NAVAL POSTGRADUATE SCHOOL

MONTEREY, CALIFORNIA

THESIS

NETTED LPI RADARS

by

Charalampos Fougias
and
Charalampos Menychtas

September 2011

Thesis Advisor: Edward Fisher
Second Reader: Wolfgang Baer

Approved for public release; distribution is unlimited

THIS PAGE INTENTIONALLY LEFT BLANK

REPORT DOCUMENTATION PAGE		*Form Approved OMB No. 0704-0188*

Public reporting burden for this collection of information is estimated to average 1 hour per response, including the time for reviewing instruction, searching existing data sources, gathering and maintaining the data needed, and completing and reviewing the collection of information. Send comments regarding this burden estimate or any other aspect of this collection of information, including suggestions for reducing this burden, to Washington headquarters Services, Directorate for Information Operations and Reports, 1215 Jefferson Davis Highway, Suite 1204, Arlington, VA 22202-4302, and to the Office of Management and Budget, Paperwork Reduction Project (0704-0188) Washington DC 20503.

1. AGENCY USE ONLY *(Leave blank)*	2. REPORT DATE September 2011	3. REPORT TYPE AND DATES COVERED Master's Thesis	
4. TITLE AND SUBTITLE Netted LPI RADAs		5. FUNDING NUMBERS	
6. AUTHOR(S) Charalampos Fougias and Charalampos Menychtas			
7. PERFORMING ORGANIZATION NAME(S) AND ADDRESS(ES) Naval Postgraduate School Monterey, CA93943-5000		8. PERFORMING ORGANIZATION REPORT NUMBER	
9. SPONSORING /MONITORING AGENCY NAME(S) AND ADDRESS(ES) N/A		10. SPONSORING/MONITORING AGENCY REPORT NUMBER	

11. SUPPLEMENTARY NOTES The views expressed in this thesis are those of the authors and do not reflect the official policy or position of the Department of Defense or the U.S. Government.   IRB Protocol number: N/A.

12a. DISTRIBUTION / AVAILABILITY STATEMENT Approved for public release; distribution is unlimited	12b. DISTRIBUTION CODE

13. ABSTRACT (maximum 200 words)

A significant number of Low Probability of Intercept (LPI) radars are used in various military applications, from guided weapons (such anti-ship missile), to large platforms (aircrafts, ships), to large systems (Integrated Air Defense Systems – IADS). The purpose of this thesis is to evaluate the performance of netted LPI radar systems. To do so, it commences with establishing the theoretical background for the LPI radar techniques and detection methods. Additionally, it presents existing LPI assets along with their operational characteristics to provide the reader with a useful tool for comparative analysis of the LPI radar market. As this work focuses on LPI radar networks, specific emphasis is given to clarifying the notion of a netted system; the conceptual and mathematical background for such are presented in a separate chapter.

14. SUBJECT TERMS Networks, LPI, Radar			15. NUMBER OF PAGES 323
			16. PRICE CODE
17. SECURITY CLASSIFICATION OF REPORT Unclassified	18. SECURITY CLASSIFICATION OF THIS PAGE Unclassified	19. SECURITY CLASSIFICATION OF ABSTRACT Unclassified	20. LIMITATION OF ABSTRACT UU

NSN 7540-01-280-5500

Standard Form 298 (Rev. 2-89)
Prescribed by ANSI Std. 239-18

THIS PAGE INTENTIONALLY LEFT BLANK

NETTED LPI RADARs

Charalampos Fougias
Major, Hellenic Air Force
B.S., Hellenic Air Force Academy, 1995

Charalampos Menychtas
Lieutenant, Hellenic Navy
B.S., Hellenic Naval Academy, 2002

Submitted in partial fulfillment of the
requirements for the degree of

MASTER OF SCIENCE IN SYSTEMS ENGINEERING

from the

NAVAL POSTGRADUATESCHOOL
September 2011

Authors: Charalampos Fougias
               Charalampos Menychtas

Approved by: Edward Fisher
               Thesis Advisor

               Wolfgang Baer
               Co-Advisor

               Dan Boger
               Chairman, Department of Information Sciences

THIS PAGE INTENTIONALLY LEFT BLANK

ABSTRACT

A significant number of Low Probability of Intercept (LPI) radars are used in various military applications, from guided weapons (such anti-ship missile), to large platforms (aircrafts, ships), to large systems (Integrated Air Defense Systems – IADS). The purpose of the present thesis is to evaluate the performance of netted LPI radar systems. To do so, it commences with establishing the theoretical background for the LPI radar techniques and detection methods. Additionally, it presents existing LPI assets along with their operational characteristics to provide the reader with a useful tool for comparative analysis of the LPI radar market. As this work focuses on LPI radar networks, specific emphasis is given to clarifying the notion of a netted system; the conceptual and mathematical background for such are presented in a separate chapter.

THIS PAGE INTENTIONALLY LEFT BLANK

TABLE OF CONTENTS

THIS PAGE INTENTIONALLY LEFT BLANK

LIST OF FIGURES

LIST OF TABLES

THIS PAGE INTENTIONALLY LEFT BLANK

LIST OF ACRONYMS AND ABBREVIATIONS

ALCM: Air Launched Cruise Missile

AOA: Angle of Arrival

AOR: Area of Regard

AWGN: Additive White Gaussian Noise

ARM: Anti-Radiation Missile

BPSK: Binary Phase Shift Keying

CVR: Crystal Video Receiver

CW: Continuous Wave

CWD: Choi-Williams Distribution

DECM: Deceptive Electronic Countermeasures

DOA: Direction of Arrival

DoD: Department of Defense

EA: Electronic Attack

ECM: Electronic Countermeasures

ELINT: Electronic Intelligence

EP: Electronic Protection

ES: Electronic Support

ESM: Electronic Support Measure

EW: Electronic Warfare

FDOA: Frequency Direction of Arrival

FH: Frequency Hopping

FLIR: Forward Looking Infra-Red

FM: Frequency Modulation

FMCW: Frequency Modulation Continuous Wave

FOV: Field of View

FSK: Frequency Shift Keying

HPBW: Half-Power Beamwidth

IADS: Integrated Air-Defense System

IFF: Identification of Friend or Foe

IFM: Instantaneous Frequency Management

IR:	Infra-Red
ISAR:	Inverse Synthetic Aperture Radar
JSR:	Jamming to Signal Ratio
LAN:	Local Area Network
LPI:	Low Probability of Intercept
MIMO:	Multiple-Input Multiple-Output
MSRS:	Multiple Radar System
MTI:	Moving Target Indicator
NCW:	Net-centric Warfare
OODA:	Observation- Orientation- Decision- Action
OTHT:	Over the Horizon Targeting
POI:	Probability of Intercept
PSD:	Power Spectral Density
PSK:	Phase Shift Keying
PSL:	Peak Sidelobe
QMFB:	Quadrature Mirror Filter Bank
RBPC:	Random Binary Phase Code
RCS:	Radar Cross-Section
RF:	Radio Frequency
RMS:	Root Mean Square
RNFR:	Random Noise Radar plus FMCW
RNFSR:	RNFR plus sine
RNR:	Random Noise Radar
RWR:	Radar Warning Receiver
SAR:	Synthetic Aperture Radar
SEI:	Specific Emitter Identification
SIGINT:	Signal Intelligence
SNR:	Signal-to-Noise Ratio
SNJR:	Signal to Noise and Jamming Ratio
SOJ:	Stand-Off Jamming
SSJ:	Self-Screening Jamming
STC:	Sensitivity Time Control

STFT: Short-Time Fourier Transform

TDOA: Time Difference of Arrival

UV: Ultra Violet

WVD: Wigner-Ville Distribution

THIS PAGE INTENTIONALLY LEFT BLANK

ACKNOWLEDGMENTS

Charalampos Fougias Acknowledgments:

I would like to thank all people who have helped and inspired me during my thesis study.

First of all, I would like to extend my utmost gratitude to my advisors Mr. Edward Fisher and Dr. Wolfgang Baer for their valuable guidance, mentorship and monumental patience. They were always accessible and willing to help with my research.

Mr. Edward Fisher deserves special thanks because I had the fortune to take one of his classes, and during that class I was inspired to explore this area of study.

A special thanks to my "brother-in-arms" in this thesis, Charalampos Menychtas, for his contributions, timeless investment, and commitment to this thesis.

I would like to thank the Hellenic Air Force for providing me the opportunity to study at the Naval Postgraduate School.

I would also like to thank my parents for providing me countless opportunities and for fostering a learning environment in which ethos integrity, discipline and hard work measure one's potential to achieve.

To my wife, Arieta, thank you for blessing me with unconditional love and unending support throughout my career and especially here at Monterey, California far away from family and friends. Few, if any, men share my luck.

To my daughter, Kalia, thank you for bringing me such joy and inspiration to keep going.

Last, I would like to dedicate this thesis to my wife Arieta and my daughter Kalia.

Charalampos Menychtas Acknowledgments:

I would like to thank the Hellenic Navy for giving me the opportunity to compete for, and earn postgraduate education at the Naval Postgraduate School. My studies in this institution have broadened my horizons both as an officer and as an individual and have asserted my view that knowledge is the most powerful weapon.

I am deeply indebted to the NPS faculty, which willingly assisted my academic inquiries and pursuits throughout my studies. Among the various professors I had the honor of being taught by, my thesis advisors, Mr. Edward Fisher and Dr. Wolfgang Baer, deserve the greatest of appreciation for their insightful comments and continuous support that made this project feasible.

I would also like to express my acknowledgements to Major Fougias, for his contribution and fruitful cooperation on this thesis work.

This work is dedicated to my family.

I. INTRODUCTION

A. BACKGROUND

The "classic" situation between radar and intercept receivers has been that the latter has no difficulty detecting and jamming the radar, and even sometimes its sidelobes, at long ranges. To counter that performance degradation, radar engineering is focused in concealing the radar emissions from the adversary (the analogy of that situation, at the target level, is to have low target Radar Cross Section [RCS] to achieve minimal returns to the radar receiver, to adopt special tactics to avoid detection, etc.). Several radar techniques have been developed to conceal radar from intercept receivers: power management, wide operational bandwidth, frequency agility, antenna sidelobe reduction, and advanced scan patterns (modulations). The types of radars that utilize such techniques are called Low Probability of Intercept (LPI) radars.

In this "Radar versus Jammer" game, both sides have exhibited remarkable adaptability: the jammer industry has replied with more sophisticated intercept receivers that try to match the LPI radar processing gain. As a response, an increasing number of LPI radars are incorporated into integrated air defense systems, IADS modern platforms, and weapons, such as anti-ship missiles and littoral weapon systems. The next step to improve the EP aspect of such systems is to associate a number of LPI assets in a net centric sense.

Examining the effect of modern jammers in net centric vs. non-centric IADS, we can draw useful conclusions on the effectiveness of the former: is there a comparative advantage of such a system vs. a non-netted one? And if there is, can it be evaluated?

B.   SCOPE OF THE THESIS

This thesis provides a comprehensive volume of two major elements in Electronic Warfare: LPI technology and network configurations. Although the existing literature dealing individually with LPI technology is not only wide but also constantly updated (Lee 1991, McRitchie and McDonald 1999, Kadambe and Adali 1998, Burgos-Garcia et al. 2000,D. Adamy 2001, Baker and Hume 2001, Skolnik 2001, Gau 2002, Lynch Jr. 2004, Wiley 2006,Pace 2009), scholarly efforts providing insights in network configurations of such assets is, by comparison, less extensive. In this context, this thesis intends to fill this literature gap and provide a more comprehensive volume covering both academic realms on the same work.[1]

To do so, it commences with establishing the theoretical background for LPI radar techniques and detection methods. Additionally, it presents the existing LPI assets along with their operational characteristics, thus providing the reader with a useful tool for comparative analysis of the LPI radar market. As this works

---

[1] The 2008 paper of Chen and Pace presents a basic framework for simulation of network enabled radar systems, but, apart from being limited in breadth, its scope is limited in the evaluation of the jamming effect in general radar topology. Y. Q. Chen and Phillip E. Pace, "Simulation of Information Metrics to Assess the Value of Networking in A General Battlespace Topology," in *Proc. of the IEEE International Conf. on System of Systems Engineering* (IEEE, June 2008).

intends to elucidate the concept of LPI networks, special emphasis shall be given to clarifying the notion of a netted system; the theoretical and mathematical background of such is presented in a separate chapter.

C.   RESEARCH QUESTIONS

Primary:

What is the jamming effect on a netted LPI radar-based IADS versus non-netted IADS?

Secondary:

What is LPI radar and how does it gain its advantage?

What is netted radar network and how does it gain its advantage?

How are LPI radars most effectively netted?

How effective is EA on LPI netted networks?

D.   METHODOLOGY

The methodology used in this thesis research will consist of the following steps.

Articles, books, periodicals, thesis, IEEE, and DoD documents related to the subject will be collected and thoroughly examined. MATLAB simulation regarding the IADS configuration under evaluation shall be applied to assist the comprehensive aspect of the thesis. With the MATLAB simulation, we will design an LPI IADS system that can be operated in netted or autonomous configuration, and we will examine its overall behavior under different jamming operational techniques. The answers to questions stated in

the above section will be established in a reasonable fashion.

E.   BENEFITS OF THE STUDY

The results of this thesis will be used to support ongoing efforts by the Hellenic Armed Forces. This thesis will enhance the perspective and knowledge of Electronic Warfare officers, related project officers, and technical personnel. The comprehensive approach of the LPI concept attempted in this paper will assist the Hellenic Armed Forces in evaluating future needs and requirements of Electronic Warfare systems on both netted and non-netted configurations.

F.   THESIS OUTLINE

The thesis research and findings are organized in the following manner:

Chapter I comprises the introductory section of the thesis.

Chapter II describes the LPI radar theory of operation and techniques (waveforms, modulation) used in this thesis work. It gives to the reader the theoretical basis of the LPI radar operation.

Chapter III presents the airborne, maritime, and land-based LPI radars available in the industry.

Chapter IV describes detection methods of LPI radars. For this purpose EP receivers and signal processing algorithms are examined in detail. Examples of EP receiver systems used in real operational environments are also given.

Chapter V discusses jamming methods for LPI radars.

Chapter VI introduces the idea of networks and attempts to clarify the concept of net-centric warfare (NCW).

Chapter VII looks more specifically into netted LPI Radar Systems, addressing their advantages and disadvantages.

Chapter VIII employs simulation of selected net centric IADS configuration via MATLAB.

Finally, conclusions are summarized in Chapter IX.

THIS PAGE INTENTIONALLY LEFT BLANK

II. LPI RADAR THEORY OF OPERATION AND TECHNIQUES

The objective of this chapter is to enlighten the reader about the applicable techniques for LPI radar systems as well as to give some examples of airborne, maritime and land-based LPI radar systems.

A.   DEFINITIONS

In today's battlefield, radar faces many threats from Electronic Attack (EA) and Anti-Radiation Missiles (ARMs). This situation brought about the need for the radar to try to "see" the target without enabling the target's passive intercept receiver and/or other enemies' intercept receiver (not on board the target) to intercept the radar's signal. To answer that need, radars were developed that apply various LPI techniques. These radars are called LPI radar.

LPI radar is one form of RF Stealth. It tries to hide one's RF emissions, or its active signature, by implementing various techniques such as using very low signal levels and/or specially constructed waveforms (those will be analyzed later in this thesis).

Active signature is defined as all the observable emissions from a platform: acoustic, chemical (soot and contrails), communications, radar, IFF, IR, laser, and Ultra-Violet (UV) (Lynch 2004, 3).

Radar signature reduction requires the use of various techniques that can minimize the radar's radiated power density at possible intercept receiver locations. The role of tactics is also important when one wants to minimize

7

radar's active signature because by correct and thoughtful tactics implementation one can reduce significantly exposure time during emission.

B.   LPI RADAR EVOLUTION HISTORY

The "classic" situation between radar and intercept receivers has been that the intercept receiver has no difficulty detecting the radar, and even sometimes its sidelobes, at long ranges. That happens because the radar transmitted wave has to "travel" twice the distance—from radar to target (intercept receiver) and back—for the radar to detect the target. In the case of the intercept receiver onboard the target, the wave has to travel only the "one way" (Skolnik 2001, 7). That can easily be seen by the following range equations for radar versus intercept receiver (ESM):

$$P_R^{RDR} = \frac{P_T G_T^2 \lambda^2 \sigma_t}{\left(4\pi\right)^3 R_{RDR}^4} \quad (2.1)$$

$$P_R^{ESM} = \frac{P_T G_T G_R \lambda^2}{(4\pi)^2 R_{ESM}^2} \quad (2.2)$$

Where:

P_T = Transmitter Power

G_T = Gain of RADAR Ant

P_R^{RDR} = RADAR received signal power

P_R^{ESM} = ESM received signal power

λ = Wavelength

σ_t = Target's RADAR Cross Section (RCS)

G_R = Gain of ESM Receiver Ant

R_{RDR} = RADAR detection range

R_{ESM} = Intercept's receiver detection range

From the above equations we can clearly see that the RADAR received signal power is proportional to $1/R_{RDR}^4$ whereas the intercept received signal power is proportional to $1/R_{ESM}^2$. So the considering all other factors between RADAR and intercept receiver the same or comparable (atmospheric losses, processing gains of both receivers etc) the path loss ($1/R_{ESM}^2$ versus $1/R_{RDR}^4$) created a great advantage for the intercept receiver.

The increased signal processing gain obtainable from radar has given radar the potential ability to alter that balance, on the assumption that the intercept receiver cannot duplicate the radar's processing gain.

LPI radar is designed to be difficult to detect by passive radar detection equipment (such as a radar warning receiver (RWR) or other ESM equipment) while it is searching for or tracking a target. This characteristic is desirable because it allows finding and tracking an opponent without alerting them to the radar's presence.

LPI radars are generally transmitting weak signals that the intercept receiver has difficulty detecting above its threshold.

Many combined features help the LPI radar prevent its detection by modern intercept receivers. These features are

centered on the antenna (antenna pattern and scan patterns), the transmitter radiated waveform and LPI radar power management features.

The capability of LPI radar to stay undetected heavily depends upon the intercept receiver's characteristics and vice versa. So in order to understand LPI radars we must understand the nature of the ESM receivers. The purpose of an ESM receiver is to detect, sort and classify an unknown radar (Lynch 2004, 11).

The ESM receiver achieves the detection of the radar signal by having the necessary sensitivity and processing power to detect a signal of specific power over a given distance.

Sorting is the task of separating different emitters, in a dense signal environment where many signals in different or the same frequency band from various directions are intercepted, so that they can then be classified.

Classification is the task of identifying emitter type (or even the specific emitter) and determining the respective weapon system that the emitter is carried on.

LPI radar uses continuous wave (CW), wide bandwidth, low power signals on the order of a few watts (or even lower in the order of magnitude of mWatts) making its detection difficult. Unlike conventional radars, which emit high-energy pulses in a narrow frequency band, LPI radar

emits low energy pulses over a wide frequency band. Wideband CW techniques include:

- Linear and nonlinear frequency modulation (FMCW)

- Phase modulation (Bi-phase codes such as Barker Code, poly-phase codes such as Frank, P1, P2, P3 and P4 Code).

- Frequency hopping (FSK, Costas sequence FSK technique).

- LPI signals are typically modulated by a periodic function such as Barker Code, Frank Code, P1 Code, P2 Code, P3 Code and P4 Code.

The purpose of this modulation is to generate a "unique" waveform signature that can be detected by the radar receiver when scattered back at very low S/N levels.

C. BASIC PRINCIPLES OF LPI RADAR OPERATION

Various features and techniques can be implemented with radar to reduce its active signature, make it an LPI radar and ultimately prevent its detection by modern intercept receivers.

1. Power Management

Power management is the ability to control the power level emitted by the antenna, and limit the power to the appropriate range/radar Cross Section (RCS) detection requirement (Pace 2009, 16).

The idea is that since most intercept receivers would expect an increase in received power by the radar as the distance decreases, the ability of the LPI radar to adjust its radiated power to lower levels as the target approaches

can make the intercept receiver change its priorities for Electronic Attack (EA) on the LPI radar.

From the LPI radar's point of view, as can be seen in equation 2.1, as the distance from the target is decreasing R_{RDR}, the LPI radar by trying to keep the level of its received power scattered back from the target P_R^{RDR} close to its minimum discernable level, with all other factors the same, reduces its radiated power level P_T.

From the intercept receiver's point of view, as can be seen in equation 2.2, by decreasing the radiated power P_T with all other factors the same (including the distance between LPI radar and intercept receiver), the received power by the intercept receiver P_R^{ESM} decreases, which in turn is translated by the intercept receiver as an increase of the distance between the LPI radar and the intercept receiver.

2. Waveform Shaping

Conventional RADARs use waveforms comprised of pulse trains that have a very high peak power P_T and a low duty cycle $DC = P_{ave} / P_T$. These kinds of waveforms are easily detectable by intercept receivers. Since the detection of a target relies upon the total back scattered power to the radar receiver, modern radar use special waveforms that:

- Disperse the power of one pulse in many pulses (that will hit the same target) and integrate them together (coherently or non-coherently) taking their added effect, as we can see in Figure 1. That is pulse compression (for

12

pulsed radar) and is based on the fact that what matters to radar detection is the total amount of energy reflected back from the target.
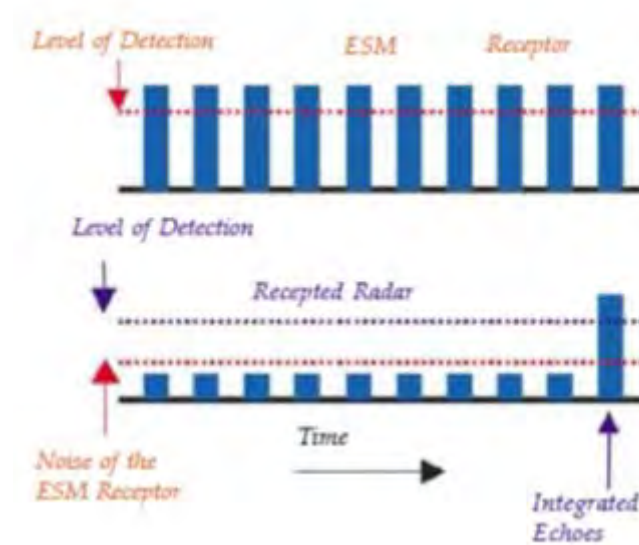
Figure 1.   Pulse Compression

• Disperse the power in low energy pulses over a wide frequency band, as we can see in Figure 2. That can be done by using a CW waveform properly modulated by techniques mentioned earlier. This is the main technique used in LPI radar that uses FM modulation ramps, but as we reported previously there are other types of modulating the CW wave used at an LPI radar. LPI radar has low P_T but high P_{ave}.

Figure 2.   FMCW

In general, waveform shaping techniques provide the extra processing gain that gives radar its main advantage with respect to ESM receivers, but it also forms a power management "like" method to reduce the peak power of the radar.

3.   **Antenna Design**

a.   *Low Level Antenna Sidelobes*

Radar applications generally demand low sidelobe antennas for the following reasons, which are also the advantages of achieving low sidelobes (Lynch 2004, 354):

- If the sidelobes are large enough, they radiate a large portion of the total radiated energy of the antenna. That fact would cause a reduction of the main beam energy and consequently the decrease of the antenna gain.

- Low sidelobes reduce clutter returns (they cover most of the space around the antenna, and since the antenna is pointing at the point of interest, their returns are mostly unwanted clutter).

14

- Low sidelobes reduce interference (mostly from nearby friendly transmitters).

- Low sidelobes reduce ECM susceptibility and probability of intercept (high levels of sidelobes make jamming easier and, since they cover most of the space around the antenna, can expose it easily at various bearings).

Typical sidelobe levels for conventional radar are around -20 dB whereas for LPI radar the acceptable level is around -45 dB (Pace 2009, 8). It is rather easy to manufacture antennas with sidelobe levels of -35 to -40 dB, and with extreme care it is possible to go even lower (-50 or -55 dB). However, considerably lower sidelobes are difficult to achieve, primarily as a result of manufacturing tolerances (Lynch 2004, 354).

One other effect of the ultra-low sidelobe antenna, apart from the fact that it will make it difficult for an ESM receiver (not located at the target – not a part of the target systems) to intercept and locate the radar, is that these types of antennas are very directional. In other words, they have very narrow Half Power Beam Widths (HPBW) both in azimuth and in elevation. According to the following formula (Skolnik 2001, 541),this will also give the radar antenna a much higher gain and thus require less transmitted power, which will also enhance the LPI feature of the radar (as $\theta_{Horizontal}^{3dB}$ and/or $\theta_{Vertical}^{3dB}$ increases then also G_T increases):

$$G_T \approx \frac{26,000}{\theta_{Vertical}^{3dB} \times \theta_{Horizontal}^{3dB}} \text{ (2.3)}$$

15

Where:

$\theta_{Vertical}^{3dB}$: Radar antenna vertical half power (3dB) beam width

$\theta_{Horizontal}^{3dB}$: Radar antenna horizontal half power (3dB) beam width

G_T : Gain of radar antenna

The combined transmitter/antenna efficiency is defined by the Effective Radiated Isotropic Power (EIRP):

$$EIRP = P_T G_T \text{ (2.4)}$$

Where:

P_T = Transmitter Power

G_T = Gain of radar antenna

So for a given EIRP that we have to accomplish, if we provide a better antenna design that gives a higher gain, then the transmitted power out of our transmitter P_T can be lower (as G_T increases then P_T also increases for the same $EIRP = P_T G_T$).

The general formula for the gain of an antenna is (Lynch 2004, 353):

$$G = \frac{4\pi A_{eff}}{\lambda^2} = \frac{4\pi \rho A_{ph}}{\lambda^2} \text{ (2.5)}$$

Where:

A_{eff} : Effective area of antenna

16

A_{ph} : Physical area of antenna

ρ : Antenna efficiency factor

λ : Wavelength

  Of course, the increase in gain of an antenna for a given frequency (and wavelength) has to happen either by improving its efficiency factor ρ or by increasing its physical dimensions A_{ph}. The first factor poses technical difficulties (like RF spillover or under-illumination, etc.), and the second factor requires a lot of "real

estate" that in the case of airborne applications is a major limiting factor (for increasing G then either ρ or A_{ph} increases).

  A typical polar diagram of low sidelobe antennas versus normal antennas is given in Figure 3 (Lynch 2004, 4). In order to achieve such a pattern for these low sidelobes we have to sacrifice some of the main lobe gain and some of the utilization of the total aperture area (under-illumination).
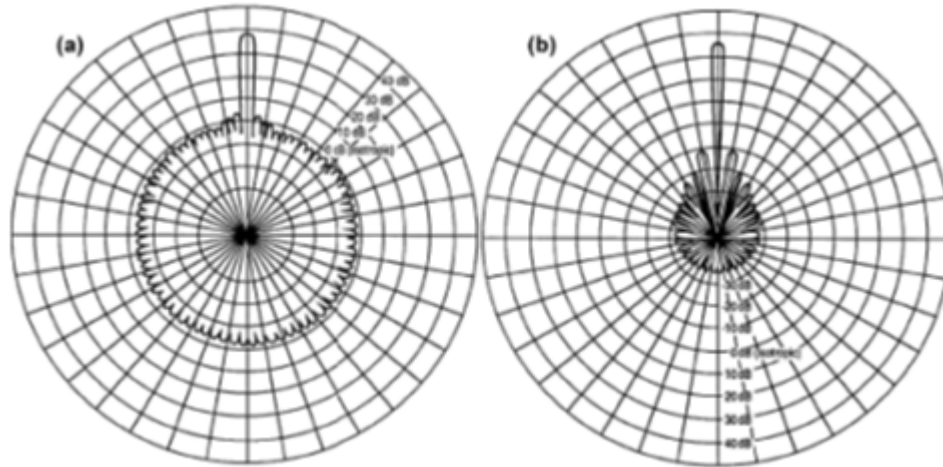
Figure 3.   Conventional (a) and Low Sidelobe Antenna
Patterns (b)

Typical technical approaches to reduce the sidelobes are the use of parallelogram shapes and separable illumination functions. These solutions aid in reducing the sidelobes, but more is required to manufacture an antenna with really low sidelobes. The most effective technical approach that we can apply in order to reduce the sidelobes to really low values (-60dB) is amplitude weighting across the aperture (or tapering). The disadvantage of this process is the decrease of the main lobe gain. The amplitude weighting function also needs to be robust in the sense that small errors will not destroy the desired performance, and the weighting values are achievable with real hardware (Lynch 2004, 374).

b.   *Antenna Scan Patterns*

When radar is intercepted, the next task is for the intercept receiver to identify it. Identification happens often by the type of scanning they perform, as modern intercept receivers can be programmed to identify

scan patterns. That applies also to LPI radar as well. LPI radar cannot avoid detection forever and so eventually will be detected (intercepted) by the intercept receiver. At this point it may be possible to identify by the scan pattern.

The LPI radar can use irregular scan patterns in order to avoid identification by the intercept receiver. That process can be implemented both in mechanically steering antennas and electronically steering antennas, but the electronically steered ones provide more flexibility in adjusting the scan pattern parameters. Some of these techniques include, but are not limited to, creation of multiple beams to scan different scan volumes; creating beams with different frequencies; use of aperiodic scan cycles; or non-scanning single beam transmit/multi-beam receive strategies (Pace2009, 10-13).

4. Carrier Frequency Selection

Due to atmospheric absorption (mainly due to H_2O and O_2) certain frequencies have higher attenuation than others, as we can see in Figure 4. LPI radar can exploit that fact by operating at these frequencies. Due to the high absorption of RF energy at these frequencies, the incident power at the intercept receiver will be much lower compared to other frequencies that are not affected by the H_2O and O_2 molecules, so the probability of intercepting LPI radar that operates at these frequencies is much lower. Another tactic should be to operate the LPI radar at a frequency that the intercept receivers are not accustomed to. For long-range LPI systems, such a consideration—

choosing a carrier frequency in a high atmospheric absorption band—is not beneficial because the return signal is greatly attenuated. However, for close range LPI systems it is an advantage because they can further lower their signature apart from practicing power management.
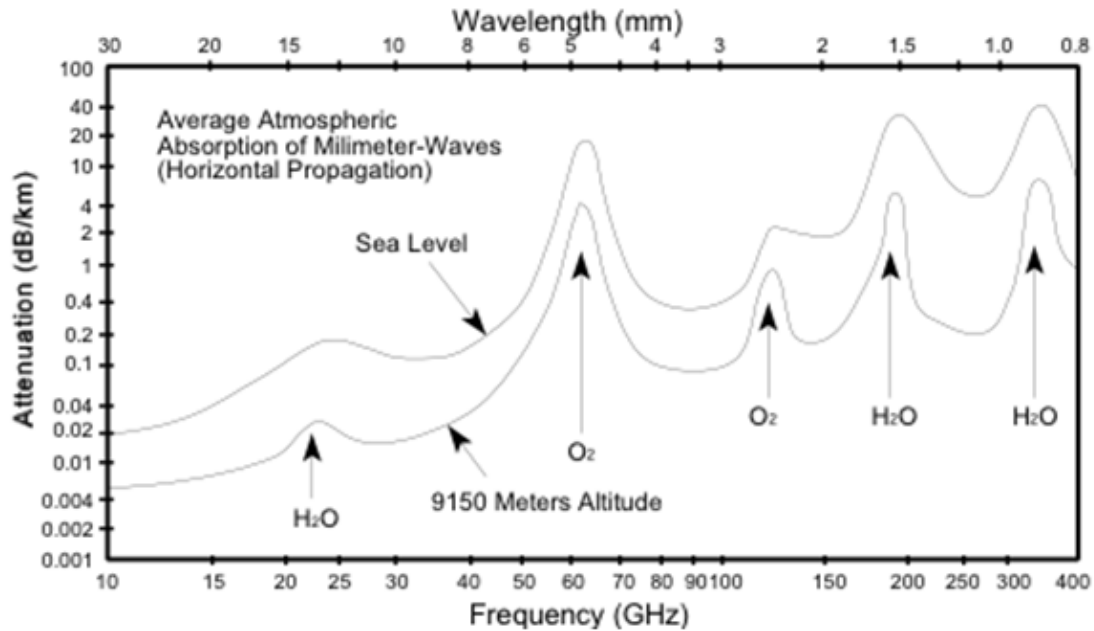
Figure 4.   Atmospheric Attenuation vs Frequency[2].

5.   High Receiver Sensitivity

Sensitivity is a critical factor in the operation of LPI radar. Sensitivity, in general, is defined as the product of the minimum signal to noise ratio required at the input times the noise power in the input bandwidth times the noise figure of a given receiver (D. L. Adamy 2004, 43); it is the lowest signal the receiver can accept and perform its function (i.e. detect targets). The higher

---

[2]Naval Air Systems Command 1999, 5-1.

the sensitivity the lower the signal the receiver can accept to perform its function.

The respective formula for the LPI radar receiver is the following (Pace 2009, 26):

$$\delta_R = kT_0 F_R B_R SNR_{required}^R \quad (2.6)$$

Where:

δ_R : LPI radar sensitivity

k : Boltzmann's constant

F_R : LPIR receiver noise factor

T_0 : Standard noise temperature (Kelvin)

B_R : LPI radar receiver bandwidth

$SNR_{required}^R$: LPI Radar receiver input SNR required

The relationship between LPI radar max range and sensitivity is the following (Pace 2009, 26):

$$R_{max}^R = \left[\frac{P_T G_T G_R \lambda^2 \sigma_t}{(4\pi)^3 \delta_R L} \right]^{\frac{1}{4}} \quad (2.7)$$

Where:

P_T : Transmitter power

G_T : Gain of transmitting radar antenna

G_R : Gain of receiving radar antenna

λ : Wavelength

σ_t : Target's Radar Cross Section (RCS)

L: Transmission losses

δ_R: LPI Radar (LPIR) sensitivity

It is clear from the above formula that for higher sensitivity we get higher LPI radar max range (when sensitivity increases then δ_R decreases and R_{max}^R increases). It is imperative for LPI radar to have very high receiver sensitivity, since the received signals (scattered back from targets) have extremely low power. That happens because the initially emitted signals have very low power as well.

Factors that can improve the LPI radar performance with respect to the sensitivity of the LPI radar receiver are the reduction of the receiver noise figure F_R and the design for lower signal to noise ratio required for detection.

6. Processing Gain of LPI Radar

The definition of processing gain of radar in general is the ratio between the signal to noise ratio of the processed signal over the signal to noise ratio of the unprocessed signal(Pace 2009, 28):

$$PG_R = \frac{SNR_{Ro}}{SNR_{Ri}} \ (2.8)$$

Where:

SNR_{Ri}: Input SNR at the radar signal integrator

SNR_{Ro}: Output SNR at the radar signal integrator

At this point, and in order to clarify the concept of the processing gain of the LPI radar and how that affects the battle of detection between radar and intercept receiver, we can consider the maximum interception range of an intercept receiver(Pace 2009, 28):

$$R_{max}^I = \left[\frac{P_T G_T' G_I \lambda^2 L_1}{(4\pi)^2 \delta_I L_{RT} L_{IR}} \right]^{\frac{1}{2}} \quad (2.9)$$

Where:

$L_1 = e^{-2\alpha R}$: One-way atmospheric transmission factor

L_{RT} : Loss between intercept receiver's receive antenna and receiver

L_{IR} : Loss between intercept receiver's receive antenna and receiver

We can use both δ_R and δ_i to quantify the advantage of the LPI radar by taking their ratio (Pace 2009, 29-30):

$$\delta = \frac{\delta_I}{\delta_R} = \left(\frac{F_I B_{Ii}}{F_R B_{Ro}} \right) \left(\frac{SNR_{Io}}{SNR_{Ro}} \right) \left(\frac{PG_R}{PG_I} \right) \quad (2.10)$$

Where:

F_R : LPI radar receiver noise factor

F_I : Intercept receiver noise factor

B_{Ii} : Intercept receiver input bandwidth

B_{Ro}: LPI radar output receiver bandwidth

SNR_{Io}: Minimum SNR required at the output of the receiver of the intercept receiver for detection.

SNR_{Ro}: Minimum SNR required at the output of the LPI radar receiver for detection.

$PG_R = \dfrac{SNR_{Ro}}{SNR_{Ri}}$: LPI radar processing gain

$PG_I = \dfrac{SNR_{Io}}{SNR_{Ii}}$: Intercept receiver processing gain

Taking into account the relationship between sensitivities δ_R and δ_i and maximum ranges R_{max}^R and R_{max}^I respectively, we get the following relationship:

$$\frac{R_{max}^I}{R_{max}^R} = R_{max}^R \left[\frac{1}{\delta} \left(\frac{4\pi}{\sigma_t} \right) \frac{G_T' G_I L_1}{G_T G_R L_2} \right]^{1/2} \quad (2.11)$$

From the Equations (2.10) and (2.11) we can see that:

$$\frac{R_{max}^I}{R_{max}^R} \propto \sqrt{\frac{1}{\delta}} \Rightarrow \frac{R_{max}^I}{R_{max}^R} \propto \sqrt{\frac{\delta_R}{\delta_I}} \quad (2.12)$$

For $R_{max}^I / R_{max}^R < 1$ we can say that the LPI radar is quiet and cannot be intercepted by the intercept receiver (radar prevails).

For $R_{max}^I / R_{max}^R > 1$ we can say that the intercept receiver prevails.

For $R_{max}^I / R_{max}^R = 1$, equation (2.11) gives:

$$R_{max}^{R} = \left[\delta \left(\frac{\sigma_t}{4\pi} \right) \frac{G_T G_R L_2}{G_T' G_I L_1} \right]^{1/2} \quad (2.13)$$

and the radar cannot be intercepted beyond the range it can detect targets (this is the maximum detection range of the LPI radar without being intercepted by the intercept receiver, and simultaneously it is the maximum intercept receiver detection range).

The processing gain advantage for LPI radar can be achieved by the performance of coherent processing and the use of special waveforms.

a. Coherent Processing

The LPI radar knows exactly the characteristics of its transmitted waveform so it can match its receiver and processing to its own signal, whereas an intercept receiver operates in a much denser environment (where other signals are present) and has to perform detailed parametric measurements/calculations in order to identify the receiving signal characteristics (D. Adamy 2001). That demands much more processing power on the part of the intercept receiver or some knowledge – probably from ELINT – of the general radar signal characteristics.

b. LPI Waveforms

We mentioned previously that the main feature of LPI radar is to disperse the power in low energy CW waveforms over a wide bandwidth and period of time. That produces very low amplitude signals that are covered in the noise floor. The general types of LPI radar wideband waveforms are the following:

- Linear and non-linear Frequency Modulating Continuous Wave (FMCW) radar.

- Phase modulating techniques including polyphase and polytime modulation.

- Frequency Shift Keying (FSK) techniques (frequency hopping techniques).

- Noise techniques

FMCW waveform, due to its importance and high popularity as used waveform in LPI radars, will be examined in depth in the present chapter. For the rest of the LPI waveforms we will provide a short description and notetheir advantages and disadvantages. A more detailed description of the other LPI waveforms will be presented in the Appendix.

(1) FMCW. CW radar uses unmodulated waveforms, and they cannot measure the target's range and speed. By modulating the CW transmit frequency either linearly or non-linearly (e.g., with a sinusoidal function), range and speed information can be obtained by correlating the transmitted signal with the return signal. The most popular method of modulating the CW wave is linear Frequency Modulation (FM) and especially triangular modulation (Skolnik 2001, 195).

FMCW waveforms, also called "chirps", are the most common among LPI radar because they provide many advantages; the most important of which are (Pace 2009, 81-82):

- It has a simple architecture and can be implemented with simple solid-state transmitters.

- Gives high resolution due to the large modulation bandwidth.

- Due to the very high duty cycle and the very low peak power, the intercept receiver's intercept range is significantly reduced.

- Due to the nature of the transmitted waveform (deterministic), the form of the return waves is predicted and any return wave that does not match the transmitted one will be suppressed. So it is resistant to interference and jamming.

- High range resolution can be obtained without the need of a wide IF and video bandwidth (the IF and video bandwidth can be matched to the data rate instead of the RF bandwidth to give the required range resolution).

- The Sensitivity Time Control (STC) function, which controls the attenuation of the returns of closing targets in order to avoid saturation, can be easily implemented.

Some problems/disadvantages of linear and non-linear FMCW radar are the following (Lynch 2004, 294), (Pace 2009, 94-95):

- To achieve high-resolution systems leads to very high bandwidth front-end signal processing.

- Valid (real) targets can be hidden within the transmitter noise sidebands. That can be countered by using weighting in the matched filter response.

- Power leakage from transmitter to receiver will decrease the receiver's sensitivity, which in turn will lead to the "loss" of valid targets.

- They have high side-lobe levels (to the order of 13dB down the value of the peak response).

Figure 5 shows the form of the triangular linear FMCW transmit waveform as well as the form of the received signal (Pace 2009, 87).
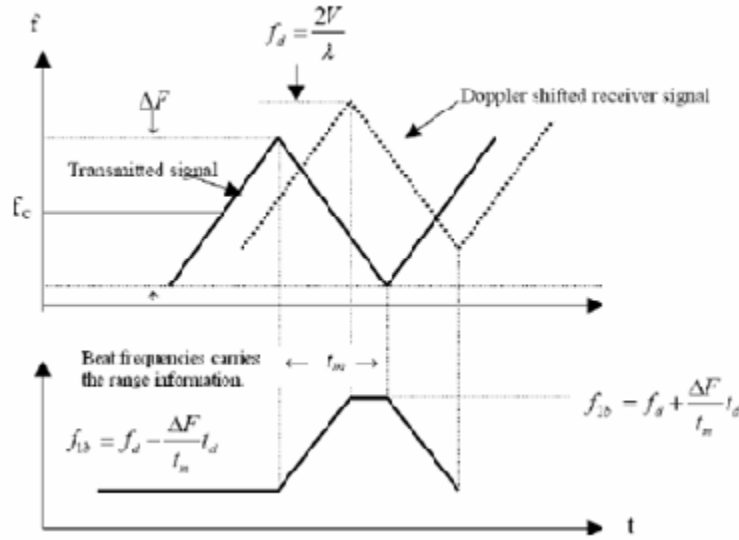
Figure 5.   Linear FMCW Triangular Waveform

For the first section (increasing slope) of the triangular FMCW waveform we have the following mathematical expressions (Pace 2009, 86-87):

Frequency: $$f_1(t) = f_c - \frac{\Delta F}{2} + \frac{\Delta F}{t_m} t \quad (2.14)$$

For $0 < t < t_m$ zero elsewhere.

28

Phase: $$\varphi_1(t) = 2\pi \int_0^t f_1(x)dx = 2\pi\left[\left(f_c - \frac{\Delta F}{2}\right)t + \frac{\Delta F}{2t_m}t^2\right] \quad (2.15)$$

Assuming $\varphi_0 = 0$ at $t = 0$

Transmit signal: $$s_1(t) = a_0 \sin\left\{2\pi\left[\left(f_c - \frac{\Delta F}{2}\right)t + \frac{\Delta F}{2t_m}t^2\right]\right\} \quad (2.16)$$

for $0 < t < t_m$.

For the second section (decreasing slope) of the triangular FMCW waveform we have the following relations(Pace 2009, 87-88):

Frequency: $$f_2(t) = f_c + \frac{\Delta F}{2} - \frac{\Delta F}{t_m}t \quad (2.17)$$

for $0 < t < t_m$ zero elsewhere.

Phase: $$\varphi_2(t) = 2\pi \int_0^t f_2(x)dx = 2\pi\left[\left(f_c + \frac{\Delta F}{2}\right)t - \frac{\Delta F}{2t_m}t^2\right] \quad (2.18)$$

Assuming $\varphi_0 = 0$ at $t = 0$

Transmit signal: $$s_2(t) = a_0 \sin\left\{2\pi\left[\left(f_c + \frac{\Delta F}{2}\right)t - \frac{\Delta F}{2t_m}t^2\right]\right\} \quad (2.19)$$

for $0 < t < t_m$.

Where:

f_c : Carrier frequency

ΔF : Modulation bandwidth

t_m : Modulation period

The received signal from the target is delayed in time by the round trip propagating time and has reduced amplitude due to the various losses encountered from propagation, scattering, atmosphere and others. The mathematical expression of the return signal is the following (Pace 2009, 100):

- For the first section (increasing slope) of the triangular FMCW waveform:

$$s_{1r}(t) = b_0 \sin\left\{2\pi\left[\left(f_c - \frac{\Delta F}{2}\right)(t-t_d) + \frac{\Delta F}{2t_m}\left(t-t_d\right)^2\right]\right\} \quad (2.20)$$

- For the second section (decreasing slope) of the triangular FMCW waveform:

$$s_{2r}(t) = b_0 \sin\left\{2\pi\left[\left(f_c + \frac{\Delta F}{2}\right)(t-t_d) - \frac{\Delta F}{2t_m}\left(t-t_d\right)^2\right]\right\} \quad (2.21)$$

Where:

t_d: Round trip propagation time

The received signal then is amplified, mixed, and demodulated with the opposite slope "chirp". That is the matched filtering process of the FMCW, and results in an output pulse whose amplitude is proportional to the square root of the time-bandwidth product ($\sqrt{t_m B_T}$) (Lynch 2004, 293-294).

The range resolution of the FMCW radar is given by (Pace 2009, 102):

30

$$\Delta R = \frac{c}{2\Delta F} = \frac{c\Delta\text{T}}{2} \text{ (2.22)}$$

In order for the FMCW radar to have high resolution (in other words small ΔR) the modulation bandwidth has to be high.

In Figure 6, by using the MATLAB LPIT TOOLBOX, we see an example of the in-phase up-ramp FMCW signal with parameters $f_c = 1kHz$, $f_s = 7kHz$, $SNR = 0dB$, $\Delta F = 250Hz$, $t_m = 20\mu\sec$.
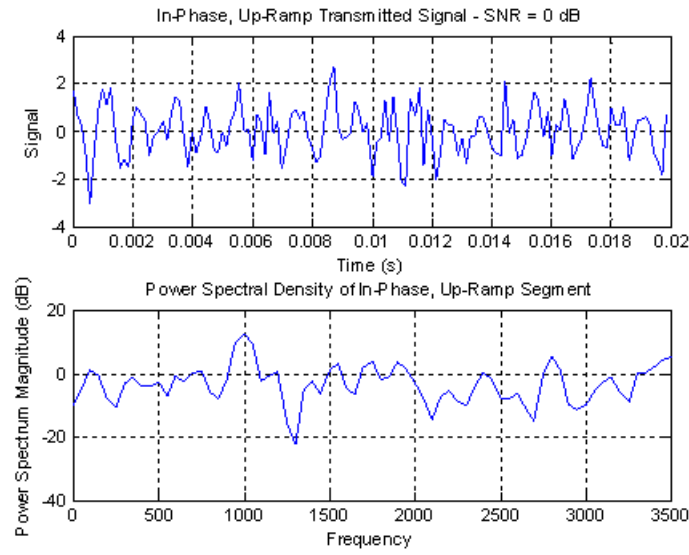
Figure 6.   Linear FMCW In-Phase Ramp-up Signal

(2) Phase Modulating Techniques. Phase modulating techniques (Phase Shift Keying – PSK) have a wide bandwidth and achievable low probability ambiguity function (PAF) side-lobe levels (Pace 2009, 125). That is

31

the major advantage of the PSK techniques over the linear and non-linear FMCW technique discussed previously.

The choice of the PSK code that will be used in LPI radar implementation heavily affects LPI radar performance. The designer first has to select the required bandwidth (which is the inverse of the selected sub-code period) in order to achieve the desired range resolution.

A trade-off has to be expected here because in the case of "big" targets, where we do not need such high resolution and the whole target can "fit" in one range bin, we can get target detection, but this results in a narrow bandwidth signal which is a negative factor since we want to avoid our own detection. On the contrary, if the designer decides to have a high range resolution, that results in dividing the target's echo in many range bins, which requires much larger transmitted power in order to detect the target and thus decreases the ability of the radar to remain "quiet"(Pace 2009, 126).

PSK techniques, and mainly polyphase techniques that can have an extremely long code period, provide high range resolution waveforms and high SNR processing gain for radar. In combination with power management techniques, these can regulate the maximum detection range of radar as well as keep the target's SNR constant while the target is closing(Pace 2009, 126).

The transmitted signal of the PSK LPI radar has the following form (Pace 2009, 126-127):

Complex representation $s(t) = Ae^{j(2\pi f_c t + \varphi_\kappa)}$ (2.23)

In phase representation $\qquad$ $I = A\cos(2\pi f_c t + \varphi_\kappa)$ (2.24)

Quadrature representation $\qquad$ $Q = A\sin(2\pi f_c t + \varphi_\kappa)$ (2.25)

Where:

f_c = Carrier frequency

φ_k = Phase modulation function

Within a code period, the signal is phase shifted N_c times with phase φ_k (which depends on the type of the PSK code used), every t_b seconds, (which is the sub-code period) according to the specific code sequence. The signal characteristics of PSK LPI radar are the following (Pace 2009, 127):

The total code period is: $\qquad$ $T = N_c t_b$ (2.26)

The code rate is: $\qquad$ $T = 1/T = 1/N_c t_b$ (2.27)

The range resolution is: $\qquad$ $\Delta R = \dfrac{ct_b}{2}$ (2.28)

The unambiguous range is: $\qquad$ $R_{un} = \dfrac{cT}{2} = \dfrac{cN_c t_b}{2}$ (2.29)

The bandwidth is: $\qquad$ $B = \dfrac{f_c}{cpp} = \dfrac{1}{t_b}$ (2.30)

Where:

N_c = Number of subcodes.

t_b = Subcode period.

cpp = Number of cycles of the carrier frequency per subcode.

A summary of the advantages and disadvantages of Phase modulating techniques is presented in Table 1.

CODE TYPES		ADVANTAGES	DISADVANTAGES
Polyphase Codes	Barker codes	1. All waveforms spread the signal of LPI radar both in frequency and in power. 2. There are many codes and code lengths to choose from when implementing LPI radar. 3. Provide low probability of detection (due to very low signal levels). 4. Provide low probability of interception (due to very low signal levels). 5. Large phase values N for polyphase codes provide: • high range resolution ΔR • large compression ratio • high processing gain PG • low auto correlation sidelobes (PSL – Peak Sidelobe Level) 6. Decreased sub-code width in polyphase codes results in fewer cycles per phase and increased bandwidth B which also contributes to the high processing gain. 7. Perfect PAF (Periodic Autocorrelation Function) for Frank, P1, P3 and P4. 8. Decreased minimum phase state (bit duration) for polytime codes gives large waveform bandwidth	1. Polyphase codes demand a very complex match filter at the receiver. 2. Barker codes discovered so far are only for subcode number less than 63. 3. P2 does not have a perfect PAF. 4. Polytime codes waveform generation is very complicated. 5. Polytime codes do not provide such low PSL as the polyphase ones. 6. All waveforms demand (in general) complex hardware for their implementation.
	Frank codes		
	P1		
	P2		
	P3		
	P4		
Polyphase Codes	T1(n)		
	T2(n)		
	T3(n)		
	T4(n)		

Table 1.   Phase Modulating Techniques Advantages/ Disadvantages

(3) Frequency Shift Keying (FSK) Techniques. Frequency shift keying is another way to lower the probability of intercept. It is a kind of Frequency Hopping (FH) technique with application to CW radar. The whole process is based on the fact that the transmitting frequency of radar changes in time over a wide bandwidth. It must be noted that in the FSK case of LPI radar we are considering the FH as the change in the CW carrier frequency f_c over time over a preselected set of frequencies. We need to make that distinction because it is very easy to confuse the CW radar FH technique with the frequency agility technique that is applies to pulsed radar.

Since the intercept receiver does not know the next frequency that LPI radar will use (out of the predefined set of frequencies – FH sequence), it is impossible for the intercept receiver to perform reactive jamming on FH LPI radar.

One significant difference between FSK techniques and FMCW techniques is that in FMCW techniques, we spread the energy of the wave in various frequencies and in this way we present a very low Power Spectral Density (PSD) to the intercept receiver. That, demands very high sensitivity and other techniques implemented into the intercept receiver (to be discussed in later chapters) in order to overcome such a low PSD. In the FH techniques there is no dispersal of the power in the frequency domain but in the time domain over different frequencies, which does not lower the PSD of the signal (Pace 2009, 188).

The transmitted frequency f_j is chosen from the FH sequence $\left\{f_1, f_2, ..., f_N\right\}$ of available frequencies for transmission at a set of consecutive time intervals $\left\{t_1, t_2, ..., t_N\right\}$. The FH CW signal is:

$$s(t) = A e^{j2\pi f_j t} \text{ (2.31)}$$

A summary of advantages and disadvantages of FSK techniques is presented in Table 2.

CODE TYPES	ADVANTAGES	DISADVANTAGES
Costas Codes Hybrid FSK/PSK Matched FSK/PSK	1. Provide low probability of interception (due to frequency hopping) 2. All waveforms spread the signal of the LPI radar in frequency. 3. Demand simple architecture for generating large bandwidth B signals. 4. Demand simple architecture for track processing. 5. Ease of implementation when using digital architecture. 6. Range resolution ΔR depends only on the hop rate (which lays on the secrecy of the FH algorithm used). 7. Secrecy of the FH sequence that is used. 8. FH performance depends a little on the code used so a large variety of codes can be used as long as certain properties are met. 9. Hybrid FSK/PSK signals LPI characteristics are further increased (as long as both FSK and PSK properties are satisfied)	1. Generation of spurious frequencies and high levels of phase noise by using complex circuitry that is required for the generation of such waveforms. 2. Output bandwidth limited by the speed of digital devices, when using digital architecture. 3. Have a higher probability of detection compared to the PSK signals because they present a higher PSD to the intercept receiver 4. In a dense environment with LPI emitters, there is high probability of mutual interference. We have to apply special care to orthogonality of FH sequences in order to avoid that.

Table 2.   Phase Modulating Techniques Advantages /Disadvantages

(4) Noise Techniques. Random Noise Radar (RNR) is not a new concept but it was not realizable until recently due to hardware constraints with respect to processing. The development of solid state RF components and VLSI circuits helped the advancement of RNR. The idea

behind RNR is to transmit a random or random-like low power microwave waveform. That waveform can also be modulated by a lower frequency waveform.

The main applications of RNR are covert surveillance and reconnaissance, target detection and tracking, through-the-wall imaging, ground penetration, foliage penetration profiling, Synthetic Aperture Radar (SAR) and Inverse Synthetic Aperture Radar (ISAR). There are various types of noise techniques used; the four best known are Random Noise Radar (RNR), RNR plus FMCW (RNFR), RNFR plus sine (RNFSR) and Random Binary Phase modulation (RBPC)(Pace 2009, 207).

A summary of the advantages and disadvantages of noise techniques is given in Table 3.

CODE TYPES	ADVANTAGES	DISADVANTAGES
Random Noise RADAR (RNR) Random Noise RADAR & FMCW (RNFR) Random Noise RADAR & FMCW & sine (RNFSR) Random Binary Phase Modulation (RBPC)	1. Due to the nature of their waveforms they have good Electronic Protection (EP) properties. 2. They transmit waveforms with very low instantaneous power spectral density, so they are very difficult to detect because they are concealed within ambient thermal noise. 3. They provide significant processing gain. 4. Even if they are detected, due to the randomness of the waveform, it is highly unlikely to be identified. So apart from LPI they have also Low Probability of Identification (LPID). 5. They are relatively inexpensive to build. 6. The use of wideband noise waveforms can result in high resolution and reduced ambiguities in range and Doppler estimation.	1. They are susceptible to deception jamming (repeater techniques). 2. They cannot simultaneously measure range and Doppler. 3. There are a lot of considerations regarding their electromagnetic influence on small signal receiver devices as GPS receivers, cell phones, LANs etc. 4. The two-dimensional sequential search required to detect targets with unknown position, which is a necessary feature for most military applications, is not yet technologically feasible.

Table 3.   Noise Techniques Advantages/Disadvantages

THIS PAGE INTENTIONALLY LEFT BLANK

III. EXAMPLES OF AIRBORNE, MARITIME AND LAND-BASED LPI RADARS

This chapter examines LPI radar applications, giving examples of airborne, maritime and land-based LPI systems. A list of some of today's LPI radar systems is given in Table 4 (Pace 2009, 63). This list does not include only early warning, fire control, or navigation radar but other types of equipment that use LPI waveforms as well (radar altimeters, precision approach landing systems, etc.).

Category	System	Description
AIRBORNE	AN/APN-232	Radar Altimeter
	HG-9550	Radar Altimeter
	GRA-2000	Radar Altimeter
	PA-5429	Radar Altimeter
	CMRA	Cruise Missile Radar Altimeter
	AHV-2XX0	Family of Radar Altimeters
	AD-1990	Radar Altimeter
	AN/APS-147	Maritime Surveillance Radar
	AN/APQ-181	Fire Control Radar
	AN/APG-77	Fire Control Radar
	LANTIRN	Low Altitude Navigation and Targeting Infra-Red for Night
	RBS-15 Mk3	Radar Missile Seeker
MARITIME	Pilot	Surveillance and Navigation Radar
	Scout	Surveillance and Navigation Radar
	Smart-L	Surveillance Radar
	VARIANT	Surface and Air Target, Gun Fire Detection Radar
LAND	AN/SPN-46 (V)	Precision Approach Landing System
	TALS	Tactical Automatic Landing System
	Eagle	Fire Control Radar
	HARD-3D	Fire Control and Surveillance Radar
	POINTER	Air Surveillance Radar
	PAGE	Air Surveillance Radar
	CRM-100	Surface Target Detection Radar
	JY-17A	Battlefield Surveillance Radar

Table 4.   Examples of LPI Radars

A.   AIRBORNE LPI RADARS

1.   AN/APN-232 Combined Altitude Radar Altimeter

The AN/APN-232 is a solid-state, Frequency Modulated (FM), Continuous Wave (CW) radar altimeter manufactured by Navcom Defense Electronics (pictured in Figure 7). It is comprised of a transceiver, signal data converter, antennas and an indicator unit. LPI is achieved via automatic power management that takes into account the aircraft's attitude and altitude and the terrain type being over-flown, as well as via the use of FMCW technology that spreads the radar altimeter's bandwidth over a 100 MHz region and thus provides a spread spectrum capability. It provides both analogue and digital outputs in order to be compatible with different avionics platforms (www.janes.com 2011).
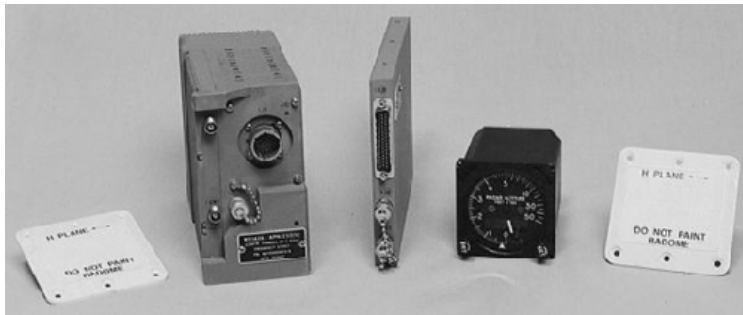
Figure 7.   AN/APN-232

2.   HG-9550 Radar Altimeter

The HG-9550 is manufactured by Honeywell (pictured in Figure 8). It is an LPI radar altimeter with capabilities that include frequency agility, power management and code/pulse repetition frequency jitter. It has the ability to vary the system track rate and Electronic Counter-Counter Measures (ECCM) response as functions of real-time inputs. It is also pre-programmable (track rate, ECCM

response, sensitivity, altitude range and output formats).
Its radio frequency sections are based on gallium arsenide
(GaAs) monolithic microwave integrated circuitry (MMIC)
(www.janes.com 2011).

Figure 8.   HG9550

3.   GRA-2000 Radar Altimeter

The GRA-2000 is manufactured by BAE Systems and it
will replace older types of radar altimeters on the
majority of tactical jets, helicopters and transport
aircraft employed by the US Department of Defense (pictured
in Figure 9). It has a modular design that allows 100%
backward compatibility with legacy radar altimeters and
thus eliminates A-kit costs (cabling, brackets, etc.) and
allows the reuse of the existing antennas.

It has a very simple and durable design (single I/F
down convert, elimination of multiple power amplifier
circuits), and uses a highly effective waveform (low power
output) and advanced signal processing (high processing
gain) that allows it to extend its accuracy, performance
envelope (roll, pitch, and altitude), and jamming
resistance, thereby providing LPI capabilities beyond
legacy systems. The waveform generation and signal

43

processing are all software controlled, allowing for customization (www.janes.com 2010).

Figure 9.   GRA-2000

4.   PA-5429 Radar Altimeter

The PA-5429 is manufactured by the South African company Tellumat. It is a pulsed airborne radar altimeter that provides altitude above ground level (AGL) for heights from 0 to 5,000 ft. It operates in the mid-J-band (~15 GHz) and provides both analogue and discrete interfaces. It incorporates LPI and comprehensive anti-jamming features (www.janes.com 2007).

5.   CMRA – Cruise Missile Radar Altimeter

The CMRA is manufactured by Honeywell and was developed specifically for cruise missile programs, including the Air Launched Cruise Missile (ALCM) and Tomahawk missiles. It is a derivative product in which a variety of features from other Honeywell altimeters are incorporated. The system has the capability to perform terrain correlation and navigation functions (www.janes.com 1994).

6. AHV-2XX0 Family of Radar Altimeters

These altimeters are manufactured by Thales Communications and are designed to meet the latest helicopter/transport aircraft (AHV-2100), fighter aircraft (AHV-2930) and missiles/UAV (AHV-2500) requirements. They use an improved FMCW technique that provides enhanced accuracy, integrity, immunity to multipath, and reduced power consumption. LPI is achieved through power management of the RF output. The combination of a narrow receiver bandwidth with high-performance digital signal processing provides resistance to jamming (www.janes.com 2010, www.thalesgroup.com 2011). A picture of the AHV-2XX0 family of radar altimeters is presented in Figure 10.
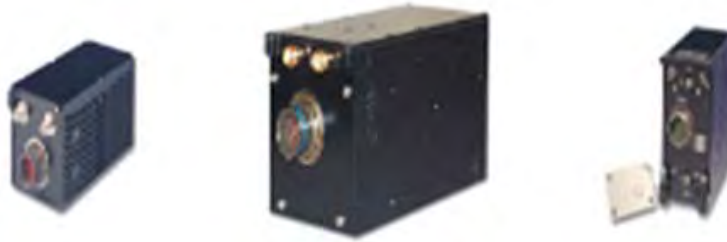
Figure 10.   AHV-2XX0 Family of Radar Altimeters

7. AD-1990 Radar Altimeter

The AD-1990, manufactured by Selex Galileo, is a covert radar altimeter, designed to meet the UK Royal Air Force's (RAF) needs in the 1990s. It was a form fit and function replacement for the original altimeter of the RAF Tornado aircraft. Its digital signal processing techniques allow the simultaneous tracking of height, both above the ground and above obstacles such as trees. Its covert operation (LPI) is achieved by spreading the transmitted signal over a very wide bandwidth through the application

of pseudo-random phase modulation and adaptive power tailoring (power management) which in addition gives a high resistance to jamming. It provides both analogue and digital outputs (www.janes.com 2010).

8. AN/APS-147 Radar

Telephonics Corporation's The AN/APS-147 is a maritime Inverse Synthetic Aperture Radar (ISAR) that equips the U.S. Navy's (USN) MH-60R multi-mission helicopter. It uses high-throughput signal and data processing and is fully programmable. It uses a collection of waveforms and has a very low output power compared to traditional maritime surveillance radars. The latter, combined with frequency agility, provides significant LPI characteristics to this radar. Some of its important features are the flexible modular design, production of high-resolution images, low input power, simple design that provides high reliability and maintainability and a fully programmable signal processor with multiple waveform exciter and high-throughput rates (www.janes.com 2010). The AN/APS-147 radar onboard a MH-60R helicopter is seen in Figure 11.

Figure 11.   AN/APS-147 Radar (Antenna Under Helicopter Cockpit--Red Arrow)

9.   AN/APQ-181 Radar

The AN/APQ-181 is manufactured by Raytheon Space and Airborne Systems. It is a multi-mode radar for the B-2 bomber. It operates in the Ku-band (12.5 to 18 GHz) and was designed for LPI functionality that complements the stealth character of the B-2 bomber. Various individually effective design and operating techniques are used in this radar that, when integrated together, greatly diminishes the effectiveness of enemy intercept receivers. The radar has in total 21 operating modes, amongst them precision position and velocity update measurement, altitude measurement, radar-generated imagery, synthetic aperture radar (SAR) mode and production of topographic map-like high-quality images. All the previous modes contribute to the achievement of a high-accuracy inertial navigation, which permits its autonomous navigation without the aid of GPS or other external navigation aids as well as the precise location and identification of assigned targets. It has two antennas, located on the left and right below the leading edge of the platform's wing/body at 2.4 m outboard of the aircraft center line, that are electronically steered in two dimensions and feature a monopulse feed design to facilitate fractional beamwidth angular resolution (www.janes.com 2010).

10.   AN/APG-77 Radar

The AN/APG-77 is manufactured by Northrop Grumman Electronic Systems and Raytheon Space and Airborne Systems for the F-22 fighter aircraft. It is an X-band (8 to 12.5 GHz) multimode Active Electronically Scanned Array (AESA)

radar. Its low observability AESA antenna has approximately 2,000 transceiver modules that incorporate MMIC technology and also provide a low radar RCS. It is advertised to offer long-range, multi-target, all-weather, stealth vehicle detection, electronic intelligence gathering and multiple missile engagement capabilities. It provides all aspect air-to-air, dogfight and air-to-surface operating modes that are also effective in a heavy clutter environment. Unconfirmed sources suggest that it has an operating range of 193 km. It has a very high bandwidth when operating in intelligence gathering mode (approximately 2 GHz bandwidth when it is functioning in a forward-looking, high-gain, passive listening mode). It offers Ultra High-Resolution (UHR) modes that are claimed to have a 31 cm resolution at ranges in excess of 161 km (www.janes.com 2011).A picture of the AN/APG-77 radar antenna is given in Figure 12.

Figure 12.   AN/APG-77 Radar Antenna

11.   LANTIRN (Low-Altitude Navigation and Targeting Infra-Red for Night)

The LANTIRN system is manufactured by Lockheed Martin Missiles & Fire Control. It is used by F-16 and F-15E fighter aircraft. It is a ground attack integrated system

that has two pods: the AN/AAQ-13 navigation pod and the AN/AAQ-14 targeting pod. The AN/AAQ-13 navigation pod contains a wide FoV (Field of View) FLIR (Forward Looking Infra-Red), and the AN/APN-237 Ku-band (12.5 to 18 GHz) terrain-following radar from Raytheon. The FLIR uses a single MCT (mercury cadmium telluride) array and the picture is displayed to the pilot on a wide FoV holographic HUD. This provides the pilot with night vision for safe flight at low level. The terrain-following radar enables the pilot to operate at very low altitudes. It uses advanced signal processing to provide wide azimuth coverage, which in turn allows more violent maneuvering of the aircraft. This is because the system can provide directional inputs to the pilot or the flight control computer, whereas older systems only provided pitch-up commands. The terrain following radar can be linked directly to the aircraft's autopilot to automatically maintain a preset altitude down to 100 feet while flying over virtually any kind of terrain. It has five modes: Normal, Weather, ECCM, LPI, and Very Low Clearance (VLC). Pictures of the LANTIRN pod aboard and F-16 fighter aircraft and the AN/AAQ-13 navigation pod, respectively, are given in Figures 13 and 14.

Figure 13.   LANTIRN Pods on F-16--Red Arrows
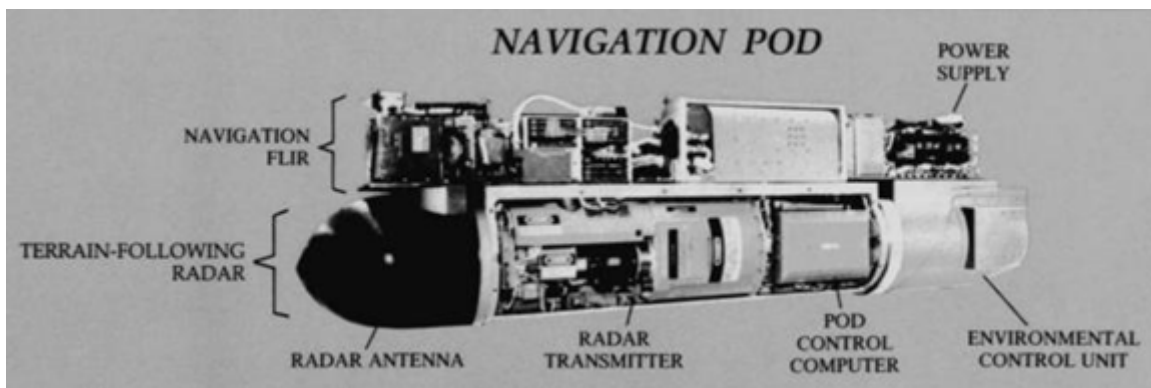
Figure 14.   AN/AAQ-13 Navigation Pod

12.   RBS-15 Mk3 Missile Seeker

The RBS-15 is manufactured by Saab Dynamics AB. It is a medium range radar guided anti-ship/land-attack missile. The RBS-15 Mk2's radar seeker uses FMCW technology and has a very low power output (in the mWatt range) (Pace 2009, 59). The broadband, frequency-agile radar with its digital processing is claimed to provide a high ECCM performance. The RBS-15 Mk3 missiles have an improved monopulse high Ku-band (35 GHz) radar seeker (www.janes.com 2010). Further developments (already tested) of the seeker are the introduction of an LPI radar using FMCW wave spread-

spectrum technology, improvements of the angular resolution and target discrimination of the seeker through synthetic aperture radar (SAR) techniques, as well as studies to integrate the seeker with an imaging infra-red (IIR) sensor (www.janes.com 2011).

B.   MARITIME LPI RADARS

1.   Pilot Radar

The Pilot is manufactured by Saab Bofors Dynamics. It is an X-band (8 to 12.5 GHz) LPI navigation and threat detection radar. It uses the FMCW transmission technique and it is suitable for coast guard vessels, fast attack craft, fast patrol boats, frigates, submarines and coastal/land surveillance applications. It can function both in stand-alone and add-on configurations. In the add-on configuration the Pilot radar uses the X-band antenna of the platform's existing radar, which can be any available pulsed navigation radar system. The aforementioned capability uses a wave-guide switch that allows either the Pilot or the conventional radar's transceiver to use the antenna as required. Other important features of the Pilot radar are the low average power output, the 2.4 m range cell resolution, the resistance to electronic support system detection and/or anti-radiation missile attack, and the use of a "fully" solid-state transceiver(www.janes.com 2010).A picture of the Pilot radar onboard a Visby-class corvette is given in Figure 15.

Figure 15.   Pilot Radar on Visby-class Corvette (Radar
Antenna--Red Arrow)

2.   Scout Radar

The Scout is manufactured by Thales Netherlands. It is
an I-band (8 to 10 GHz) LPI surface surveillance and
tactical navigation radar, and is an improved version of
the Pilot radar. This improvement has to do mainly with the
FMCW transmission technique used by the Scout radar. It
incorporates a dual array antenna that features optimal
isolation between transmit and receive elements in order to
maximize range performance. It can function both in stand-
alone and add-on configurations. In the add-on
configuration, an I-band pulse radar uses the Scout dual
array antenna (with the addition of a waveguide and
waveguide switch) for both pulsed and FMCW functionality.
Other important features of the Scout radar are the low
average power output (10mW to 1 W selectable by the user),

the extremely high range resolution and the use of a "fully" solid-state transceiver (www.janes.com 2011).A picture of the Scout radar is given in Figure 16.

Figure 16.   Scout Radar

3.   Smart-L Radar

The Smart-L is manufactured by Thales Netherlands. It is an L-band (1 to 2 GHz) air/surface surveillance and target designation radar. It is a multi-beam radar that provides medium range detection of small "stealth" air targets, long-range detection of conventional aircraft, surface surveillance and maritime patrol aircraft guidance support. Some of the important features of the Smart-L radar are the use of parallel receiver channels, the digital beam forming, the broadband frequency operation and frequency agility, the low antenna sidelobe values and the use of a "fully" solid-state transmitter (www.janes.com 2011).A picture of the Smart-L radar is given in Figure 17.

Figure 17.   Smart-L Radar

4.   VARIANT Radar

VARIANT is manufactured by Thales Netherlands. It is a dual-band, 2-D, surveillance and target indication radar. It operates in G-band (4 to 6 GHz) and I-band (8 to 10 GHz). Some of its important features are full coherency, pulse Doppler clutter suppression and the use of the FMCW technique that provides its LPI characteristics (www.janes.com 2011). A picture of the VARIANT radar is given in Figure 18.

Figure 18.   VARIANT Radar

5. AN/SPN-46 (V) Precision Approach Landing System

The AN/SPN-46(V) is manufactured by Textron Defense Systems. It is a precision approach landing system that provides simultaneous and automatic control for up to two aircraft during final approach and landing aboard aircraft carriers and other landing platforms. The heart of the system is a precision dual-band automatic acquisition/tracking radar that features cross-band beacon and aircraft skin tracking. It operates in X-band (8 to 12.5 GHz) and K-band (20 to 40 GHz) (www.janes.com 2010). A picture of the AN/SPN-46 radar is given in Figure 19.

Figure 19.   AN/SPN-46 (V)[3]

C.   LAND-BASED LPI RADARS

1.   TALS--Tactical Automatic Landing System

The TALS is manufactured by Sierra Nevada Corporation. It is an Automatic Unmanned Aerial Vehicle (UAV) recovery/tactical automatic landing system that provides a day/night, all weather, automatic landing and take-off capability for UAVs operating in tactical or fixed-base land environments. It operates in K-band (35 GHz ±150 MHz)

---

[3]www.navair.navy.mil 2011

and it has a wide bandwidth (up to 20 MHz), which gives the radar its LPI characteristics (www.janes.com 2011). A picture of the TALS is given in Figure 20.

Figure 20.   TALS

2.   Eagle Fire Control Radar

The Eagle is manufactured by Saab Group. It is a "silent" millimetric system that is used in mobile ground and naval-based air defense applications. It operates within the K-band (35 GHz center frequency) and is optimized for low altitude target tracking. Its LPI characteristics come from the fact that it uses pulse compression, a high gain antenna with low sidelobe values, and a low output peak power figure. The manufacturer claims that its antenna radiation pattern, in combination with its transmission technique, makes it impossible for escort/standoff jammers to degrade its performance. It also incorporates an operating mode that allows simultaneous pulse-to-pulse frequency agility and Moving Target

Indication (MTI) (www.janes.com 2010). The Eagle fire control radar is seen in Figure 21.

Figure 21.   Eagle Fire Control Radar

3.   HARD-3D Radar

The HARD-3D is manufactured by Saab Group. It is an all-solid-state 3D-search-and-acquisition radar designed for use in short-range air defense systems such as the Atlas Short Range Air Defense (ASRAD). The electronically scanned beam in elevation achieves the 3D capability of the radar. Its LPI characteristics are due to its very low electromagnetic signature, (low output peak power 240 W, low average power 30 W), its broadband frequency agility, the low sidelobes and the narrow antenna beam (www.janes.com 2011). The HARD-3D radar is seen in Figure 22.

Figure 22.   HARD-3D Radar

4.   POINTER Radar

The POINTER is manufactured by Ericsson Microwave Systems. It is an LPI all-solid-state 3D radar that operates in X-band and has been designed to integrate into short-range air defense missile systems such as the Mistral, Stinger and Starburst. The technology implemented on the Pointer radar came from the developer's experience with Eagle and HARD-3D radars. The Pointer radar is a further development of the HARD-3D radar (www.janes.com 2005). The Pointer radar is seen in Figure 23.

Figure 23.   Pointer Radar

5. PAGE Radar

The Portable Air defense Guard Equipment (PAGE) is manufactured by Thales Netherlands. It is a man-portable/vehicle-mounted J-band (10-20 GHz) low-level air surveillance radar designed for use in very short-range air defense applications involving both anti-aircraft guns and man-portable air defense equipment. It uses the FMCW technique, which in combination with its very low power output (20 W) can make the system "nearly undetectable" by electronic support and radar warning receivers (www.janes.com 2011). The PAGE radar is seen in Figure 24.

Figure 24.   PAGE Radar

6. CRM-100 Radar

The CRM-100 is manufactured by Przemyslowy Instytut Telecomunikacji (PIT), Poland. It is a "quiet," LPI, solid-state, FMCW radar designed to detect and track up to 40 sea surface targets and automatically handoff data to a command system. Some of its applications are monitoring of "sea borders" for "fraud" traffic and illegal immigrants, monitoring of economic interest zones, and search and rescue. It operates in X-band (8-12.5 GHz) and its transmit

power is very low (1mW – 1W). Its LPI characteristics are due to the FMCW technique and the power management (www.janes.com 2011). The CRM-100 radar is seen in Figure 25.

Figure 25.   CRM-100

7.   **JY-17A Radar**

The JY-17A is manufactured by ECRIEE, China. It is a battlefield surveillance radar that operates in X-band (8-12.5 GHz). It is a fully coherent, solid-state sensor suitable for ground or vehicle based applications. It is designed to detect, localize and identify moving targets on the battlefield (including low-flying air vehicles) in "severe" electronic countermeasures and clutter

environments. Specific role applications include battlefield surveillance, artillery fire adjustment, border surveillance and high-value asset protection. Its main features are the modular design, the LPI functionality, its solid-state transmitter, digital pulse compression, pulse-Doppler filter bank processing and automatic target detection and tracking (www.janes.com 2004).

THIS PAGE INTENTIONALLY LEFT BLANK

IV. DETECTION OF LPI RADARS

As discussed in Chapter II, one of the main characteristics of the LPI technology is its wideband nature. The concept behind utilizing wideband techniques is to spread the radiated power over a large bandwidth, in order to produce a Power Spectral Density (PSD) below the noise level of the receiver. By reducing the input power at the receiver, signal detection relies on extending the integration time period, during which a special integration procedure must be applied to exclude noise being added in the same amount (Burgos-Garcia, et al. 2000).

Another point of concern for the receiver is the element of sensitivity, as the detection of the wideband LPI signal has to take place against a background saturated with short duration, conventional radar signals in the same band (Denk 2006). Without neglecting the centrality of the sensitivity factor, the performance trends in radar warning receivers are primarily improvements to obtain higher dynamic range and higher frequency resolution, not in the direction of improved sensitivity (Lynch Jr. 2004).

Signal processing comprises another critical area of consideration for the receiver. LPI radars can integrate their reflected signals coherently over the whole of the integration time, thus narrowing the receiver noise bandwidth and increasing sensitivity. On the other hand, ES receivers cannot coherently detect the radar's signals and hence they cannot narrow their bandwidths in the same manner (Fuller 1990). In most cases today, the signal processor in an intercept receiver is considerably less

powerful than its counterpart in radars or data links. Based on netted situational awareness, modern processors will also be dynamically programmed to threat frequency bands (see Chapter V).

The increased sophistication of modern radar systems results in an electro-magnetic environment where the receiver should expect very few pulses. Staggered PRF and frequency agility techniques, which can be implemented by track-while-scan or LPI radar, further complicate the issue of identification. This is especially true for LPI CW radars and digital pulsed radars that utilize an enormous number of complex modulations; as these modulations can result in many reports for a single diverse emitter, they render accurate identification more difficult (Pace 2009).

The situation is exacerbated in the presence of ultra-wideband sources such as spread spectrum communication signals, impulse radars and impulse jammers. Sources such as ultra wideband SAR and ISAR imaging radar, whether intercepted intentionally or not, can significantly raise the noise floor of the receiver, disabling the ability of the EW receiver to detect the important threats of interest (Pace 2009). In addition, the EW receiver must have high power detection and protection circuits at the front end to protect itself from deliberate destruction by directed energy weapons.

Reaction time is another crucial challenge for LPI detectors, especially in the face of modern range Doppler imaging missiles: employing sophisticated FMCW modes to improve target aiming accuracy and reject eventual decoys,

power managed seekers adjust the transmitter power in such a manner that the received power at the EW receiver is kept constant.

All aforementioned concerns have been quantified into seven generic factors that need to be taken into account for the LPI radar signals to be detected by Electronic Warfare Support (ES) receivers (Lynch Jr. 2004):

1. LPI system mainlobe power at the intercept receiver

2. LPI system sidelobe power level at the intercept receiver

3. Area of mainlobe and sidelobes on the ground or at a certain threat altitude

4. Time of Area of Regard (AOR) illumination for mapping, tracking, or targeting

5. Intercept receiver density and search time

6. Intercept receiver detection response

7. Power management strategy

The vital task of detection is followed by classification, a process that requires sorting the signal into groups having similar parameters that distinguish one LPI radar signal from another:

- LPI radar type

- Carrier frequency

- Modulation bandwidth

- Modulation period

- Code period

• Time and angle of arrival.

Subsequent correlation with an electronic emission library (database) can then aid in signal tracking and response management (identification). This process, commonly known as Specific Emitter Identification (SEI), attempts to fingerprint the emitters that are intercepted. Several algorithms have been investigated for doing SEI but their details remain classified (Pace 2009, 402). The research conducted for this thesis indicates that Fourier analysis remains the fundamental tool. Commencing from this basic tool, more complex signal processing techniques have evolved, such as the Short Time Fourier Transform (STFT), which aims at tracking signal parameters over time. More sophisticated techniques have also been developed, called time-frequency and bi-frequency distributions, to identify the different modulation schemes used by the LPI radar (e.g., Wigner Ville Distribution (WVD) and Quadrature Mirror Filter Bank (QMFB) [Pace 2009, 405-510]).

A.   ES RECEIVER CHALLENGES

To detect LPI radar signals, ES receivers have to overcome two major difficulties:

- Processing gain of the LPI radar

- High sensitivity requirement

1.   Radar Processing Gain

In the second chapter of this thesis, range factor α was defined as $\alpha = R_I$. Assuming R_I to be the detection range of the interceptor and R_r the detection range of the radar, range factor can be defined as:

$$\alpha = \frac{R_I}{R_R} \quad (4.1)$$

If $\alpha > 1$, the radar will be detected by the intercept receiver platform. If $\alpha \leq 1$, the radar can detect the platform while the intercept receiver platform cannot detect the radar.

When the same radar antenna is used to both transmit and receive ($G_{Tx} \approx G_{Rx}$) and an omnidirectional intercept antenna ($G = 1$) is used for the interceptor, then a certain energy or average power transmitted range factor α can be expressed directly in terms of the radar waveform, antenna pattern and radar cross section as:

$$\alpha = \frac{R_I}{R_R} = K\sqrt{\frac{G_{Ti}}{RG_{T\gamma}} \cdot \frac{1}{\tau B_i} \cdot \sqrt[4]{\frac{1}{\sigma}}} \quad (4.2)$$

where K is the constant parameter of the equation, G_{Ti} is the antenna gain in the direction of the interceptor, B_i is the equivalent noise bandwidth of the intercept receiver, τ is the integration time of the LPI radar, and σ is the radar cross section of the target. This equation indicates that the value of α is directly proportional to the square root of the radar antenna gain in the direction of the interceptor, to the fourth root of the radar cross section and inversely proportional to the time-bandwidth factor (τB_i), which also comprises the processing gain of the radar receiver over the intercept receiver (Lee 1991, 55).

2. High Sensitivity Requirement

Some ES receivers do not have sufficient sensitivity for the detection of LPI radar signals. Jim P. Lee states that for an over-the-horizon operation (OTHT), system sensitivity should be no less than -100dBmi. Accounting for the pre- and post-detection bandwidth of the receiver, Lee provides a formula different than the one provided in Chapter II (Equation [2.6]) for the calculation of sensitivity:

$$\delta_1 = n_I SNR_i G_i B_1^\gamma \left(2B_2\right)^{1-\gamma} \quad (4.3)$$

Where:

n_i: Receiver noise power density

SNR_i: The threshold signal-to-noise ratio

G_i: Intercept receiver antenna gain

B_1: Pre-detection bandwidth

B_2: Post-detection bandwidth, and

γ: A parameter ranging between $0<\gamma<0.5$.(Lee 1991, 55)

In Equation (4.3), the pre-detection bandwidth B_1 defines the instantaneous bandwidth of the intercept receiver over which it can detect signals. The post-detection bandwidth B_2 defines the maximum modulation rate that the intercept receiver can measure. The parameter γ determines the effective bandwidth of the receiver and

varies from a value of 0.5 when $B_1 < B_2$, (characteristic of a wide-open, high probability of intercept receiver), to a value of 0 when the two bandwidths are comparable (characteristic of a high sensitivity search receiver).

A careful examination of Equation (4.3) reveals that the ES receiver has three basic means for increasing its sensitivity: increasing the antenna gain, reducing the pre-detection bandwidth, and reducing the post-detection bandwidth. In order to improve sensitivity further, both the noise figure and transmission loss of the ES receiver should be minimized.

The first two means involve a probability of intercept (POI) loss by reducing either the angular or frequency instantaneous coverage. The third merely represents a reduction in the measurement bandwidth of the intercept receiver. Therefore, for operation against high duty cycle LPI waveforms, there is scope within conventional ES receivers for increasing sensitivity at negligible cost by reducing the post-detection bandwidth without compromising the POI (Ruffe and Stott 1992, 200-202).

B.   TYPES OF ES RECEIVERS FOR LPI RADAR DETECTION

There are six general kinds of intercept receiver implementation (see Table 5). The first and simplest class is wideband channelized Crystal Video Receivers (CVRs) with RF preamplifiers. The second class, which is widely used, is Instantaneous Frequency Measuring (IFM), usually employing preamplifiers and wideband channelization. The third class is digitally controlled scanning superheterodyne/homodyne receivers, which are characterized

by narrowband filters that are swept over the frequency range of interest. Fourth are completely channelized high-dynamic-range intercept receivers that are characterized by wide frequency coverage but broken into reasonably small filter bins, implemented with multiple discrete filters to provide very high dynamic range. Fifth are transform receivers (microscan, Bragg cell, or compressive), which in essence form a filter bank from a frequency-dispersive or optical device. Sixth and last are hybrids of the above types, which allow cueing of high-resolution, high-dynamic-range analysis receivers.

Parameter/Type	CVR	IFM	Superhet.	Channelized	Transform	Cueing
Instantaneous Bandwidth	Excellent	Poor	Poor	Good	Good	Excellent
Simultaneous signals	Poor	Excellent	Poor	Good	Good	
Frequency Resolution	Poor	Good	Excellent	Good	Good	Excellent
Dynamic Range	Good	Fair	Excellent	Very Good	Fair	Excellent
Usable Sensitivity	Poor	Fair	Excellent	Good	Fair	Excellent

Table 5.   Intercept Receiver Typical Performance[4]

The performance trends in radar warning receivers are primarily improvements to obtain higher dynamic range and higher frequency resolution, not in the direction of improved sensitivity.[5] Research indicates that the usable sensitivity is always limited by the environment and not by Boltzmann's constant (Lynch Jr. 2004). The second area where improvements will occur is signal processing. In most cases today, the signal processor in an intercept receiver

---

[4]Lynch Jr., 117.

[5]For an argument in favor of improved sensitivity, see: Aytug Denk, *Detection and Jamming Low Probability of Intercept (LPI) Radars*, Master's Thesis, Electronic Warfare, Naval Postgraduate School (NPS) (Monterey: NPS, 2006).

is considerably less powerful than its counterpart in radars or data links. Processors also will be dynamically programmed to treat frequency bands based on netted situational awareness. The rate of the developments in signal processing is so great relative to the rest of the technology that dramatic improvements in signal processing can be expected over the coming decades. What this will require of stealth systems is spreading the emissions over wider and wider operating bands and creating more complex operating and spoofing waveforms.

1.   Crystal Video Receiver

CVRs are the most common types of intercept receivers, one of their most common commercial uses being radar automobile speed trap detectors. In fact, the simplest ELINT system is the crystal video type consisting of an antenna, a detector, and a video amplifier (Wiley, ELINT: The Interception and Analysis of Radar Signals 2006, 57–63). A typical CVR block diagram is provided in Figure 26.
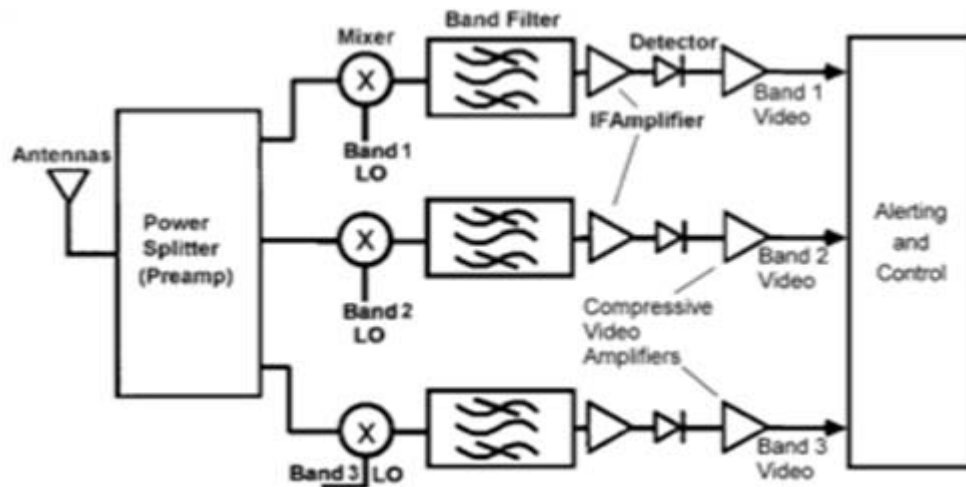
Figure 26.   CVR Block Diagram

It consists of one or several omni-directional antennas, which are frequency multiplexed into a small number of RF amplifier channels. (CVRs have broad channelization, e.g., X, Ku, IR, and UV). Subsequent to this channelization, which typically might be 1 GHz in bandwidth, the output is detected and compressed in a log compressive video amplifier. The amplitude-compressed outputs in each of the bands are then processed with respect to pulse train shape, angle of arrival, and general frequency of operation.

In their simplest form, CVRs have too much sensitivity and create many false alarms unless thresholds are set very high (−35 to 40 dBm). Extra sensitivity can be provided with the use of an additional low-noise RF preamplifier: from a level of −35 to −55 dBm without a preamp, an RF preamplifier may increase its sensitivity down to −85 dBm.

The tangential sensitivity of a CVR is:

$$TSS = kTF\left(6.31B_v + 2.5\sqrt{2B_{RF}B_v - B_v^2} + \frac{AB_v}{\left(GF\right)^2} \right) \quad (4.4)$$

Where:

k : Boltzmann's constant ($1.38 \cdot 10^{-23}$ W/K)

T : Room temperature ($290K$)

F : Noise figure of amplifiers ahead of detector

B_v : Video bandwidth (Hz)

B_{RF} : RF bandwidth (Hz)

A: Diode parameter

G: Gain of the amplifiers ahead of the detector

The diode parameter is given by the formula:

$$A = \frac{4F^{\nu}R}{kTC^2} \quad (4.5)$$

Where

R: Dynamic impedance of the detector (Ω)

C: Detector sensitivity (V/W)

CVRs are very mismatched in the optimal detection sense, but they were designed for high peak power and short ranges, for which they are quite adequate. The crystal video receiver is characterized by broad instantaneous bandwidth and low sensitivity. Front-end bandwidths are typically 200 MHz up to 4 GHz.

The advantages of such a system are that the design is simple by military standards, relatively inexpensive, not spoofed by complex waveforms, and in a low-density signal environment, every bit as good as the more elaborate receivers. The principal disadvantage is lack of selectivity, which is a severe problem in dense signal environments. Its sorting capability is limited, because frequency resolution and angle of arrival accuracy is usually poor. In addition, sensitivity is usually limited by RF preamplifier bandwidth. The sensitivity limitation, however, is usually not significant, because the poor

selectivity prevents the handling of very many signals so that noise limited thresholds can never be approached.

2. Instantaneous Frequency Management Receivers (IFM)

A leading member of the channelized receiver family, IFMs were developed in response to the need to measure the frequency on each pulse. IFMs are essentially a CVR with the addition of a frequency sensing method, usually dividing the signal into two paths with a short delay inserted in one of them. The IFM receiver principal can be understood from Figure 27. The frequency measuring reference in this scheme is a delay line, which results in the channelizing of the frequency spectrum to an accuracy that is on the order of the reciprocal of the delay line time length.
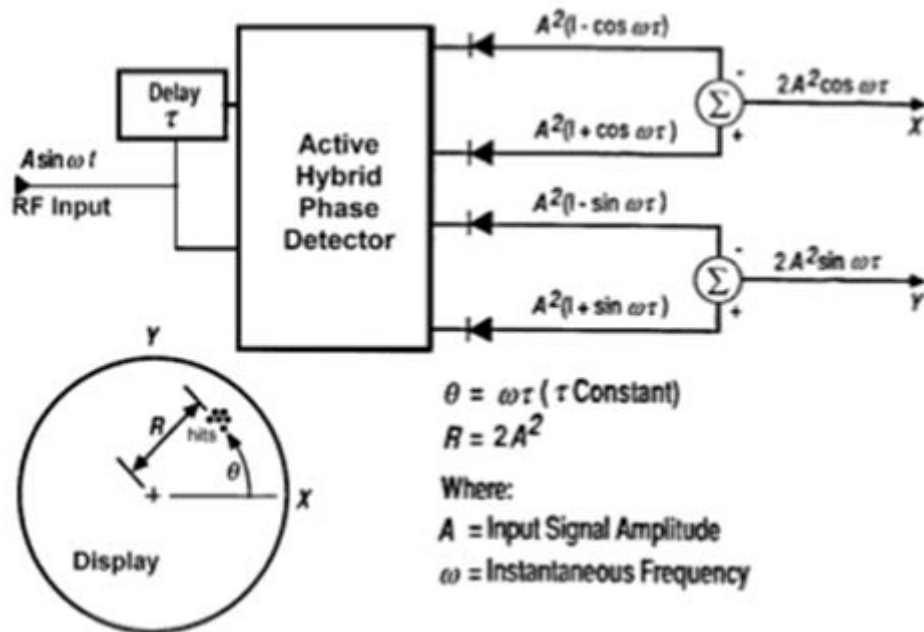
Figure 27.   IFM Principle

74

Indeed, by comparing the phase of the signals, the phase shift ends proportional to the carrier frequency:

$$\theta = 2\pi f \tau \quad (4.6)$$

Where:

θ : Phase shift (radians)

f : Carrier frequency (Hz)

τ : Differential delay (sec)

As the frequency is proportional to the phase difference, for a given delay, the unambiguous band covered is that for which the phase-change is $1/\tau$ (Wiley, ELINT: The Interception and Analysis of Radar Signals 2006, 74).

Intensity is usually thresholded to control noise. The signal above that threshold is usually log compressed by a pre-emphasis circuit so that there is a correspondence with a range reticle on the display. Modern digital IFMs have multiple delay lines with binary ratios and thresholded outputs that are encoded into a frequency tag word as shown in Figure 28.

IFM 1
$r = \theta 1$

IFM 2
$z = 0.2$

IFM as in
Fig 3.4

Low Pass
Filter /
Integrator

Digital
Encoder

Antenna

Power
Splitter
(PreAmp)

IFM n
$z = 0.1 * 2^n$

Threshold

Intercept /
Frequency
Tag Word
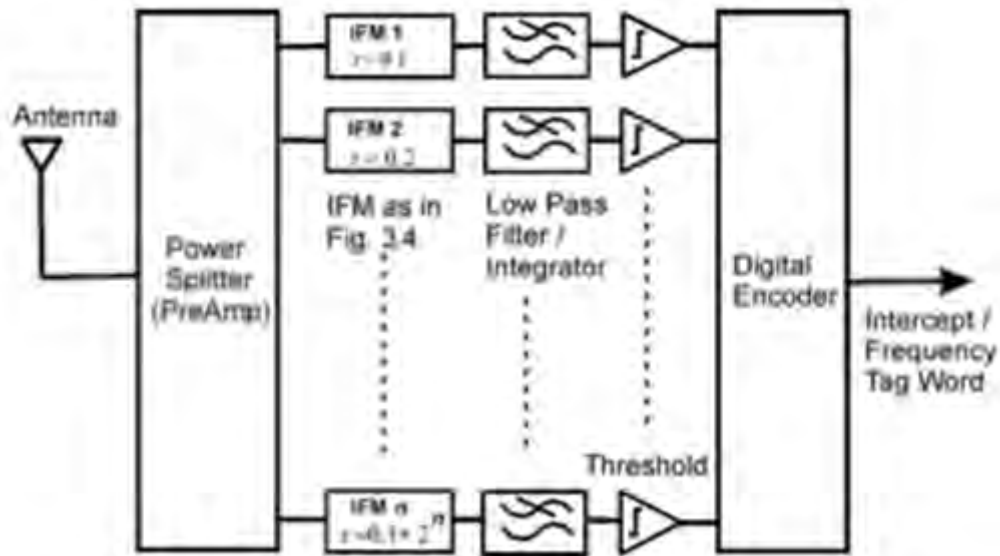
Figure 28.   Digital Multioctave IFM Block Diagram

The major advantages of an IFM are its good frequency accuracy and moderate to good sorting capability in an interference-free or low-signal-density environment. In addition, IFMs are not confused by wide-bandwidth modulations such as chirp and frequency hopping. With a low-noise preamp, sensitivities can reach a level of −85 dBm. In general, however, performance is not degraded by noise, but by signal density and processing capacity.

The major disadvantage of the IFM receiver is its complexity, which unavoidably renders it more expensive than CVRs. The absence of a high dynamic range frequency preselection ahead of the IFM renders it vulnerable to overlapping or pulse-on-pulse signal environments. Usually, in the presence of overlapping pulses, dynamic ranges are never greater than 25 dB, and the more overlapping pulses, the greater the number of false targets (Lynch Jr. 2004, 123).

The IFM is generally a good compromise between channelized and crystal video intercept receivers for many applications.

3.   Superheterodyne Receiver

This type of receiver is the most widely used design in nearly all applications. It uses a local oscillator to convert the incoming signal to a fixed intermediate frequency (IF). After this mixing process (heterodyning), the IF amplifier need operate at only one frequency and its characteristics can be precisely controlled (bandwidth, center frequency, gain, band edge roll-off, group delay). One of the most common channelization schemes used today is the digitally controlled scanning superheterodyne design (Figure 29).
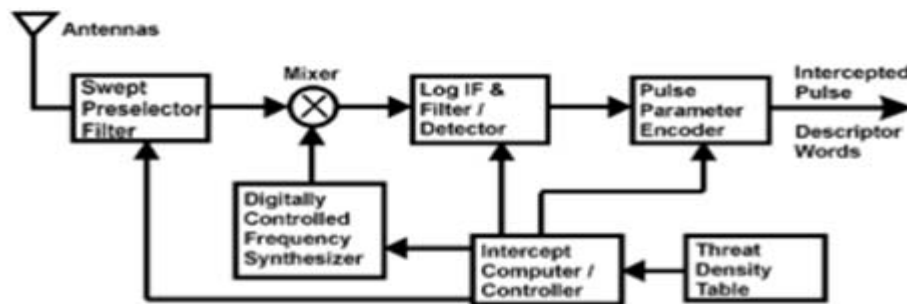
Figure 29.   Digitally Controlled Superheterodyne Receiver Block Diagram

The scanning superheterodyne receiver in Figure 31 consists of a swept preselection filter: e.g., swept YIG resonator, a swept local oscillator, a narrowband intermediate frequency filter detector, a logarithmic amplitude compressor, and a signal encoder. All subunits are digitally controlled by computer as to frequency, sweep rate, and threshold by a threat table. The effects of

harmonic distortion are reduced with the use of a pre-selection filter, the bandwidth of which is determined by the local oscillator harmonic spacing; the higher the local oscillator frequency, the wider the preselector bandwidth can be. The controlled frequency synthesizer successively locates the narrowband IF filter-detector across the band of interest by means of the mixer output signal (usually the first difference term). The bandwidth of the IF filter is selected to be approximately matched to the narrowest pulse to be detected. Subsequent to filtering, the pulses are detected and amplitude compressed. Amplitude compression is required to compress the typical 10^{12}dynamic range down to even 100:1 (Wiley, ELINT: The Interception and Analysis of Radar Signals 2006, 125). The encoder output usually includes the pulse amplitude, pulse width, time of arrival, frequency, and special parameters, i.e., CW or FM waveforms.

The scanning superhet has a single or small number of narrowband filters whose frequency locations are swept according to some pre-programmed strategy. The tradeoff for their improved noise performance—due to their narrowband nature—is a large mismatch with respect to the intercepted signal. Usually, the sweep rate is low in dense threat bands and high in bands in which there are few threats.

The dynamic range for superhets is extremely high and is often limited by the threat table to a value related to lethal range. For example, the threshold for the AN/ALR-56M Radar Warning Receiver (RWR) is programmed by frequency band based on the threat effective engagement range that reduces pulse traffic in the receiver.

Figure 30.   AN/ALR-56M Radar Warning Receiver (RWR)

4.   Channelized Receivers

In this type of receiver, multiple simultaneous frequency bands, roughly matched to the target emitter spectrum, are completely processed and detected. As each channel is an autonomous radio receiver tuned to a particular filter characteristic, the assembly of several channels produces a fully parallel receiver with inherently high data rate capabilities (Fuller 1990, 1-10). The goal is to achieve a large probability of intercept simultaneously with a high degree of sensitivity.

A typical channelized system block diagram is depicted in Figure 31.
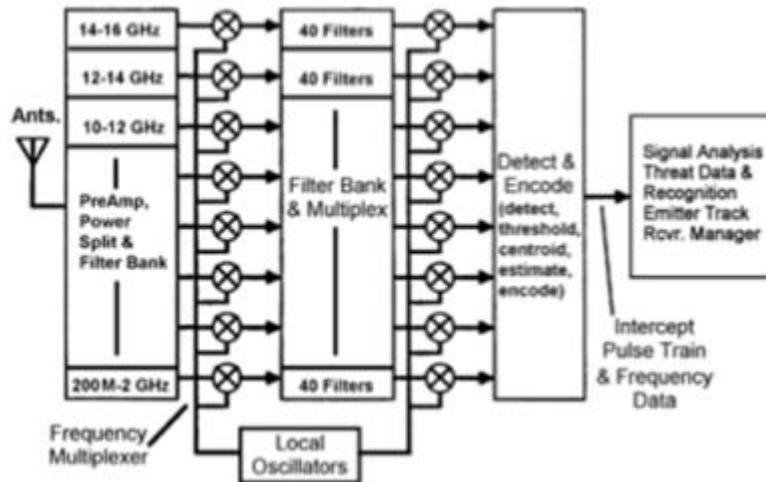
Figure 31.   Channelized Intercept Receiver Block Diagram

It consists of an antenna or set of antennas, multiplexers, and filters. RF channels are frequency multiplexed to an intermediate frequency where multiple local oscillators place 50 to 200 MHz segments of the received band into narrow filters. The outputs of these individual filters are down-converted again, folded in frequency by re-sampling to save hardware, detected, and video filtered. Those sampled outputs are encoded in amplitude, phase, pulse width, and so on (Lynch Jr. 2004, 126).

A channelized receiver's major advantage is that sensitivity is usually limited only by thermal noise, because sorting problems are minimized. In addition, channelized receivers have excellent frequency resolution, which not only provides good sorting capability but also minimizes interference in a dense signal environment. Finally, the reduced processing load allows dramatically improved usable sensitivity and much better emitter classification (Lynch Jr. 2004, 128).

The disadvantages of such systems occur primarily in issues of complexity and cost. Other limitations have to do with the spectral purity of the multiplicity of local oscillators and signal ambiguity in a dense emitter environment caused by folding. The narrow bandwidth may also result in some desensitization or false targets when chirp, frequency-hopping, or phase-coded signals are utilized by the target emitters.

5.   Transform Intercept Receivers

This type of receiver approximates a Fourier transform. Among the most common ways of implementing them, are compressive devices such as Brag cells and microscans, designed to operate at scan times on the order of the pulse lengths from the target emitter class. The microscan compressive receiver—practically a channelized receiver—suffers the same inherent disadvantages as an IFM receiver: limitation in instantaneous dynamic range. As David Lynch notes, instantaneous dynamic range limitations can be a source of serious implications in dense emitter environment. Another inherent shortfall, inevitable due to the non-linearities that exist in all receivers, has to do with harmonic distortion caused by simultaneously received multiple signals. This distortion ends in signal misclassification in frequency, direction, amplitude, number of pulses present, and so on. An additional side effect of nonlinearities is small signal suppression; consequently, in an environment in which LPI systems co-exist with conventional systems, the conventional emitter may completely mask the LPI systems (Lynch Jr. 2004, 128).

6.   Cueing Systems/Hybrid Systems

Cueing or hybrid systems are a combination of two or more of the previous receiver types. Alerting, angle and frequency estimates from the first receiver (coarse receiver) are used to cue a second receiver with higher resolution and dynamic range for tracking, sorting, and classification. Adequate signal storage is provided by wideband delay lines so that the coarse receiver can command the high-resolution receiver to the correct frequency band and angular quadrant for high-resolution measurement. A typical block diagram is shown in Figure 32.
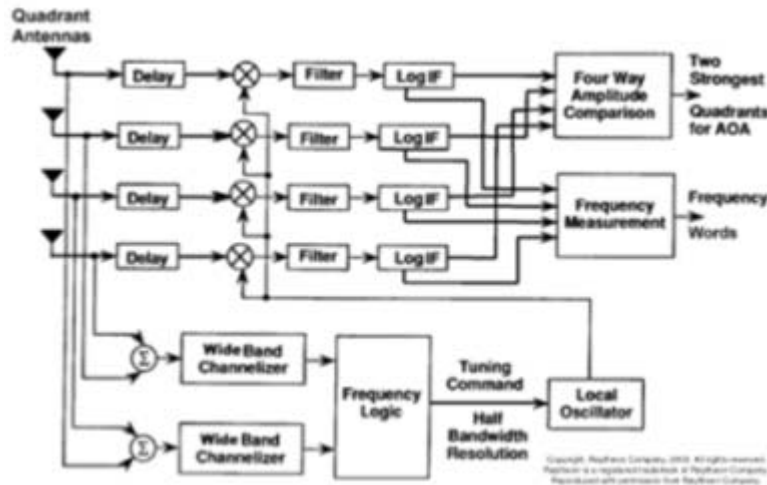
Figure 32.   Hybrid Receiver Block Diagram

Hybrid receivers are capable of wide coverage while still providing high enough resolution to simplify processing, which allows higher sensitivity.

One major advantage of this configuration is its higher resolution analysis band, which can separate overlapping pulse trains and similar signals with greater ease. This happens because the probability of many signals

over a narrower angle and frequency space is greatly reduced, allowing thus higher sensitivity to be used, as a consequence of reduced probability of processor overload.

The disadvantages of the hybrid class of receiver are complexity, cost, and sensitivity to overload if all the signals come from the same quadrant and frequency bands (which they often do in wartime).

Parameter /Type	CVR	IFM	Superhet.	Channelized	Transform	Cueing
Frequency Coverage	4-32GHz	1-18GHz	0.5-18GHz	0.2-18GHz	1-10GHz	0.2-35GHz
Bands	3	5	6	8	4	18
RF Bandwidth	Octave	Octave	500MHz	2GHz	1GHz	2GHz
Video Bandwidth	20MHz	20MHz	10MHz	10MHz	2GHz	10MHz
Sensitivity	-35 to -55dBbm	-65 to -85dBbm	-85dBm	-85dBm	-75dBm	-85dBm
Instantaneous dynamic range at frequency separation	45dB@ 85MHz	65dB@ 275MHz	70dB @1GHz	0dB @10MHz 50dB @30MHz 70dB @200MHz	0dB @3MHz 30dB @30MHz 50dB @300MHz	0dB @10MHz 50dB @30MHz 70dB @200MHz
Pulse traffic capacity	<100k pps	<100k pps	<1Mpps	1Mpps, processor limited	150Mpps, processor limited	>1Mpps, processor limited
Frequency Resolution	Octave	Octave	10MHz	10MHz	3MHz	10MHz
Frequency accuracy	-	0.001 of band center	0.001 of band center	3MHz	3MHz	3MHz
Adjacentpulse recovery time	300nsec	50nsec	10µsec	200nsec	200nsec	200nsec
Coverage scan rate	1sec	1sec	1sec	1sec	0.3µsec	1sec
Advantages	Simple, broad instant bandwidth, inexpensive, easy to use if sensitivity low	Good frequency resolution, god sorting capacity in low-density signal environment, handles wideband modulation	Very good sorting capability, high usable sensitivity, good in dense signal environments, very good frequency resolution	Sensitivity limited only by ambient and thermal noise, good frequency resolution, excellent sorting capacity in dense signal environment	Good frequency resolution, wide instantaneous bandwidth, good sensitivity	Best dynamic range on a small emitter subset, good in dense signal environment, good for broadband emitters
Disadvantages	Limited sensitivity. Limited to low density signal environment, very limited sorting capability	Confused by overlapping pulses, more complex and expensive than CVR	Long scan times, narrow bandwidth limits, detection of wideband modulation, low probability of intercept for transient emitters	Complex, expensive, narrow bandwidth limits, detection of wideband modulation	Complex, expensive, poor dynamic range limits in dense signal environment, difficult signal processing	Complex, expensive, longer search time

Table 6.　　　Typical ES Receivers' Performance Parameters[6]

[6]Lynch Jr., 123-169.

C.   DETECTION ACCURACY

1.   Detection Finding Techniques

The three basic ways in which emitters can be located are triangulation (determination of two lines of bearing from known locations to the emitter), determination of distance and one line of bearing, and determination of two mathematically described curves that cross the emitter's location (D. L. Adamy. 2004, 156). To measure the direction of arrival (DOA) of the emitter signals in the first two approaches, Adamy has listed five principal direction finding (DF) techniques.

a.   Rotating Directional Antenna

This technique exploits the relation between the gain pattern of a rotating antenna and the angle from its bore sight: knowing the pattern of the antenna's gain, two or more intercepts within the antenna main beam are sufficient to determine the orientation which would place the signal at the antenna bore sight. As the DF accuracy is dependent on the size of the beam and consequently on the size of the antenna, this approach is very common in naval EW assets where the antenna size is not a major concern.

b.   Multiple Antenna Amplitude Comparison

This approach utilizes the difference in amplitude ratio between two differently oriented antennas that both intercept the same signal. As no large antennas are needed, it is widely used in aircraft radar warning receivers (RWRs), yet its accuracy is typically low (5^0–15^0)

c. *Watson Watt*

This technique uses three antennas in line, separated a quarter-wavelength apart. The sum and difference patterns of the outside antennas generate a cardioid vs. angle graph; switching among eventual symmetrical pairs causes rotation of the cardioid graph, allowing DF measurement. The Watson-Watt approach provides moderate DOA accuracy (approximately 2.5^0RMS).

d. *Doppler*

This technique utilizes a rotating and a non-moving antenna; the received signal frequency in the rotating antenna follows a sinusoidal Doppler shift pattern relative to the signal received at the non-moving antenna. The direction of signal arrival is the angle at which the Doppler shifts from positive to negative. Typical accuracy for this technique is 3^0.

e. *Interferometer*

Interferometry in direction finding is based on measuring the phase of a received signal at each of two antennas. The emitter bearing is then computed utilizing the phase difference between them (D. L. Adamy.2004, 162-3).

As the biggest exploitable weakness for stealth emitters in intercept receivers is the angle of arrival (AOA), a weakness that also cascades into range estimation, two major methods have been developed for its measurement: amplitude angle of arrival and phase angle of arrival. In both methods, there is a signal-to-noise-limited lower bound on measurement accuracy. Assuming a matched filter in

the presence of white noise (best case), then the lower bound rms error will be (Lynch Jr. 2004, 149):

$$\sigma_\theta \geq \frac{\lambda\sqrt{3}}{\pi\ell\cos\theta\sqrt{2SNR}} \quad (4.7)$$

Where

ℓ : Aperture length (m) and

θ : AOA of the intercepted signal

f.   Amplitude Angle of Arrival

Due to its simplicity, amplitude comparison is the primary method used in most RWRs where broadband cavity-backed spiral antennas are used in each in each quadrant. For bandwidths around 20 GHz, David Lynch estimated that this type of antenna has the following gain pattern.
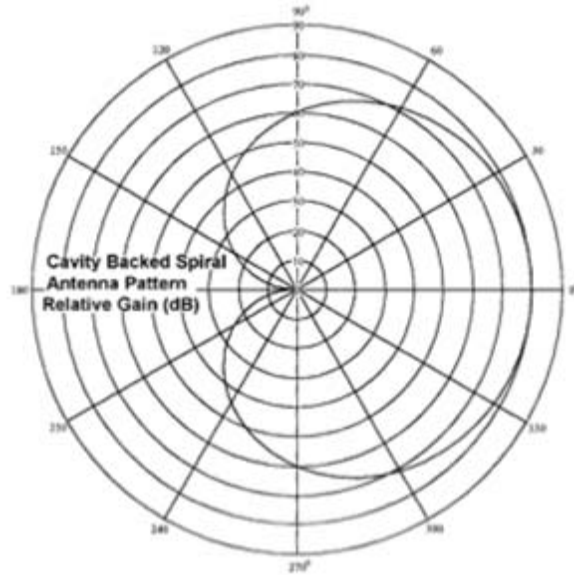
Figure 33.   Broadband Cavity Backed Spiral Gain Pattern[7]

Lynch went on to draw the patterns' overlap of the antennas, as they are all mounted on the same interceptor.
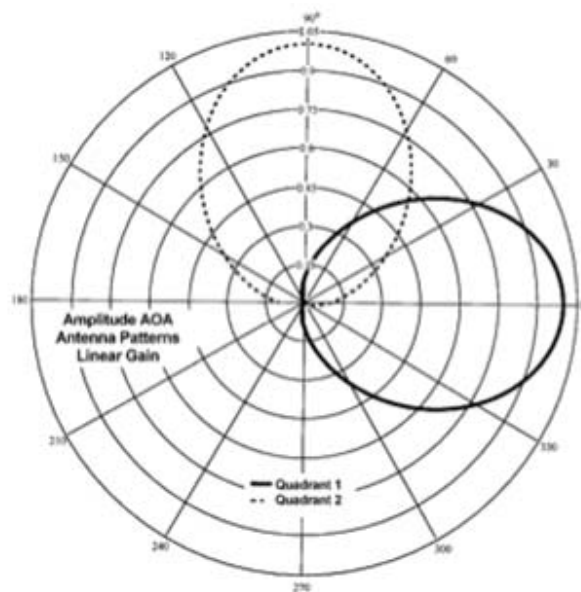
Figure 34.   Amplitude AOA Pattern Displacement[8]

---

[7]Lynch Jr., 150.

The system structure to estimate the AOA is fairly simple: after its filtering, each quadrant signal passes through a logarithmic amplifier, and the difference between any two quadrants is multiplied by an angle scale factor and fitted to a correction curve to estimate angle of arrival. For a set of three idealized quadrant antennas, the angle of arrival measurement by amplitude would look as follows.
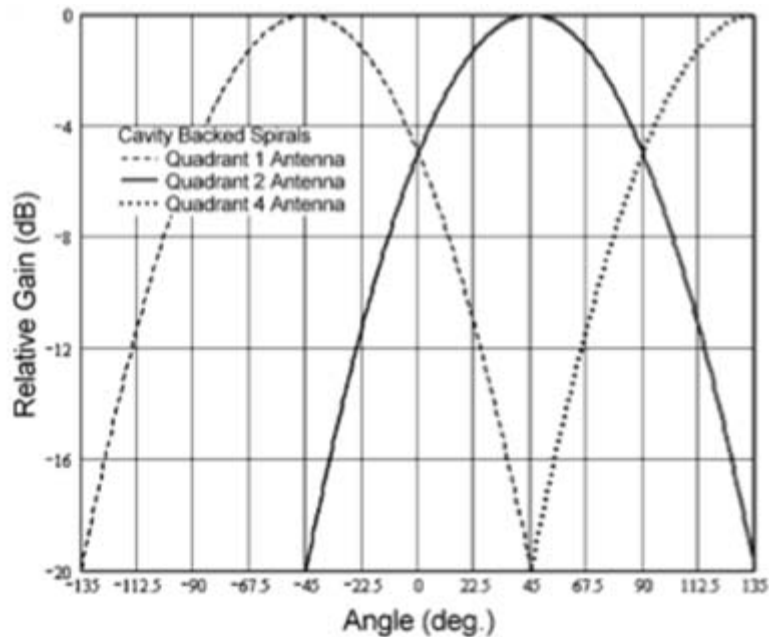
Figure 35.   Angle of Arrival Measurement by Amplitude Comparison[9]

Figure 35 shows three idealized quadrant antenna patterns; it can be seen that the differences can be used to uniquely determine the AOA if the signal-to-noise ratio

[8]Lynch Jr., 151.

[9]Lynch Jr., 152.

is high (recall Equation [4.7]). The mathematical calculation of the emitter angle, assuming a 90^0 antenna spacing is given by:

$$\theta_E = \frac{(20\log Q_i) - (20\log Q_{i+1})}{k_m} \quad (4.8)$$

and

$$Q_i = E_o e^{-k^2\left(\theta_B - i\frac{\pi}{2}\right)} \quad (4.9)$$

where:

Q_i: Antenna pattern in the   quadrant

k_m: $-8.68\pi k^2$

E_o: Peak output voltage of the quadrant antenna and amplifiers before log compression

k : $5/(3\theta_B)$

θ_E: True direction of the emitter

θ_B: 1/4 Power antenna beamwidth

AOA errors are of course not rare and are generally attributed to deviations from ideal logarithmic conversion, deviations from ideal gain pattern, component temperature, and time drift and amplifier linearity. To compensate for this deficiency, which, although not severe, is also present in phase comparison AOA, periodic calibration (of a magnitude of second to minutes) is

performed in most of these systems, and the measurements in each frequency band are then corrected by a calibration table.

g. *Phase Angle of Arrival*

As per its name, this technique is based on the time of arrival difference of the emitter's signal at two or more antennas, by comparing the relative phases from each of them with the assistance of a phase discriminator as follows.
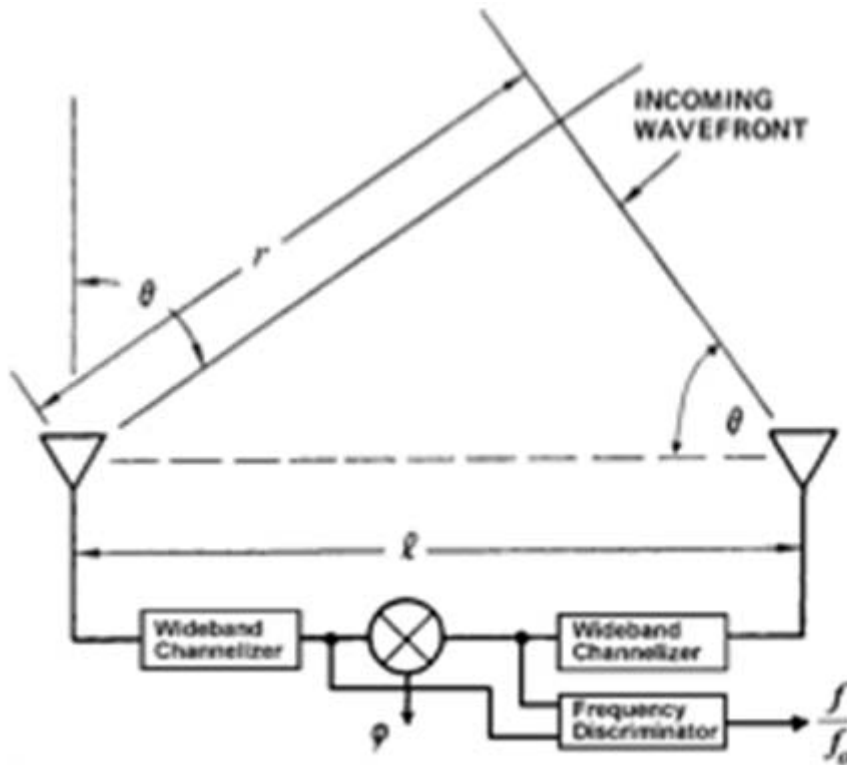
Figure 36.   Phase Comparison AOA Measurement

The two antennas form a baseline. An incoming wavefront from a distant source will arrive as almost a plane wave. For a wavefront arriving to the antenna baseline at an angle of θ, the distance r of its source

(emitter) to the antenna is $\ell\sin\theta$. Assuming a single incoming frequency, the measured phase will be:

$$\varphi = \frac{2\pi f\ell}{c}\sin\theta \xrightarrow{c=f_o\lambda_o} \varphi = \frac{2\pi f}{cf_o}\cdot\frac{\ell}{\lambda_o}\sin\theta \quad (4.10)$$

And solving for , the phase comparison AOA is:

$$\theta_E = \arcsin\left(\frac{\lambda_o f_o}{2\pi\ell f}\varphi\right) \quad (4.11)$$

It is obvious that for the phase AOA to be accurate, the frequency of the arriving signal must be correctly measured. The frequency filters before and after the phase detector and the frequency discriminator in parallel with it aim at providing the most accurate possible measurement. Note that at low SNR levels or large bandwidth measurement, phase AOA is better than amplitude AOA, yet is still quite limited.

Just as for amplitude comparison AOA, phase deviations from an ideal antenna pattern, ideal RF and IF conversion, component temperature/time drift, frequency discriminator errors, and linearity issues on the amplifier and phase detector will result in AOA errors (Lynch Jr. 2004, 159).

2. Precision Emitter Location Techniques

This section will discuss the two most widely used targeting techniques: time difference of arrival (TDOA) and frequency difference of arrival (FDOA). Although they are used in conjunction, often with less accurate location systems, each technique will be addressed separately.

a. *Time Difference of Arrival (TDOA)*

The concept of this method is based on our knowledge of transmission speed. Knowing that the signal travels at the speed of light, all the detector needs to know is the exact time the signal left the transmitter. The exact propagation distance will be:

$$d = c\Delta t \ (4.12)$$

Where:

d : Propagation distance

Δt : Propagation time

c : Speed of light (3×10^8 m/sec)

Obviously, determination of the time of departure is feasible only when dealing with cooperative signals. When dealing with hostile emitters, we have no way of knowing when the signal left the transmitter; the only measurable information is the time it arrives at the receiver. To overcome this, TDOA suggests measuring the difference in time of arrival between two sites whose positions are known. If the measuring is done accurately, the transmitting site is located along a hyperbolic curve (D. L. Adamy. 2004, 164). More specifically, each TDOA forms a hyperbola, or isochrone,[10] the intersection of which provides a potential location of the emitter. A schematic

---

[10] "An isochrone is a hyperbolic line containing all of the locations at which an emitter could be located for a fixed difference in propagation path length to the two sites, causing a fixed time difference of arrival for a signal"; in: David L. Adamy, *EW 102: A Second Course in Electronic Warfare* (Norwood, MA: Artech House Publishers, 2004), 165.

diagram of isochrones for various values of TDOA between two aircraft is shown in Figure 37.
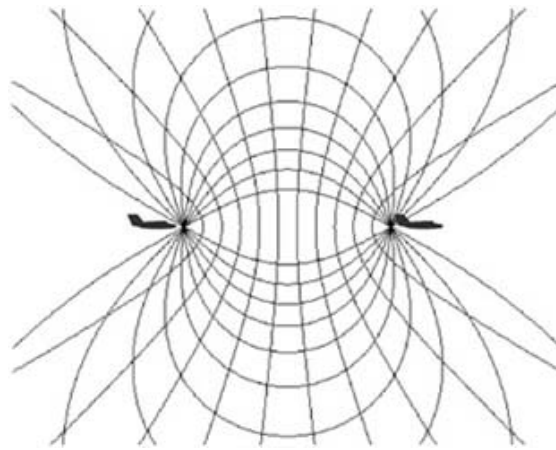
Figure 37.   Isochrone Lines; Two Aircraft Time
                    Difference of Arrival

As depicted above, the location problem is still not solved, as a hyperbola is an infinite curve. To determine the actual location of the transmitter a third receiver is required.
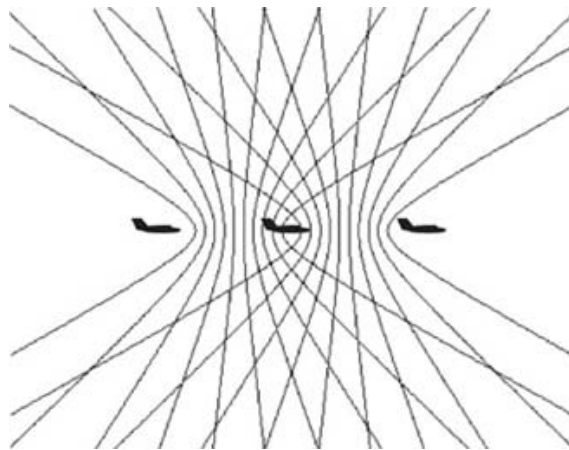
Figure 38.   Isochrone Lines; Two Aircraft Time
                    Difference of Arrival

Note that Figure 38 is a two-dimensional depiction; in reality, isochrones cover three-dimensional

space. Regardless of the depiction, the intersection of the same TDOA hyperbolas provides the location of the transmitting site.

According to David Lynch Jr., the root mean square (RMS) error lower bound for a time-of-arrival estimate, assuming a rectangular intercepted pulse with a matched filter in the presence of white noise, is given by the formula (Lynch 2004):

$$\sigma_{TOA} \geq \frac{T\sqrt{3}}{\pi\sqrt{2SNR}} \quad (4.13)$$

$$\sigma_{TOA} \geq \frac{T\sqrt{3}}{\pi\sqrt{2SNR}} \quad (4.13)$$

Where

T : Pulsewidth

Note that this formula additionally assumes that the measuring timebase or clock is orders of magnitude more accurate than the measured interval, which is not always true. In the case of PRI interval measuring, Equation (4.13) becomes:

$$\sigma_{PRI} \geq \frac{c_m}{2B\sqrt{nSNR}} \quad (4.14)$$

Where:

c_m : Multipath scintillation coefficient (typically 2).

As David Adamy notes, for an accurate measurement of the emitter location, it is necessary that the receiver sites be precisely known. This task can be executed by GPS; yet, for moving receivers, such as ship or aircraft mounted

devices, it is necessary to consider the instantaneous receiver locations when calculating the isochrone and emitter location (D. L. Adamy. 2004, 167).

b. Frequency Difference of Arrival (FDOA)

This technique involves the measurement of the difference between the received frequencies at two moving receivers from a single transmitter, generally stationary. As this difference is caused by the Doppler shift, this method is also known as Differential Doppler (DD).

The frequency measured in a fixed receiver from a moving transmitter is given by the formula:

$$f_R = f_T \left(1 + \frac{v_r \cos\theta}{c} \right) \quad (4.15)$$

Where:

f_R : Received frequency

f_T : Transmitted frequency

v_R : Receiver speed

θ : Angle from the receiver velocity vector to the transmitter

c : Speed of light ($3 \cdot 10^8 m/\sec$)

In the case of two moving receivers that receive the same signal from different locations, the difference between the two receives frequencies given by the formula:

$$\Delta f = \frac{f_T}{c}\left(v_2\cos\theta_2 - v_1\cos\theta_1\right) \quad (4.16)$$

Where:

Δf : Difference in frequency

f_T : Transmitted frequency

v_1 : Receiver No1 speed

v_2 : Receiver No2 speed

θ_1 : True spherical angle from the velocity vector of receiver No1 to the transmitter

θ_2 : True spherical angle from the velocity vector of receiver No2 to the transmitter

c : Speed of light ($3\cdot10^8 m/\sec$)

The intersection between the three-dimensional surface defining all of the possible transmitter locations which would produce such a Δf, and a plane, such as the Earth surface, results in a curve called *isofreq*. As in the TDOA method, the frequency measurement cannot on its own define a location; it only defines a curve of possible solutions (D. L. Adamy. 2004, 169). Accurate location of the transmitter can be determined from the intersection of isofreqs from three or more baselines (i.e. triangulation); yet, accuracy depends on the precision of the frequency measurement as well. For a rectangular intercepted pulse with a matched filter in the presence of white noise, the rms error lower bound for a frequency estimate will be:

$$\sigma_f \geq \frac{\sqrt{3}}{\pi T \sqrt{2SNR}} \quad (4.17)$$

Where

T : Pulsewidth

Accounting for the filter mismatch and multipath scintillation, David Lynch Jr. provides a more realistic formula for rms frequency measurement:

$$\sigma_f \geq \frac{c_m B}{\sqrt{2SNR}} \quad (4.18)$$

Where:

c_m : Multipath scintillation coefficient (typically 2).

B : Detection bandwidth of the intercept receiver.

Similarly, the phase error would be:

$$\sigma_\varphi \geq \frac{c_\varphi}{\sqrt{2SNR}} \quad (4.19)$$

Where:

σ_φ : Phase detector coefficient (usually between $2^{0.5}$ and 2^{11} .

D.   SIGNAL PROCESSING ALGORITHMS

As discussed in Chapter II, the main characteristic of LPI technology is its sensitivity (δ). To quantify this LPI radar advantage compared to the intercept receiver, Wiley introduced the notion of *sensitivity advantage*, which he defined as the ratio for the signal power needed at the

intercept receiver (P_{IR}) to that needed at the LPI radar (P_{RT}) to detect the target (Wiley 1976, 3):

$$\delta_{adv} = \frac{P_{IR}}{P_{RT}} = \frac{4\pi}{\sigma_T}\left(\frac{G_T' G_I L_{RR}}{G_T G_r L_{IR}}\right)\left(\frac{R_T^2}{R_I}\right)^2 \quad (4.20)$$

Where:

σ_T : RCS of the target

G_T : Bore sight gain of the LPI radar's directive transmit antenna

G_T' : Gain of the LPI radar's transmit antenna sidelobe in the direction of the intercept receiver

G_I : Gain of the intercept receiver's antenna

G_r : Gain of the radar's receive antenna

L_{RR} : Loss in the intercept receiver

L_{IR} : Loss between the radar's antenna and receiver

R_T : Radar to target range and

R_I : Radar to intercept receiver range.

The formula indicates that the sensitivity advantage (δ_{adv}) depends on the intercept receiver characteristics and should be a high value, on the order of 50 dB, for a case where we have a simple receiver against an LPI radar (Lima 2002, 2). From the receiver perspective, a way to improve the sensitivity and thus enhance the detection process is

improving the spectral analysis of the signal: time frequency signal processing, correlation techniques and algorithms are major tools in the game to overcome the processing advantage of the LPI radar. However, increasing the sensitivity of the receiver allows for detecting sidelobes of the emitter, but at the same time obligates the receiver to process a significantly large number of signals (Denk 2006). To demodulate the LPI waveform and identify the emitter parameters (i.e., carrier frequency, bandwidth, modulation period, modulation bandwidth and time of arrival), Fourier analysis has been the major tool. However, more complex processing techniques have evolved, such as short time Fourier (tracks signal parameters over time) or time-frequency and bi-frequency distributions. The latter two, which aim at identifying the exotic modulation schemes of the LPI waveform, include techniques such as the Wigner distribution, the Choi-Williams distribution, quadrature mirror filtering, and cyclostationary processing (Stephens 1996). To introduce the reader to the fundamentals of frequency distribution for LPI detection, this thesis will address the former two methods; for a comprehensive analysis on the issue of frequency distribution, the work of Leon Cohen (Cohen 1989) and Phillip Pace (Pace 2009, 405–548) can provide further useful insights.

1. Wigner Ville Distribution (WVD)

The WVD is a three-dimension function that relates the amplitude of the signal to a frequency and a time component. Its greatest advantage is that it exhibits the highest signal energy concentration in the time-frequency

plane for linearly modulated signals (Pace 2009, 406); for nonlinear frequency modulated signals, higher order time frequency representations have been researched (Katkovnik and Stankovic 1998).

The WVD of input signal ___ is defined as:

$$W_x(t,\omega) = \int_{-\infty}^{+\infty} x\left(t + \frac{\tau}{2}\right) x^*\left(t - \frac{\tau}{2}\right) e^{-i\omega x} d\tau \quad (4.21)$$

Where:

t : Time variable and

ω : Angular frequency variable ($2\pi f$).

Stankovic and Stankovic showed that windowing the data results with a rectangular window, the WVD can be written as (Stankovic and Stankovic 1994):

$$W(l,\omega) = 2 \sum_{n=-N+1}^{N-1} x(l+n) x^*(l-n) w(n) w(-n) e^{-i2\omega n} \quad (4.22)$$

Where:

$x(l)$: A sample time series with l a discrete time index ranging from $-\infty$ to $+\infty$

$w(n)$: A rectangular window-function of length $2N - 1$ and amplitude 1.

Substituting the kernel function[11]

---

[11]A kernel is an arbitrary function named by Claasen and Mecklenbrauker in: T.A.C.M Claasen and W.F.G Mecklebrauker, "The Wigner Distribution-a Tool for Time-Frequency Signal Analysis; Part Ill: Relations With Other Time-Frequency Signal Transformations," *Philips J. Res.* 35: 372-389. In general, the kernel may depend explicitly on time and frequency and in addition may also be functional on the signal.

$$f_1(n) = x(l+n)x^*(l-n)w(n)w(-n) \quad (4.23)$$

Equation (4.22) becomes (Pace 2009, 406):

$$W(l,\omega) = 2 \sum_{n=-N+1}^{N-1} f_1(n)e^{-i2\omega n} \quad (4.24)$$

Equation (4.24) renders clear that the choice of N affects the resolution of the WVD. Note that the data length M limits the N according to the formula:

$$N \leq \frac{M+1}{2} \quad (4.25)$$

Sampling the continuous frequency variable ω:

$$\omega = \frac{\pi k}{2N} \quad , k = 0,1,2,\ldots,(2N-1) \quad (4.26)$$

and modifying the kernel indexes to fit the standard DFT algorithms as follows:

$$W\left(l,\frac{\pi k}{2N}\right) = 2 \sum_{n=0}^{2N-1} f_1'(n)e^{-i2\frac{\pi k}{2N}n} \quad (4.27)$$

Where:

$$f_1'(n) = \begin{cases} f_1(n), & 0 \leq n \leq N-1 \\ 0, & n = N \\ f_1(n-2N), & N+1 \leq n \leq N-1 \end{cases} \quad (4.28)$$

the WVD functions becomes:

$$W(l,k) = 2\sum_{n=0}^{2N-1} f_1'(n)e^{-i\frac{\pi k}{N}n} \quad (4.29)$$

which is the fundamental equation used to calculate the WVD of the detected signals.

The greatest deficit of the WVD is arguably the fact that it contains *cross terms* (ghost terms) between every pair of signal components. Several formulations have been suggested to remove them (Kadambe and Adali 1998). In addition, WVD is extremely costly with respect to computation time, and although hardware improvements are being researched—such as more efficient coding algorithms in combination with a very fast digital processor of a Field Programmable Gate Array (FPGA) (Milne and Pace 2002)— extraction of the detailed modulation parameters is still expensive. Moreover, the signal must be known for relatively large periods of time to derive useful results (Denk 2006, 69). Despite these elements, WVD is considered to be able to identify frequency and time changes in most LPI radar signals (Gau 2002, 147).

2.   Choi Williams Distribution

The Choi-Williams distribution (CWD) was first proposed by Hyung-Ill Choi and William J. Williams in 1989 (Huyng and Williams 1989) and aimed at minimizing the cross terms so prevalent in the WVD. Choi and Williams realized that a careful choice of the kernel function in the three-dimensional distribution (time-frequency-phase) can minimize the cross terms and still retain the desirable properties of the self-terms.

Indeed, the generalized class of bilinear transformation with good resolution in both time and frequency, first presented by Cohen(Cohen 1989, 943), was simplified by Pace (Pace 2009, 446):

$$C_f(t,\omega,\varphi) = \frac{1}{2\pi} \iiint e^{j\left(\xi\mu - \tau\omega - \xi\tau\right)} \varphi\left(\xi,\tau\right) A\left(\mu,\tau\right) d\mu d\tau d\xi \quad (4.30)$$

Where:

$\varphi\left(\xi,\tau\right)$: Is a kernel function

and

$$A\left(\mu,\tau\right) = x\left(\mu + \frac{\tau}{2}\right) x^*\left(\mu - \frac{\tau}{2}\right) \quad (4.31)$$

Where:

$x\left(\mu\right)$: The time signal

$x^*\left(\mu\right)$: The complex conjugate.

Substituting the existing kernel function with Choi Williams' suggestion:

$$\varphi\left(\xi,\tau\right) = e^{-\frac{\xi^2\tau^2}{\sigma}} \quad (4.32)$$

where σ is a positive scaling factor, the CWD of the signal becomes:

$$CWD_{x(t,\omega)} = \int_{\tau=-\infty}^{\infty} e^{-i\omega\tau} \left[\int_{-\infty}^{+\infty} \sqrt{\frac{\sigma}{4\pi\tau^2}} G\left(\mu,\tau\right) A\left(\mu,\tau\right) d\mu \right] d\tau \quad (4.33)\ ^{12}$$

Where:

---

[12] The bracketed term in Equation (4.31) is the estimation of the time-indexed autocorrelation function.

$$G(\mu,\tau) = e^{\sigma\left(\frac{\mu-t}{2\tau}\right)^2} \quad (4.34)$$

The discrete form of the Choi Williams distribution is:

$$CWD_{x(t,\omega)} = 2\sum_{\tau=-\infty}^{\infty} e^{-j2\omega t} \sum_{\mu=-\infty}^{\infty} \frac{1}{\sqrt{\frac{4\pi n^2}{\sigma}}} e^{-\sigma\left(\frac{\mu-1}{2\tau}\right)^2} x(\mu+\tau)x^*(\mu-\tau) \quad (4.35)$$

Applying a windowing procedure similar to that in the WVD, the CWD takes the form:

$$CWD_{x(1,\omega)} = 2\sum_{n=-L}^{L} S(1,n)e^{-j2\omega n} \quad (4.36)$$

with the kernel being:

$$S(1,n) = W(n)\sum_{\mu=-\frac{M}{2}}^{\frac{M}{2}} \frac{1}{\sqrt{\frac{4\pi n^2}{\sigma}}} e^{-\left[\sigma\left(\frac{\mu-1}{2\tau}\right)\right]^2} x(\mu+\tau)x^*(\mu-\tau) \quad (4.37)$$

where $W(n)$ is a symmetrical window with nonzero values on the interval $-L$ to L and, $W(\mu)$ a uniform rectangular window of amplitude 1 for the range $-M/2$ to $M/2$; the choice of N and M determine the frequency resolution of the CWD and the range at which the function will be defined. The analysis by Choi and Williams proves that decreasing the size of $W(n)$, apart from reducing the cross terms, affects the frequency resolution of the distribution; in other words, there is direct relationship between the reduction of the cross terms and the frequency resolution obtained from the distribution.

System	RF (GHz)	Az. (deg)	El. (deg)	Sensitivity (dBm)	Antenna Gain (dB)	Azimuth accuracy (deg)	Update time	Type	Deployment
DZ 9001	1-18	100	20	-70	10-30	3	2	Superhet	Ground
BM/KJ 8602	0.7-18	360	60	-40	0	15	1	CVR	Airborne
MCS-93	0.8-18	100	45	-80	10-20	3	1	Superhet	Ground
Strategie	0.8-18	180	45	-80	6	1	1	Interferometer	Ground
Phalanger	1-18	360	45	-50	3	1	1	Int./Transform	Airborne
CR2700	0.5-18	360	20	-80	20-40	1	4-8	Superhet	Ground
Kingfisher	2-18	360	40	-60	0	2	4-8	Int./IFM	Airborne
Sirena/SPO-10/15/23	6-21	360	45	-55	0	45	1	CVR	Airborne
NRS-1/pole dish	2-4,8-17	360	45	-70to-35	24-36	0.3	Minutes	Superhet	Ground
RPS-1,2,3	0.5-37.5	360	45	-70to-35	20-35	0.3	Minutes	Superhet	Ground
RPS-5/twin box	0.5-10	360	45	-80to-50	10-20	5	2-8	Superhet	Ground
Weasel	0.7-18	360	45	-80	10,30	1	4	Hybrid	Ground
Zeus	0.5-18	360	90	-50	0	20/quadrant	2-8	IFM/Hybrid	Airborne
ALR-52	0.5-18	360	15-35	-70	13-26	2	1	IFM	Airborne
ALR-56	0.5-20	360	30	-50	0	20/quadrant	2-8	Superhet	Airborne
ALR-69	0.5-18	360	30	-50	0	20/quadrant	2-8	CVR	Airborne
WLR-11	0.5-18	360	45	-70	0	20/quadrant	1	IFM	Ship

Table 7.   Typical Deployed Intercept Receivers[13]

---

[13]Lynch Jr., 19.

V. JAMMING METHODS FOR LPI RADARS

A. CONCEPTUAL CLARIFICATIONS

In its modern conception, electronic attack entails the offensive use of the EM spectrum to disable the enemy's combat capabilities, involving both nondestructive (soft kill) and destructive (hard kill) actions. Jamming is an example of a soft kill action that aims to dilute the effectiveness of an enemy weapon system through confusion, distraction, deception, or seduction. Due to their different mechanisms, soft and hard kill systems have generally been separately employed; however, to optimize performance, both have to be employed in a cooperative manner. In this chapter, we address the soft kill type of measures, trying to look more specifically into the particularities of the LPI radar.

1. EA Radar Jamming Waveforms

There are basically two types of radar that must be jammed by EA equipment. The first is the surveillance radar, which locates the position of a target within a large coverage volume. Conceptually, the search radar can be modeled as a rotating antenna beam whose main lobe sequentially scans the search volume while its sidelobes provide response in all directions. The matched filter maximizes the received SNR, which then depends on the energy received from the target and the receiver noise spectral density.

The second major type is the tracking radar, which is usually given high priority in the hierarchy of EA threats

because it is associated with the terminal phases of a weapon system.[14] The function of the EA system is to cause the tracking radar to break lock, thus removing the guidance information being used by the weapon to converge on the target.

In the EA context presented above, Schleher notes the two fundamental ways to introduce jamming into radar (Schleher 1999, 147). The first is to raise the receiver noise level by injecting external noise through the radar's antenna, through either the main lobe or the sidelobes. The second way is to introduce spurious signals into the radar's main lobe or sidelobe in order to confuse or deceive the radar with respect to the location of the real target. The closer the transmitted false targets replicate the actual radar transmitter waveform, the greater the radar's response to these false targets will be. Any deviation in either the envelope or the phase structure of the jamming signal with respect to the actual transmitted waveform will cause a mismatch loss, which must be compensated for by an extra jamming power. For this reason, deception jammers usually repeat the radar's signal with both a coherently related time delay and frequency translation. The probability for achieving this is presented in the next paragraph.

2. LPI Jamming Probability: The Issue of Interception

The most comprehensive work on LPI interception is arguably that of Stove, Hume and Baker, who in 2004

---

[14]To say that a tracking radar is locked onto a target implies that a weapon is directed at the target.

presented a paper examining the evolving relationship between advanced LPI radar designs and future trends in ESM receiving capability. To determine the key factors that influence the detection of LPI radar signals, the authors computed the performance of ESM and radar systems for a number of cases, including not just simple interception, but also the extraction of information from intercepted signals. The authors concluded that this relationship is far from straightforward, being not only probabilistic, but also dependent on environmental and operational factors. In addition, they demonstrated that it is never possible to be completely certain that a radar system has not been detected and that the most appropriate way to implement an LPI radar design is always closely related to the tactical environment in which the radar system will be used.

The key equation to conceptualize the probabilistic nature of LPI signal interception is Shannon's theorem:

$$C = Wlog_2\left(1 + SNR\right) \quad (5.1)$$

For the detection threshold level of 17dB SNR, each interception may be assumed to provide the opportunity for extracting 5.7 bits of information concerning the LPI radar. The authors hypothesized that in order to exploit transmissions, the following information is needed:

- Scan timing, i.e., where the radar is pointing at any time,

- Carrier frequency,

- Modulation bandwidth,

- Modulation or code period,

• Synchronization, i.e., when the modulation pattern starts.

Assuming that each of these parameters must be known to 4 bits precision, 20 bits of information are needed to characterize the radar; that is, without trying to replicate its waveform in any detail. Denk makes two interesting observations: first, the scan timing and carrier frequency can readily be derived from the way in which the intercept is made. Second, information on the LPI radar can effectively be obtained from multiple looks at the receiver output (Denk 2006, 87). After this process is concluded, 12 bits giving 36dB SNR of information has to be recovered from the signal.[15]

According to Stove et al. the problem with attempting to match the jamming receiver for a single-look interception and exploitation is that it is more efficient in energy terms to obtain information from separate looks at lower SNR. For example, sending 8 bits of information at once requires 24dB SNR in the channel's information bandwidth, whereas sending the same information in two messages of 4bits each requires twice as much time but only 12dB SNR; that is a total energy saving of 9dB(Stove, Hume and Baker 2004).

---

[15] According to Stove et al, in some conventional ES receivers this sensitivity is achieved through integrating multiple looks, using a receiver with a wider bandwidth than the signal's information bandwidth. In: A. G. Stove, A. L. Hume and C. J. Baker, "Low Probability of Intercept Radar Strategies," *IEEE Proceedings-Radar Sonar and Navigation* (Artech House) 151, no. 5 (October 2004): 249-260.

B.   LPI RADAR JAMMER DESIGN REQUIREMENTS

As the extraction of LPI signal data is necessary for its successful jamming, most scholarly efforts address the issue of interception (McRitchie and McDonald 1999; Pace 2009). Jamming techniques for LPI radars, which we discuss in the end of this chapter, do not differ from jamming techniques for conventional radars. As a consequence, the battle between the jammer and the LPI is constrained in the interception phase, which precedes that of the actual jamming.

According to Denk, the major factor that determines the design, and ultimately the effectiveness, of an LPI system is bandwidth (Denk 2006, 88).

1.   Bandwidth

Denk differentiated between the jammer RF bandwidth and the detector video bandwidth, arguing that both parameters affect jamming by their comparative size. In jammer RF bandwidth, too wide a bandwidth allows too much signal to enter the detector and unnecessarily degrades the receiver noise figure, while too narrow a bandwidth eliminates too much of the signal lowering the average power to the detector. In detector video bandwidth, a wide video bandwidth provides for fast rise and fall times necessary for processing narrow pulses, but this is done at the expense of allowing more noise to the detector as well. As McRitchie and McDonald note, a carefully designed jammer should address both of these design areas (McRitchie and McDonald 1999).

Another way to look at the effect of bandwidth is through the notion of *burn through range*, a concept that indicates the range at which the radar overcomes the jamming effect:

$$R_{max} = \left[\frac{P_T G_T}{4\pi(SJR)_{min}} \frac{\sigma}{P_J G_J} \frac{B_J}{B_r} \frac{L_J}{L_R} \right] \quad (5.2)$$

Where:

P_T: Peak Power transmitted (W)

G_T: LPI radar antenna gain

σ: RCS (m^2)

B_J: Jammer bandwidth (Hz)

L_J : Jammer system Losses

SJR: Signal-to-jamming ratio

P_J: Jammer power density (W/Hz)

G_J: Jammer antenna gain

B_r: LPI radar bandwidth

L_R: Jammer power density

The term B_J/B_r represents the ratio between the jamming and radar bandwidths. If this term approaches a value of 1 to 5, then the jamming is considered spot jamming. If $B_J \square B_r$ then barrage noise is being used. It is to the advantage of the jammer (R_{max} is minimum) to be in spot jamming mode (Schleher 1999, 151).

2. Radar Receiver Sensitivity Advantage

Picking up the work of Wiley (Wiley, Electronic Intelligence: The Analysis of Radar Signals 1976), Gerd Schrick studied the relationship between the pre-detection bandwidths of the two receivers (interceptor and LPI) and the *radar receiver sensitivity advantage* (Schrick 1990).As we showed in Chapter IV, the radar receiver sensitivity advantage (δ_{adv}) is defined as the ratio of the signal power at the ELINT receiver (P_E) to that needed at the radar receiver (P_R) (Equation 4.20). Shrick showed that the formula for δ_{adv} can be written as:

$$\delta_{adv} = \frac{B_E}{B_R} \frac{G_R}{G_E} \quad (5.3)$$

Where:

B_E: Intercept receiver (ELINT) bandwidth

B_R: Receiver bandwidth

G_E: Processing gain of ELINT antenna

G_R : Gain of receiver antenna

Although Schrick expected the intercept receiver bandwidth B_E to be larger than B_R for convenience in intercepting a variety of signals, he noted that B_E can be made to match that of the signal to be intercepted once the nature of the signal is known. It is therefore reasonable, he concludes, to choose the value of B_E / B_R between 1 and 100 (Schrick 1990, 110).

The maximum processing gain of the radar is achieved when the target echo is coherently integrated for the entire time the transmitted signal strikes the target (T_o). In this case the maximum radar processing gain is $B_R T_o$. If the radar makes use of both coherent and non-coherent integration, the processing gain would be reduced from this value. If the coherent integration time is T_c, the total radar processing gain would be:

$$\left(B_R T_C \right)\left(T_o / T_C \right)^{\gamma} \quad (5.4)$$

where γ is the non-coherent integration efficiency, typically 0.7 to 0.8.[16]

The intercept receiver processing gain can be as small as 1 if there is no post-detection integration (or filtering). However, the prudent intercept receiver designer would plan to use non-coherent integration for a time (TE) comparable to the radar's integration time, T_o. This provides a processing gain of:

$$G_E = \left(B_E T_E \right)^{\gamma} \quad (5.5)$$

This strategy provides the best chance of detecting the LPI radar but has the disadvantage of obscuring the details of the radar's pulse compression code. Combining equations (5.3), (5.4) and (5.5), Schrick reaches the following radar receiver sensitivity advantage formula:

---

[16] The minimum value for γ is approximately 0.5; in: D. K. Barton, *Radar System Analysis* (Norwood, MA: Artech House, 1982).

$$\delta_{adv} = \left(B_E T_C\right)^{1-\gamma} \left(\frac{T_o}{T_E}\right) \quad (5.6)$$

If $T_E = T_o$ and $B_E = B_R$, the radar receiver sensitivity advantage is as small as it can be, which is:

$$\delta_{adv} = \left(B_R T_C\right)^{1-\gamma} \quad (5.7)$$

At the limit, when the interceptor makes maximum use of non-coherent integration and matches the instantaneous bandwidth of the radar, δ_{adv} depends only on the time-bandwidth product of the radar waveform raised to the $1-\gamma$ power. With the radar instantaneous bandwidth being determined by the range resolution required for a particular mission or application, Schrick suggests that the best strategy for the LPI radar designer is to make the coherent integration time as long as possible (Schrick 1990, 110).

C. ANTIJAM ADVANTAGE OF LPI

As we discussed in Chapter IV, signals associated with LPI communications have special modulations designed to make them difficult for normal type receivers to detect. This spreading is accomplished via one of the basic spreading modulation techniques: frequency hopping, chirp, and direct sequence spread spectrum. Assuming that the jamming signal is spread across the whole spread spectrum frequency range for an LPI communication system, Adamy drew the anti-jam advantage of the LPI as shown in Figure 39.
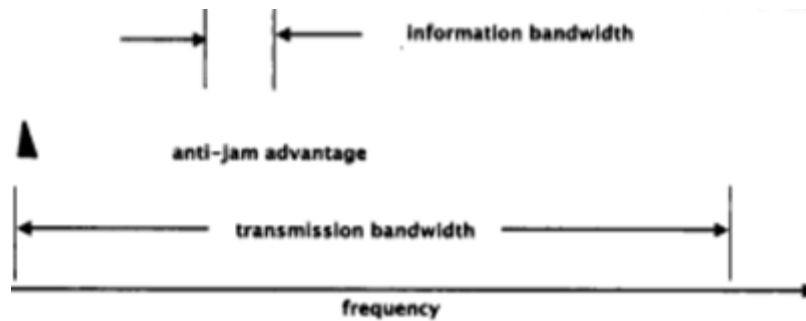
Figure 39.   The Anti-jam Advantage of LPI Communication

The anti-jam advantage is defined as the amount of signal power that must be received at an LPI system receiver location to provide the same jamming-to-signal ratio (JSR) that would be achieved if the entire jamming signal power were within the bandwidth of a non-spread system receiver. This is the ratio between the information bandwidth and the transmission bandwidth of the LPI signal. Bearing in mind that each of the spread spectrum techniques requires the input signals to be digital, Adamy noted that successful jamming requires only 0dB JSR and significantly less than 100 percent duty cycle (D. L. Adamy, Jamming LPI Signals 2009). As shown in figure 40, the bit error rate[17] can never be greater than 50 percent, regardless of the JSR; increasing the jamming power above this point causes very few additional errors. Empirical evidence indicates that when the bit error rate is at least 33 percent over a few milliseconds, no information can be recovered from the jammed signal.

---

[17] The bit error rate is the number of incorrectly received bits divided by the total number of bits received.
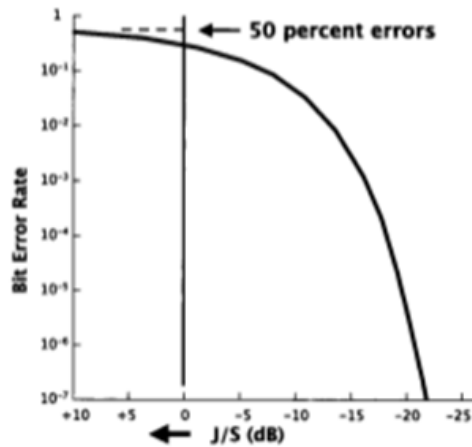
Figure 40.   The Bit Error Rate in a Digital Receiver
Cannot Exceed 50 Percent; a 0dB JSR Reaches this Level
of Errors;[18]

In the paragraphs to follow, we present the latest
trend in jamming LPI.

D.   JAMMING

1.   FSK

For FSK radars, the anti-jam advantage depicted in
figure 39 is based on the assumption that the jammer knows
only the full hopping range and must spread its jamming
power over that full frequency range. Denk provides an
interesting example to illustrate this: assume an FSK radar
that has a 2000 frequency hopping sequence which is random
or unknown to the ES receiver. The FSK radar can be said to
have a jamming advantage of 2000, which converts to 33dB.
This means that it takes 33dB more jammer power to achieve
a given JSR against this frequency hopper than would be
required if it were a fixed-frequency conventional radar.

---

[18]D. L. Adamy, Jamming LPI Signals 2009

117

Denk argues that the most effective jamming technique for FSK is "follower jamming", which entails a detection of the frequency of each hop and then jamming on that frequency (follower). As Adamy notes, this method requires a sophisticated and extremely fast frequency measurement technique in order to deny the enemy the transmitted information in each hop (D. L. Adamy, EW 101: A First Course in Electronic Warfare 2001). An extra consideration is the fact that the frequency hopping sequence of FSK radar is unknown and appears random to the ES receiver. Unless this frequency sequence is solved, the possibility of a jammer following the changes in frequency is highly remote (Denk 2006, 99).

2. PSK

Phase coded signals can be affected mostly by VGPO-type techniques.[19] If the jammer introduces an additional Doppler shift, this will be interpreted by the radar as an additional phase shift, causing a spreading of the received signal and thus a decrease in the effective processing gain (Denk 2006, 93). If the Doppler shift is enough, a corresponding loss of integration gain within the radar processor should be expected (Denk 2006, 93; McRitchie and McDonald 1999).

McRitchie and McDonald suggest that range bin masking should also be quite effective. They argue that if a section of the radar waveform recorded by DRFM or repeater

---

[19]VGPO is a method of capturing the velocity gate of a Doppler radar and moving it away from the skin echo. It is similar in essence to the RGPO, but is used against CW or Doppler velocity tracking radar systems. The CW or pulse Doppler frequency, which is amplified and retransmitted, is shifted in frequency (velocity) to provide an apparent rate change or Doppler shift.

is used by the jammer as its transmit waveform, the truncation will cause an increase in the sidelobe levels of the processed return. Total signal loss may occur as a side effect of the merging of the sidelobes[20]; however, this will degrade the SNR of the true target return, thus causing a loss in processing gain (McRitchie and McDonald 1999).

3.   FMCW

The main characteristic of FMCW radars that renders them difficult to detect is their wideband waveforms. Potential jammers have a significant problem measuring the waveform parameters with sufficient accuracy to match the jamming waveform (Pace 2004, 455). The situation is exacerbated in a real-world environment, where an FMCW radar operates among several radar systems in the same frequency band. An extra difficultly derives from the deterministic aspects of the FMCW radar. According to Pace, the fact the return target signature has a form that can be predicated (deterministic) provides the FMCW with significant suppression capabilities of many interfering waveforms that are uncorrelated (Pace 2009, 455).

Nevertheless, if the modulation period t_m and modulation bandwidth ΔF can be determined, then coherent deception jamming is feasible and very effective, since the jammer waveform looks like the radar waveform (Pace 2004, 455). Relevant literature suggests two major coherent deception EA techniques:

---

[20] According to Denk, the merging of the sidelobes can create a threshold problem; in Aytug Denk, *Detection and Jamming Low Probability of Intercept (LPI) Radars*, Master's Thesis, Electronic Warfare, Naval Postgraduate School (NPS) (Monterey: NPS, 2006), p.93.

The first is by producing false range targets. In an FMCW radar, this can be achieved by slightly shifting the return frequency. Such a shift is expected to create an equivalent shift in the apparent range of the signal as it passes through the radar processor.

The second coherent EA technique is VGPO. Employed in most Deceptive Electronic Countermeasure (DECM) systems, VGPO signals repeat a frequency-shifted replica of the received radar signal, initially programmed so that the repeated signal is within the passband of the Doppler filter containing the target return. This is designed to allow the jammer to capture the Doppler filter containing the target through the radar's automatic gain control (AGC) action. The repeated jammer signal is then swept in frequency until the maximum expected Doppler frequency of the radar is achieved. Then the repeated signal is switched off, forcing the victim radar to reacquire the target (Schleher 1999, 22).

Adamy suggests two approaches: the first requires prediction of the frequency-versus-time characteristics of the signal and the use of a jammer to direct energy to the receiver at the same frequency as the FM signal it is attempting to receive. This will allow the maximum jammer-to-signal ratio (JSR) to be achieved for any given jammer power and jamming geometry (D. L. Adamy 2001).

The second approach is to cover all or part of the modulation range with a broadband jamming signal. This jamming technique focuses the jamming power over a fraction of the frequency modulation range that will allow the JSR ratio in the jammed portion to cause a high rate of bit

errors in the digital modulation which is carrying the signal's information. The fraction of the jammed range depends on the jammer power, the effective radiated power of the modulated transmitter, and the relative ranges of the transmitter and the jammer to the jammed receiver.

Noting that the SNR in the LPI receiver is already at quite a low value, McRitchie and McDonald propose that a narrow band Doppler noise may also be quite effective. A Digital RF Memory (DRFM) can be used to focus the available power of the jammer and inject Doppler noise only a few KHz wide, matching to the instantaneous bandwidth of the FMCW radar (McRitchie and McDonald 1999).

In the following table, we present the currently deployed EA systems with the caveat that a measure of effectiveness against LPI assets is unavailable in present literature.

	Platform	Function	Characteristics
ALQ-99E	EA-6B, EF-111A	Support	Search Radar Jamming, 10 transmitters, analysis receivers, directional antennas
ALQ-162B	A-4, A-6, A-7, F-4, F-14, F-18	Self-protection	Coverage through I/J band, 1-kW peak power, 4% to 5% duty, track radar jamming, typical 60-degree fore/aft coverage, repeater transponder modes
ALQ-136	Army Helicopters	Self-protection	I/J-band jammer, AA artillery radar jammer, threat programmable
ALQ-131	F-16C, F-111, A-7, A-10, F-15, F-4	Self-protection	Dual mode pod jammer, CVR/ SHR analysis receiver, phased array
ALQ-161	B-1B	Self-protection	Coverage through I band, search and track radar jamming, monopulse and Doppler radar jamming, software controllable, phased array
ALQ-162 (shadowbox)	F-16C, F-18, RC-12D, RV-1D	Self-protection	CW jammer, chopped repeater lightweight, threat programmable, +60 degree switchable coverage
ALQ-165 (ASPJ)	F-16C, F/A18, F-14, AV-8B	Self-protection	Covered frequency range in two bands, pulse/CW capability, analysis receivers, threat programmable
ALQ-135 (TEWS)	F-15C	Self-protection	High powered transmitters, power management, integrated with ALR-56C

122

	Platform	Function	Characteristics
ALQ-172	B-52G/H	Self-protection	Track/search radar jamming, steerable jam beams, software programmable, phased array antenna, monopulse radar jamming
ALQ-184 (V)	F-4, F-15. F-16, A-7, A-10, F-111	Self-protection	Pod jammer, Rotman lens, medium power miniature TWTs, transponder and repeater jamming, high ERP
SLQ-32V (3)	Ships	Self-protection	Lens fed array, crystal video and IFM receivers, medium power miniature TWTs, tactical display, transponder and receiver jamming, high ERP

Table 8.   Modern EA Systems[21]

---

[21]Schleher 1999, 145.

THIS PAGE INTENTIONALLY LEFT BLANK

VI. NETWORKS AND NETCENTRIC WARFARE (NCW)

A.   INTRODUCTION

As with other sensors, LPI radar systems can be networked together as part of a network-centric warfare (NCW) architecture to gather and share surveillance and targeting data. In the case of LPI systems, this capability is "covert" in nature. In this chapter, we discuss the NCW notion on the three-layer architecture suggested by Phillip E. Pace: the information layer, the sensor layer, and the weapons layer. To point out the centrality of the NCW notion in the modern battlefield, our analysis commences by distinguishing between the concepts of *platform-centric warfare* and *network-centric warfare*. It is followed by a quantification of the NCW operational value, where central notions such as *Connectivity Measure*, *Network Rich*, and *Network Richness* are introduced.

B.   NETWORK-CENTRIC WARFARE

Network centric warfare is defined as military operations that exploit state-of-the art sensor information and network technologies to integrate widely dispersed human decision makers, weapons, situation and targeting sensors, and forces into a highly adaptive comprehensive system to achieve unprecedented mission effectiveness (Pace 2009, 320).

In a platform-centric architecture, a single asset is the epicenter of operations. Peripheral weapons, each with its own sensor(s) establish what Pace calls a "stovepipe communication system," transmitting the data back and

forth. The numerous platforms needed in architectures of this type limit the Command and Control (C2) capabilities as well.

Evolving from the platform-centric concept, NCW integrates a distributed system of C2, sensors and weapons into a *grid*, in order to collect, process, and disseminate an uninterrupted flow of data among the various nodes. Its main characteristic is the exponential effect it has on the combat power of the overall architecture: for N number of nodes, it gives a total force value of N^2, compared to N for a platform-centric system (Pace 2009, 321).

C. NCW REQUIREMENTS

Among the several prerequisites for establishing a viable NCW operation, bandwidth is arguably the most central: next to a wideband transmit/receive capability to sustain the compression and transportation of large amounts of data, a wideband Local Area Network (LAN) that will process and distribute the data to the various sensors and weapons is required. Along with bandwidth requirements, the issue of *information processing capability* and *information management* is also critical. Having these elements in mind, several questions arise regarding the formation of an NCW architecture (Pace 2009, 322):

- How do different degrees of networking affect the strategic, operational and tactical outcome?

- What is the optimal network topology (physical, virtual, arrangement of nodes)?

- How will the network impact the C2?

126

- What is the correct balance of sensors, shooters and network technology?

- How can degradation of network processing be quantified (i.e., in the event of an electronic attack)?

As Pace notes, the complexity of the relationships between the network space and the battle space makes answering these questions difficult; a schematic depiction is provided in Figure 41.
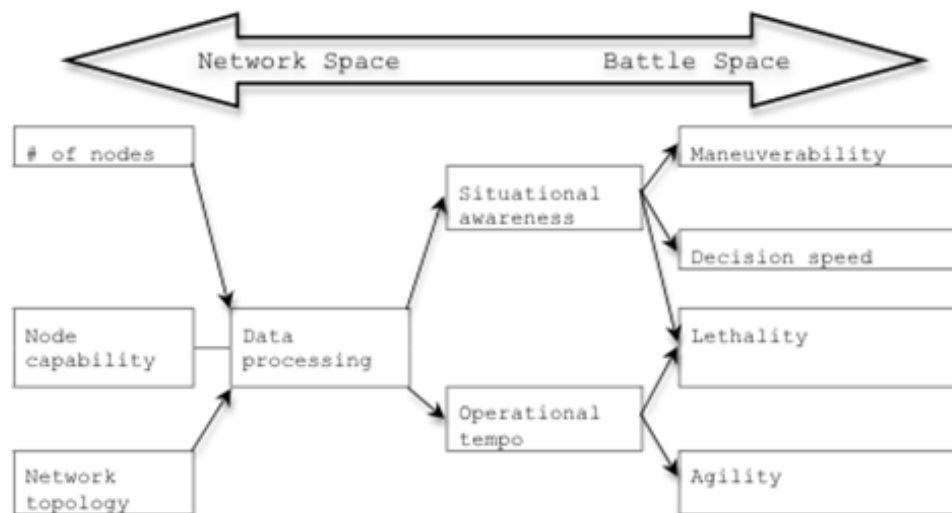
Figure 41. Relationship Between Network Space and Challenges[22]

To establish a solid theoretical foundation prior to quantifying the metrics for information grid analysis, we provide the definitions of the various NCW requirements.

---

[22]Pace 2009, 323.

1. Situational Awareness

Situational awareness is "the ability to have accurate real time information of friendly, enemy, neutral and non-combatant locations; a common, relevant picture of the battlefield scaled to specific levels of interest and special needs" (Stein, Garska and McIndoo 2000).

In practice, situational awareness is built by continuous snapshots that are gathered from the theater of operations and sent to the C2 center. The refreshing of the snapshots, deriving mainly from the number of the nodes and their processing capabilities, results in greater information flow; consequently, situational awareness is mainly determined by information processing capability (Kruse, Adkins and Holloman 2005).

2. Maneuverability

In the NCW context, maneuverability is defined as the capability to perform a strategic or tactical movement. To clarify this generic definition, Pace approaches the maneuverability concept considering three of its properties: speed, safety and cost. The effect of speed on maneuverability is obvious—the greater the speed, the greater the capability of movement. Safety has the opposite effect, as all additional precautions reduce the tempo. Last but not least, high maneuverability networks require complex, and thus, costly assets and structure. Studying the various aspects of battle topology situational awareness, Chen and Pace schematically depict their interaction with maneuverability as shown in Figure 42.

Figure 42.   Maneuverability[23]

3.   Decision Speed and Operational Tempo

The notion of the Observation-Orientation-Decision-Action (OODA) loop was first developed by John Boyd in his monumental work entitled *A Discourse on Winning and Losing*, commonly known as "The Green Book" (Boyd 1987). A central concept in military strategy, the OODA loop is shown in Figure 43.

Figure 43.   OODA Loop

To quantify the maximum network operational tempo—an important attribute when considering the fusion of netted radar data—Pace examines each phase separately. In the observation-orientation phase, the *characteristic tempo* λ_T, is defined as "the speed in which the situational awareness is processed in order to orient (or adjust) the force to

---

[23]Chen and Pace 2008.

the current situation" (Pace2009, 323). Moving to the decision phase, the *decision tempo* λ_c refers to the "speed to make a decision for action", and is mathematically described as the sum of the characteristic tempo λ_T and the deployment tempo λ_d. After the deployment, the overall speed at which the situational response is made is the sum of the characteristic tempo and a *fighting tempo* λ_f. The *maximum operational tempo* Λ_{OODA} is the defined as the inverse of the maximum frequency to complete the OODA cycle.

4. Agility

Highly affecting the operational tempo, agility in the NCW context is defined as "the ability of an organization to sense and respond to advancement opportunities in order to stay ahead and competitive in a turbulent battlefield quickly." To better convey the notion of agility, Pace graphically depicted the interrelation between operational tempo and force agility as in figure 44.

Figure 44.   Operational Tempo vs. Force Agility[24]

---

[24]Pace 2009, 325.

Pace did not provide any formulas or other means to quantify agility, which, along with maneuverability and situational awareness, remain abstract terms in relevant literature.[25] A careful study of the definition and Figure 46 indicate that the higher the operational tempo, the higher the agility of the force.

5. Lethality

Another abstract term utilized by Pace to assess the various NCW requirements is lethality, which is defined as "the ability to damage an enemy" (Pace 2009, 325). Obviously the use of the term is not constrained to the NCW realm but can also pertain to non-netted configuration, that is asset-to asset- confrontation. For the purpose of this thesis, lethality, where used, shall represent a measure of jamming effectiveness against LPI assets, whether in netted configuration or not.

D. METRICS FOR INFORMATION GRID ANALYSIS

As previously discussed, the total capability of the network is greatly affected by the number of nodes. However, quantification of this capability has been difficult to achieve as, among other issues, each node differs significantly from each other; consequently, relevant analysis has often provided misleading results (Ling, Moon and Kruzins 2005). In this section, we introduce the latest metrics designed to quantify the general value inherent in the information network topology.

---

[25] Our research indicates that these terms appear only in Philip Pace's work: Phillip E. Pace, *Detecting and Classifying Low Probabilty of Intercept Radars*, 2nd Edition (Norwood, MA: Artech House, 2009).

1.   Generalized Connectivity Measure

The generalized connectivity measure of a network of sensors or weapons is defined as the sum of the value of all the nodes and their connections scaled by the lengths of the routes and their directionality (P. E. Pace, 2009, 325). Its mathematical expression is (Ling, Moon and Kruzins 2005):

$$C_M(t) = \sum_{\mu=1}^{N_T} K_\mu(t) \sum_{\nu=1}^{N_\mu} \sum_{\gamma=1}^{N_{\mu,\nu}} L_\gamma^{\mu,\nu}(d,t) \quad (6.1)$$

Where:

N_T : The number of nodes in the network

N_μ : The total number of nodes connected to the node μ

$N_{\mu,\nu}$: The total number of possible *routes*[26] connecting the pair of nodes μ and ν.

$K_\mu(t)$: The capability value of node μ; $K_\mu(t) \geq 0$

$L_\gamma^{\mu,\nu}$: The information flow parameter of the route γ connecting nodes μ and ν : $L_\gamma^{\mu,\nu} \geq 0$. It depends on the length of the route and it is also a function of time. The functional dependence of $L_\gamma^{\mu,\nu}$ on the length of the route δ (number of links[27]), can be simplified by separating it into a time independent component, and a time dependent coefficient, scaled by the route length d raised to the

---

[26] The term *route* refers to the possible connection from one node to another.

[27] The term *link* represents the direct connection between any two nodes. One route contains one or more links.

power ξ. The value of $F_\gamma^{\mu,\nu}(t)$, is a minimum of zero and reaches a maximum of one the route γ.. Eqn. (6.1) then becomes:

$$C_M(t) = \sum_{\mu=1}^{N_T} K_\mu(t) \sum_{\gamma=1}^{N_\mu} L_\gamma^{\mu,\nu} \sum_{\gamma=1}^{N_{\mu,\nu}} \frac{F_\gamma^{\mu,\nu}(t)}{(d_\gamma)^\xi} \quad (6.2)$$

2. Reference Connectivity Measure

Reference connectivity measure refers to a fully connected network, that is, a network that has all nodes fully connected with bidirectional links where each of the nodes has a capability value of $K_\mu = 1$: (Ling, Moon and Kruzins 2005). Consequently, the resulting *reference network* has the highest connectivity measure of any network with the same number of nodes.

The reference connectivity measure depends only on the total number of nodes. Its mathematical expression is:

$$C_M^R = N_T(N_T - 1)\left(1 + \frac{N_T - 2}{2} + \ldots + \frac{(N_T - 2)(N_T - 3)\ldots 2 \cdot 1}{N_T - 1}\right) \quad (6.3)$$

The term $N_T(N_T - 1)$ represents the number of possible connections in a given network with N_T nodes. The numerator in each of the terms inside the square brackets is the number of possible routes of the length given in the denominator.

3. Network Reach

Network reach is dimensionless term created to provide a means of normalizing the connectivity measure (Ling, Moon

and Kruzins 2005). As Pace notes, normalization by the reference network allows us to investigate the varying degrees of network connection, the non-identical nodes/links and the effect of broken symmetries (Pace 2009, 329). The latter becomes significant in cases of reduced network performance, such as when evaluating the effect of EA on the whole architecture. The formula for network reach is (Ling, Moon and Kruzins 2005):

$$I_R = \frac{C_M}{C_M^R} \quad (6.4)$$

4.   Extended Generalized Connectivity Measure

The concept of the generalized connectivity measure was developed in order to analyze network architectures with routes not able to maintain full capability in the flow of sensor information (Chen and Pace June 2008). In the network shown in Figure 45, the limited capability value of nodes 2 $\left(K_2 = 0.5\right)$ and 3 $\left(K_3 = 0.5\right)$ constrain the information flow when data follows the route: node 1→ node 2 →node 3.
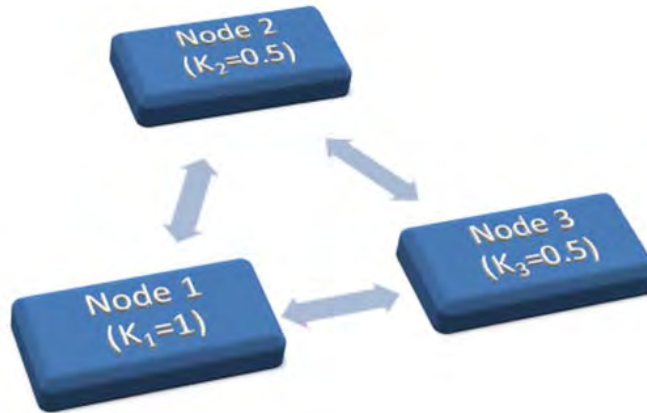
Figure 45.   Three-node Network Example

To account for this limitation, Pace suggests an extended definition of connectivity measure as (Pace 2009, 333):

$$C_{M_e}(t) = \sum_{\mu=1}^{N_T} \sum_{\nu=1}^{N_\mu} \sum_{\gamma=1}^{N_{\mu,\nu}} \frac{K_\gamma F_\gamma^{\mu,\nu}}{d_\gamma} \quad (6.5)$$

Where:

K_γ: The K_μ with the lowest capability value (bottleneck) in route γ.

K_γ considers the starting node and exchangers but not the receiving node because in military networks, many nodes only receive data, without equivalent processing capability for transmitting.

Pace concludes that, by comparing C_M to C_M^R, and by disabling nodes in the reference and the real network and recalculating both values, the robustness of network can be quantified. This comparison can provide a clear representation of the real network under attack (Pace 2009, 333).

5. Entropy and Network Richness

a. Entropy

The concept of entropy is central to our analysis, as it is directly linked to the calculation of the information rate λ. In information theory, *entropy* is a measure of the uncertainty associated with a random variable. The concept of entropy was analytically studied by Claude E. Shannon, who, in his monumental 1948 work on communication signals, studied entropy in the context that

135

quantifies the expected value of information contained in a message. Applying Shannon's approach to net-centric architecture, we note that at each node, the data exchange rate has a direct impact on the operational tempo of the grid. Assuming a set of J possible sample values by:

$$S = \left\{ x_1, x_2, \ldots x_J \right\} \quad (6.6)$$

and assuming that the probability of the source output x_j is p_j, the amount of information sent when the message is transmitted is:

$$I(j) = -log_2(p_j) \quad (6.7)$$

where p_j is the probability of transmitting the message. Shannon's entropy (or uncertainty) of the source is described by the formula:

$$H(S) = E\left\{ I(j) \right\} = -\sum_{j=1}^{J} p_j log_2(p_j) \quad (6.8)$$

The information rate of the source is then:

$$\lambda = \frac{H}{T} \left(bits / sec \right) \quad (6.9)$$

where T is the time required to send the message. A related measure is the channel capacity or:

$$C = Blog_2(1 + SNR)\left(bits / sec \right) \quad (6.10)$$

where B is the channel Bandwidth and SNR the signal-to-noise power ratio (not in dB) at the receiver input (Shannon 1948). Pace notes that the channel capacity can be

used as a unifying principle for both electronic attack (EA) and electronic protection (EP) actions in EW: all EA actions can be considered an attempt to reduce the bandwidth of an adversary signal and/or to reduce the SNR and all EP actions as an attempt to increase bandwidth and/or increase SNR (Pace 2009, 333).

To demonstrate this, Pace provides three examples:

Example 1: When an LPI emitter uses frequency hopping as an EP measure, protection against jamming necessitates a large total bandwidth; if the same emitter wants to protect against interception only, then only a small instantaneous bandwidth is required. In this case, the large total bandwidth makes it difficult for the jammer to set on the transmission frequency, thus limiting the reduction in SNR to that provided by barrage jamming.

Example 2: Applying repeater or gate stealing EA techniques requires a certain reduction of SNR within the bandwidth of the victim's receiver to be effective. The corresponding EP technique might utilize a combination of guards and filters to recognize and eliminate the unwanted jamming signal, thereby protecting the SNR.

Example 3: To avoid adversary exploitation, a LPI emitter uses a very large bandwidth with low average power density, which reduces the probability of intercept. However, the energy over the bandwidth can be summed to extract the information from the signal. Therefore, the transmitter compensates for the low SNR with increased

bandwidth to transmit the information at fast enough rates. The jammer can achieve high SNRs only over small portions of the bandwidth.

b.   *Network Richness*

Within the sensor network, each node is able to process the information at its own rate; by combining the various node information rates, we can quantify the network's richness. The information rate λ_T of a node μ is the rate at which the network information is processed by the node. The minimum information rate λ_μ^{min}, of the node is the minimum rate that information must be processed for generating decision-level knowledge from the sensor network data. From Shannon's information entropy theory, the knowledge function is defined as (Ling, Moon and Kruzins 2005):

$$Q\left(\lambda_\mu\right) = \begin{cases} 0, & \lambda_\mu \geq e\lambda_\mu^{min} \\ ln\left(\dfrac{e\lambda_\mu}{\lambda_\mu^{min}}\right), & \lambda_\mu^{min} < \lambda_\mu < e\lambda_\mu^{min} \\ ln\left(\dfrac{e\lambda_\mu^{min}}{\lambda_\mu^{min}}\right) = 1, & \lambda_\mu \geq e\lambda_\mu^{min} \end{cases} \quad (6.11)$$

Using the knowledge function, Ling et al. defined the network richness R_Q as the average rate at which information entropy (or knowledge) is generated from the network shared data (Ling, Moon and Kruzins 2005):

$$R_Q = \frac{\sum_{\mu=1}^{N_T} \lambda_\mu Q\left(\lambda_\mu\right)}{N_T} \quad (6.12)$$

138

Equation (6.12) leads us to two major observations:

- If a node cannot provide data at a rate above its minimum value , it degrades the overall value $\lambda_\mu Q(\lambda_\mu)$.

- There is little advantage to generating sensor data faster than knowledge can be generated and absorbed.

6. Maximum Operational Tempo

The maximum information exchange rate of a network is determined by the following factors:

- The number of nodes;

- The communication and sensor technologies employed;

- The information data transfer rates, and

- The network topology.

To quantify this rate within an OODA loop, Pace introduces the term *characteristic tempo* λ_T, a concept that relates the network topology to its ability to gather situational awareness. In a net-centric architecture *characteristic tempo* is defined as the product of the network reach I_R and the network richness R_Q (Pace 2009, 336):

$$\lambda_T = I_R R_Q \quad (6.13)$$

Figure 46 shows the tempo parameters of the sensor network OODA loop:

Figure 46.   Time Spent in Each OODA Cycle Phase[28]

The variable Δt_1 represents the time from observation to orientation and is limited by the information exchange time; Δt_2 is the time from orientation to decision and is dominated by the decision speed; Δt_3 is the time from decision to action and must be greater than the information exchange time (command time) and deployment time; Δt_4 is the time from action to observation and is always greater than the sum of information exchange time and fighting time.

The lower limits for each of the Δt_i presented above are as follows:

$$\Delta t_1 \geq \frac{1}{\lambda_T} \quad (6.14)$$

---

[28] Pace 2009, 336.

$$\Delta t_2 \geq \frac{1}{\lambda_{C_2}} \quad (6.15)$$

$$\Delta t_3 \geq \frac{1}{\lambda_T} + \frac{1}{\lambda_d} \quad (6.16)$$

$$\Delta t_4 \geq \frac{1}{\lambda_T} + \frac{1}{\lambda_f} \quad (6.17)$$

Where:

λ_T: Characteristic tempo

λ_{C_2}: Decision tempo

λ_d: Deployment tempo

λ_f: Fighting tempo

Using the aforementioned parameters, the maximum tempo of the network to perform an entire OODA loop (*maximum operational tempo*) can be defined as (Pace 2009, 337):

$$\Lambda_{OODA} \leq \left(\frac{1}{\lambda_T} + \frac{1}{\lambda_{C_2}} + \frac{1}{\lambda_T} + \frac{1}{\lambda_d} + \frac{1}{\lambda_T} + \frac{1}{\lambda_f} \right)^{-1} \quad (6.18)$$

7. Example

To demonstrate the interrelation of the aforementioned parameters, a network-enabled example is provided below: A nuclear submarine (capability value $K_{submarine} = 1$) has launched a cruise missile to destroy an adversary Multiple Launch Rocket System (MLRS) as shown in Figure47.
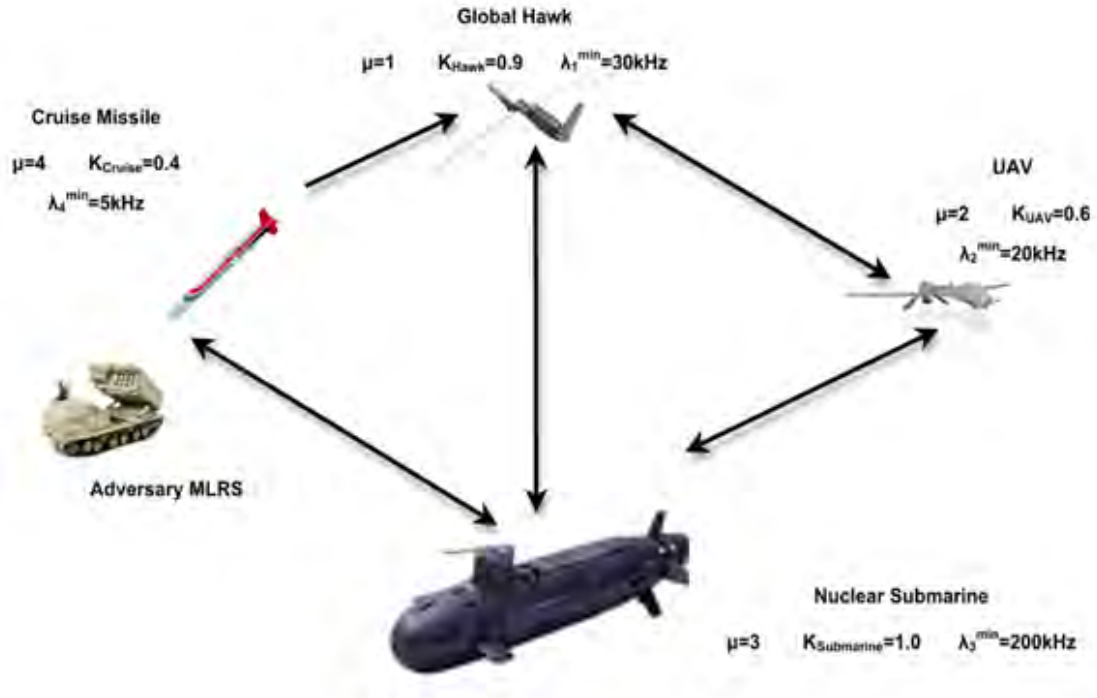
Figure 47.   Network Topology

To follow up with the damage report, a tactical UAV flies to the target and a Global Hawk UAV covers the intelligence, surveillance and reconnaissance (ISR) component. Due to its limited connectivity and signal rerouting options, the cruise missile capability value is assumed to be $K_{cruise} = 0.4$.[29] The Global Hawk also has a limited rerouting capability and is given a capability value of $K_{Hawk} = 0.9$.[30]

Assuming each link to have a flow component of either 1 or 0. (i.e., $F = L = 1,0$), the reference connectivity measure is:

---

[29] Note its unidirectional link to the Global Hawk.

[30] In reality, no tactical UAV is fast enough to follow a cruise missile; the choice of the assets is imaginary and aims at visualizing an operational scenario, not at providing a real-combat configuration.

$$C_M^R = N_T\left(N_T - 1\right)\left[1 + \frac{N_T - 2}{2} + \frac{\left(N_T - 2\right)\cdot\left(N_T - 3\right)}{3}\right] \Rightarrow$$

$$\Rightarrow C_M^R = 4\cdot\left(4-1\right)\left[1 + \frac{4-2}{2} + \frac{\left(4-2\right)\cdot\left(4-3\right)}{3}\right] \Rightarrow C_M^R = 32$$

To calculate the network reach, we break our process into five steps.

Step I: Calculating $\sum\dfrac{F^{1\nu}}{d}$:

$N_{11} = 0$

$N_{12} = 2$	1	2	$\sum\dfrac{F^{12}}{d} = \dfrac{1}{1} + \dfrac{1}{2} = \dfrac{9}{6}$
	1	1	
	2	3	
		2	

$N_{13} = 2$	1	2	$\sum\dfrac{F^{13}}{d} = \dfrac{1}{1} + \dfrac{1}{2} = \dfrac{9}{6}$
	1	1	
	3	2	
		3	

$N_{14} = 2$	1	2	$\sum\dfrac{F^{14}}{d} = \dfrac{1}{2} + \dfrac{1}{3} = \dfrac{5}{6}$
	1	1	
	3	2	
	4	3	
		4	

Step II: Calculating $\sum\dfrac{F^{2\nu}}{d}$:

$N_{21} = 3$	1	2	3	$\sum\dfrac{F^{21}}{d} = \dfrac{1}{1} + \dfrac{1}{2} + \dfrac{1}{3} = \dfrac{11}{6}$
	2	2	2	
	1	3	3	
		1	4	
			1	

$N_{22} = 0$

$N_{23}=2$	1	2	$\displaystyle\sum\frac{F^{23}}{d}=\frac{1}{1}+\frac{1}{2}=\frac{9}{6}$
	2	2	
	3	1	
		3	

$N_{24}=2$	1	2	$\displaystyle\sum\frac{F^{24}}{d}=\frac{1}{2}+\frac{1}{3}=\frac{5}{6}$
	2	2	
	3	1	
	4	3	
		4	

Step III: Calculating $\displaystyle\sum\frac{F^{3v}}{d}$:

$N_{31}=3$	1	2	3	$\displaystyle\sum\frac{F^{31}}{d}=\frac{1}{1}+\frac{2}{2}=\frac{9}{6}$
	3	3	3	
	1	2	4	
		1	1	

$N_{32}=3$	1	2	3	$\displaystyle\sum\frac{F^{32}}{d}=\frac{1}{1}+\frac{1}{2}+\frac{1}{3}=\frac{11}{6}$
	3	3	3	
	2	1	4	
		2	1	
			2	

$N_{33}=0$

$N_{34}=3$	1	$\displaystyle\sum\frac{F^{34}}{d}=\frac{1}{1}=\frac{6}{6}$
	3	
	4	

Step IV: Calculating $\displaystyle\sum\frac{F^{4v}}{d}$:

$N_{41}=3$	1	2	3	$\displaystyle\sum\frac{F^{41}}{d}=\frac{1}{1}+\frac{1}{2}+\frac{1}{3}=\frac{11}{6}$
	4	4	4	
	1	3	3	
		1	2	
			1	

$N_{42}=3$	1	2	3	$$\sum\frac{F^{42}}{d}=\frac{2}{2}+\frac{1}{3}=\frac{8}{6}$$
	4	4	4	
	1	3	3	
	2	2	1	
			2	

$N_{43}=3$	1	2	3	$$\sum\frac{F^{43}}{d}=\frac{1}{1}+\frac{1}{2}+\frac{1}{3}=\frac{11}{6}$$
	4	4	4	
	3	1	1	
		3	2	
			3	

$$N_{44}=0$$

Step V: The network reach will be:

$$I_R=\frac{1}{C_M^R}C_M\Rightarrow I_R=\frac{1}{C_M^R}\left[\sum_{\mu=1}^{N_T=4}K_\mu\sum_{\gamma=1}^{N_{\mu\nu}}\frac{F_\gamma^{\mu\nu}}{d}\right]\Rightarrow$$

$$\Rightarrow I_R=\frac{1}{C_M^R}\left[K_1\sum\frac{F^{1\nu}}{d}+K_2\sum\frac{F^{2\nu}}{d}+K_3\sum\frac{F^{3\nu}}{d}+K_4\sum\frac{F^{4\nu}}{d}\right]\Rightarrow$$

$$\Rightarrow I_R=\frac{1}{32}\left[0.9\cdot\frac{23}{6}+0.6\cdot\frac{25}{6}+1\cdot\frac{26}{6}+0.4\cdot\frac{30}{6}\right]\Rightarrow I_R\cong0.3838$$

This example manifests the centrality of two elements in the network reach concept regarding a net-centric architecture: the number of nodes and the capability value. The number of nodes affects the network reach, and thus the overall performance of the network by means of the parameter $\sum\frac{F^{\mu\nu}}{d}$; if we increase the number μ of nodes, the square bracketed term in the previous relationship will

increase accordingly. The capability value affects the bracketed term by means of altering the multiplying factor K_i inside it.

As the capability value K_i is the parameter that is mostly affected by EA, to better comprehend its impact on network performance, we recalculate the network reach assuming that a hostile jammer degrades the Global Hawk performance into $K_{Hawk} = 0.6$, and the UAV performance into $K_{UAV} = 0.4$; the new value will be:

$$I_R = \frac{1}{C_M^R} C_M \Rightarrow I_R = \frac{1}{C_M^R} \left[\sum_{\mu=1}^{N_T=4} K_\mu \sum_{\gamma=1}^{N_{\mu\nu}} \frac{F_\gamma^{\mu\nu}}{d} \right] \Rightarrow$$

$$\Rightarrow I_R = \frac{1}{C_M^R} \left[K_1 \sum \frac{F^{1\nu}}{d} + K_2 \sum \frac{F^{2\nu}}{d} + K_3 \sum \frac{F^{3\nu}}{d} + K_4 \sum \frac{F^{4\nu}}{d} \right] \Rightarrow$$

$$\Rightarrow I_R = \frac{1}{32} \left[0.6 \cdot \frac{23}{6} + 0.4 \cdot \frac{25}{6} + 1 \cdot \frac{26}{6} + 0.4 \cdot \frac{30}{6} \right] \Rightarrow I_R \cong 0.3219$$

The situation can be exacerbated if the EA is so effective that it ultimately takes one link down. Assuming that the link removed is the one connecting the aircraft carrier to the cruise missile, the network topology will be as follows:
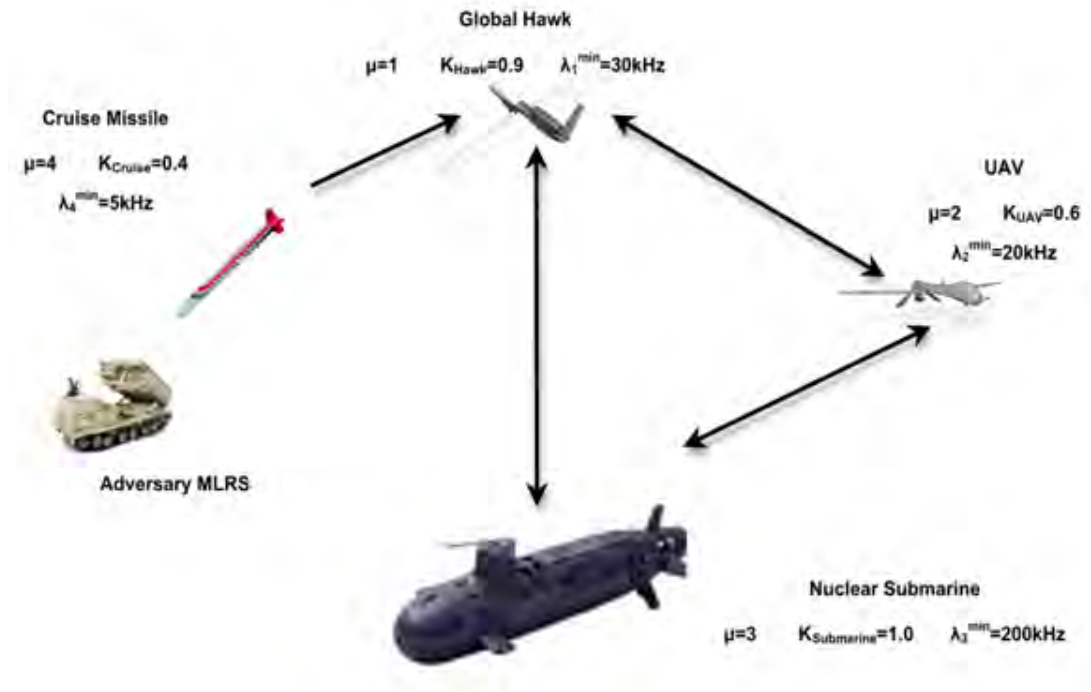
Figure 48. Network Topology after EA

Since the number of nodes is unaltered, the reference connectivity measure remains the same:

$$C_M^R(EA) = 32$$

To calculate the new network reach, we work similarly:

Step I: Calculating $\sum \dfrac{F^{1v}}{d}$:

$$N_{11} = 0$$

	1	2	
$N_{12} = 2$	1	1	$\sum \dfrac{F^{12}}{d} = \dfrac{1}{1} + \dfrac{1}{2} = \dfrac{9}{6}$
	2	3	
		2	

	1	2	
$N_{13} = 2$	1	1	$\sum \dfrac{F^{13}}{d} = \dfrac{1}{1} + \dfrac{1}{2} = \dfrac{9}{6}$
	3	2	
		3	

147

$N_{14} = 0$

Step II: Calculating $\sum \dfrac{F^{2v}}{d}$:

<table>
<tr><td rowspan="4">$N_{21} = 2$</td><td>1</td><td>2</td><td rowspan="4">$\sum \dfrac{F^{21}}{d} = \dfrac{1}{1} + \dfrac{1}{2} = \dfrac{9}{6}$</td></tr>
<tr><td>2</td><td>2</td></tr>
<tr><td>1</td><td>3</td></tr>
<tr><td></td><td>1</td></tr>
</table>

$N_{22} = 0$

<table>
<tr><td rowspan="4">$N_{23} = 2$</td><td>1</td><td>2</td><td rowspan="4">$\sum \dfrac{F^{23}}{d} = \dfrac{1}{1} + \dfrac{1}{2} = \dfrac{9}{6}$</td></tr>
<tr><td>2</td><td>2</td></tr>
<tr><td>3</td><td>1</td></tr>
<tr><td></td><td>3</td></tr>
</table>

$N_{24} = 0$

Step III: Calculating $\sum \dfrac{F^{3v}}{d}$:

<table>
<tr><td rowspan="3">$N_{31} = 2$</td><td>1</td><td>2</td><td rowspan="3">$\sum \dfrac{F^{31}}{d} = \dfrac{1}{1} + \dfrac{1}{2} = \dfrac{9}{6}$</td></tr>
<tr><td>3</td><td>3</td></tr>
<tr><td>1</td><td>2</td></tr>
<tr><td></td><td>1</td></tr>
</table>

<table>
<tr><td rowspan="3">$N_{32} = 2$</td><td>1</td><td>2</td><td rowspan="3">$\sum \dfrac{F^{32}}{d} = \dfrac{1}{1} + \dfrac{1}{2} = \dfrac{9}{6}$</td></tr>
<tr><td>3</td><td>3</td></tr>
<tr><td>2</td><td>1</td></tr>
<tr><td></td><td>2</td></tr>
</table>

$N_{33} = 0$

$N_{34} = 0$

Step IV: Calculating $\sum \dfrac{F^{4v}}{d}$:

<table>
<tr><td rowspan="3">$N_{41} = 2$</td><td>1</td><td rowspan="3">$\sum \dfrac{F^{41}}{d} = 1$</td></tr>
<tr><td>4</td></tr>
<tr><td>1</td></tr>
</table>

	1	2	
$N_{42} = 2$	4	4	$\sum \dfrac{F^{42}}{d} = \dfrac{1}{2} + \dfrac{1}{3} = \dfrac{5}{6}$
	1	1	
	2	3	
		2	

	1	2	
$N_{43} = 2$	4	4	$\sum \dfrac{F^{43}}{d} = \dfrac{1}{2} + \dfrac{1}{3} = \dfrac{5}{6}$
	1	1	
	3	2	
		3	

$$N_{44} = 0$$

The new network reach will be:

$$I_R^{EA_2} = \frac{1}{C_M^R} C_M \Rightarrow I_R^{EA_2} = \frac{1}{C_M^R} \left[\sum_{\mu=1}^{N_T=4} K_\mu \sum_{\gamma=1}^{N_{\mu\nu}} \frac{F_\gamma^{\mu\nu}}{d} \right] \Rightarrow$$

$$\Rightarrow I_R^{EA_2} = \frac{1}{C_M^R} \left[K_1 \sum \frac{F^{1\nu}}{d} + K_2 \sum \frac{F^{2\nu}}{d} + K_3 \sum \frac{F^{3\nu}}{d} + K_4 \sum \frac{F^{4\nu}}{d} \right] \Rightarrow$$

$$\Rightarrow I_R^{EA_2} = \frac{1}{32} \left[0.6 \cdot \frac{18}{6} + 0.4 \cdot \frac{18}{6} + 1 \cdot \frac{18}{6} + 0.4 \cdot \frac{16}{6} \right] \Rightarrow I_R^{EA_2} \cong 0.2208$$

The performance of the network is significantly lower in the presence of EA, as expected, since a crucial network link was taken out. In comparative terms, the example renders clearly that the absence of a link affects the performance of the network; in this case by a factor of approximately 68% (0.3219 compared to 0.2208). The deficiency of the "network reach" term, as introduced and defined by Pace, lies in the fact that there is no absolute value that can be used as a reference for evaluation. In other terms, it is a useful tool of evaluating similar, or nearly similar networks, but provides no clue regarding the performance of an individual network.

E.   NETTED LPI RADAR SYSTEMS

Despite recent advantages in mono-static radar systems (collocated single transmitter and receiver), two major disadvantages are inherent: they offer little to counter stealth technology and they only offer a single perspective for each radar (Hume and Baker October 2001). The development of stealth technology has primarily been aimed at defeating the mono-static radar by the use of absorbing materials and non-reflective structural designs that minimize the scattered energy reflected into the hemisphere, in the direction from which the signal arrives. The limited energy returned to the emitter from the stealth target makes it very difficult to detect the target. In addition, due to terrain obscuration, ground based or low-flying mono-static radar systems often do not have a line of sight (LOS) to the target and therefore cannot provide detection.

Due to this single perspective, the richer information contained in multiple perspectives is missed. When a number of cooperative radar systems are distributed spatially and networked together, they can provide the opportunity to view the target from a number of different aspect angles. In multi-frequency radar networks, each radar performs a significant amount of local preprocessing. Outcomes of the local preprocessing can then be delivered to a central processor through a communication link. The preprocessing limits the amount of information that needs to be passed on to make a final detection decision. These systems use

different frequencies to cope with interference rejection, but each receiver is unable to process the information from all transmitters.

Netted radar systems, sometimes referred to as Multiple-Input-Multiple-Output (MIMO) radar systems, consist of a number of distributed radar systems (transmit and receive sensors) each having the ability to transmit independent orthogonal waveforms (to avoid interference) and the ability to receive and process synchronously all waveforms that are transmitted. Figure 49 depicts an example of a MIMO netted radar system with three radar nodes connected by a network:
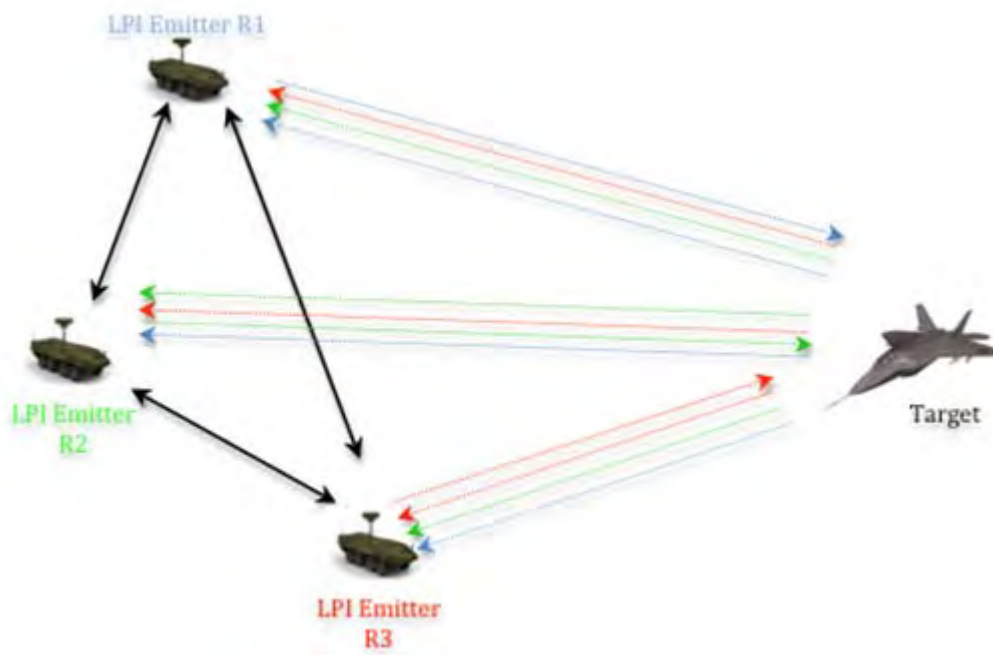
Figure 49.   Three-node MIMO Netted Radar System[31]

All three radars have acquired and are tracking the target with their antenna beams. The LPI Emitters R1, R2,

---

[31]Pace 2009, 346.

and R3 each transmit a different waveform but receive and process all three waveforms that are collected from the target. The use of the network allows each node to share its target information non-coherently (using orthogonal waveforms) or coherently. The implementation of networked radar systems has become feasible due to recent advantages in large bandwidth wireless networks, high capacity transmission lines, multichannel electronically scanned antennas, high-speed, low-cost digital processors, and precise synchronization systems (Teng et al. 2007).

VII. NETTED RADAR SYSTEMS -- ADVANTAGES AND DISADVANTAGES

A.   MULTISITE RADAR SYSTEMS CATEGORIZATION

A Multisite Radar System (MSRS) is one that includes several spatially separated transmitting, receiving and/or transmitting-receiving facilities where information of each target from all sensors are fused and jointly processed (Chernyak 1998, 3). This definition covers both multi-static radars (radars that have one transmitter and several receiving stations spatially separate from each other) as well as multi-radar systems that are comprised of many transceiver radars spatially separate from with each other. The latter is also called a netted radar system.

Netted radar systems can be realized by the interconnecting different types of transceiver radars. This thesis examines netted radar systems realized by interconnecting several LPI radars (netted LPI radars).

The two main differences between netted LPI radar systems and a single LPI radar are the several spatially separated stations (LPI radars) and the fusion (joint processing) of the target information. These two features give netted LPI radars their main benefits.

MSRSs can be further classified by the following attributes (Chernyak 1998, 3-6).

1.   Type of Targets of Interest

These can be divided into active, passive and active/passive. This classification is heavily dependent on the characteristics of the target of interest. If the

target is a radiating target then it can be served by a passive MSRS; if the target is non-radiating it can be served by an active MSRS. The active/passive MSRS can serve both radiating and non-radiating targets.

2.   The Degree of Spatial Coherence

The spatial coherence of an MSRS is the ability to maintain a strong dependence between signal RF phases between separated stations[32]. Spatial coherence of an MSRS is actually the phase stability of its equipment. MSRSs are classified into three categories.

a.   *Spatially Coherent MSRSs*

These provide almost full utilization of the electromagnetic field spatial structure. They require precise time synchronization, precise frequency control and precise phase control; this demands they be implemented with many stations (several dozen or more), creates difficulties in the inter-station phasing implementation, and are very complicated and expensive to build. To build such MSRSs, usually the designers keep the station base-length small, which leads to the loss of critical waveform information by the MSRSs and thus reduces the advantages of the spatial coherence.

b.   *Short-Term Spatial Coherent MSRSs*

In these MSRSs the equipment phase stability is maintained within short time intervals, mainly for the used

---

[32] We must distinguish between the spatial coherence of the MSRS and the spatial coherence of the signal at the inputs of the MSRS receiving stations. The latter depends on the baselengths between stations, signal wavelength, target size and fluctuation of the propagating medium.

signal duration at least. The inter-station phase shifts are assumed to be random and mutually independent and in this context they do not contain useful information. The joined signal processing in these kinds of MSRSs can use all the information contained in the signal complex envelopes in plots and tracks from different stations. Consequently they do not require inter-station phase control, but they require time synchronization and frequency control. These facts permit their implementation with a few stations only, reducing complexity and implementation cost compared with the spatially coherent system. The resolution and accuracy characteristics no longer depend on carrier frequency, but on frequency bandwidth. The loss of information--compared to the spatially coherent system--can be compensated for by increasing the baselines.

c. *Spatially Incoherent MSRSs*

In these MSRSs, the inter-station phase information and its changes in time are not used. They utilize information contained only in signal real envelope relations, plots and tracks from separated stations. Only time synchronization of the separated stations is necessary. These types of MSRSs are much simpler than the other types of MSRSs but due to the loss of the phase information there are certain power and information losses. Of course, the spatial incoherence does not rule out the temporal coherence of each station before information fusion (e.g., measurement of Doppler shifts and target

155

radial velocity in each radar). Table 9 summarizes the characteristics of the degree of spatial coherence design criterion of an MSRS.

MSRS Type	Advantages	Disadvantages
Spatially coherent	• Full utilization of the EM field spatial structure.	• Require precise time synchronization, frequency control and phase control • Complicated. • Expensive. • Require many stations (radars).
Short term Spatially coherent	• Utilize the information contained in the signal complex envelopes • Do not require inter-station phase control • Implementation with a few stations only • Reduced complexity and implementation cost compared with the spatially coherent ones	• They require precise time synchronization and frequency control.
Spatially incoherent	• Utilize information containing only in signal real envelope • Only time synchronization of the separated stations is necessary • They are simpler than the other types of MSRSs • They have the least cost compared to the other types of MSRSs.	• There are certain power and information losses due to the loss of the phase information.

Table 9.   Degree of Spatial Coherence Summary

3. Information Fusion Level

MSRSs can be categorized into four classes. In each class, both analog and digital transmission lines can be used.

a. *Radio Signal Integration Level*

All signals, noise and interference are subject to joint processing. Information is either transmitted immediately by the stations as raw data or after preliminary linear filtering. This type of fusion level requires high capacity wideband transmission lines.

b. *Video Signal Integration Level*

After phase elimination at each station, all signals, noise and interference are subject to joint processing. The required capacity of the transmission lines is slightly reduced but there are certain power and especially information losses. This type of fusion leads to no spatial coherence, which is why it's seldom used.

c. *Plot[33] Integration Level*

There is initial information processing at the station level (signal thresholding and parameter estimation) and only useful information is transmitted for fusion. The partial processing done at the stations has to do with the preliminary decision of existence or not of a target; the final decision is made at the fusion center

---

[33] A *plot* is a result of individual target detection and parameters measurement or a measurement of target's coordinates and their derivatives when an "instantaneous" target state is estimated without taking into account previous measurement results.

(decentralized or distributed detection). This in effect reduces greatly the required capacity of the transmission lines.

d. Track Integration Level

Apart from the initial information processing at the station level, secondary information processing occurs resulting in target track information. Those track data are then transferred to the fusion center where false tracks are eliminated and true track parameters are estimated more accurately. The required transmission line capacity is similar to the plot integration level. Table 10 summarizes the characteristics of the information fusion level design criterion of an MSRS.

MSRS Type	Advantages	Disadvantages
Radio signal	• No information losses.	• Require high capacity transmission lines. • Require complicated fusion processing.
Video signal	• All information but phase is transmitted to the fusion center.	• Require high capacity transmission lines but with less capacity than those for radio signals. • There cannot be spatial coherence with this type of fusion.
Plot	• Only useful information is transmitted to the fusion center (plot). • Require low capacity transmission lines.	• Reduced power and information characteristics of the MSRS.
Track	• Only track data are transmitted to the fusion center. • Require low capacity transmission lines.	• Reduced power and information characteristics of the MSRS

Table 10.   Information Fusion Level Summary

4.   Degree of Autonomy of Signal Reception

MSRSs can be categorized into three classes; in each class both analog and digital transmission lines can be used.

a.   Independent (Autonomous) Signal Reception

Stations (radars) of this MSRS type are designed to receive scattered signals from targets illuminated by the same radar only. These are generally spatially incoherent MSRSs that use the plot or track level of fusion. They are often called netted radar.

159

b.   *Cooperative Signal Reception*

Stations (radars) of such an MSRS are designed to receive and process echoes from targets illuminated by any radar or MSRS station. They provide better power and information characteristics than do independent ones. An example of such an MSRS is a multi-static radar with one transmitting and many receiving stations.

c.   *Independent - Cooperative Signal Reception*

Stations (radars) of such an MSRS are designed to do both independent and cooperative signal reception.

5.   Station Location and Mobility

MSRSs can be categorized into five classes.

a.   *Ground-Based MSRSs With Stationary Stations*

These systems, even though they may be comprised of mobile ground stations, require the stations' positions to be fixed during MSRS operation.

b.   *Ground-based MSRSs With Mobile Stations*

These systems are comprised of mobile ground stations that can change positions during the MSRS operation.

c.   *Transmitter (or Receiver) on Platforms, Receiver (or Transmitter) Ground-based.*

These systems have one part of the MSRS (transmitter or receiver) on a platform (i.e., aircraft, satellite) and the other (receiver or transmitter respectively) fixed on the ground.

d.   *All Stations on Platforms*

All stations (transmitters, receivers or transceivers) are placed on platforms (aircraft, vehicles, satellites).

e.   *Shipborne*

All stations (transmitters, receivers or transceivers) are placed on ships.

B.   ADVANTAGES OF MULTISITE RADAR SYSTEMS

The advantages of a MSRS system over a mono-static radar or a number of radars that are not integrated in a system are briefly discussed here (Chernyak 1998, 9–21; Pace 2009).

1.   Capability to Form Coverage Area of Required Configuration for Expected Environments

It is apparent that the actual geometry of an MSRS (that can also be tailored to each specific application), in combination with the fusion algorithms that are used, gives an area coverage advantage over a mono-static radar or a system of radars that are not integrated.

2.   Power Advantages

Adding transmitting and/or receiving stations to a mono-static radar (and thus forming an MSRS) upgrades the total power and/or sensitivity of the system. There are also some other significant advantages in the case of cooperative signal reception (as described in paragraph 4.b above), where if the baseline distances are sufficiently long or when the target is illuminated by sufficiently separated stations, there is a significant power gain due

to fluctuation smoothing. That gain can also be obtained by MSRSs that apply independent signal reception (as described in paragraph 4.a above) but use different carrier frequencies.

3.   Detection of Stealth Targets

Stealth technology primarily aims to defeat the mono-static radar by the use of radar absorbing materials (RAM) and non-reflective structural designs that minimizes the scattered energy reflected back into the hemisphere from which the signal arrives. Most stealth assets are designed to hide their front aspect angle from radar. Having a netted radar system (MSRS) (which covers an area from various aspect angles), can in effect negate the advantage of a stealth asset because some number of the stations comprising the MSRS will view the target from a number of different aspect angles.

4.   High Accuracy of the Position Estimation of a Target

An MSRS can estimate target coordinates through range measurements from several spatially separated stations (either several mono-static netted radars or multi-static radar system). As one can see in Figure 50, for the respective MSRS category (netted mono-static and multi-static) the resulting error after the fusion is the intersection of the individual errors.
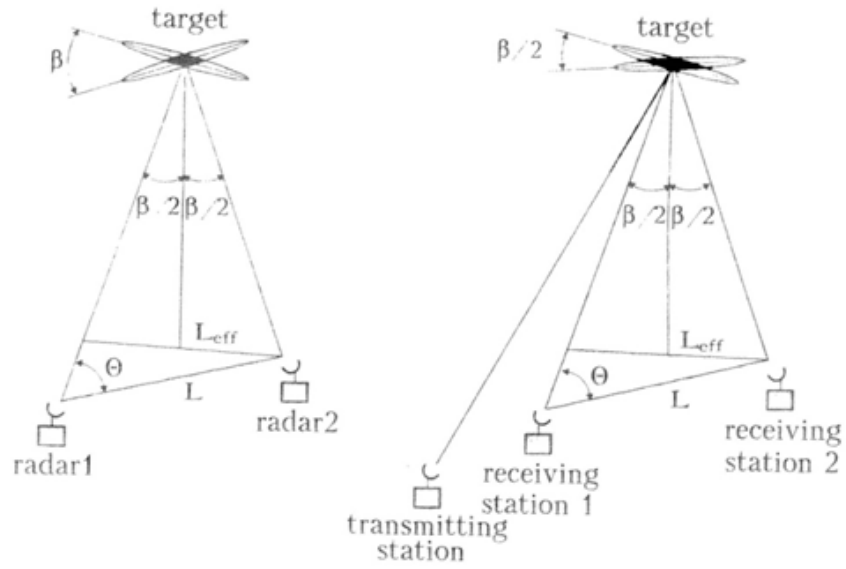
Figure 50.   Netted Mono-static (left) Multi-static (right) Increase of Angular Coordinate Measurement Accuracy[34]

The formulas for calculating this error for the two cases are:

$$\sigma_\theta = \sigma_R \sqrt{\frac{2}{L\sin\theta}} \approx \sigma_R \sqrt{\frac{2}{L_{\mathit{eff}}}} \quad (7.1)$$

$$\sigma_\theta = \sigma_{R\Sigma} \sqrt{\frac{2}{L_{\mathit{eff}}}} \approx 2\sqrt{\frac{2\sigma_R}{L_{\mathit{eff}}}} \quad (7.2)$$

Where:

σ_θ: RMS error of angle estimation in the bi-static plane

σ_R: RMS error of range measurements

L: Baselength (distance between radars)

L_{eff}: Effective baselength

---

[34]Chernyak 1998, 10.

$\sigma_{R\Sigma}$: RMS error of range sum measurements

c : Speed of light

σ_{T} : RMS error of time arrival

Equations (7.1) and (7.2) suggest that if the range measurements are very accurate (e.g., wideband signals such as FMCW are used and thus σ_{R} decreases) or the stations have large baselengths (L_{eff} increases) we can achieve a very low RMS error of angle estimation compared to a single mono-static radar.

In cases where the baselengths are small or the range measurements are not that accurate, there is no significant improvement in the angular accuracy. In that event the bearing measurements of the separate stations play the major role in angle accuracy improvement.

Redundant measurements of the targets coordinated can also be used for position accuracy refinement as well as for higher tracking accuracy when in a tracking mode of operation.

5. Possibility of Estimating Target's Velocity and Acceleration Vectors by the Doppler Method

By performing Doppler frequency shift measurements at several spatially separate stations, one can estimate the velocity vector of a target. That fact is of great importance for accurate target tracking. Consider the case depicted in Figure 51.
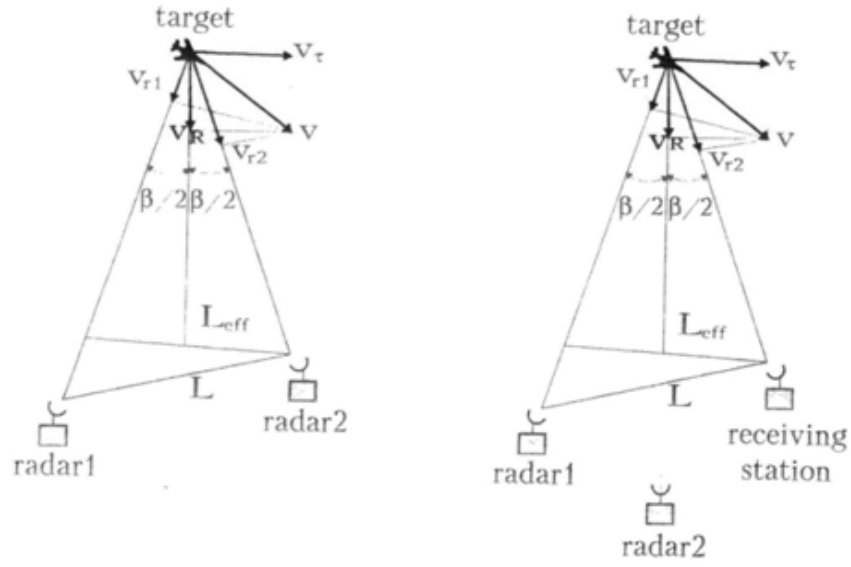
Figure 51.   Netted Mono-static (left) Multi-static
(right) Target Velocity Vector Measurement by the
Doppler Method[35]

For the configuration in Figure 51:

$$F_{D1} = \frac{2V_{r1}}{\lambda} \quad (7.3)$$

$$F_{D2} = \frac{2V_{r2}}{\lambda} \quad (7.4)$$

$$\sigma_{vR} = \sigma_F \left[\frac{\lambda/2}{\sqrt{2} \cdot \cos(\beta/2)} \right] \approx \sigma_F \frac{\lambda}{2\sqrt{2}} \quad (7.5)$$

$$\sigma_{v\tau} = \sigma_F \left[\frac{\lambda/2}{\sqrt{2} \cdot \sin(\beta/2)} \right] \approx \sigma_F \frac{\lambda}{\sqrt{2}} \frac{R}{L_{eff}} \quad (7.6)$$

Where:

F_{D1} : Doppler frequency measures by radar 1

_____

[35]Chernyak 1998, 12.

F_{D2}: Doppler frequency measures by radar 2

V_{r1}: Target radial velocity with respect to radar 1

V_{r2}: Target radial velocity with respect to radar 2

V_R: Target radial velocity

V_τ: Target tangential velocity

σ_F: RMS error of Doppler frequency measurement (assumes the same for both radars)

σ_{vR}: RMS error of target's radial velocity

$\sigma_{v\tau}$: RMS error of target's tangential velocity

λ: Wavelength

R: Target range

L: Baselength (distance between radars)

L_{eff}: Effective baselength

For the above formula approximations it is assumed that the effective baselength is much less than the target range ($R/L_{eff} >> 1$).

In the case of a single radar (i.e., radar 2 in the left part of the Figure 51), we get the following results:

$$F_D = \frac{2V_R \cos(\beta/2)}{\lambda} \quad (7.7)$$

$$\sigma_{vR} = \sigma_F \left[\frac{\lambda}{2\cos(\beta/2)} \right] \approx \frac{\lambda\sigma_F}{2} \quad (7.8)$$

$$\sigma_{v\tau} = \sigma_F \left[\frac{\lambda}{\sqrt{2}\cdot\sin(\beta/2)} \right] \approx \sigma_F \lambda\sqrt{2}\,\frac{R}{L_{eff}} \quad (7.9)$$

From the above equations, we can see that in the case of single radar σ_{vR} increases by a factor of $\sqrt{2}$ and increases $\sigma_{v\tau}$ by a factor of 2. By estimating the speed of the Doppler shift variations or by differentiating the velocity vector components one can get the target's acceleration vector, which promotes track accuracy and tracking quality in general, especially when the target is maneuvering aggressively.

6. Capability to Measure Three Coordinates and Velocity Vector of Radiation Sources

Mono-static and bi-static radars can determine only signal direction of arrival (DOA) when operating in a passive mode with a frequency compatible radiating target (bearing of the radiation source). In contrast, MSRSs in passive mode can obtain three coordinates as well as their derivatives. This can be done by triangulation and/or hyperbolic methods. As discussed in paragraphs 4 and 5, an MSRS comprised of four or more stations can obtain all three components of the source velocity vector simply by Doppler frequency shift measurements. Using triangulation we can estimate the source velocity by differentiating the position estimates only.

The aforementioned capability (determination of targets coordinates and velocity vector) is a very important feature especially in the case of self-screening jamming where the target is revealed by its own jammer (home on jammer).

7.   Increase of Resolution Capability

In order to demonstrate this capability we will consider a simple case scenario involving an MSRS comprised of two mono-static radars that have the same angle and range resolution.

Figure 52.   Angular Resolution of MSRS[36]

We assume that in the aforementioned setup radar 1 cannot resolve the two targets because they lie in the same angle and range resolution cell, whereas radar 2 can resolve them. The equivalent angular resolution of the two

---

[36]Chernyak 1998, 15.

radars, when target range R is several times greater than L_{eff} ($R/L_{eff} \gg 1$) is:

$$\delta\theta \approx \frac{\delta R}{L_{eff}} = \frac{c}{2L_{eff}\Delta F} \quad (7.10)$$

Where:

$\delta_R = c/\Delta F$: Angular resolution of each radar (assume same radar)

c: Speed of light

ΔF: Radar signal bandwidth

L_{eff}: Effective baselength

If instead of two mono-static radars we had one mono-static (transceiver) and one receiving station, then, assuming $R/L_{eff} \gg 1$, the equivalent angular resolution of the two radars is:

$$\delta\theta \approx \frac{\delta R}{L_{eff}} = \frac{c}{L_{eff}\Delta F} \quad (7.11)$$

It is obvious from the formulas (7.10) and (7.11) that when the product $L_{eff}\Delta F$ is large enough, the beamwidth of an MSRS is much less than the beamwidth of a usual antenna (i.e., for parabolic reflectors $\delta\theta > BW_{3dB}$). In cases where the angle between the baseline L and the target direction is small, the L_{eff} decreases significantly and the product $L_{eff}\Delta F$ is decreased as well resulting in lower angular resolution.

In MSRSs that perform passive triangulation, the resolution is determined by the intersection of the antenna beamwidths. When $R/L_{eff} \gg 1$ the respective formulas for range resolution and angle resolution are:

$$\delta R \approx \frac{R^2}{L_{eff}\delta\alpha} \quad (7.12)$$

$$\delta\theta \approx R\delta\alpha \quad (7.13)$$

Where:

$\delta\alpha$: Antenna beamwidth of receiving stations

In MSRSs that use the hyperbolic method the resolution is determined by the extent of the of the envelope's main lobe of the signal mutual correlation function (expressed as delay $\delta\tau \approx 1/\Delta F$ or range difference $\delta R \approx c/\Delta F$). When $R/L_{eff} \gg 1$, the respective formulas for range resolution and angle resolution are:

$$\delta\theta \approx \frac{\delta R}{L_{eff}} = \frac{c}{L_{eff}\Delta F} \quad (7.14)$$

$$\delta R \approx \frac{R^2\delta(\Delta R)}{L_{eff}^2} \approx \frac{R^2 c}{L_{eff}^2\Delta F} \quad (7.15)$$

It has to be noted that high spatial resolution can be achieved only for spatially correlated signals at the inputs of the stations; when stochastic signals at the inputs of the stations are uncorrelated spatial resolution cell cannot be formed.

8.   Increase of Target Handling Capacity

Handling capacity is the maximum number of targets that a given radar can handle in a certain time interval.

Mechanical scanning radars scan in a constant rate determined by the antenna servo electronics. Their handling capacity is limited by the processing hardware and software. Electronically scanning radars have better handling capacity than do mechanical ones, by using electronically scanning antennas. Their handling capacity is limited by the processing hardware and software, and by their power and accuracy characteristics. Since processing resources of such radars are usually very high, the main limiting factor is power. An approximate formula that describes the relation of target handling capacity versus power of electronically scanning radar is as follows.

$$n_t = \frac{P_{tr}T}{\Delta E} = \frac{kP_{ave}T}{\Delta E} \quad (7.16)$$

Where:

n_t : Number of simultaneous tracked targets

P_{tr} : Mean power allowed for target tracking ($P_{tr} = kP_{ave}$)

T : Average time interval between illuminations to maintain track

ΔE : Transmitted energy per illuminations

P_{ave} : Average radar power

k : Coefficient determining the fraction of average radar power used for radar tracking ($k < 1$)

It is suggested from equation (7.16) above that an MSRS having several transmitting stations can achieve higher P_{ave}, so it can have increased target handling capacity. Even in the case of the same P_{ave} an MSRS, by better position measurement accuracy and velocity vector estimation, can increase significantly the time interval between illuminations T. This further increases target handling capacity

9. Increase of "Signal Information" Body

Signal information refers to the information extracted from the target echoes (geometrical and physical target characteristics, target movement about its center of mass, etc.). When the target is observed by many stations almost simultaneously, its signal information body is significantly larger than when the target is observed by one mono-static radar. By measuring amplitudes, phases and polarization parameters of signals received by spatially separate stations (MSRS stations), a target's size, form and relative movement (about its center of mass) can be estimated with higher accuracy and in a shorter time interval (as demonstrated in the previous paragraphs).

10. Increase of Jamming Resistance

MSRSs can use the same anti-jamming methods used by mono-static radars on an individual (per station) basis. To effectively increase their resistance to jamming, MSRSs have several inherent features and can make use some other specific techniques.

172

a. *Resistance to Sidelobe Jamming*

Sidelobe cancellation can be easily performed in an MSRS[37], whereas it is more difficult for a mono-static radar.   In this way, sidelobe noise-like jamming can be effectively defeated.

b. *Resistance to Main Lobe Jamming*

When the MSRS station is a transceiver station, a jammer can effectively jam its main lobe (using various techniques as against a mono-static radar) resulting in the loss of target information. This state of play changes dramatically in favor of the station when the station is passive (receiving only or in transceiver in passive mode), because the direction from the jammer to the station is not known.

In the case of main lobe jamming of a number of spatially separate stations (transceiving stations whose bearing can be located by the jammer), the jammer has to divide its available power to all of those stations (spreading its power to a much larger solid angle). The result is low jamming signal power density at each station, which is relatively easier for each station to overcome. The same effect occurs when the stations are passive and the jammer cannot determine station direction; it therefore

---

[37]Sidelobe cancelation can be performed by adaptive interference cancelation. This function monitors the received signal and identifies interference when present. Several antenna elements (the actual radiating and receiving components) are combined to form a null or cancelation in the direction of the interference. That procedure is easier to perform in an MSRS that already has many transceiving components (antennas of each of the nodes) than in a mono-static radar. There are ways to perform this function in a mono-static radar that has Active Electronically Steering Array (AESA) antenna in combination with additional antennas (specific for this purpose), but in the case of an MSRS it is an inherent feature of the radar net.

has to spread its power to a large solid angle, again resulting in low jamming power density at each station.

When the MSRS stations also transmit in different frequencies, then the jammer is in an even worse situation, because apart from the wide solid angle it has to spread its power to different narrow frequency bands, which further decreases the jamming power density at each station. Such MSRSs are virtually immune to narrowband jamming and much less vulnerable to deception and repetitive pulse jamming.

In the special case of spatially coherent and short-term spatially coherent MSRSs, which have the capability of canceling noise-like interferences without suppressing target echoes, targets can be detected even in the presence of intensive main lobe jamming by either jammers in close proximity to the target (stand-off jamming) or aboard the target (self-screening jamming).

11. Increase of Clutter Resistance

When transmitting and receiving stations of an MSRS are spatially separate, the intersection volume of their main lobes may be much less than the main lobe of a mono-static radar. In this way clutter returns (ground clutter) are smaller than a mono-static radar, because the intersection volume is usually far away from the receiving station. Even highly directional reflectors (like corner reflectors) are not efficient against this type of radar because the energy reflected back aims toward the transmitter, not the receiver. In the case of clutter falling in the intersection of the transmitter station's main lobe and the receiver station's sidelobe (or vice

versa), the reduction in clutter depends only on the respective antennas' (transmit or receive) sidelobe pattern. That is the reason for keeping sidelobe level low in such radars.

For MSRS that use spatially separated transceiving stations operating in different frequency ranges, narrowband chaff clutter is not efficient because it will clutter the specific frequency range it's designed for but leave the target visible to MSRS stations that do not operate in this frequency range.

MTI techniques used in mono-static radars can also be used in MSRSs, however MSRSs present some additional advantages. A target that presents zero radial velocity to mono-static radar performing MTI processing can be hidden from the radar. However, in the case of an MSRS, this target will not present zero radial velocity to all stations and so it will be tracked.

Another advantage has to do with radars performing Doppler processing. A target's speed can coincide with the "blind" speeds of a mono-static Doppler processing radar, but an MSRS station can operate in different PRFs and/or transmission frequencies, eliminating such effect.

12. Increase of Survivability and Reliability

MSRSs comprised of many stations can be dispersed spatially and can be redundant; therefore, the system has a significantly higher probability of survival than does a mono-static radar. Even the destruction or equipment failure of one or several stations does not lead to the total loss of information, but only to a decrease in

175

performance, as there are still other stations available. This effect is often called "graceful degradation". The possibility of reconfiguring an MSRS after an attack or failure enhances its graceful degradation and its reliability as well.

In the special case of "silent" receiving stations the probability of interception is much lower, making them even less vulnerable to an attack (e.g., anti-radiation missiles).

Mobile MSRSs can re-locate quickly, which lessens the probability of a successful attack against them.

MSRSs that use transceiving stations (which can be intercepted), may be positioned in a less dangerous zone, use LPI waveforms, use decoy emitters or several netted transmitters with irregular switching between them.

The survivability of an MSRS can be further improved if decentralized signal and data processing is used.

13. Technical and Operational Advantages

MSRSs that use separate transmitting and receiving stations do not require receiver protection RF components (circulators, duplexers, etc.). The required dynamic range of receivers may be significantly reduced, since the dynamic range of reflected signals received by them is much lower compared with signals of mono-static radars.

14. Detection of Non-LOS Targets

Due to terrain obscuration, ground-based or low-flying mono-static radar systems may not have a line of sight (LOS) to the target and therefore cannot provide detection,

whereas an MSRS with several stations can cover areas without losing targets. This is feasible because the probability of obtaining an LOS to the target (by at least one station) is greatly improved due to the spatial dispersion of the stations.

C.   DISADVANTAGES OF MULTISITE RADAR SYSTEMS

The disadvantages of an MSRS system over a mono-static radar or a number of radars not integrated in a system are as follows (Chernyak 1998, 22–24; Pace 2009, 346–347).

1.   Centralized Control of Spatially Separate Stations

The control of an MSRS depends on the type of MSRS (especially with respect to the degree of spatial coherency as mentioned in paragraph A.2 above and its information fusion level as mentioned in paragraph A.3 above). It can vary from simple control (target distribution among several groups of radars, tracks processing, etc.) to complex control (coordinated scanning of space, choice of operational frequencies and waveforms, position control of mobile stations, joint processing of signals, etc.). To achieve high survivability of an MSRS, partial decentralization of system control is important.

2.   Necessity of Data Transmission Conduits

All MSRSs demand reliable data transmission conduits for data or signal transmission from the stations as well as control information from the fusion center. As discussed in chapter VII, section A, paragraph 3, the capacity of such transmission conduits is determined mainly by the information fusion level the MSRS requires. The type of

such data transmission conduits (wired or wireless) is determined by station location and mobility characteristics (stationary or mobile). Data transmission conduits are essential for the operation of any MSRS and additional considerations must be made with regard to protection against interference, physical protection, redundancy and so on.

3.   Additional Requirements for Synchronization, Phasing of Spatially Separate Stations, Transmission of Reference Frequencies and Signals

Joint information processing (information fusion) requires some kind of synchronization between the stations and the fusion center (the accuracy of synchronization depends on the type of MSRS). For cooperative type MSRSs (as mentioned in paragraph A.4.b above), the transmitted frequency and signal waveform must be known by all receiving stations, which can be accomplished by either signal or special commands for station alignment transmission via the data transmission lines. Precise target coordinate measurements require precise synchronization (no more than a fraction of the inverse of signal bandwidth).

For coherent signal processing (MTI or Doppler measurements), a common reference frequency is required in each station to couple the transmitter and receiver heterodyne frequencies. It is also needed for correlation processing of received signals in active or passive/active MSRSs. The common frequency may be transmitted by the fusion center via the data transmission lines or by using a highly stable frequency standard at each station.

In spatially coherent MSRSs, in addition to precise synchronization and reference frequencies, phase synchronization is also required (the maintenance of phase relations among stations).

4. Increased Requirements to Signal and Data Processors and Computer Systems

It is obvious that by increasing the signal information body, as generally happens with an MSRS, there is a need for additional processing power compared to a mono-static radar (as mentioned in paragraph B.8 above). Factors that increase the computational effort of an MSRS compared to a mono-static radar are: the necessity for coordinate conversion from the local coordinate system of the station(s) into a common coordinate system for the MSRS; the data association of measurements (plots, tracks) from the various stations and targets determined and maintained at the fusion center; and the fact that most of the geometrical computational efforts (both at the stations or at the fusion center, depending on the type of the MSRS) are much more complicated than the ones of a mono-static radar.

5. Necessity for Accurate Station Positioning and Mutual Alignment

A main task of the fusion center is to correctly process the coordinate information coming from various stations in order to construct target tracks. To do so the stations' positions must be known and stations must be aligned. Errors in station position determination as well as the orientation of the local (station) coordinate system axes directly influence the accuracy of the output

information (target location determination) of the MSRS. The use of Global Positioning System (GPS) receivers is the solution for accurate position data.

6.   Need for Direct LOS Between Stations and Targets

Unless the MSRS is comprised of Over the Horizon Radar (OTHR), its coverage is limited by the need for LOS between stations and targets. A target should be simultaneously visible by several stations of an MSRS (transmitting and receiving or transceiving) in order for fusion to be effectively applied.

7.   High Cost

MSRSs comprised of several spatially separate stations, data transmission lines, and information fusion centers are more complex and expensive than mono-static radar. However for the comparison to be fair we have to compare systems with similar capabilities and characteristics. In this context some MSRS characteristics are not achievable by mono-static radars, whereas others can be achieved but will dramatically increase the complexity and cost of the mono-static radar. Note that MSRSs with simple stations of the same type are less expensive than a mono-static radar with similar characteristics. Also note that significant benefits can be obtained at a low cost when an MSRS is created by integrating several mono-static radars or by adding remote receiving station to these radars.

D.   SUMMARY

Although in previous years the implementation of MSRSs posed certain technical difficulties, nowadays it has become feasible due to recent advances in large bandwidth wireless networks, high capacity data transmission lines, multichannel electronically scanned antennas, high-speed, low-cost digital processors, and precise synchronization systems (Teng, et al. 2007). But, there are technical challenges that have yet to be addressed. The most important is the time and frequency synchronization for coherent operation. By using GPS as a reference-timing signal, the network can be made coherent. Another important challenge is data fusion and registration of the various data streams, which requires reliable and high-capacity communication links in the network (Derham, et al. 2007).

Table 11 summarizes the MSRS advantages among the types of MSRSs. The table's color is coded best to worst as follows: green means that the specific subtype has this advantage to the highest degree; yellow means that this subtype has this advantage to a lesser degree than those marked in green; red means that this subtype has this advantage to a lesser degree than those marked in yellow.

Table 12 summarizes the MSRS disadvantages for the types of MSRSs. It is color coded worst to best as follows: red means that the specific subtype has this disadvantage to the most serious degree; yellow means that this subtype has this disadvantage to a lesser degree than those marked green; green means that this subtype has this disadvantage to the least degree.

The purpose of the color coding of the two tables is to show the relative differences for advantages and disadvantages between MSRS subcategories. When all subtypes have the same color (either green for advantages of red for disadvantages), there is no relative difference between them with respect to the advantage or disadvantage. When there are different colors among subtypes, then there is relative difference between the subtypes).

MSRS Advantages	Type of targets of interest			Degree of spatial coherence			Information fusion level				Degree of autonomy of signal reception			Station location and mobility				
	Active	Passive	Active/Passive	Spatially coherent	Short-term spatially coherent	Spatially incoherent	Radio signal	Video signal	Plot	Track	Independent	Cooperative	Independent-Cooperative	Ground/stationary	Ground/Mobile	Tx(Rx) platforms Rx(Tx) Ground	All stations on platforms	Shipborne
Form coverage area	green	green	green	green	green	green	green	green	green	green	green	green	green	green	green	green	green	green
Power	green	green	green	green	green	green	green	green	green	green	yellow	green	green	green	green	green	green	green
Detection of stealth targets	green	green	green	green	green	green	green	green	green	green	green	green	green	green	green	green	green	green
High accuracy of position estimation	green	yellow	green	green	green	green	green	green	green	green	green	green	green	green	green	green	green	green
Possibility of estimating target's velocity and acceleration vectors	green	green	green	green	green	green	green	green	green	green	green	green	green	green	green	green	green	green
Measurement of radiating sources position and velocity	yellow	green	green	green	green	green	green	green	green	green	green	green	green	green	green	green	green	green
Increase in resolution	green	yellow	green	green	green	green	green	green	green	green	green	green	green	green	green	green	green	green
Increase of target handling capacity	green	green	green	green	green	green	green	green	green	green	green	green	green	green	green	green	green	green
Increase of signal information body	green	green	green	green	yellow	red	green	yellow	red	red	green	green	green	green	green	green	green	green
Increase in jamming resistance	yellow	green	green	green	green	yellow	green	green	green	green	green	green	green	green	green	green	green	green
Increase in clutter resistance	green	green	green	green	green	green	green	green	green	green	green	green	green	green	green	green	green	green
Increase in survivability and reliability	yellow	green	green	green	green	green	green	green	green	green	green	green	green	red	green	yellow	green	green
Technical and operational advantages	green	green	green	green	green	green	green	green	green	green	green	green	green	green	green	green	green	green
Detection of non-LOS targets	green	green	green	green	green	green	green	green	green	green	green	green	green	green	green	green	green	green

Table 11.   Summary of MSRS Advantages for Types of MSRSs

MSRS Disadvantages \ MSRS types	Type of targets of interest			Degree of spatial coherence			Information fusion level				Degree of autonomy of signal reception			Station location and mobility				
	Active	Passive	Active/Passive	Spatially coherent	Short-term spatially coherent	Spatially incoherent	Radio signal	Video signal	Plot	Track	Independent	Cooperative	Independent-Cooperative	Ground/stationary	Ground/Mobile	Tx(Rx) platforms Rx(Tx) Ground	All stations on platforms	Shipborne
Centralized control of spatially separate stations	Red	Red	Red	Red	Yellow	Green	Red	Yellow	Green	Green	Red	Red	Red	Red	Red	Red	Red	Red
Necessity of data transmission lines	Red	Red	Red	Red	Yellow	Green	Red	Yellow	Green	Green	Red	Red	Red	Red	Red	Red	Red	Red
Synchronization, phasing and reference frequencies	Red	Red	Red	Red	Yellow	Green	Red	Red	Red	Red	Green	Red	Yellow	Red	Red	Red	Red	Red
Increased requirements for signal and data processors and computer systems	Red	Red	Red	Red	Yellow	Green	Red	Yellow	Green	Green	Yellow	Red	Red	Green	Red	Yellow	Red	Red
Accurate system positioning and alignment	Red	Red	Red	Red	Red	Red	Red	Red	Red	Red	Red	Red	Red	Green	Red	Yellow	Red	Red
Need of direct LOS between target and stations	Red	Red	Red	Red	Red	Red	Red	Red	Red	Red	Red	Red	Red	Red	Red	Red	Red	Red
High cost	Yellow	Green	Red	Red	Yellow	Green	Red	Yellow	Green	Green	Yellow	Red	Red	Green	Yellow	Yellow	Red	Red

Table 12.   Summary of MSRS Disadvantages for Types of MSRSs

VIII. SIMULATION SCENARIO

Having discussed the theoretical background of the LPI principle and issues pertaining to netted and non-netted configuration of LPI systems, in this chapter we attempt to evaluate the efficiency of the latter, using the network topology depicted in Figure 53.
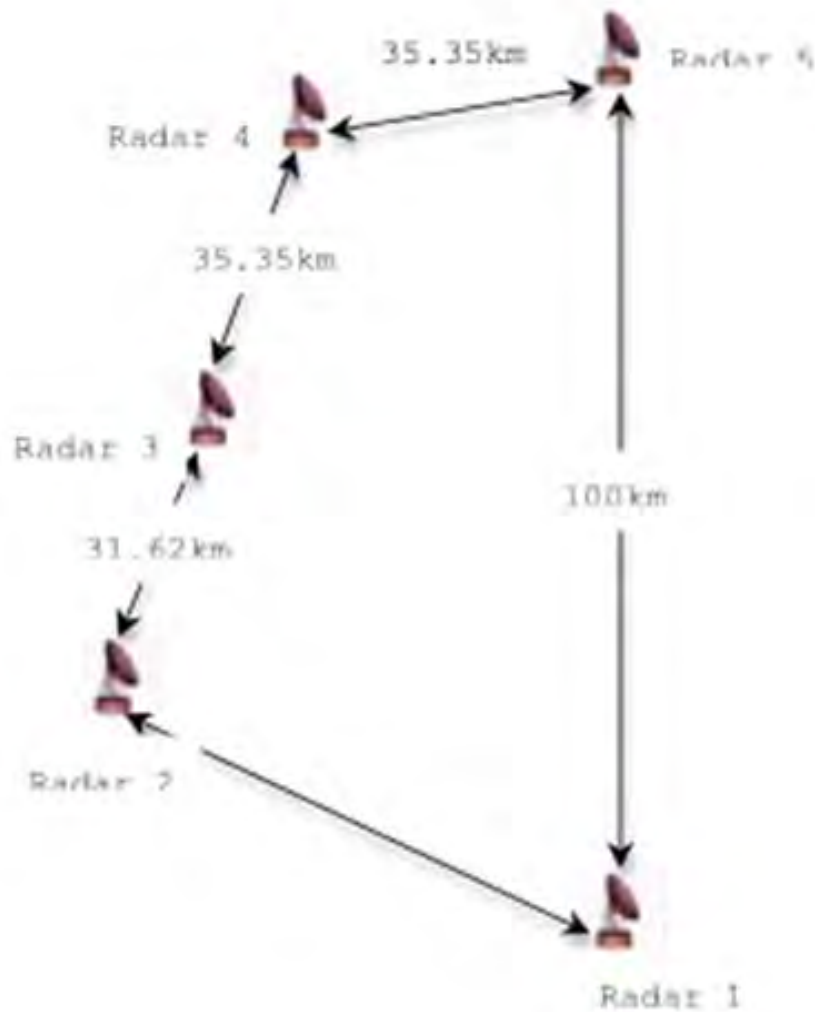

Figure 53.   Simulation Network Topology

Figure 53 depicts a five node IADS, consisting of five identical LPI radars whose task is to provide early warning in a radius of 100km.

Prior to launching LPIsimNet, we set the LPI radar characteristics based on the requirements for detection range, resolution range, and the operating central frequency of our design as shown in Table 13.

Characteristic	Symbol	Value
Radar Operating Frequency	f	9.375 GHz
Radar Required Range Resolution[38]	ΔR	1 m
Radar Required Detection Range	R	100 km
Radar ERP	ERP	10 Watt
Radar Antenna Gain	G_T, G_R	30 dB
Radar Emitted Power	P_{CW}	0.1 Watt
Target RCS	σ_T	2 sq. Meters
Target Intercept receiver antenna Gain	G_I	0 dB

Table 13.   LPI Radar & Target Characteristics

Commencing from the design requirements of Table 13, we calculated the specific parameters of the scenario:

The required modulation bandwidth (ΔF) for a range resolution of $\Delta R = 1m$ is:

---

[38] Assuming that the target against which the IADS wants to provide an early warning is an F-16, with wingspan 9.8m, the range resolution we want to achieve at max range is approximately 1m.

$$\Delta F = \frac{c}{2\Delta R} \Rightarrow \Delta F = \frac{3 \cdot 10^8}{2 \cdot 1m} \Rightarrow \boxed{\Delta F = 150 MHz}$$

For a detection range of $R = 100km$, the time delay t_d is:

$$t_d = \frac{2R}{c} \Rightarrow t_d = \frac{2 \cdot 100km}{3 \cdot 10^8} \Rightarrow \boxed{t_d = 0.667 m\sec}$$

The modulation period t_m is:

$$t_m \approx 5.5 t_d \Rightarrow t_m = 5.5 \cdot 0.667 m\sec \Rightarrow \boxed{t_m = 3.6685 m\sec}$$

And the effective modulation bandwidth $\Delta F'$:

$$\Delta F' = \Delta F(1 - \frac{t_d}{t_m}) \Rightarrow \Delta F' = 150 MHz(1 - \frac{0.667}{3.6685}) \Rightarrow \boxed{\Delta F' = 122.73 MHz}$$

The effective range resolution ΔR will therefore be:

$$\Delta R' = \frac{c}{2\Delta F'} \Rightarrow \Delta R' = \frac{3 \cdot 10^8}{2 \cdot 122.73 \cdot 10^{6'}} \Rightarrow \boxed{\Delta R' = 1.22m}$$

The coherent processing interval t_o is:

$$t_o = t_m - t_d \Rightarrow t_o = 3.6685 - 0.667 \Rightarrow \boxed{t_o = 3.0015 m\sec}$$

The spectral width of the beat frequency Δw is:

187

$$\Delta w = \frac{1}{t_o} \Rightarrow \Delta w = \frac{1}{3.0015 m \sec} \Rightarrow \boxed{\Delta w = 0.3332 kHz}$$

The velocity resolution Δv is:

$$\Delta v = \frac{\lambda \Delta w}{2} \Rightarrow \Delta v = \frac{0.032 \cdot 0.3332 \cdot 10^3}{2} \Rightarrow \boxed{\Delta v = 5.3312 \frac{m}{\sec}}$$

The effective time bandwidth product (or processing gain [PG]) is:

$$PG = t_o \Delta F' \Rightarrow PG = 3.0015 \cdot 10^{-3} \cdot 122.73 \cdot 10^6 \Rightarrow \boxed{PG = 368,374.1 = 55.66 dB}$$

Assuming that the closing speed of target is $V = 1 Mach = 300 m/\sec$) the effective beat frequencies (f'_{1b} & f'_{2b}) are:

$$f'_{1b} = \frac{2R\Delta F'}{ct_o} - \frac{2V}{\lambda} \Rightarrow f'_{1b} = \frac{2 \cdot 100 \cdot 10^3 \cdot 122.73 \cdot 10^6}{3 \cdot 10^8 \cdot 3.0015 \cdot 10^{-3}} - \frac{2 \cdot 300}{0.032} \Rightarrow \boxed{f'_{1b} = 27.241 MHz}$$

$$f'_{2b} = \frac{2R\Delta F'}{ct_o} + \frac{2V}{\lambda} \Rightarrow f'_{2b} = \frac{2 \cdot 100 \cdot 10^3 \cdot 122.73 \cdot 10^6}{3 \cdot 10^8 \cdot 3.0015 \cdot 10^{-3}} + \frac{2 \cdot 300}{0.032} \Rightarrow \boxed{f'_{2b} = 27.279 MHz}$$

The maximum beat frequency $f'_{b\max}$ is:

$$\boxed{f'_{b\max} = f'_{2b} = 27.279 MHz}$$

The sampling frequency f_s is:

$$f_s = 2f'_{b\max} = 2f'_{2b} \Rightarrow \boxed{f_s = 54.558 MHz}$$

The number of samples within the coherent processing interval N^F is:

$$N^F = f_s t_o \Rightarrow N^F = 54.558 MHz \cdot 3.0015 m\sec \Rightarrow \boxed{N^F = 163,756}$$

The Fast Fourier Transform (FFT) size N' is:

$$N' = 2^x \geq N^F \Rightarrow \boxed{N' = 2^{18} = 262,144 \geq 163,756}$$

The unambiguous range of our LPI radar R_{un} is:

$$R_{un} = N' \Delta R' \Rightarrow R_{un} = 262,144 \cdot 1.22 \Rightarrow \boxed{R_{un} = 319,815.68 m = 319.816 km}$$

Since the unambiguous range (319.816km) is much higher than the requested detection range (100km), the designer can limit the range cells within the FFT by means of filtering the input to the FFT.

In order to better comprehend the simulation results that will follow, we have to calculate the LPI radar sensitivity and, based on that calculation, determine the required SNR at the input of the LPI radar receiver to be able to perform the detection at the required detection range.

Assuming all losses equal to 1, the LPI radar sensitivity δ_R is:

$$\delta_R = \frac{P_{CW} G_T G_R \lambda^2 \sigma_T L_2}{(4\pi)^3 R^4 L_{RT} L_{RR}} \Rightarrow \delta_R = \frac{0.1 \cdot 1000 \cdot 1000 \cdot 0.032^2 \cdot 2 \cdot 1}{(4\pi)^3 (100 \cdot 10^3)^4 \cdot 1 \cdot 1} \Rightarrow$$

$$\Rightarrow \boxed{\delta_R = 0.103205 \cdot 10^{-20} Watt = -209.86 dBW}$$

The SNR required at the input of the LPI radar receiver will therefore be:

$$SNR_{Ri} = \frac{\delta_R}{kT_o F_R B_{Ri}} \Rightarrow SNR_{Ri} = \frac{0.103205 \cdot 10^{-20}}{1.38 \cdot 10^{-23} \cdot 290 \cdot 3.1623 \cdot 150 \cdot 10^6} \Rightarrow$$

$$\Rightarrow \boxed{SNR_{Ri} = 5.4366 \cdot 10^{-10} = -92.65 dB}$$

where we assumed that the noise factor at the LPI radar's receiver is $F_R = 5dB = 3.1623$ and the input bandwidth of the LPI radar receiver is matched to the LPI radar waveform: $B_{Ri} = \Delta F = 150 MHz$.

In order to check whether the intercept receiver with the design characteristics we set at Table 13 can detect the LPI emitter within the desired range, we separately calculated the maximum intercept range R_{Imax} using Equation (2.8).

The results we get for various values of sensitivity δ_I are summarized in Table 14.

Intercept receiver sensitivity δ_I	Maximum intercept range $R_{\mathrm{I}max}$
-60.00 dB	25.46 m
-80.00 dB	254.65 m
-100.00 dB	2,546.48 m
-120.00 dB	25,464.78 m
-131.88 dB	100,000.00 m

Table 14.   Maximum Detection Range vs. Intercept Receiver's Sensitivity

Studying Table 14, we notice two issues:

- The LPI radar is capable of detecting the target at the desired range, as long as the required SNR at the input of the receiver is greater than -92.65 dB ($SNR_{Ri} \geq 92.65dB$); and

- The intercept receiver cannot detect the LPI radar emissions at the maximum LPI radar detection range unless it has a sensitivity less than -131.88 dB ($\delta_R < -131.88dB$).

Having established the parameters of our design, and in order to enhance the level of realism, we assume that nodes 2 and 3 have lower decision tempo and connectivity values than do nodes 1, 4, and 5. In order to incorporate these values into a simulation scenario, and to evaluate the information network metrics and the SNR advantages of the network topology chosen, we utilize the *LPIsimNet*

software, a collection of MATLAB files developed by Chen and Pace, that can set up a sensor network with a given configuration and number of communication nodes (Chen, 2007; Chen and Pace, 2008).

For the purposes of our analysis, we examined the configuration of Figure 53 in three scenarios of increasing complexity:

The first scenario involves a 5-node LPI network and a self-jammer.

The second scenario replaces the self-jammer with a stand-off jammer and a target.

The third scenario uses two stand-in jammers (UAVs).

Each scenario is run in three stages (time indexes), representing the time steps taken by the jammer/target as it approaches the IADS. To thoroughly examine the jamming effect, our analysis is structured along two levels: the first involves the visual representation of the SNJR contour chart on each step of the scenario under examination. By doing so, we aim to provide the reader with a tool for rapid visual comparison between the different configurations. The second level pertains to numerical analysis. Its purpose is to present precise data for mathematical analysis and final conclusions. To present both levels, we have utilized the LPIsimNet software. The latter's results (SNR, JSR, S/(J+N)) are presented first for the non-netted and then for the netted configuration.

A.   SCENARIO 1: 1 SSJ

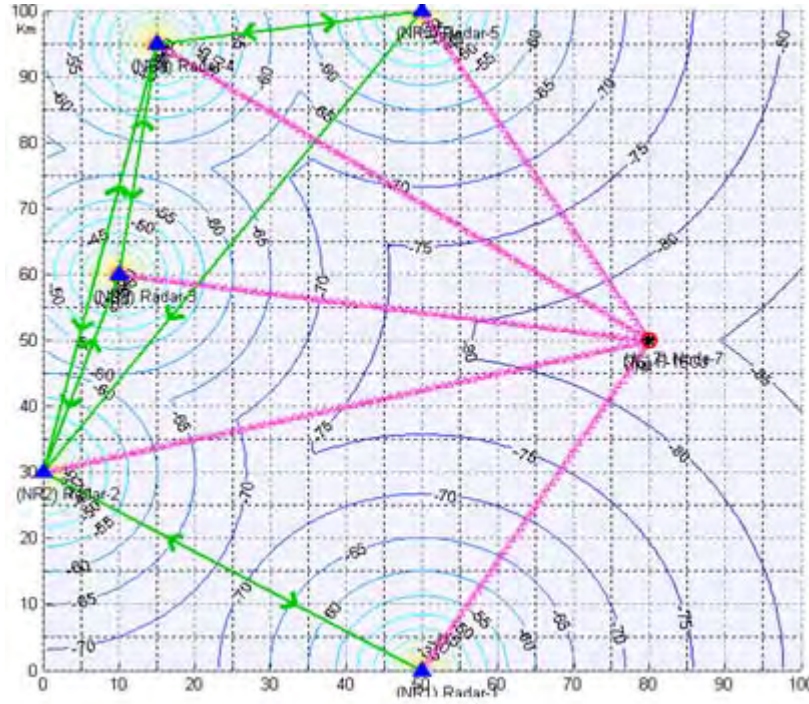### 1.   Scenario 1 Time Index 1

a.   `SNR – Non-Netted

Figure 54.   Non-Netted SNR Contour Chart at Time Index=1

For target at (80, 50):

Node	Radar Echo(W)	Noise(W)	SNR
1	$4.4646 \cdot 10^{-21}$	10^{-12}	$4.4646 \cdot 10^{-9}$
2	$1.1161 \cdot 10^{-21}$	10^{-12}	$1.1161 \cdot 10^{-9}$
3	$2.0644 \cdot 10^{-21}$	10^{-12}	$2.0644 \cdot 10^{-9}$
4	$1.3212 \cdot 10^{-21}$	10^{-12}	$1.3212 \cdot 10^{-9}$
5	$4.4646 \cdot 10^{-21}$	10^{-12}	$4.4646 \cdot 10^{-9}$

Max SNR = $4.4646 \cdot 10^{-9}$ = -83.5022 dB
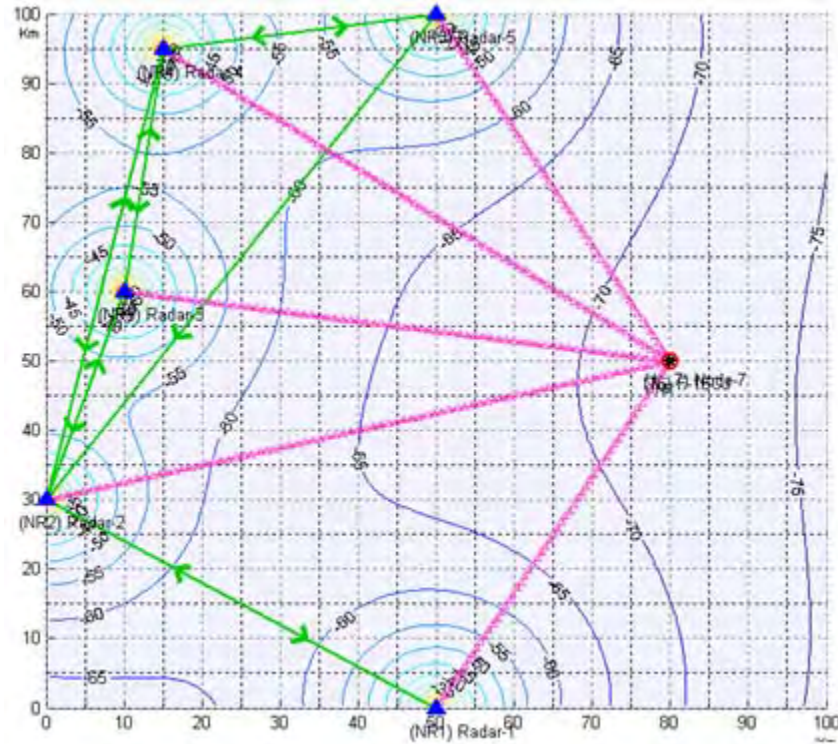
b.   *`SNR – Netted*

Figure 55.   Netted SNR Contour Chart at Time Index=1

For target at (80, 50):

Node	Radar Echo(W)	Noise(W)	SNR
1	$1.6626 \cdot 10^{-21}$	10^{-12}	$1.6626 \cdot 10^{-8}$
2	$8.313 \cdot 10^{-21}$	10^{-12}	$8.313 \cdot 10^{-9}$
3	$1.1306 \cdot 10^{-21}$	10^{-12}	$1.1306 \cdot 10^{-8}$
4	$9.0446 \cdot 10^{-21}$	10^{-12}	$9.0446 \cdot 10^{-9}$
5	$1.6626 \cdot 10^{-21}$	10^{-12}	$1.6626 \cdot 10^{-8}$

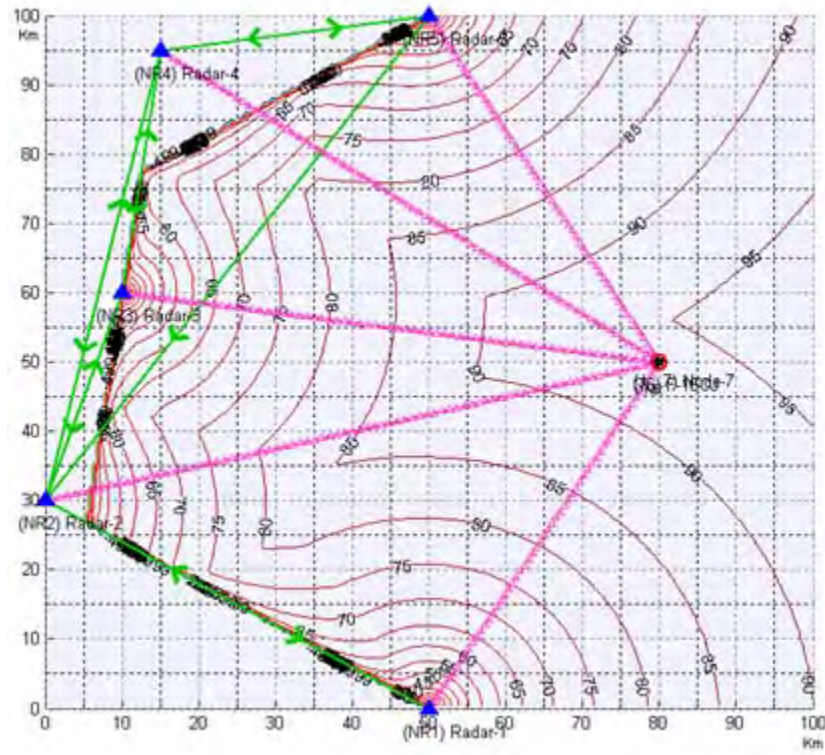|	Network disabled	Network enabled	Network improvement
SNR (dB)	–83.5022 dB	–72.082 dB	**11.42 dB**

c.   `JSR – Non-Netted

Figure 56.   Non-netted JSR Contour Chart at Time Index=1

For target at (80, 50):

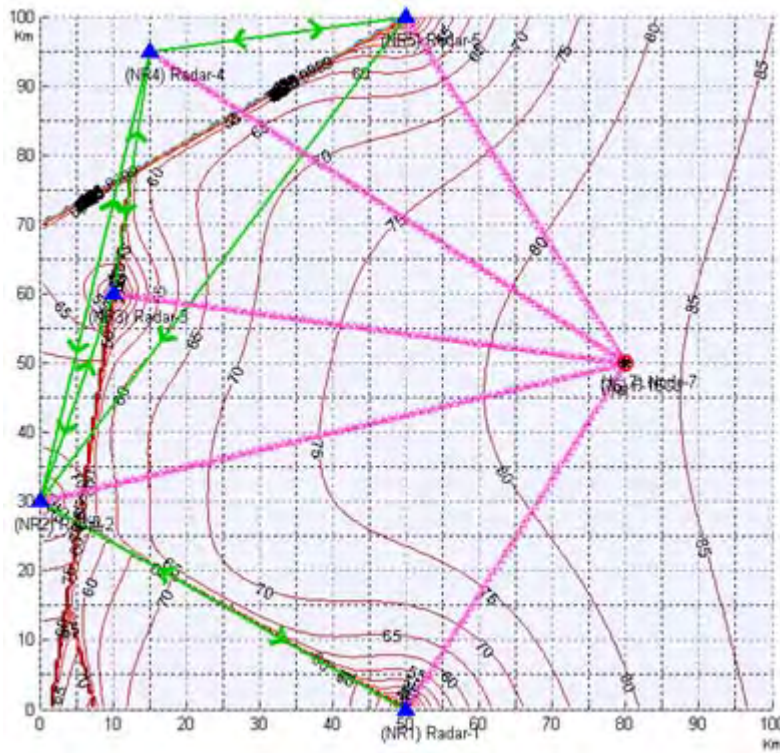| Node	Jamming Power(W)	Radar Echo (W)	JSR
1	$1.9075 \cdot 10^{-11}$	$4.4646 \cdot 10^{-21}$	4272566008.8821
2	$9.5376 \cdot 10^{-12}$	$1.1161 \cdot 10^{-21}$	8545132017.7642
3	$1.2971 \cdot 10^{-11}$	$2.0644 \cdot 10^{-21}$	6283185307.1796
4	$1.0377 \cdot 10^{-11}$	$1.3212 \cdot 10^{-21}$	7853981633.9745
5	$1.9075 \cdot 10^{-11}$	$4.4646 \cdot 10^{-21}$	4272566008.8821

Min JSR = 4272566008.8821 = 96.3069 dB

195

d. **`JSR – Netted**

Figure 57.   Netted JSR Contour Chart at Time Index=1

For target at (80, 50):

Node	Jamming Power(W)	Radar Echo (W)	JSR
1	$1.9075 \cdot 10^{-11}$	$1.6626 \cdot 10^{-20}$	1147305587.7772
2	$9.5376 \cdot 10^{-11}$	$8.313 \cdot 10^{-21}$	1147305587.7772
3	$1.2971 \cdot 10^{-11}$	$1.1306 \cdot 10^{-20}$	1147305587.7772
4	$1.0377 \cdot 10^{-11}$	$9.0446 \cdot 10^{-21}$	1147305587.7772
5	$1.9075 \cdot 10^{-11}$	$1.6626 \cdot 10^{-20}$	1147305587.7772

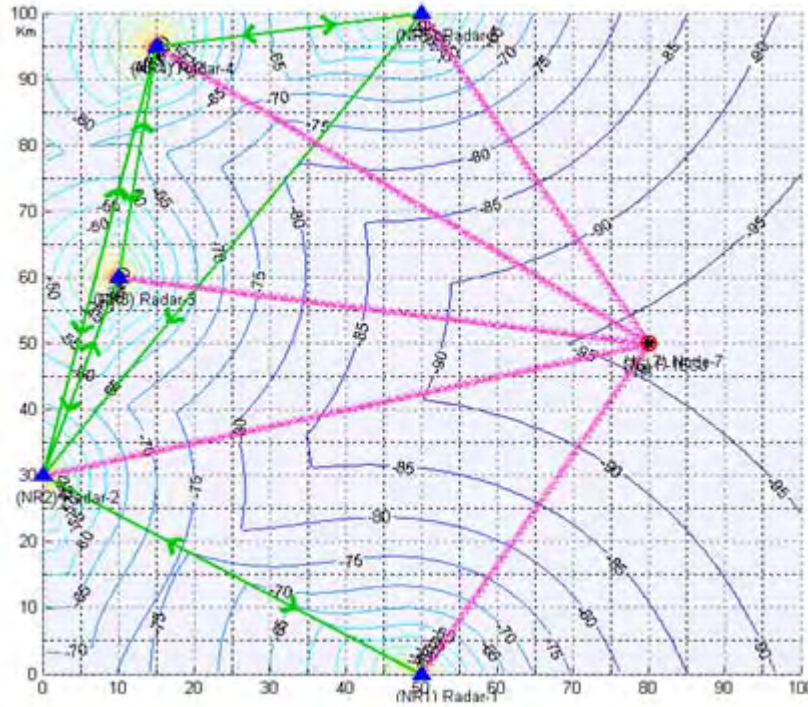|	Network disabled	Network enabled	Network improvement
JSR (dB)	96.3069 dB	83.6071	12.6998 dB

196

e.   `S/(J+N) – Non-Netted

Figure 58.   Non-netted SNJR Contour Chart at Time
Index=1

For target at (80, 50):

Node	Radar Echo	Noise Power	Jamming Power	SNJR
1	$4.4646 \cdot 10^{-21}$	10^{-12}	$1.9075 \cdot 10^{-11}$	$2.2239 \cdot 10^{-10}$
2	$1.1161 \cdot 10^{-21}$	10^{-12}	$9.5376 \cdot 10^{-12}$	$1.0592 \cdot 10^{-10}$
3	$2.0644 \cdot 10^{-21}$	10^{-12}	$1.2971 \cdot 10^{-11}$	$1.4776 \cdot 10^{-10}$
4	$1.3212 \cdot 10^{-21}$	10^{-12}	$1.0377 \cdot 10^{-11}$	$1.1613 \cdot 10^{-10}$
5	$4.4646 \cdot 10^{-21}$	10^{-12}	$1.9075 \cdot 10^{-11}$	$2.2239 \cdot 10^{-10}$

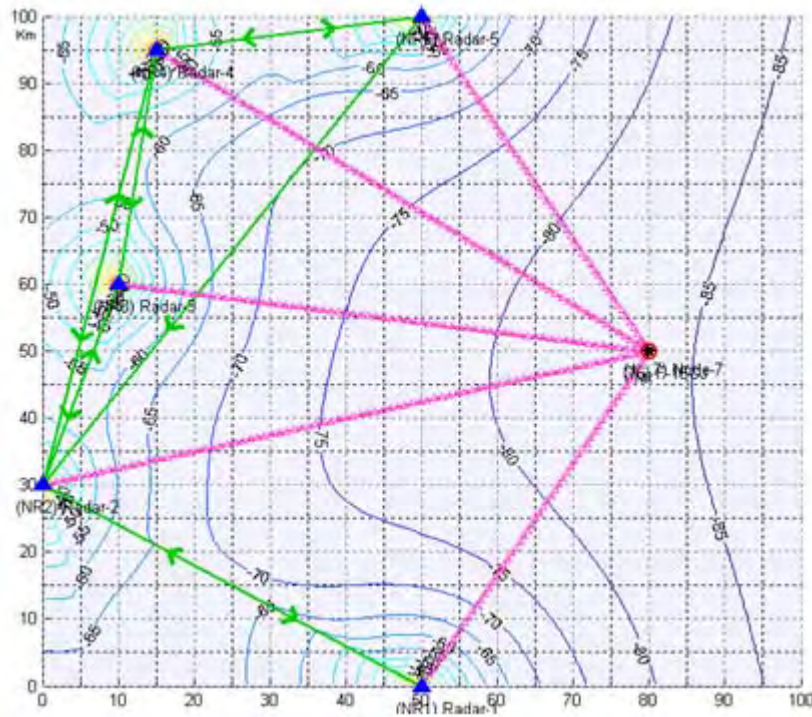Max SNJR = $2.2239 \cdot 10^{-10}$= –96.5288 dB

197

f.   S/(J+N) – Netted

Figure 59.   Netted SNJR Contour Chart at Time Index=1

For target at (80, 50):

Node	Radar Echo	Noise Power	Jamming Power	SNJR
1	$1.6626 \cdot 10^{-20}$	10^{-12}	$1.9075 \cdot 10^{-11}$	$8.2819 \cdot 10^{-10}$
2	$8.313 \cdot 10^{-21}$	10^{-12}	$9.5376 \cdot 10^{-10}$	$7.8889 \cdot 10^{-10}$
3	$1.1306 \cdot 10^{-20}$	10^{-12}	$1.2971 \cdot 10^{-11}$	$8.0922 \cdot 10^{-10}$
4	$9.0446 \cdot 10^{-21}$	10^{-12}	$1.0377 \cdot 10^{-11}$	$7.95 \cdot 10^{-10}$
5	$1.6626 \cdot 10^{-20}$	10^{-12}	$1.9075 \cdot 10^{-11}$	$8.2819 \cdot 10^{-10}$

Total SNJR = $4.0495 \cdot 10^{-9}$ = -83.926 dB

	Network disabled	Network enabled	Network improvement
SNJR (dB)	-96.5288 dB	-83.926 dB	**12.6028 dB**

198

2. Scenario 1 Time index 2 (5 LPI Radar + 1 SSJ)
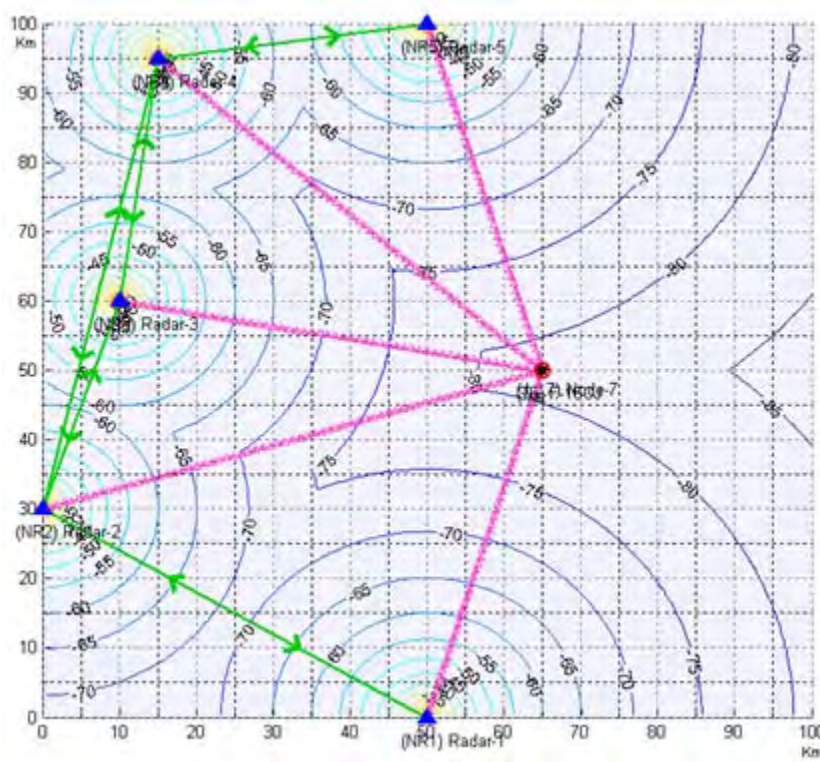
a. *SNR Non-Netted*

Figure 60. Non-netted SNR Contour Chart at Time Index=2

Analysis of SNR without Network at Time Index = 2

For target at (65, 50):

Node	Radar Echo(W)	Noise(W)	SNR
1	$6.9503 \cdot 10^{-21}$	10^{-12}	$6.9503 \cdot 10^{-9}$
2	$2.4128 \cdot 10^{-21}$	10^{-12}	$2.4128 \cdot 10^{-9}$
3	$5.2849 \cdot 10^{-21}$	10^{-12}	$5.2849 \cdot 10^{-9}$
4	$2.5206 \cdot 10^{-21}$	10^{-12}	$2.5206 \cdot 10^{-9}$
5	$6.9503 \cdot 10^{-21}$	10^{-12}	$6.9503 \cdot 10^{-9}$

Max SNR = $6.9503 \cdot 10^{-9}$ = -81.58 dB

199
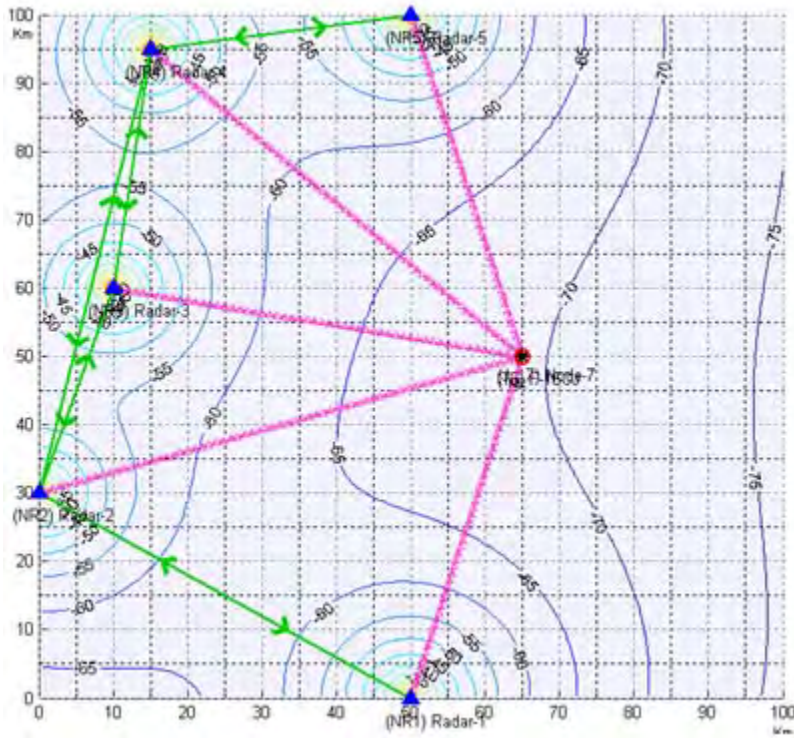
Figure 61.   Netted SNR Contour Chart at Time Index=2

For target at (65, 50):

Node	Radar Echo(W)	Noise(W)	SNR
1	$2.8242 \cdot 10^{-20}$	10^{-12}	$2.8242 \cdot 10^{-8}$
2	$1.664 \cdot 10^{-20}$	10^{-12}	$1.664 \cdot 10^{-8}$
3	$2.4627 \cdot 10^{-20}$	10^{-12}	$2.4627 \cdot 10^{-8}$
4	$1.7008 \cdot 10^{-20}$	10^{-12}	$1.7008 \cdot 10^{-8}$
5	$2.8242 \cdot 10^{-20}$	10^{-12}	$2.8242 \cdot 10^{-8}$

Total SNR = $1.1476 \cdot 10^{-7}$ = -69.4022 dB

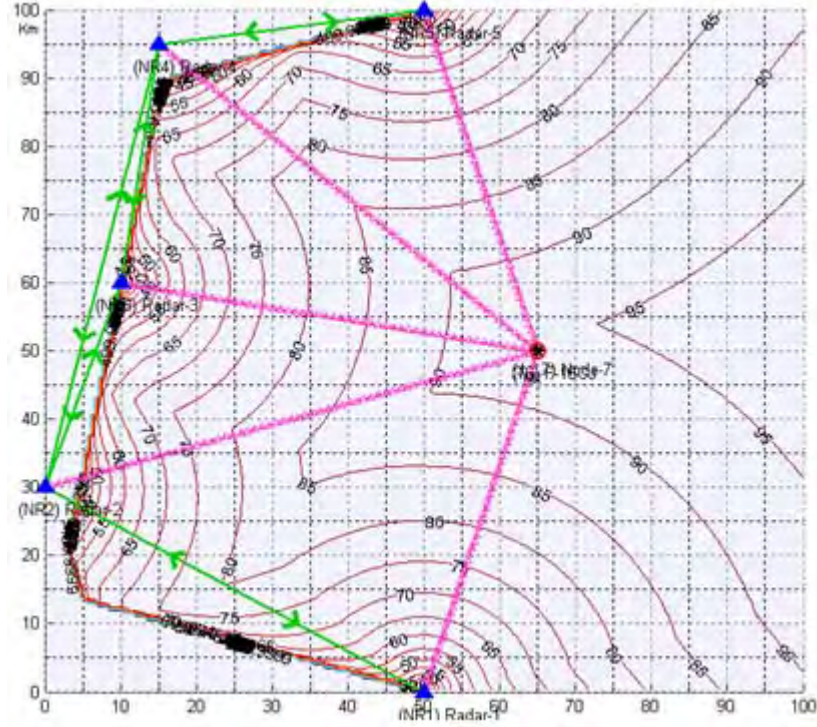|	Network disabled	Network enabled	Network improvement
SNR (dB)	-81.58 dB	-69.4022 dB	**12.1778 dB**

c.   *JSR Non-Netted*

Figure 62.   Non-netted JSR Contour Chart at Time Index=2

For target at (65, 50):

Node	Jamming Power(W)	Radar Echo (W)	JSR
1	$2.38 \cdot 10^{-11}$	$6.9503 \cdot 10^{-21}$	3424335992.4129
2	$1.4023 \cdot 10^{-11}$	$2.4128 \cdot 10^{-21}$	5811946409.1411
3	$2.0754 \cdot 10^{-11}$	$5.2849 \cdot 10^{-21}$	3926990816.9872
4	$1.4333 \cdot 10^{-11}$	$2.5206 \cdot 10^{-21}$	5686282702.9975
5	$2.38 \cdot 10^{-11}$	$6.9503 \cdot 10^{-21}$	3424335992.4129

Min JSR = 3424335992.4129 = 95.3458 dB

d. *JSR Netted*

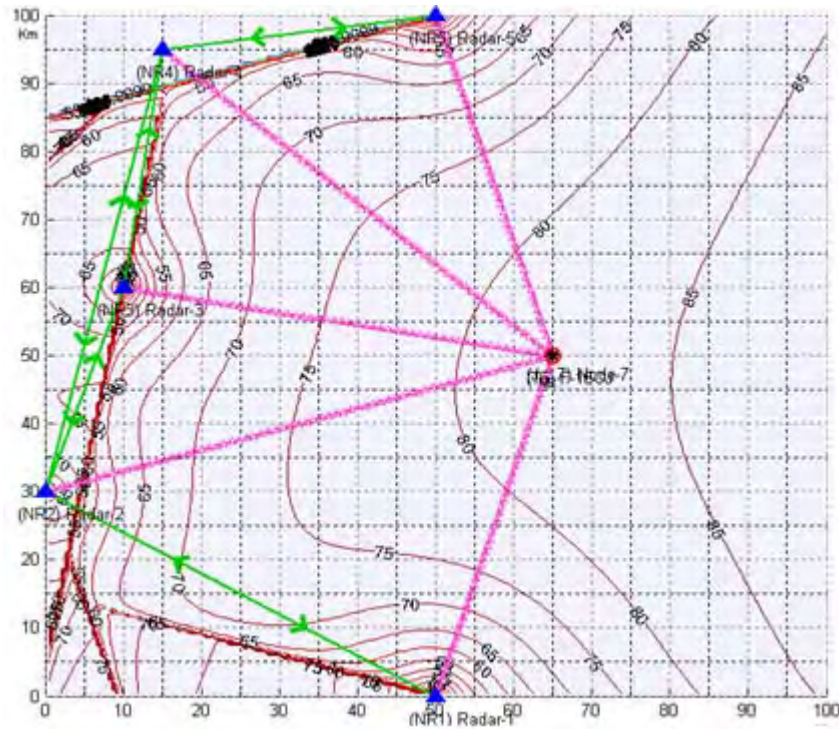

Figure 63.   Netted JSR Contour Chart at Time Index=2

For target at (65, 50):

Node	Jamming Power(W)	Radar Echo (W)	JSR
1	$2.38 \cdot 10^{-11}$	$2.8242 \cdot 10^{-20}$	842726958.2774
2	$1.4023 \cdot 10^{-11}$	$1.664 \cdot 10^{-20}$	842726958.2774
3	$2.0754 \cdot 10^{-11}$	$2.4627 \cdot 10^{-20}$	842726958.2774
4	$1.4333 \cdot 10^{-11}$	$2.4627 \cdot 10^{-20}$	842726958.2774
5	$2.38 \cdot 10^{-11}$	$2.8242 \cdot 10^{-20}$	842726958.2774

Total JSR = 168545391.6555 = 82.2672 dB

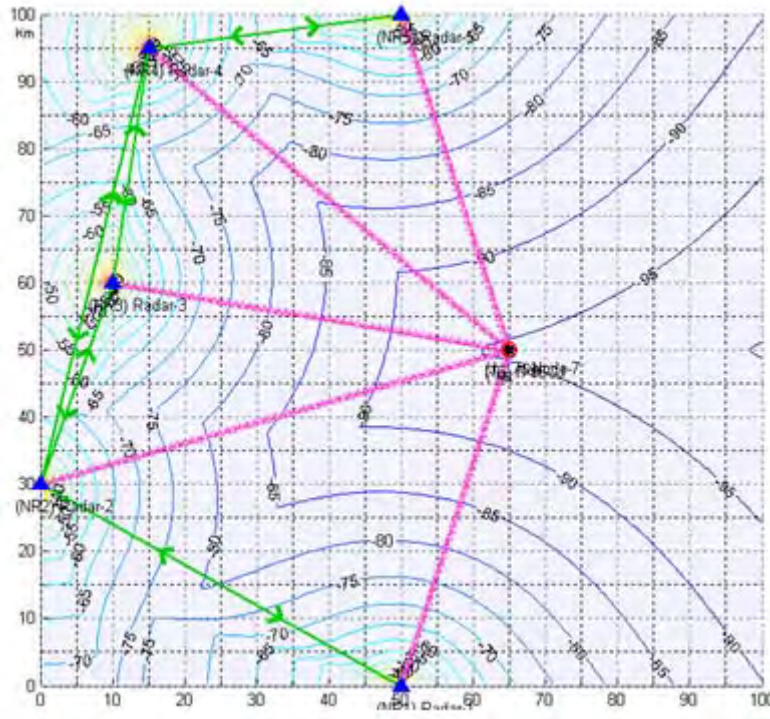|	Network disabled	Network enabled	Network improvement
JSR (dB)	95.3458 dB	82.2672 dB	**13.0786 dB**

e. S/(J+N) Non-Netted

Figure 64.   Non-netted SNJR Contour Chart at Time
Index=2

For target at (65, 50):

Node	Radar Echo	Noise Power	Jamming Power	SNJR
1	$6.9503 \cdot 10^{-21}$	10^{-12}	$2.38 \cdot 10^{-11}$	$2 \cdot 10^{-10}$
2	$2.4128 \cdot 10^{-21}$	10^{-12}	1.402310^{-11}	$1.6061 \cdot 10^{-10}$
3	$5.2849 \cdot 10^{-21}$	10^{-12}	$2.0754 \cdot 10^{-11}$	$2.4294 \cdot 10^{-10}$
4	$2.5206 \cdot 10^{-21}$	10^{-12}	$1.4333 \cdot 10^{-11}$	$1.6439 \cdot 10^{-10}$
5	$6.9503 \cdot 10^{-21}$	10^{-12}	$2.38 \cdot 10^{-11}$	$2.8025 \cdot 10^{-10}$

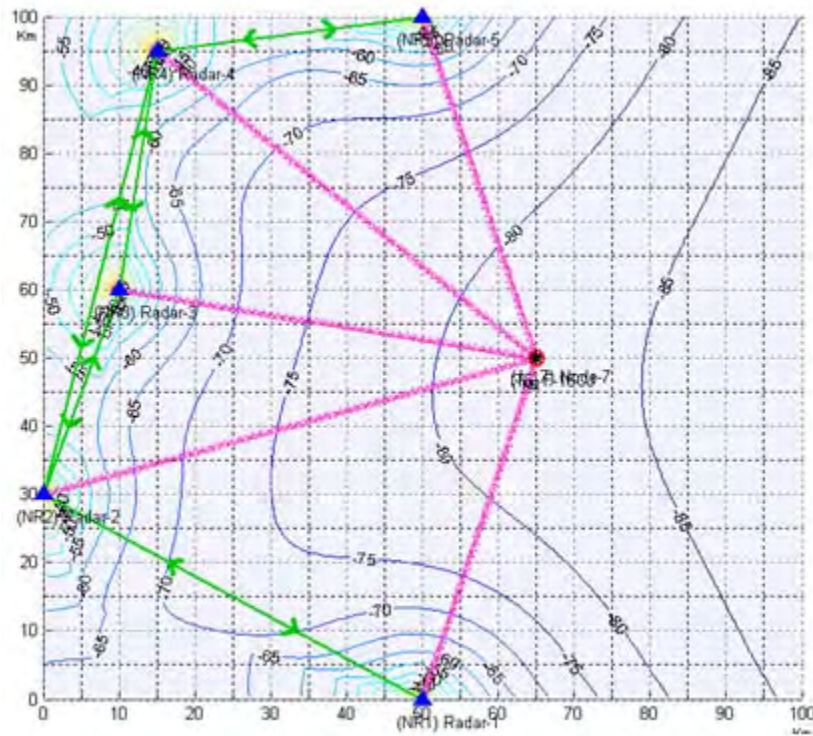Max SNJR = $2.8025 \cdot 10^{-9}$ = -95.5245 dB

203

f.   S/(J+N) Netted

Figure 65.   Netted SNJR Contour Chart at Time Index=2

For target at (65, 50):

Node	Radar Echo	Noise Power	Jamming Power	SNJR
1	$2.8242 \cdot 10^{-20}$	10^{-12}	$2.38 \cdot 10^{-11}$	$1.1388 \cdot 10^{-9}$
2	$1.664 \cdot 10^{-20}$	10^{-12}	$1.4023 \cdot 10^{-11}$	$1.1076 \cdot 10^{-9}$
3	$2.4627 \cdot 10^{-20}$	10^{-12}	$2.0754 \cdot 10^{-11}$	$1.1321 \cdot 10^{-9}$
4	$1.7008 \cdot 10^{-20}$	10^{-12}	$1.4333 \cdot 10^{-11}$	$1.1092 \cdot 10^{-9}$
5	$2.8242 \cdot 10^{-20}$	10^{-12}	$2.38 \cdot 10^{-11}$	$1.1388 \cdot 10^{-9}$

Total SNJR = $5.6265 \cdot 10^{-9}$ = -82.4976 dB

	Network disabled	Network enabled	Network improvement
SNJR (dB)	-95.5245 dB	-82.4976 dB	**13.0269 dB**

3. Scenario 1 Time index 3 (5 LPI Radar + 1 SSJ)

a. *SNR – Non-Netted*
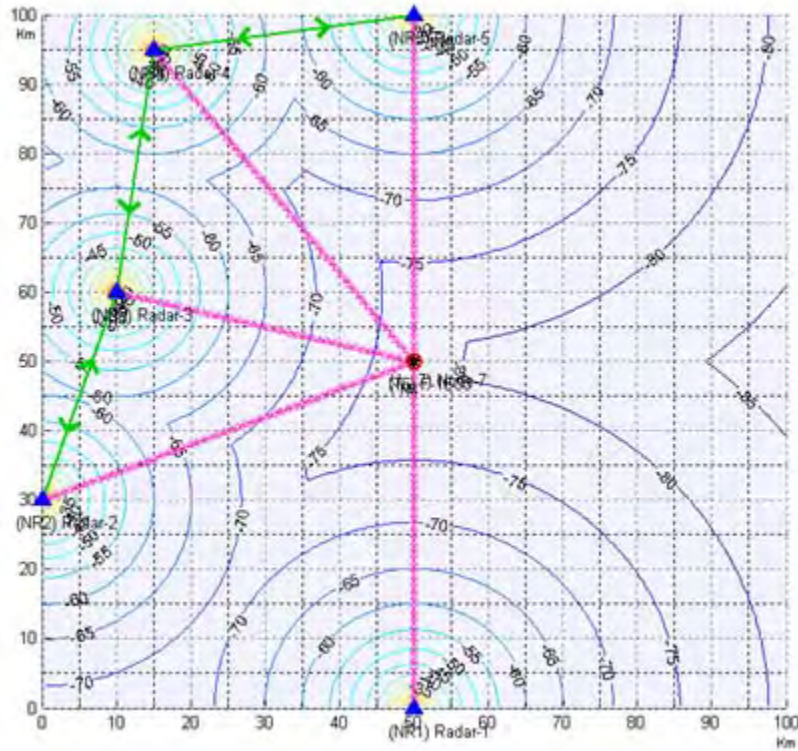
Figure 66. Non-netted SNR Contour Chart at Time Index=3

For target at (50, 50):

Node	Radar Echo(W)	Noise(W)	SNR
1	$8.2577 \cdot 10^{-21}$	10^{-12}	$8.2577 \cdot 10^{-9}$
2	$6.1368 \cdot 10^{-21}$	10^{-12}	$6.1368 \cdot 10^{-9}$
3	$1.7858 \cdot 10^{-20}$	10^{-12}	$1.7858 \cdot 10^{-8}$
4	$4.8862 \cdot 10^{-20}$	10^{-12}	$4.8862 \cdot 10^{-8}$
5	$8.2577 \cdot 10^{-21}$	10^{-12}	$8.2577 \cdot 10^{-9}$

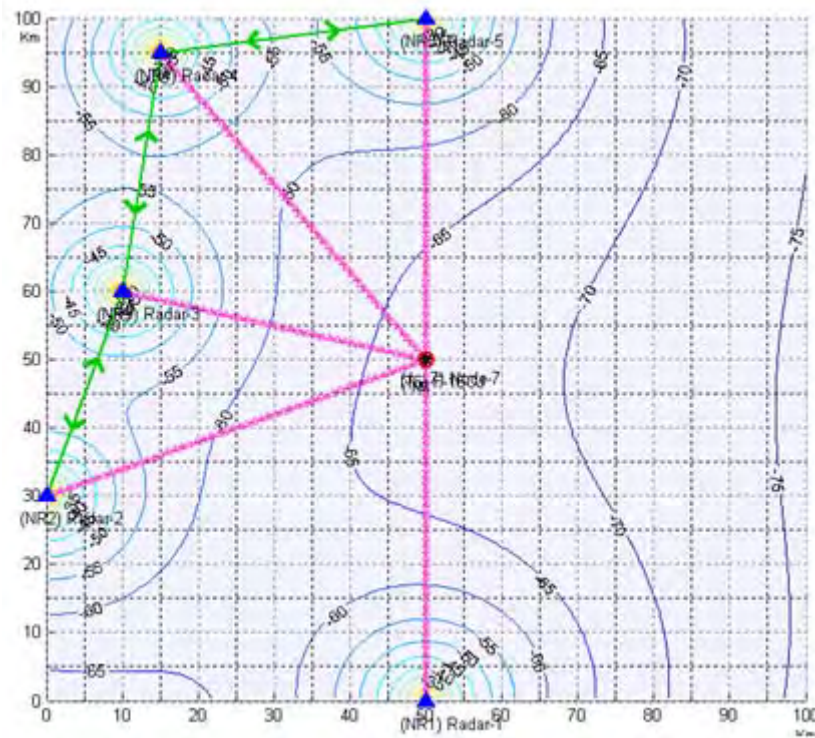Max SNR = $1.7858e \cdot 10^{-8}$ = -77.4816 dB

b.   SNR -Netted

Figure 67.   Netted SNR Contour Chart at Time Index=3

For target at (50, 50):

Node	Radar Echo(W)	Noise(W)	SNR
1	$4.213 \cdot 10^{-20}$	10^{-12}	$4.213 \cdot 10^{-8}$
2	$3.6319 \cdot 10^{-20}$	10^{-12}	$3.6319 \cdot 10^{-8}$
3	$6.1956 \cdot 10^{-20}$	10^{-12}	$6.1956 \cdot 10^{-8}$
4	$3.2407 \cdot 10^{-20}$	10^{-12}	$3.2407 \cdot 10^{-8}$
5	$4.213 \cdot 10^{-20}$	10^{-12}	$4.213 \cdot 10^{-8}$

Total SNR = $2.1494 \cdot 10^{-7}$= -66.6768 dB

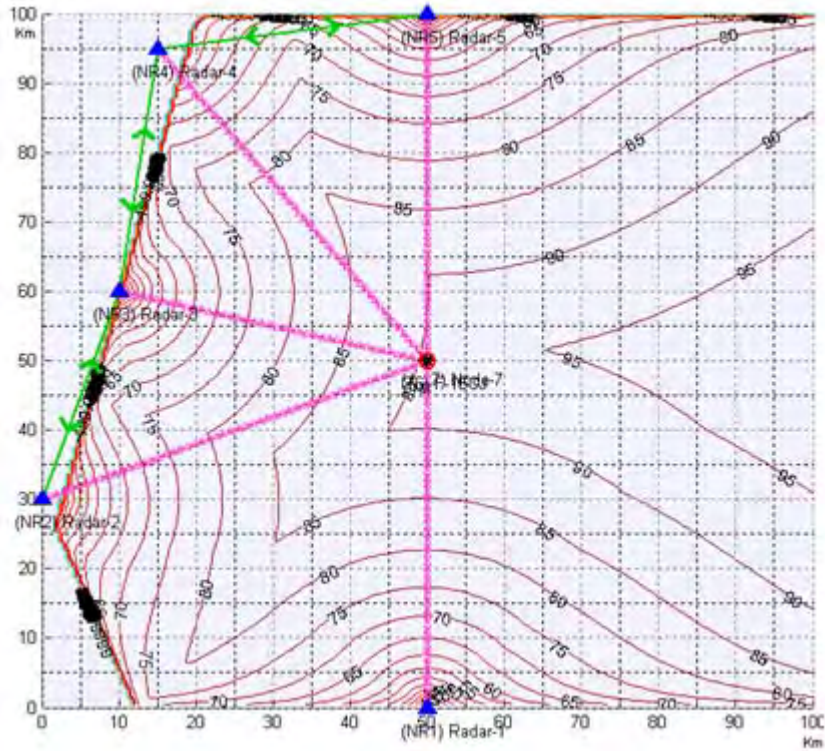|	Network disabled	Network enabled	Network improvement
SNR (dB)	-77.4816 dB	-66.6768 dB	**10.8048 dB**

c.   JSR – Non-Netted

Figure 68.   Non-netted JSR Contour Chart at Time Index=3

For target at (50, 50):

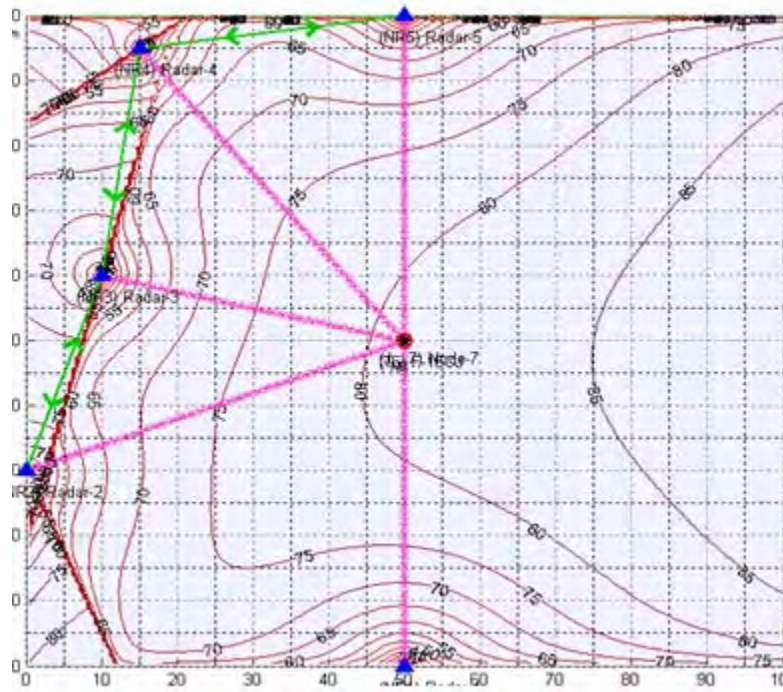| Node	Jamming Power(W)	Radar Echo (W)	JSR
1	$2.5942 \cdot 10^{-11}$	$8.2577 \cdot 10^{-21}$	3141592653.5898
2	$2.2364 \cdot 10^{-11}$	$6.1368 \cdot 10^{-21}$	3644247478.1642
3	$3.815 \cdot 10^{-11}$	$1.7858 \cdot 10^{-20}$	2136283004.4411
4	$1.9956 \cdot 10^{-11}$	$4.8862 \cdot 10^{-21}$	4084070449.6667
5	$2.5942 \cdot 10^{-11}$	$8.2577 \cdot 10^{-21}$	3141592653.5898

Min JSR = 2136283004.4411 = 93.2966 dB

d. *JSR – Netted*

Figure 69.   Netted JSR Contour Chart at Time Index=3

For target at (50, 50):

Node	Jamming Power(W)	Radar Echo (W)	JSR
1	$2.5942 \cdot 10^{-11}$	$4.213 \cdot 10^{-20}$	615770607.2805
2	$2.2364 \cdot 10^{-11}$	$3.6319 \cdot 10^{-20}$	615770607.2805
3	$3.815 \cdot 10^{-11}$	$6.1956 \cdot 10^{-20}$	615770607.2805
4	$1.9956 \cdot 10^{-11}$	$3.2407 \cdot 10^{-20}$	615770607.2805
5	$2.5942 \cdot 10^{-11}$	$4.213 \cdot 10^{-20}$	615770607.2805

Total JSR = 123154121.4561 = 80.9045 dB

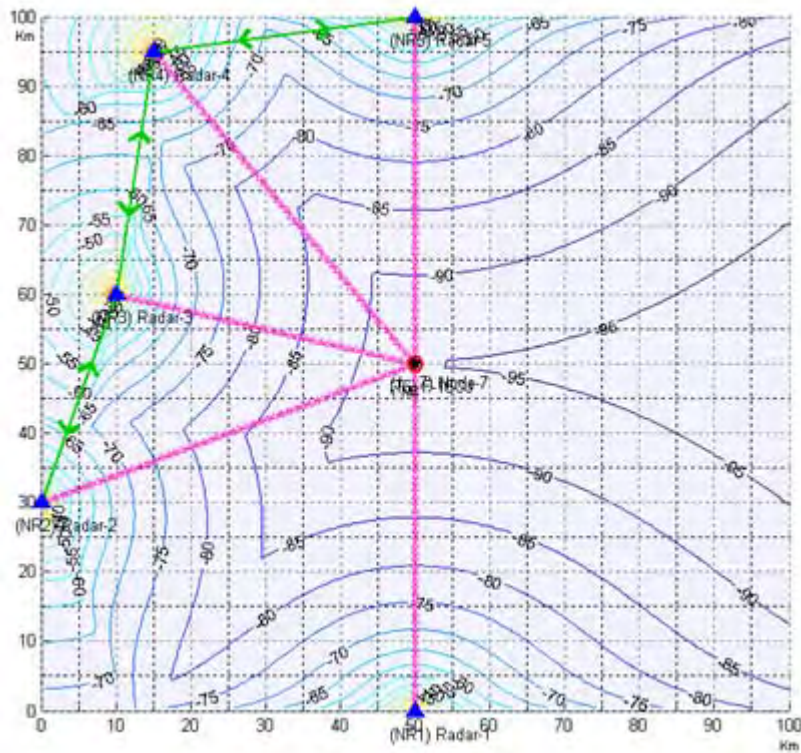|	Network disabled	Network enabled	Network improvement
JSR (dB)	93.2966 dB	80.9045 dB	**12.3921 dB**

Figure 70.   Non-netted SNJR Contour Chart at Time Index=3

For target at (50, 50):

Node	Radar Echo	Noise Power	Jamming Power	SNJR
1	$8.2577 \cdot 10^{-21}$	10^{-12}	$2.5942 \cdot 10^{-11}$	$3.065 \cdot 10^{-10}$
2	$6.1368 \cdot 10^{-21}$	10^{-12}	$2.2364 \cdot 10^{-11}$	$3.8457 \cdot 10^{-10}$
3	$1.7858 \cdot 10^{-20}$	10^{-12}	$3.815 \cdot 10^{-11}$	$4.5615 \cdot 10^{-10}$
4	$4.8862 \cdot 10^{-21}$	10^{-12}	$1.9956 \cdot 10^{-11}$	$2.3317 \cdot 10^{-10}$
5	$8.2577 \cdot 10^{-21}$	10^{-12}	$2.5942 \cdot 10^{-11}$	$3.065 \cdot 10^{-10}$

Max SNJR = $4.5615 \cdot 10^{-10}$ = -93.409 dB
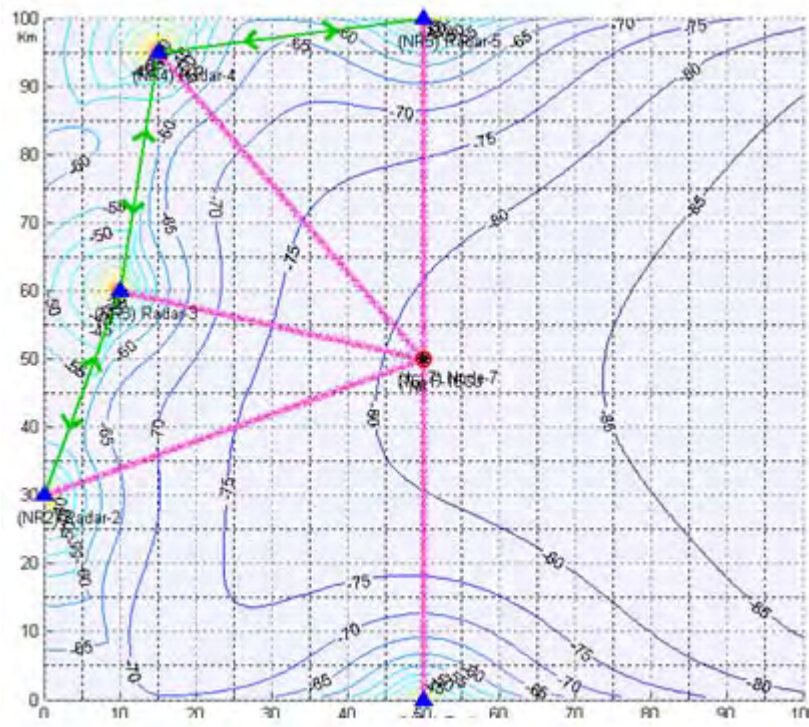
209

f.   S/(J+N) –Netted

Figure 71.   Netted SNJR Contour Chart at Time Index-3

For target at (50, 50):

Node	Radar Echo	Noise Power	Jamming Power	SNJR
1	$4.213 \cdot 10^{-20}$	10^{-12}	$2.5942 \cdot 10^{-11}$	$1.5637 \cdot 10^{-9}$
2	$3.6319 \cdot 10^{-20}$	10^{-12}	$2.2364 \cdot 10^{-11}$	$1.0 \cdot 10^{-9}$
3	$6.1956 \cdot 10^{-20}$	10^{-12}	$3.815 \cdot 10^{-11}$	$1.5825 \cdot 10^{-9}$
4	$3.2407 \cdot 10^{-20}$	10^{-12}	$1.9956 \cdot 10^{-11}$	$1.5465 \cdot 10^{-9}$
5	$4.213 \cdot 10^{-20}$	10^{-12}	$2.5942 \cdot 10^{-11}$	$1.5637 \cdot 10^{-9}$

Total SNJR = $7.8109 \cdot 10^{-9}$ = -81.073 dB

	Network disabled	Network enabled	Network improvement
SNJR (dB)	–93.409 dB	–81.073 dB	**12.336 dB**

B. SCENARIO 2: 1 STAND-OFF JAMMER & 1 TARGET

1. Scenario 2 Time Index 1

a. *SNR – Non-Netted*
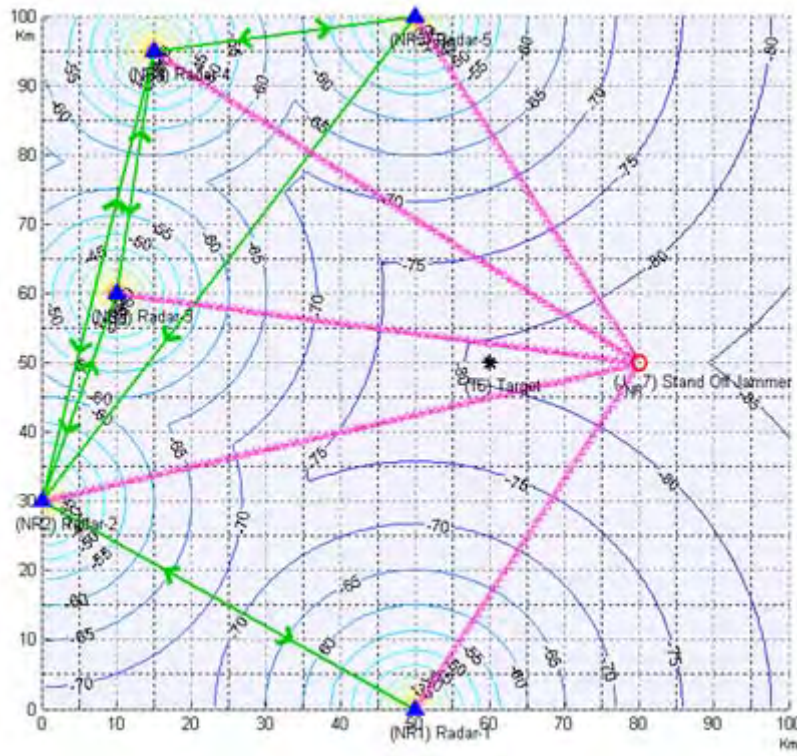
Figure 72.   Non-netted SNR Contour Chart at Time Index=1

For target at (60, 50):

Node	Radar Echo(W)	Noise(W)	SNR
1	$7.6347 \cdot 10^{-21}$	10^{-12}	$7.6347 \cdot 10^{-9}$
2	$3.2257 \cdot 10^{-21}$	10^{-12}	$3.2257 \cdot 10^{-9}$
3	$7.6347 \cdot 10^{-21}$	10^{-12}	$7.6347 \cdot 10^{-9}$
4	$3.1465 \cdot 10^{-21}$	10^{-12}	$3.1465 \cdot 10^{-9}$
5	$7.6347 \cdot 10^{-21}$	10^{-12}	$7.6347 \cdot 10^{-9}$

Max SNR = $7.6347 \cdot 10^{-9}$ = -81.1721 dB

211
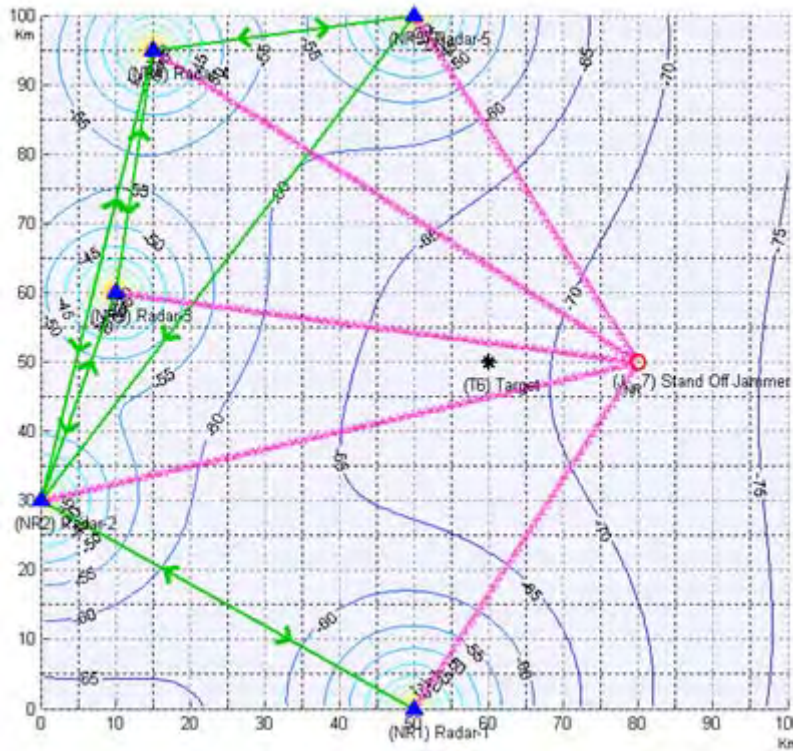
Figure 73.   Netted SNR Contour Chart at Time Index=1

For the target at (60, 50):

Node	Radar Echo (W)	Noise(W)	SNR
1	$3.2768 \cdot 10^{-20}$	10^{-12}	$3.2768 \cdot 10^{-8}$
2	$2.1299 \cdot 10^{-20}$	10^{-12}	$2.1299 \cdot 10^{-8}$
3	$3.2768 \cdot 10^{-20}$	10^{-12}	$3.2768 \cdot 10^{-8}$
4	$2.1036 \cdot 10^{-20}$	10^{-12}	$2.1036 \cdot 10^{-8}$
5	$3.2768 \cdot 10^{-20}$	10^{-12}	$3.2768 \cdot 10^{-8}$

Total SNR = $1.4064 \cdot 10^{-7}$= -68.5189 dB

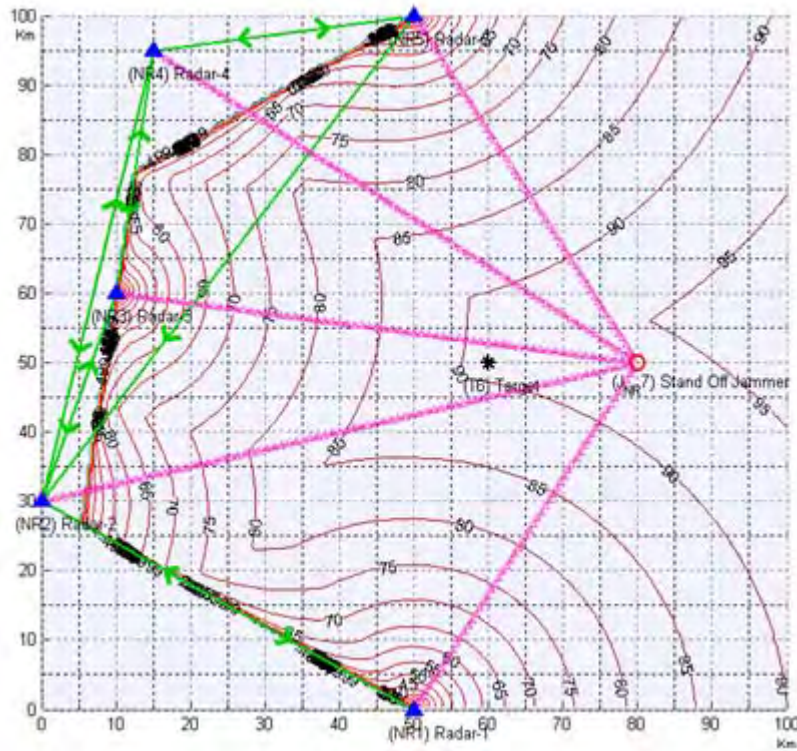|	Network disabled	Network enabled	Network improvement
SNR (dB)	-81.1721 dB	-68.5189 dB	**12.6532 dB**

c. JSR – Non-Netted

Figure 74.   Non-netted JSR Contour Chart at Time Index=1

For target at (60, 50):

Node	Jamming Power(W)	Radar Echo (W)	JSR
1	$1.7964 \cdot 10^{-11}$	$7.6347 \cdot 10^{-21}$	2352932896.9714
2	$9.5095 \cdot 10^{-12}$	$3.225 \cdot 10^{-21}$	2948083808.8287
3	$1.2951 \cdot 10^{-11}$	$7.6347 \cdot 10^{-21}$	1696357488.2551
4	$1.021 \cdot 10^{-11}$	$3.1465 \cdot 10^{-21}$	3244722585.3052
5	$1.796 \cdot 10^{-11}$	$7.6347 \cdot 10^{-21}$	2352932896.9714

Min JSR = 1696357488.2551 = 92.2952 dB

213

d. JSR –Netted
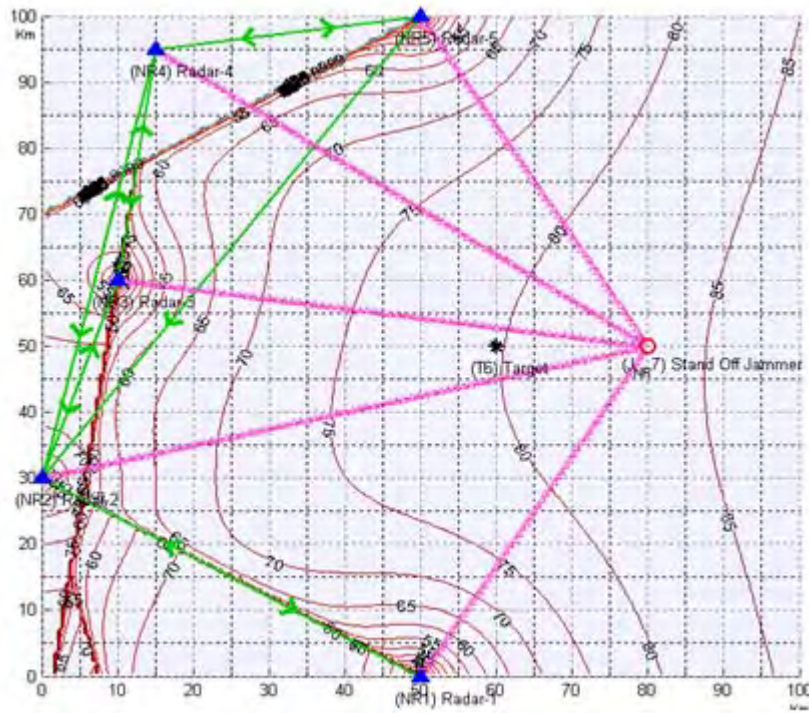
Figure 75.   Netted JSR Contour Chart at Time Index=1

For target at (60, 50):

Node	Jamming Power(W)	Radar Echo (W)	JSR
1	$1.7964 \cdot 10^{-11}$	$3.2768 \cdot 10^{-20}$	548216783.1287
2	$9.5095 \cdot 10^{-12}$	$2.1299 \cdot 10^{-20}$	446473788.393
3	$1.2951 \cdot 10^{-11}$	$3.2768 \cdot 10^{-20}$	395239339.9933
4	$1.021 \cdot 10^{-11}$	$2.1036 \cdot 10^{-20}$	485331725.6893
5	$1.7964 \cdot 10^{-11}$	$3.2768 \cdot 10^{-20}$	548216783.1287

Total JSR = 95433289.1152 = 79.797 dB

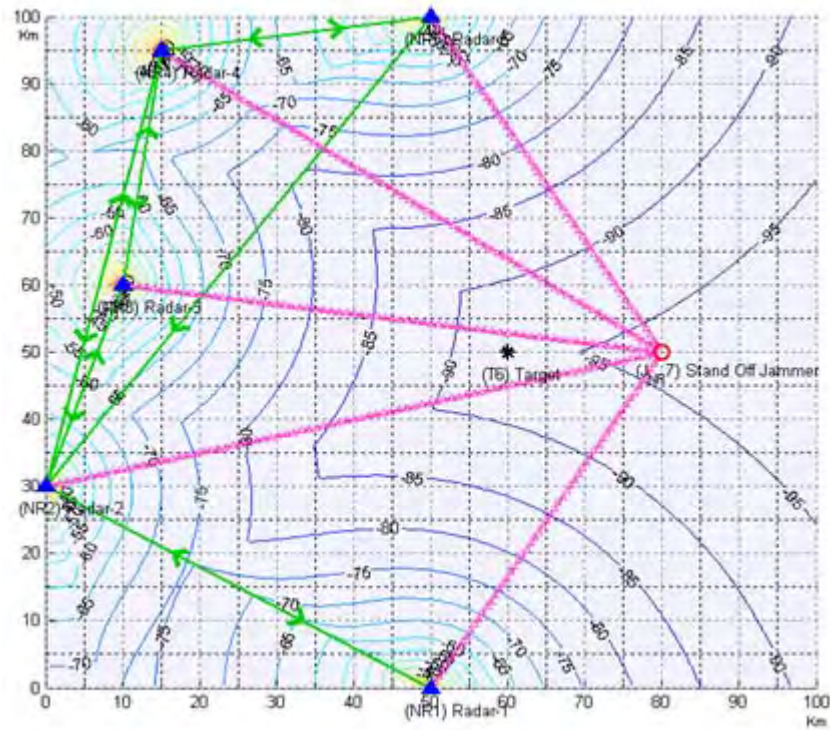|	Network disabled	Network enabled	Network improvement
JSR (dB)	92.2952 dB	79.797 dB	**12.4982 dB**

214

e. S/(J+N) – Non-Netted

Figure 76.   Non-netted SNJR Contour Chart at Time
Index=1

For target at (60, 50):

Node	Radar Echo	Noise Power	Jamming Power	SNJR
1	$7.6347 \cdot 10^{-21}$	10^{-12}	$1.7964 \cdot 10^{-11}$	$4.0259 \cdot 10^{-10}$
2	$3.2257 \cdot 10^{-21}$	10^{-12}	$9.5095 \cdot 10^{-12}$	$3.0693 \cdot 10^{-10}$
3	$7.6347 \cdot 10^{-21}$	10^{-12}	$1.2951 \cdot 10^{-12}$	$5.4724 \cdot 10^{-10}$
4	$3.1465 \cdot 10^{-21}$	10^{-12}	$1.021 \cdot 10^{-11}$	$2.807 \cdot 10^{-10}$
5	$7.6347 \cdot 10^{-21}$	10^{-12}	$1.7964 \cdot 10^{-11}$	$4.0259 \cdot 10^{-10}$

Max SNJR = $5.4724 \cdot 10^{-10}$= −92.6182 dB

f.   S/(J+N) –Netted
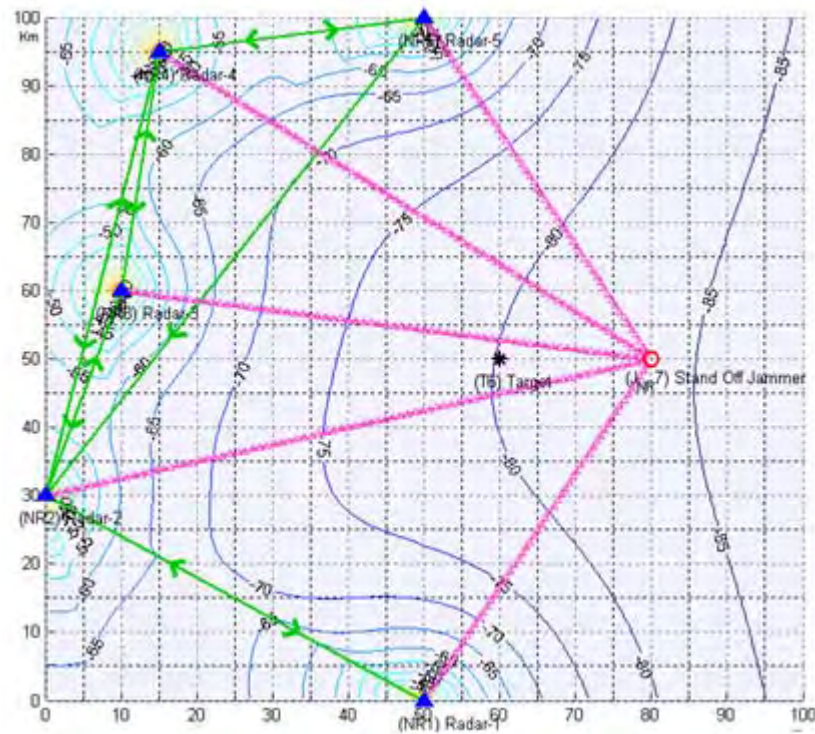
Figure 77.   Netted SNJR Contour Chart at Time Index=1

For target at (60, 50):

Node	Radar Echo	Noise Power	Jamming Power	SNJR
1	$3.2768 \cdot 10^{-20}$	10^{-12}	$1.7964 \cdot 10^{-11}$	$1.7279 \cdot 10^{-9}$
2	$2.1299 \cdot 10^{-20}$	10^{-12}	$9.5095 \cdot 10^{-12}$	$2.026 \cdot 10^{-9}$
3	$3.2768 \cdot 10^{-20}$	10^{-12}	$1.2951 \cdot 10^{-11}$	$2.3488 \cdot 10^{-9}$
4	$2.1036 \cdot 10^{-20}$	10^{-12}	$1.021 \cdot 10^{-11}$	$1.8766 \cdot 10^{-9}$
5	$3.2768 \cdot 10^{-20}$	10^{-12}	$1.7964 \cdot 10^{-11}$	$1.7279 \cdot 10^{-9}$

Total SNJR = $9.7079 \cdot 10^{-9}$ = −80.1288 dB

	Network disabled	Network enabled	Network improvement
SNJR (dB)	−92.6182 dB	−80.1288 dB	**12.4894 dB**

216

2. Scenario 2 Time Index 2

a. *SNR – Non-Netted*
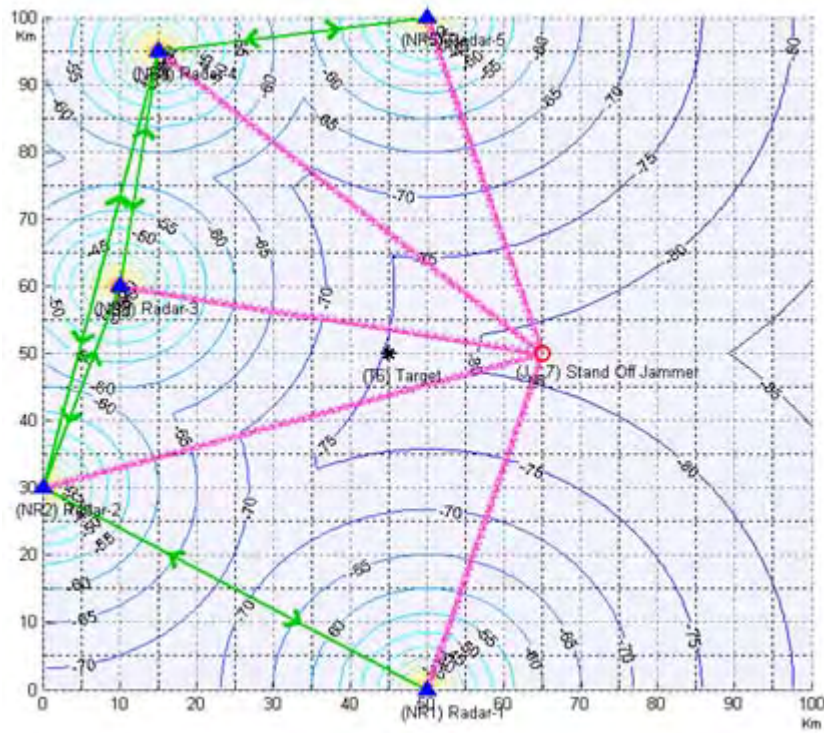
Figure 78.   Non-netted SNR Contour Chart at Time Index=2

For target at (45, 50):

Node	Radar Echo(W)	Noise(W)	SNR
1	$8.095 \cdot 10^{-21}$	10^{-12}	$8.095 \cdot 10^{-9}$
2	$8.7764 \cdot 10^{-21}$	10^{-12}	$8.7764 \cdot 10^{-9}$
3	$2.9397 \cdot 10^{-20}$	10^{-12}	$2.9397 \cdot 10^{-8}$
4	$6.0323 \cdot 10^{-21}$	10^{-12}	$6.0323 \cdot 10^{-9}$
5	$8.095 \cdot 10^{-12}$	10^{-12}	$8.095 \cdot 10^{-9}$

Max SNR = $2.9397 \cdot 10^{-8}$ = -75.3169 dB

b. *SNR –Netted*
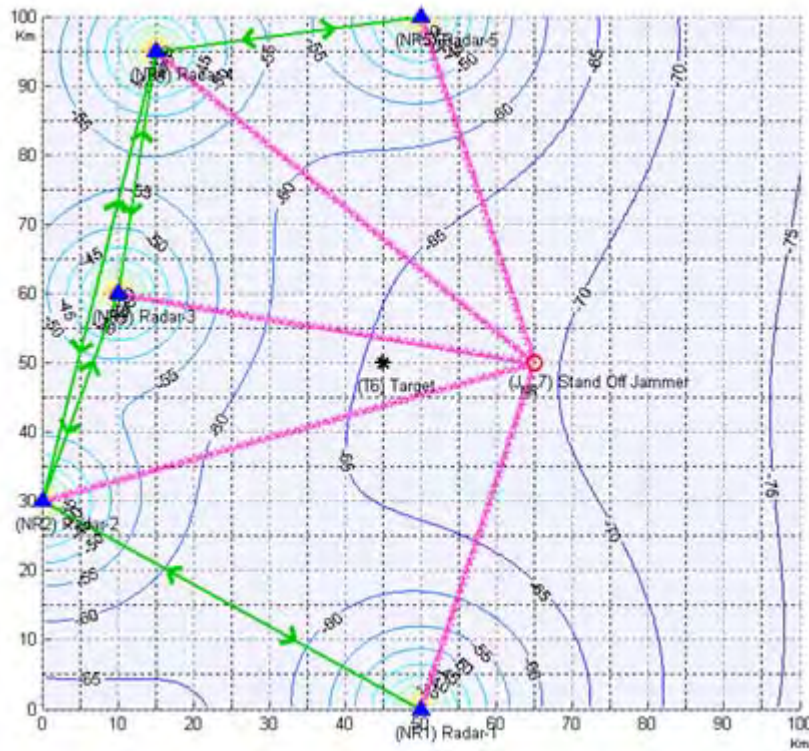
Figure 79.   Netted SNR Contour Chart at Time Index=2

For target at (45, 50):

Node	Radar Echo(W)	Noise(W)	SNR
1	$4.7033 \cdot 10^{-20}$	10^{-12}	$4.7033 \cdot 10^{-8}$
2	$4.8972 \cdot 10^{-20}$	10^{-12}	$4.8972 \cdot 10^{-8}$
3	$8.9629 \cdot 10^{-20}$	10^{-12}	$8.9629 \cdot 10^{-8}$
4	$4.0601 \cdot 10^{-20}$	10^{-12}	$4.0601 \cdot 10^{-8}$
5	$4.7033 \cdot 10^{-20}$	10^{-12}	$4.7033 \cdot 10^{-8}$

Total SNR = $2.7327 \cdot 10^{-7}$ = -65.6341 dB

	Network disabled	Network enabled	Network improvement
SNR (dB)	-75.3169 dB	-65.6341 dB	**9.6828 dB**

218
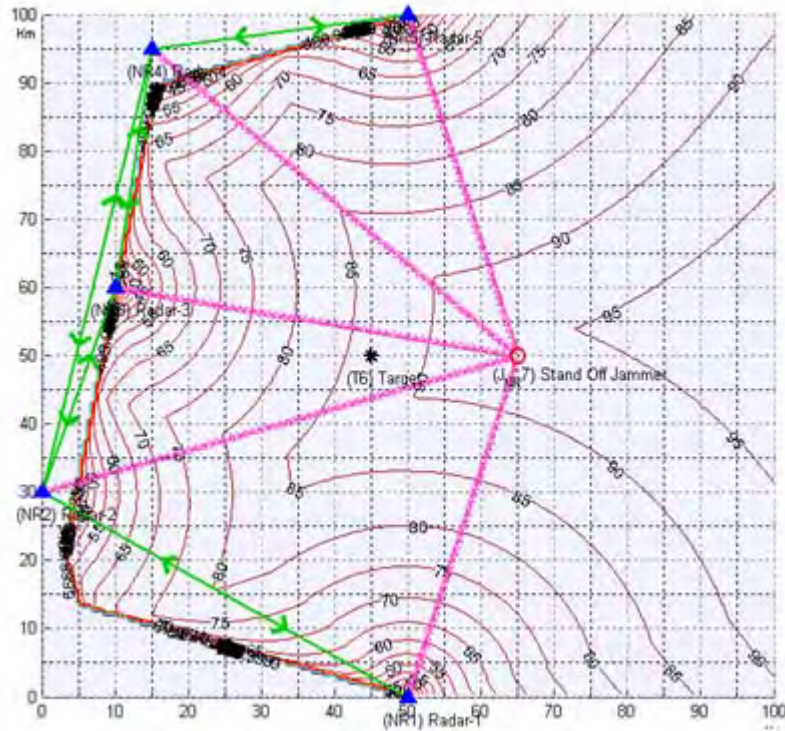
c. *JSR – Non-Netted*

Figure 80.   Non-netted JSR Contour Chart at Time Index=2

For target at (45, 50):

Node	Jamming Power(W)	Radar Echo (W)	JSR
1	$2.2003 \cdot 10^{-11}$	$8.095 \cdot 10^{-21}$	2718090550.4659
2	$1.3922 \cdot 10^{-11}$	$8.7764 \cdot 10^{-21}$	1586359166.5851
3	$2.0653 \cdot 10^{-11}$	$2.9397 \cdot 10^{-20}$	702560415.2673
4	$1.3887 \cdot 10^{-11}$	$6.0323 \cdot 10^{-21}$	2302130378.0091
5	$2.2003 \cdot 10^{-11}$	$8.095 \cdot 10^{-21}$	2718090550.4659

Min JSR = 702560415.2673 = 88.4668 dB

d. JSR –Netted
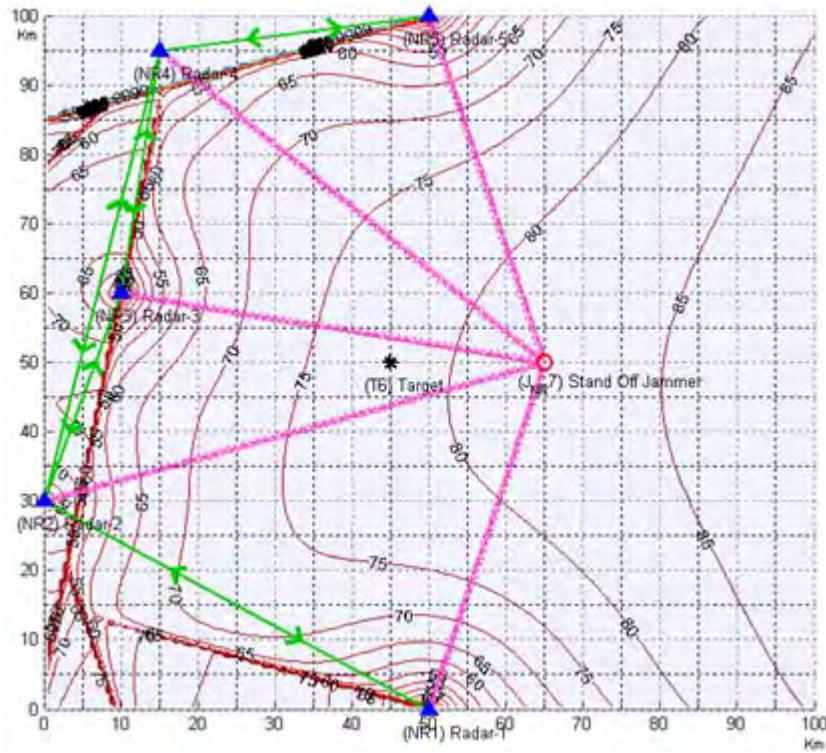
Figure 81. Netted JSR Contour Chart at Time Index=2

For target at (45, 50):

Node	Jamming Power(W)	Radar Echo (W)	JSR
1	$2.2003 \cdot 10^{-11}$	$4.7033 \cdot 10^{-20}$	467817995.0508
2	$1.3922 \cdot 10^{-11}$	$4.8972 \cdot 10^{-20}$	284291689.5865
3	$2.0653 \cdot 10^{-11}$	$8.9629 \cdot 10^{-20}$	230431678.4694
4	$1.3887 \cdot 10^{-11}$	$4.0601 \cdot 10^{-20}$	342041207.0007
5	$2.2003 \cdot 10^{-11}$	$4.7033 \cdot 10^{-20}$	467817995.0508

Total JSR = 66418763.7848 = 78.2229 dB

|	Network disabled	Network enabled	Network improvement
JSR (dB)	88.4668 dB	78.2229 dB	**10.2439 dB**

e.   S/(J+N) – Non-Netted
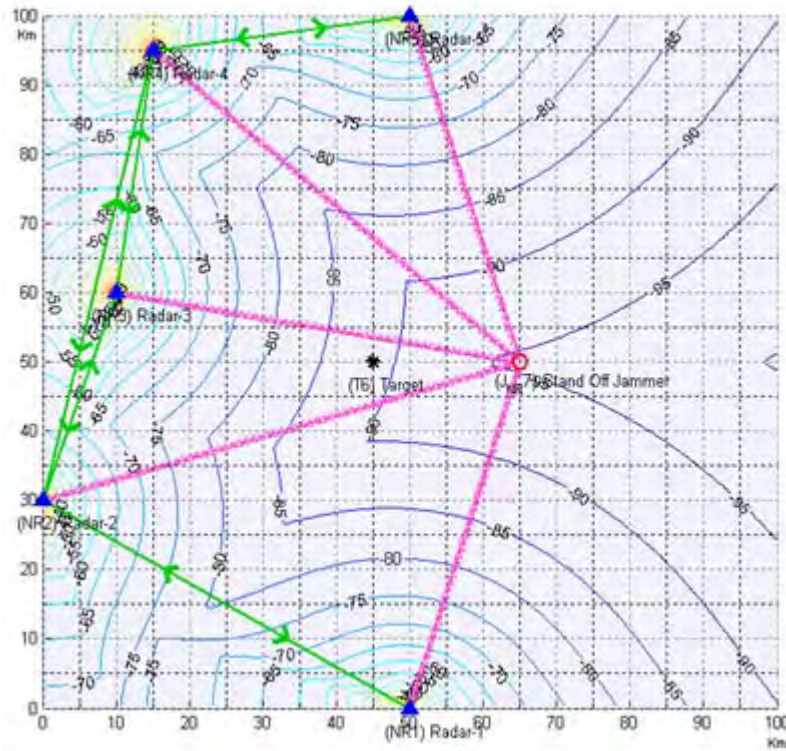
Figure 82.   Non-netted SNJR Contour Chart at Time Index=2

For target at (45, 50):

Node	Radar Echo	Noise Power	Jamming Power	SNJR
1	$8.095 \cdot 10^{-21}$	10^{-12}	$2.2003 \cdot 10^{-11}$	$3.5191 \cdot 10^{-10}$
2	$8.776 \cdot 10^{-21}$	10^{-12}	$1.3922 \cdot 10^{-11}$	$5.8813 \cdot 10^{-10}$
3	$2.9397 \cdot 10^{-20}$	10^{-12}	$2.0653 \cdot 10^{-11}$	$1.3576 \cdot 10^{-9}$
4	$6.0323 \cdot 10^{-21}$	10^{-12}	$1.3887 \cdot 10^{-11}$	$4.052 \cdot 10^{-10}$
5	$8.095 \cdot 10^{-21}$	10^{-12}	$2.2003 \cdot 10^{-11}$	$3.5191 \cdot 10^{-10}$

Max SNJR = $1.3576e \cdot 10^{-9}$ = -88.6722 dB

f.   S/(J+N) –Netted
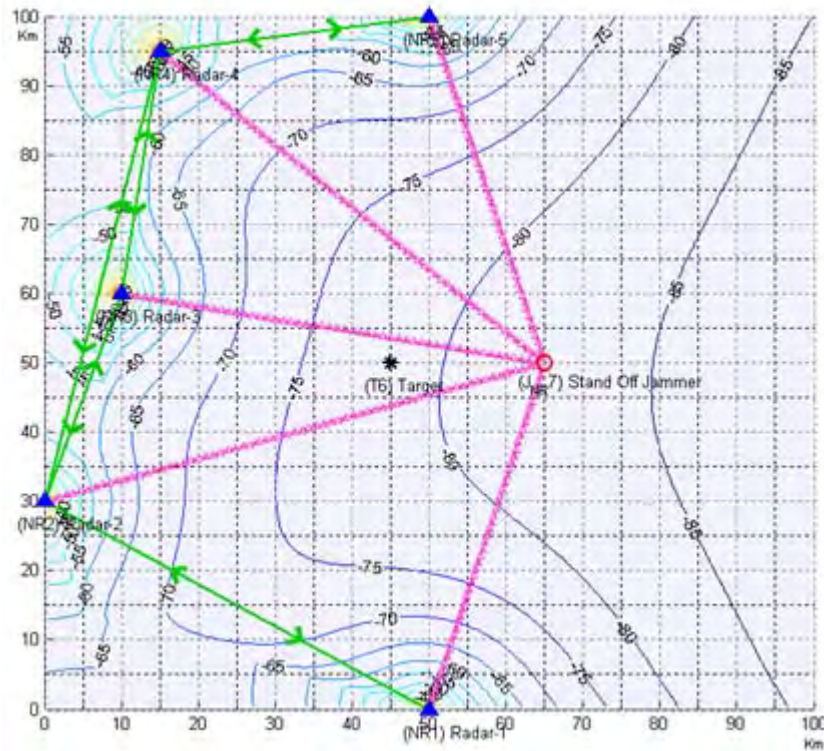
Figure 83.   Netted SNJR Contour Chart at Time Index=2

For target at (45, 50):

Node	Radar Echo	Noise Power	Jamming Power	SNJR
1	$4.7033 \cdot 10^{-20}$	10^{-12}	$2.2003 \cdot 10^{-11}$	$2.0447 \cdot 10^{-9}$
2	$4.8972 \cdot 10^{-20}$	10^{-12}	$1.3922 \cdot 10^{-11}$	$3.2818 \cdot 10^{-9}$
3	$8.9629 \cdot 10^{-20}$	10^{-12}	$2.0653 \cdot 10^{-11}$	$4.1393 \cdot 10^{-9}$
4	$4.0601 \cdot 10^{-20}$	10^{-12}	$1.3887 \cdot 10^{-11}$	$2.7272 \cdot 10^{-9}$
5	$4.7033 \cdot 10^{-20}$	10^{-12}	$2.2003 \cdot 10^{-11}$	$2.0447 \cdot 10^{-9}$

Total SNJR = $1.4238 \cdot 10^{-8}$ = -78.4656 dB

	Network disabled	Network enabled	Network improvement
SNJR (dB)	-88.6722 dB	-78.4656 dB	**10.2066 dB**

222

3. Scenario 2 Time Index 3

a. *SNR – Non-Netted*
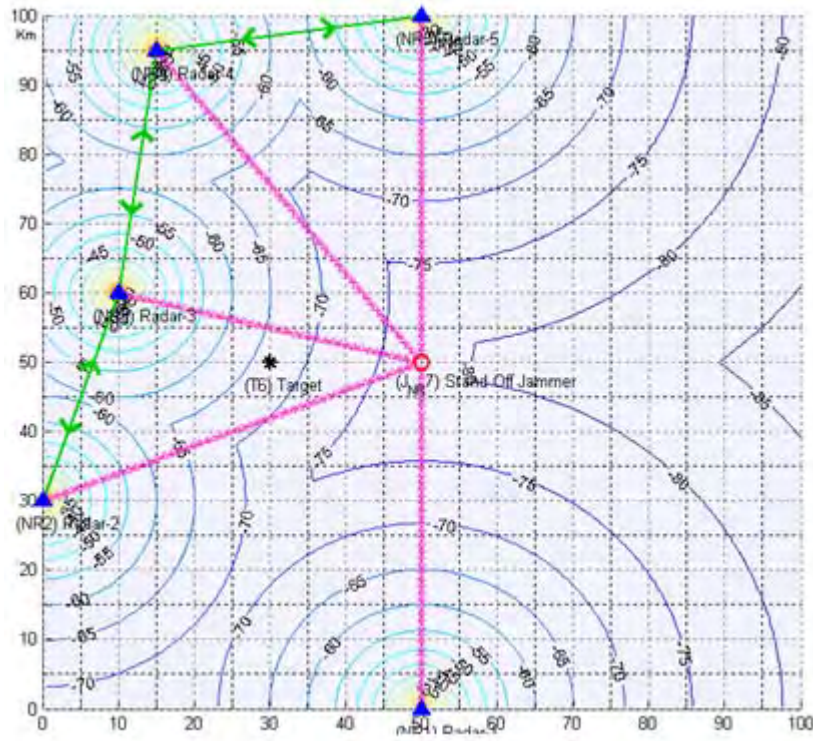
Figure 84.   Non-netted SNR Contour Chart at Time Index=3

For target at (30, 50):

Node	Radar Echo(W)	Noise(W)	SNR
1	$6.1368 \cdot 10^{-21}$	10^{-12}	$6.1368 \cdot 10^{-9}$
2	$3.0539 \cdot 10^{-20}$	10^{-12}	$3.0539 \cdot 10^{-8}$
3	$2.0644 \cdot 10^{-19}$	10^{-12}	$2.0644 \cdot 10^{-7}$
4	$1.0195 \cdot 10^{-20}$	10^{-12}	$1.0195 \cdot 10^{-8}$
5	$6.1368 \cdot 10^{-20}$	10^{-12}	$6.1368 \cdot 10^{-9}$

Max SNR = $2.0644 \cdot 10^{-7}$ = -66.852 dB

b.   *SNR –Netted*
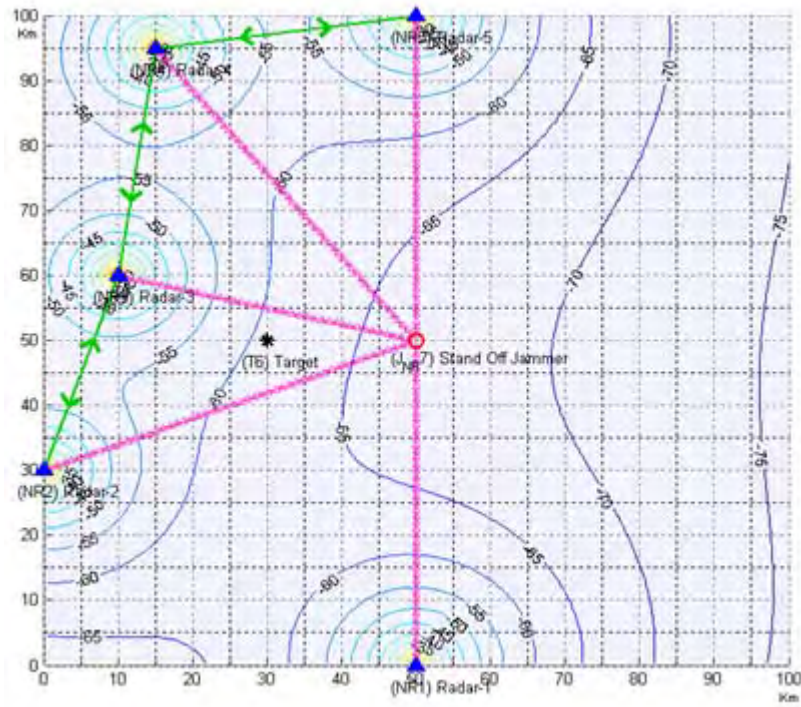
Figure 85.   Netted SNR Contour Chart at Time Index=3

For target at (30, 50):

Node	Radar Echo (W)	Noise(W)	SNR
1	$6.9466 \cdot 10^{-20}$	10^{-12}	$6.9466 \cdot 10^{-8}$
2	$1.5496 \cdot 10^{-19}$	10^{-12}	$1.5496 \cdot 10^{-7}$
3	$4.0291 \cdot 10^{-19}$	10^{-12}	$4.0291 \cdot 10^{-7}$
4	$8.9535 \cdot 10^{-20}$	10^{-12}	$8.9535 \cdot 10^{-8}$
5	$6.9466 \cdot 10^{-20}$	10^{-12}	$6.9466 \cdot 10^{-8}$

Total SNR = $7.8634 \cdot 10^{-7}$= -61.0439 dB

	Network disabled	Network enabled	Network improvement
SNR (dB)	-66.852 dB	-61.0439 dB	**5.8081dB**

c.   *JSR – Non-Netted*
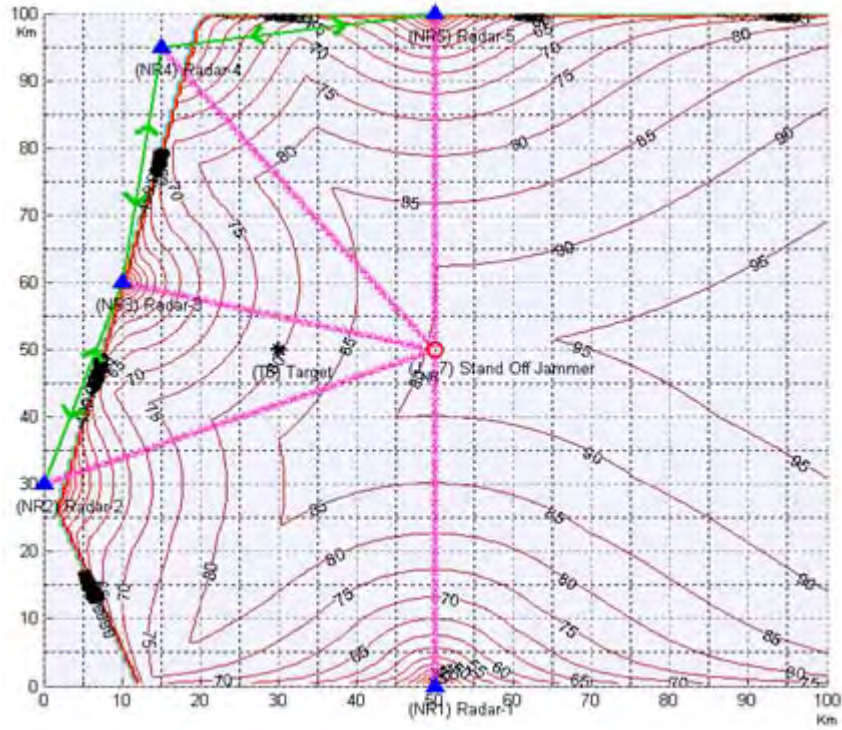
Figure 86.   Non-netted JSR Contour Chart at Time Index=3

For target at (30, 50):

Node	Jamming Power(W)	Radar Echo (W)	JSR
1	$2.4087 \cdot 10^{-11}$	$6.1368 \cdot 10^{-21}$	3924974653.5797
2	$2.1884 \cdot 10^{-11}$	$3.0539 \cdot 10^{-20}$	716607743.2427
3	$3.7242 \cdot 10^{-11}$	$2.0644 \cdot 10^{-19}$	180398946.8708
4	$1.8818 \cdot 10^{-11}$	$1.0195 \cdot 10^{-20}$	1845860091.197
5	$2.4087 \cdot 10^{-11}$	$6.1368 \cdot 10^{-21}$	3924974653.5797

Min JSR = 180398946.8708 = 82.5623 dB

d.   JSR –Netted
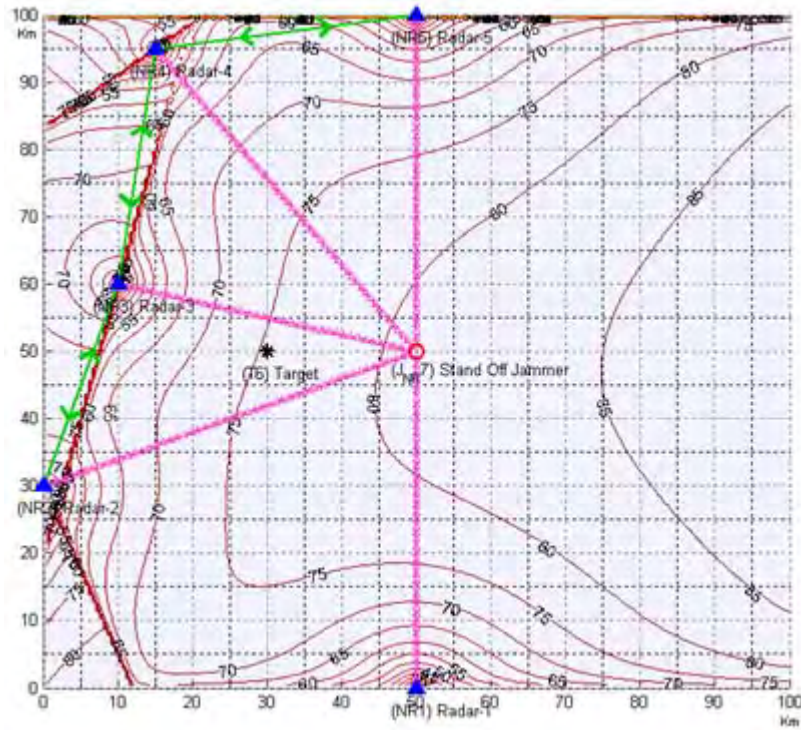
Figure 87.   Netted JSR Contour Chart at Time Index=3

For target at (30, 50):

Node	Jamming Power(W)	Radar Echo (W)	JSR
1	$2.4087 \cdot 10^{-11}$	$6.9466 \cdot 10^{-20}$	346739681.7191
2	$2.1884 \cdot 10^{-11}$	$1.5496 \cdot 10^{-19}$	141222154.1727
3	$3.7242 \cdot 10^{-11}$	$4.0291 \cdot 10^{-19}$	92433347.4377
4	$1.8818 \cdot 10^{-11}$	$8.9535 \cdot 10^{-20}$	210174948.4691
5	$2.4087 \cdot 10^{-11}$	$6.9466 \cdot 10^{-20}$	346739681.7191

Total JSR = 35179550.0136 = 75.4629 dB

|	Network disabled	Network enabled	Network improvement
JSR (dB)	82.5623 dB	75.4629 dB	**7.0994 dB**

e.   *S/(J+N) – Non-Netted*
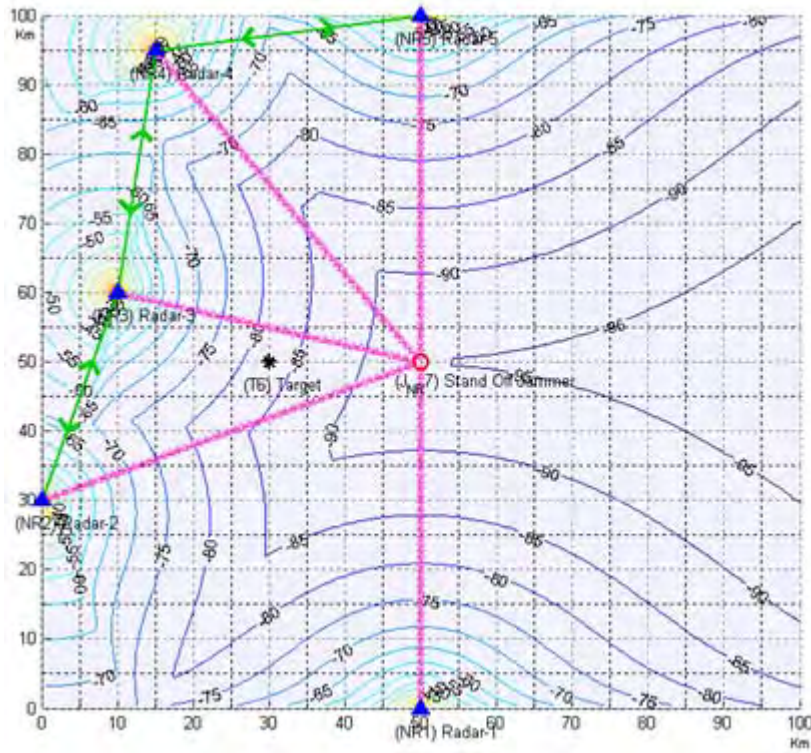
Figure 88.   Non-netted SNJR Contour Chart at Time Index=3

For target at (30, 50):

Node	Radar Echo	Noise Power	Jamming Power	SNJR
1	$6.1368 \cdot 10^{-21}$	10^{-12}	$2.4087 \cdot 10^{-11}$	$2.4462 \cdot 10^{-10}$
2	$3.0539 \cdot 10^{-20}$	10^{-12}	$2.1884 \cdot 10^{-11}$	$1.3345 \cdot 10^{-9}$
3	$2.0644 \cdot 10^{-19}$	10^{-12}	$3.7242 \cdot 10^{-11}$	$5.3983 \cdot 10^{-9}$
4	$1.0195 \cdot 10^{-20}$	10^{-12}	$1.8818 \cdot 10^{-11}$	$5.1442 \cdot 10^{-10}$
5	$6.1368 \cdot 10^{-21}$	10^{-12}	$2.4087 \cdot 10^{-11}$	$2.4462 \cdot 10^{-10}$

Max SNJR = $5.3983 \cdot 10^{-9}$ = -82.6774 dB

f.   S/(J+N)– Netted
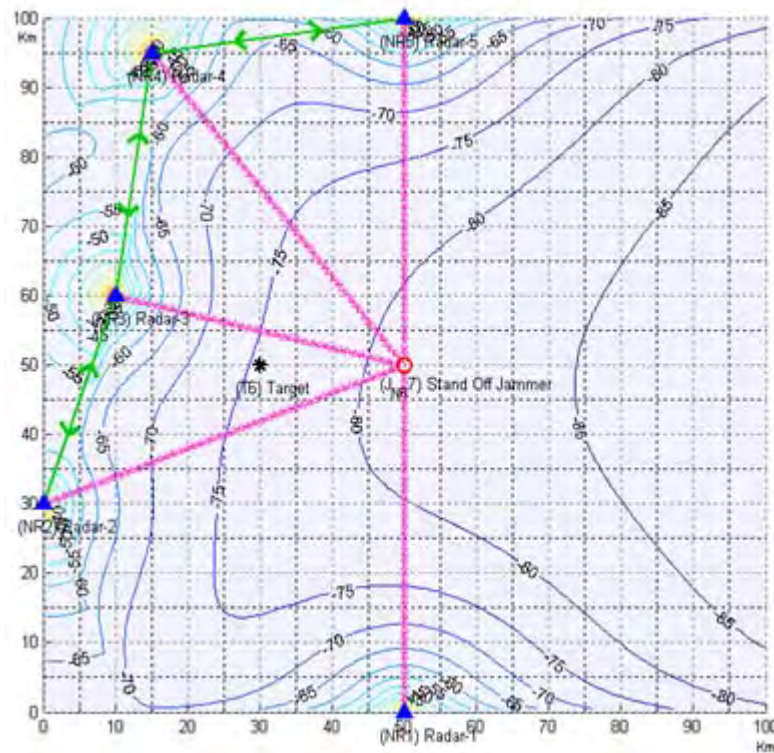
Figure 89.   Netted SNJR Contour Chart at Time Index=3

For target at (30, 50):

Node	Radar Echo	Noise Power	Jamming Power	SNJR
1	$6.9466 \cdot 10^{-20}$	10^{-12}	$2.4087 \cdot 10^{-11}$	$2.769 \cdot 10^{-9}$
2	$1.5496 \cdot 10^{-19}$	10^{-12}	$2.1884 \cdot 10^{-11}$	$6.7716 \cdot 10^{-9}$
3	$4.0291 \cdot 10^{-19}$	10^{-12}	$3.7242 \cdot 10^{-11}$	$1.0536 \cdot 10^{-8}$
4	$8.9535 \cdot 10^{-20}$	10^{-12}	$1.8818 \cdot 10^{-11}$	$4.5179 \cdot 10^{-9}$
5	$6.9466 \cdot 10^{-20}$	10^{-12}	$2.4087 \cdot 10^{-11}$	$2.769 \cdot 10^{-9}$

Total SNJR = $2.7363 \cdot 10^{-8}$ = –75.6283 dB

	Network disabled	Network enabled	Network improvement
SNJR (dB)	–82.6774 dB	–75.6283 dB	**7.049 dB**

C.   SCENARIO 3: 2 STAND IN JAMMERS

1.   Scenario 3 Time Index 1

a.   *SNR – Non-Netted*
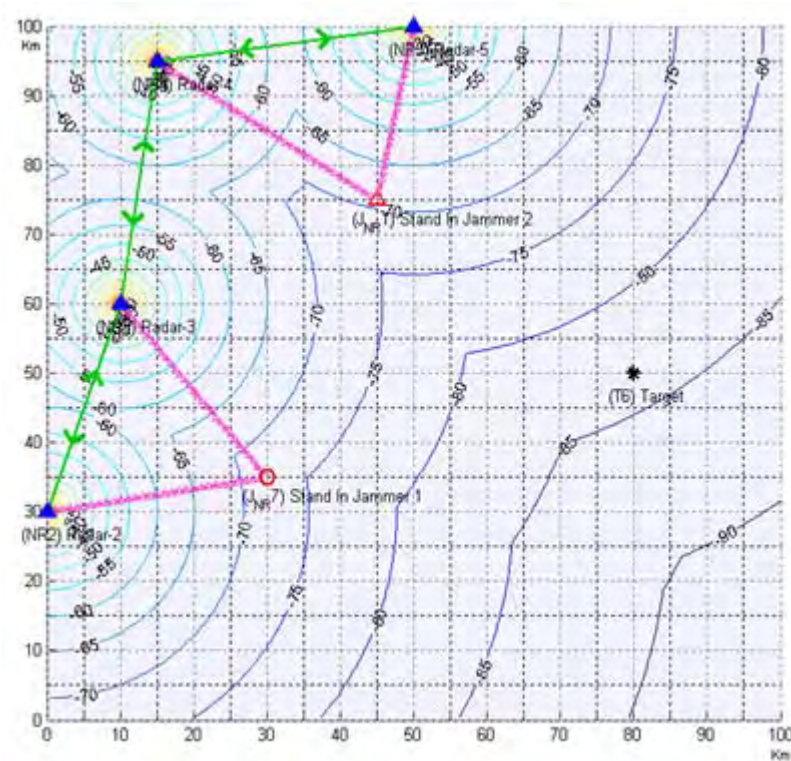
Figure 90.   Non-netted SNR Contour Chart at Time Index=1

For target at (80, 50):

Node	Radar Echo(W)	Noise(W)	SNR
2	$1.1161 \cdot 10^{-21}$	10^{-12}	$1.1161 \cdot 10^{-9}$
3	$2.0644 \cdot 10^{-21}$	10^{-12}	$2.0644 \cdot 10^{-9}$
4	$1.3212 \cdot 10^{-21}$	10^{-12}	$1.3212 \cdot 10^{-9}$
5	$4.4646 \cdot 10^{-21}$	10^{-12}	$4.4646 \cdot 10^{-9}$

Max SNR = $4.4646 \cdot 10^{-9}$ = -83.5022 dB

229

b.   SNR – Netted
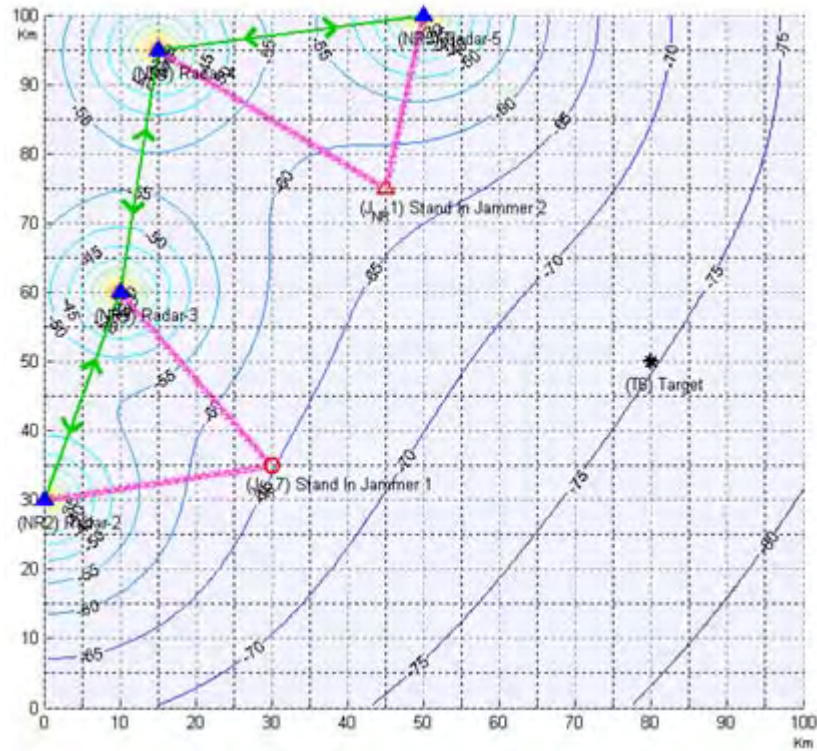
Figure 91.   Netted SNR Contour Chart at Time Index=1

For target at (80, 50):

Node	Radar Echo(W)	Noise(W)	SNR
2	$6.0808 \cdot 10^{-21}$	10^{-12}	$6.0808 \cdot 10^{-9}$
3	$8.2698 \cdot 10^{-21}$	10^{-12}	$8.2698 \cdot 10^{-9}$
4	$6.6159 \cdot 10^{-21}$	10^{-12}	$6.6159 \cdot 10^{-9}$
5	$1.2162 \cdot 10^{-20}$	10^{-12}	$1.2162 \cdot 10^{-9}$

Total SNR = $3.3128 \cdot 10^{-8}$ = -74.7981 dB

	Network disabled	Network enabled	Network improvement
SNR (dB)	-83.5022 dB	-74.7981 dB	**8.7041 dB**

c. JSR – Non-Netted
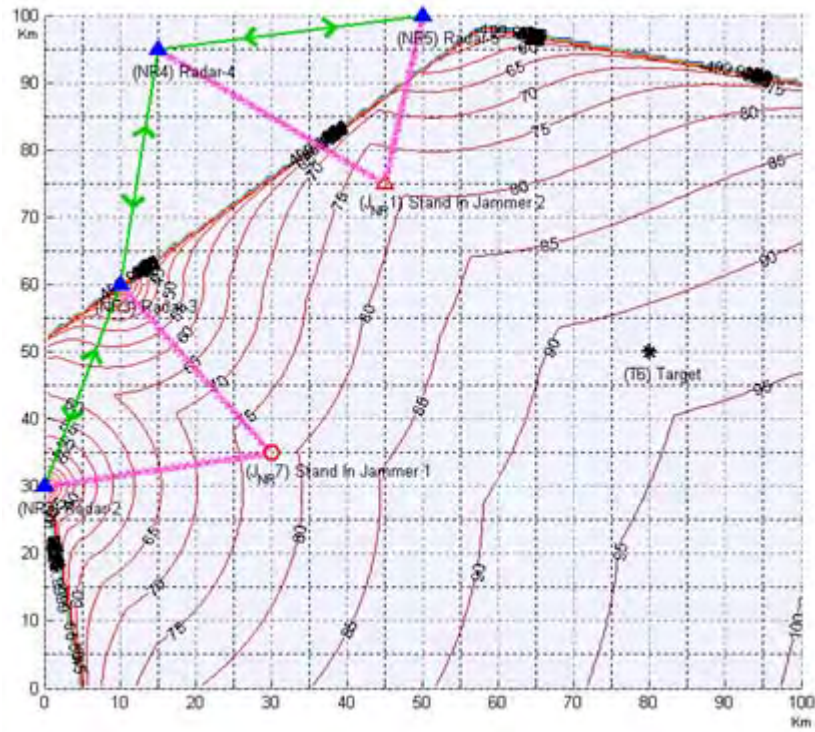
Figure 92.   Non-netted JSR Contour Chart at Time Index=1

For target at (80, 50):

Node	Jamming Power(W)	Radar Echo (W)	JSR
2	$6.9891 \cdot 10^{-12}$	$1.1161 \cdot 10^{-21}$	6261820912.0461
3	$4.6117 \cdot 10^{-12}$	$2.0644 \cdot 10^{-21}$	2233896340.3644
4	$4.9881 \cdot 10^{-12}$	$1.3212 \cdot 10^{-21}$	3775371748.1475
5	$7.383 \cdot 10^{-12}$	$4.4646 \cdot 10^{-21}$	1653677775.5514

Min JSR = 1653677775.5514 = 92.1845 dB
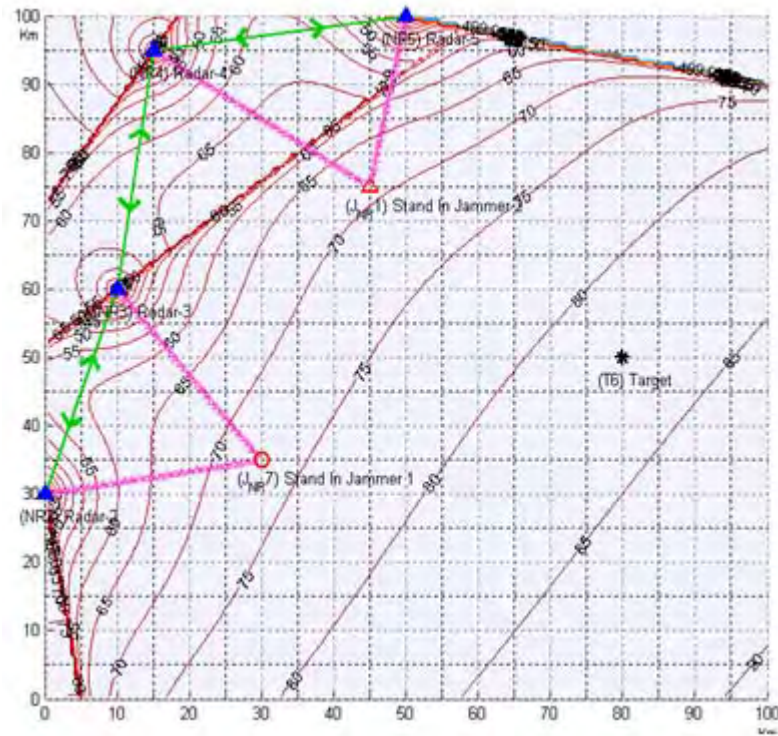
Figure 93.   Netted JSR Contour Chart at Time Index=1

For target at (80, 50):

Node	Jamming Power(W)	Radar Echo (W)	JSR
2	$6.9891 \cdot 10^{-12}$	$6.0808 \cdot 10^{-21}$	1149379756.2493
3	$4.6117 \cdot 10^{-12}$	$8.2698 \cdot 10^{-21}$	557654005.671
4	$4.9881 \cdot 10^{-12}$	$6.6159 \cdot 10^{-21}$	753965576.7226
5	$7.383 \cdot 10^{-12}$	$1.2162 \cdot 10^{-20}$	607077010.1143

Total JSR = 177405020.9081 = 82.4897 dB

	Network disabled	Network enabled	Network improvement
JSR (dB)	92.1845 dB	82.4897 dB	**9.6948 dB**

e. S/(J+N) – Non-Netted
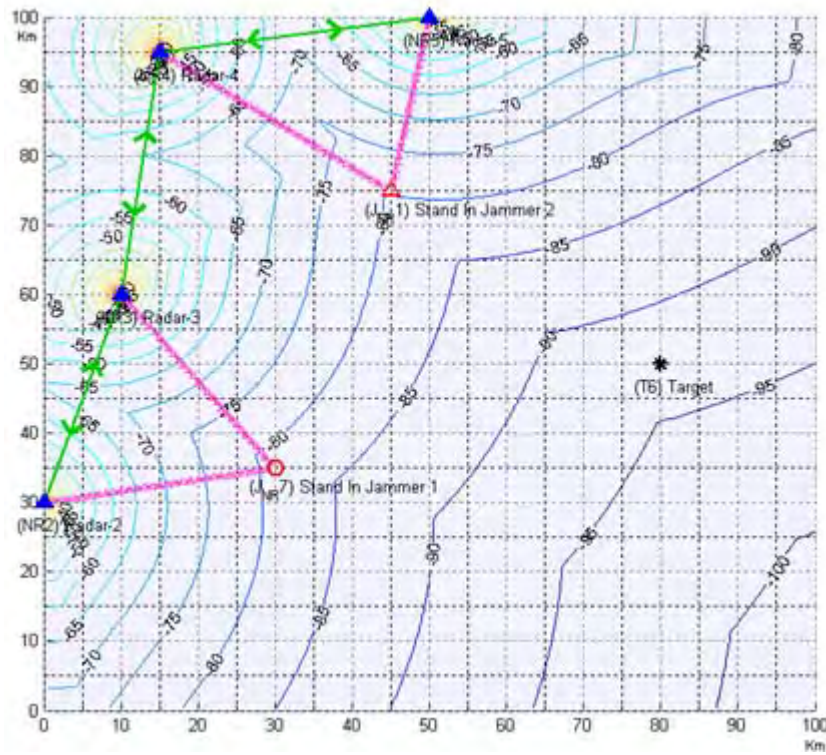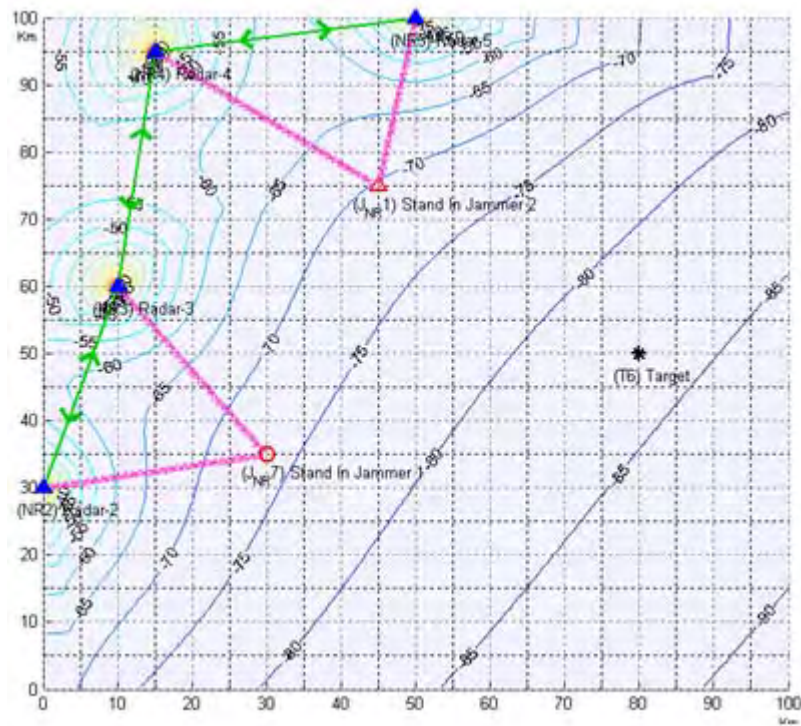

Figure 94.   Non-netted SNJR Contour Chart at Time
Index=1

For target at (80, 50):

Node	Radar Echo	Noise Power	Jamming Power	SNJR
2	$1.1161 \cdot 10^{-21}$	10^{-12}	$6.9891 \cdot 10^{-12}$	$1.3971 \cdot 10^{-10}$
3	$2.0644 \cdot 10^{-21}$	10^{-12}	$4.6117 \cdot 10^{-12}$	$3.6788 \cdot 10^{-10}$
4	$1.3212 \cdot 10^{-21}$	10^{-12}	$4.9881 \cdot 10^{-12}$	$2.2064 \cdot 10^{-10}$
5	$4.4646 \cdot 10^{-21}$	10^{-12}	$7.383 \cdot 10^{-12}$	$5.3258 \cdot 10^{-10}$

Max SNJR = $5.3258 \cdot 10^{-10}$= -92.7362 dB

233

f.   S/(J+N)- Netted

Figure 95.   Netted SNJR Contour Chart at Time Index=1

For target at (80, 50):

Node	Radar Echo	Noise Power	Jamming Power	SNJR
2	$6.0808 \cdot 10^{-21}$	10^{-12}	$6.9891 \cdot 10^{-12}$	$7.6113 \cdot 10^{-10}$
3	$8.2698 \cdot 10^{-21}$	10^{-12}	$4.6117 \cdot 10^{-12}$	$1.4737 \cdot 10^{-9}$
4	$6.6159 \cdot 10^{-21}$	10^{-12}	$4.9881 \cdot 10^{-12}$	$1.1048 \cdot 10^{-9}$
5	$1.2162 \cdot 10^{-20}$	10^{-12}	$7.383 \cdot 10^{-12}$	$1.4507 \cdot 10^{-9}$

Total SNJR = $4.7904 \cdot 10^{-9}$ = -83.1963 dB

	Network disabled	Network enabled	Network improvement
SNJR (dB)	-92.7362 dB	-83.1963 dB	**9.5399 dB**

234

2. Scenario 3 Time Index 2

a. *SNR – Non-Netted*
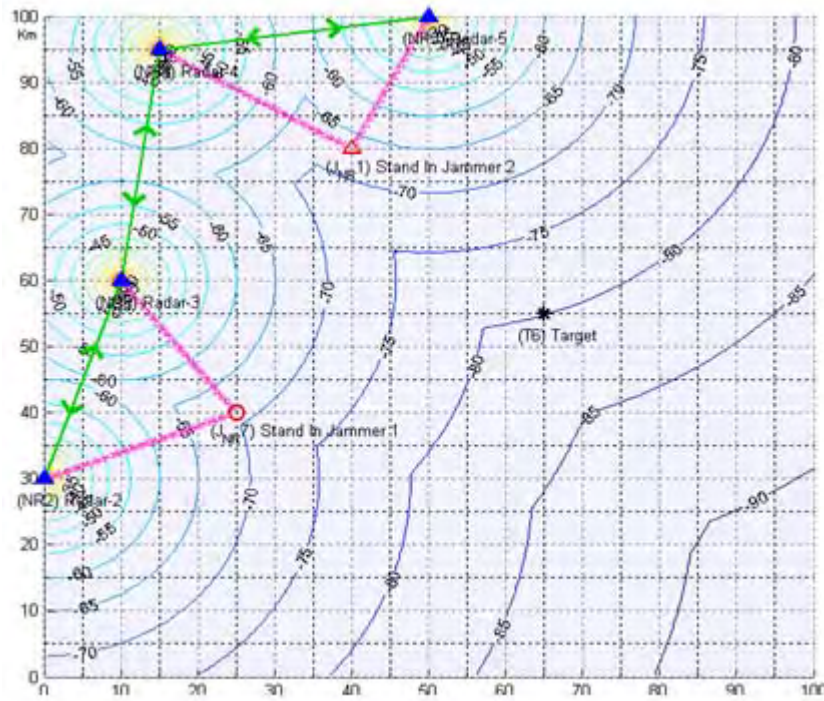
Figure 96. Non-netted SNR Contour Chart at Time Index=2

For target at (65, 55):

Node	Radar Echo(W)	Noise(W)	SNR
2	$2.1941 \cdot 10^{-21}$	10^{-12}	$2.1941 \cdot 10^{-9}$
3	$5.548 \cdot 10^{-21}$	10^{-12}	$5.548 \cdot 10^{-9}$
4	$3.0702 \cdot 10^{-21}$	10^{-12}	$3.0702 \cdot 10^{-9}$
5	$1.0195 \cdot 10^{-20}$	10^{-12}	$1.0195 \cdot 10^{-8}$

Max SNR = $1.0195 \cdot 10^{-8}$ = -79.9163 dB

b.   SNR – Netted
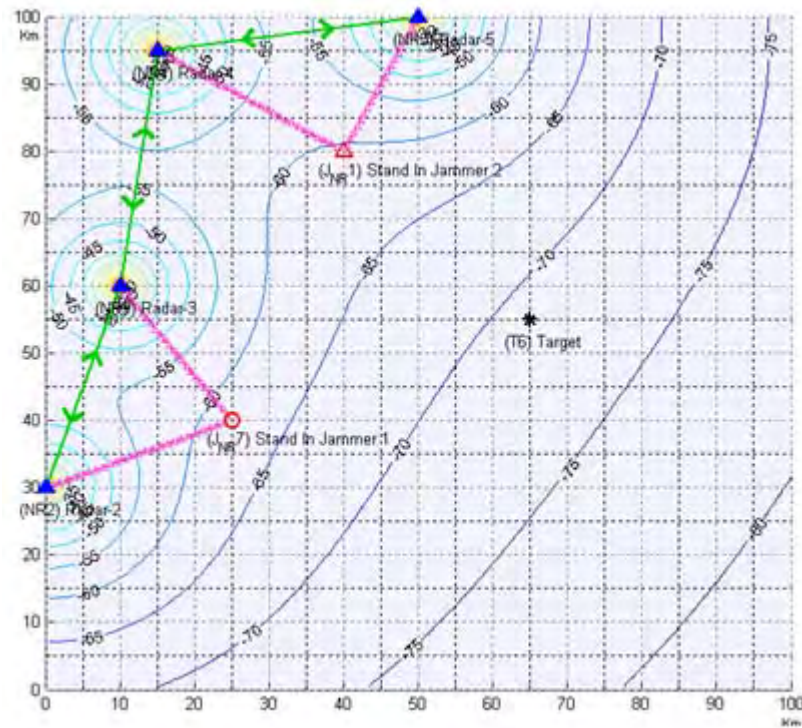
Figure 97.   Netted SNR Contour Chart at Time Index=2

For target at (65, 55):

Node	Radar Echo(W)	Noise(W)	SNR
2	$1.3008 \cdot 10^{-20}$	10^{-12}	$1.3008 \cdot 10^{-8}$
3	$2.0685 \cdot 10^{-20}$	10^{-12}	$2.0685 \cdot 10^{-8}$
4	$1.5387 \cdot 10^{-20}$	10^{-12}	$1.5387 \cdot 10^{-8}$
5	$2.8039 \cdot 10^{-20}$	10^{-12}	$2.8039 \cdot 10^{-8}$

Total SNR = $7.712 \cdot 10^{-8}$= –71.1283 dB

	Network disabled	Network enabled	Network improvement
SNR (dB)	–79.9163 dB	–71.1283 dB	**8.788 dB**

236
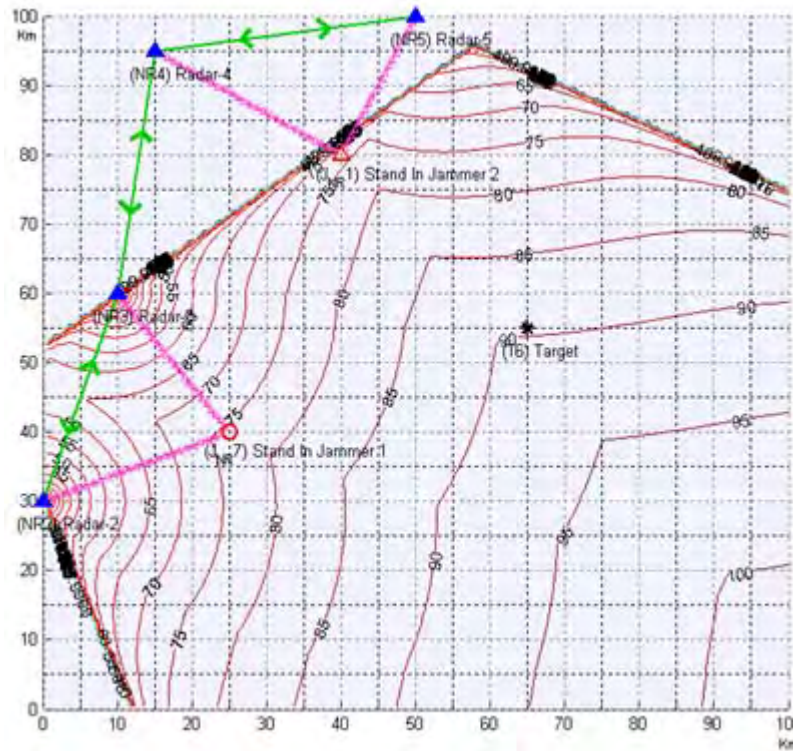
c.   JSR – Non-Netted

Figure 98.   Non-netted JSR Contour Chart at Time Index=2

For target at (65, 55):

Node	Jamming Power(W)	Radar Echo (W)	JSR
2	$8.9448 \cdot 10^{-12}$	$2.1941 \cdot 10^{-21}$	4076774915.7844
3	$6.9522 \cdot 10^{-12}$	$5.548 \cdot 10^{-21}$	1253087303.8055
4	$7.5613 \cdot 10^{-12}$	$3.0702 \cdot 10^{-21}$	2462799115.4328
5	$9.172 \cdot 10^{-12}$	$1.0195 \cdot 10^{-20}$	899683794.9771

Min JSR = 899683794.9771 = 89.5409 dB

d.   JSR – Netted
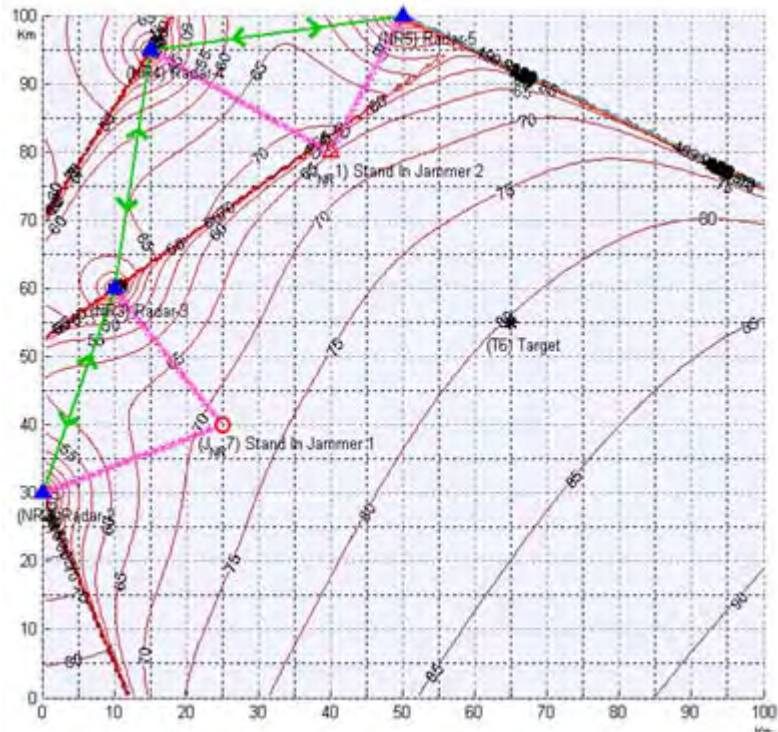
Figure 99.   Netted JSR Contour Chart at Time Index=2

For target at (65, 55):

Node	Jamming Power(W)	Radar Echo (W)	JSR
2	$8.9448 \cdot 10^{-12}$	$1.3008 \cdot 10^{-20}$	687640094.5942
3	$6.9522 \cdot 10^{-12}$	$2.0685 \cdot 10^{-20}$	336099360.6127
4	$7.5613 \cdot 10^{-12}$	$1.5387 \cdot 10^{-20}$	491395673.1209
5	$9.172 \cdot 10^{-12}$	$2.8039 \cdot 10^{-20}$	327109815.3063

Total JSR = 105023736.6453 = 80.2129 dB

	Network disabled	Network enabled	Network improvement
JSR (dB)	89.5409 dB	80.2129 dB	**9.328 dB**

238
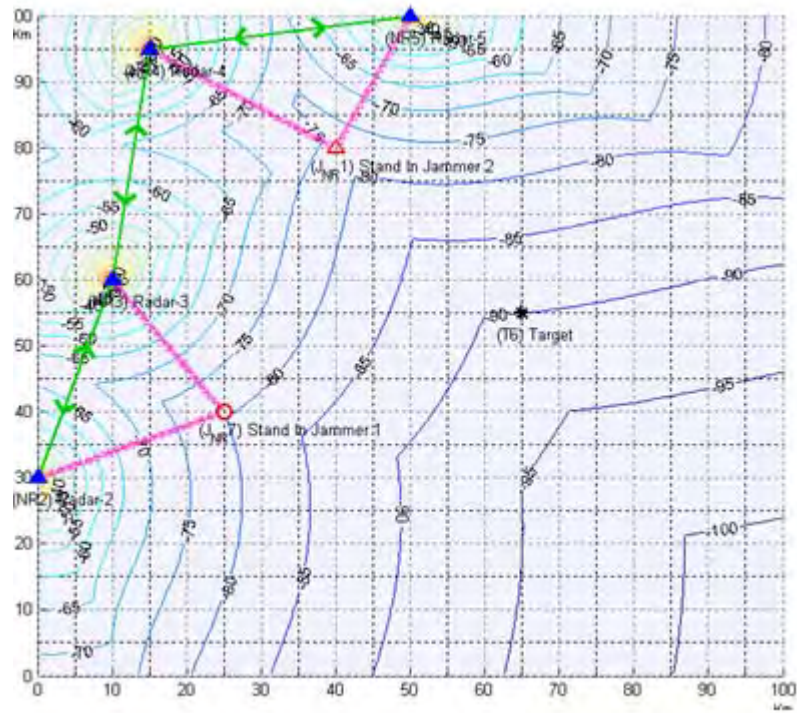
e. S/(J+N) – Non-Netted

Figure 100. Non-netted SNJR Contour Chart at Time
Index=2

For target at (65, 55):

Node	Radar Echo	Noise Power	Jamming Power	SNJR
2	$2.1941 \cdot 10^{-21}$	10^{-12}	$8.9448 \cdot 10^{-12}$	$2.2063 \cdot 10^{-10}$
3	$5.548 \cdot 10^{-21}$	10^{-12}	$6.9522 \cdot 10^{-12}$	$6.9768 \cdot 10^{-10}$
4	$3.0702 \cdot 10^{-21}$	10^{-12}	$7.5613 \cdot 10^{-12}$	$3.5861 \cdot 10^{-10}$
5	$1.0195 \cdot 10^{-20}$	10^{-12}	$9.172 \cdot 10^{-12}$	$1.0022 \cdot 10^{-9}$

Max SNJR = $1.0022 \cdot 10^{-9}$ = -89.9903 dB

239

f.   S/(J+N)-Netted
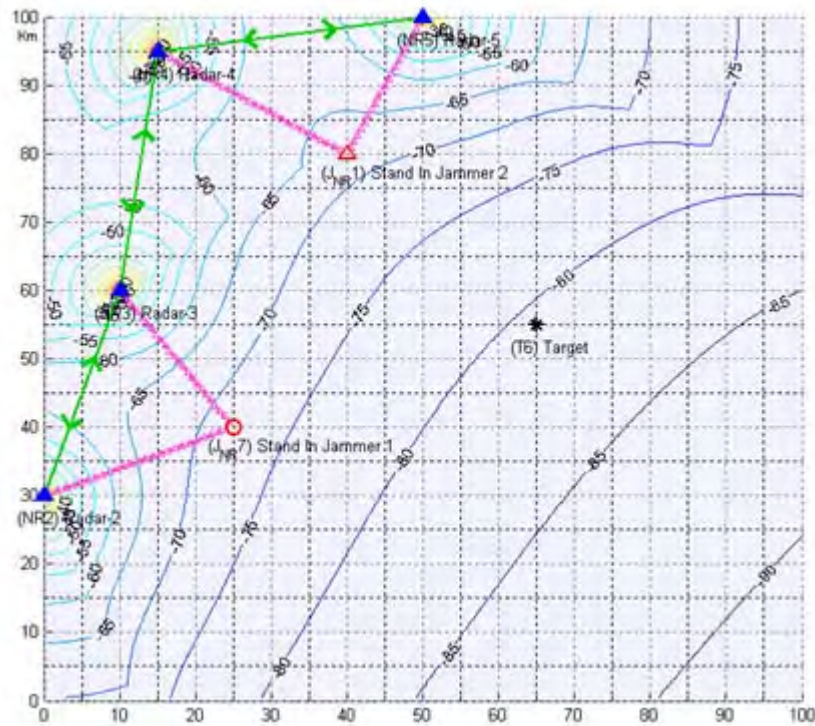
Figure 101. Netted SNJR Contour Chart at Time Index=2

Analysis of SNJR with Network at Time Index = 2

For target at (65, 55):

Node	Radar Echo	Noise Power	Jamming Power	SNJR
2	$1.3008 \cdot 10^{-20}$	10^{-12}	$8.9448 \cdot 10^{-12}$	$1.308 \cdot 10^{-9}$
3	$2.0685 \cdot 10^{-20}$	10^{-12}	$6.9522 \cdot 10^{-12}$	$2.6012 \cdot 10^{-9}$
4	$1.5387 \cdot 10^{-20}$	10^{-12}	$7.5613 \cdot 10^{-12}$	$1.7973 \cdot 10^{-9}$
5	$2.8039 \cdot 10^{-20}$	10^{-12}	$9.172 \cdot 10^{-12}$	$2.7565 \cdot 10^{-9}$

Total SNJR = $8.463 \cdot 10^{-9}$ = -80.7247 dB

	Network disabled	Network enabled	Network improvement
SNJR (dB)	-89.9903 dB	-80.7247 dB	**9.2656 dB**

3. Scenario 3 Time Index 3

a. *SNR – Non-Netted*
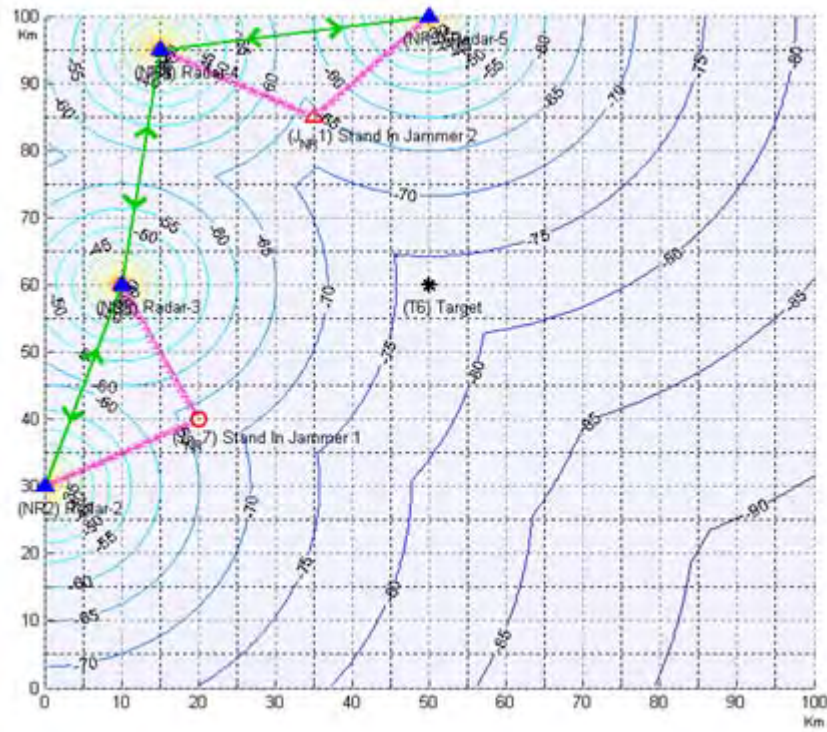
Figure 102. Non-netted SNR Contour Chart at Time Index=3

For target at (50, 60):

Node	Radar Echo(W)	Noise(W)	SNR
2	$4.4646 \cdot 10^{-21}$	10^{-12}	$4.4646 \cdot 10^{-9}$
3	$2.016 \cdot 10^{-21}$	10^{-12}	$2.016 \cdot 10^{-8}$
4	$8.5982 \cdot 10^{-21}$	10^{-12}	$8.5982 \cdot 10^{-9}$
5	$2.016 \cdot 10^{-20}$	10^{-12}	$2.016 \cdot 10^{-8}$

Max SNR = $2.016 \cdot 10^{-8}$ = -76.955 dB
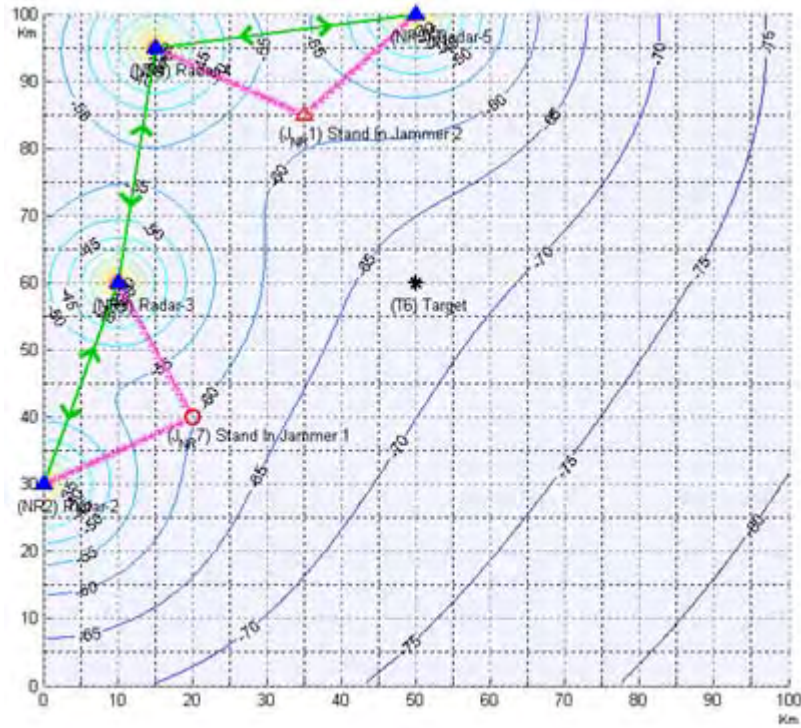
Figure 103. Netted SNR Contour Chart at Time Index=3

For target at (50, 60):

Node	Radar Echo(W)	Noise(W)	SNR
2	$2.9635 \cdot 10^{-20}$	10^{-12}	$2.9635 \cdot 10^{-8}$
3	$6.2974 \cdot 10^{-20}$	10^{-12}	$6.2974 \cdot 10^{-8}$
4	$4.1126 \cdot 10^{-20}$	10^{-12}	$4.1126 \cdot 10^{-8}$
5	$6.2974 \cdot 10^{-20}$	10^{-12}	$6.2974 \cdot 10^{-8}$

Total SNR = $1.9671 \cdot 10^{-7}$= -67.0618 dB

	Network disabled	Network enabled	Network improvement
SNR (dB)	-76.955 dB	-67.0618 dB	**9.8932 dB**

242
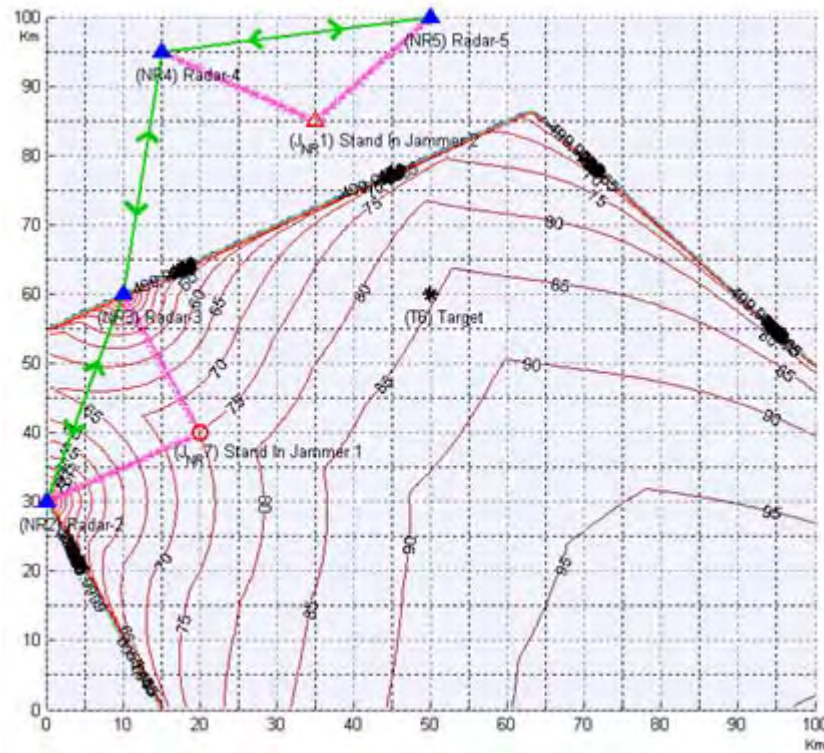
c. *JSR – Non-Netted*

Figure 104. Non-netted JSR Contour Chart at Time Index=3

For target at (50, 60):

Node	Jamming Power(W)	Radar Echo (W)	JSR
2	$1.2933 \cdot 10^{-11}$	$4.4646 \cdot 10^{-21}$	2896787150.5551
3	$5.8009 \cdot 10^{-12}$	$2.016 \cdot 10^{-20}$	287736411.3834
4	$1.2305 \cdot 10^{-11}$	$8.5982 \cdot 10^{-21}$	1431176785.5706
5	$1.0191 \cdot 10^{-11}$	$2.016 \cdot 10^{-20}$	505501347.6305

Min JSR = 287736411.3834 = 84.5899 dB

d. JSR –Netted
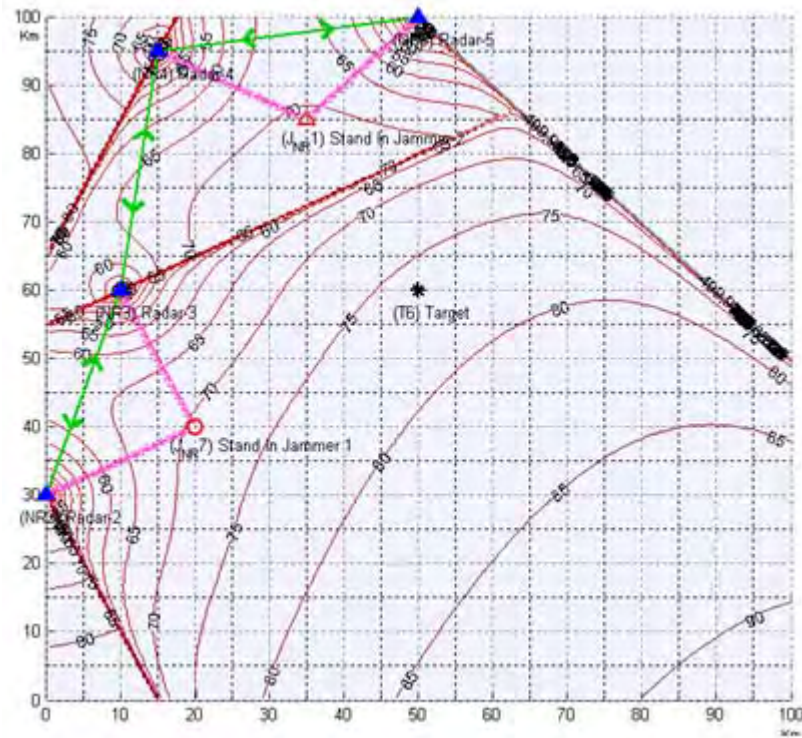
Figure 105. Netted JSR Contour Chart at Time Index=3

For target at (50, 60):

Node	Jamming Power(W)	Radar Echo (W)	JSR
2	$1.2933 \cdot 10^{-11}$	$2.9635 \cdot 10^{-20}$	436410669.8761
3	$5.8009 \cdot 10^{-12}$	$6.2974 \cdot 10^{-20}$	92115461.446
4	$1.2305 \cdot 10^{-11}$	$4.1126 \cdot 10^{-20}$	299216053.5551
5	$1.0191 \cdot 10^{-11}$	$6.2974 \cdot 10^{-20}$	161830369.937

Total JSR = 44113617.6938 = 76.4457 dB

	Network disabled	Network enabled	Network improvement
JSR (dB)	84.5899 dB	76.4457 dB	**8.1442 dB**

244
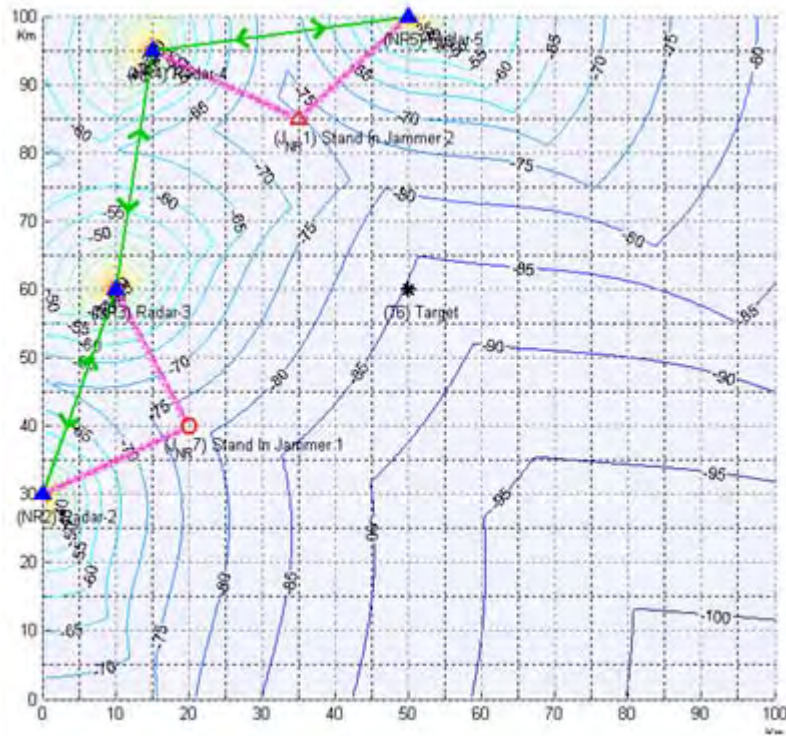
e.   S/(J+N) – Non-Netted
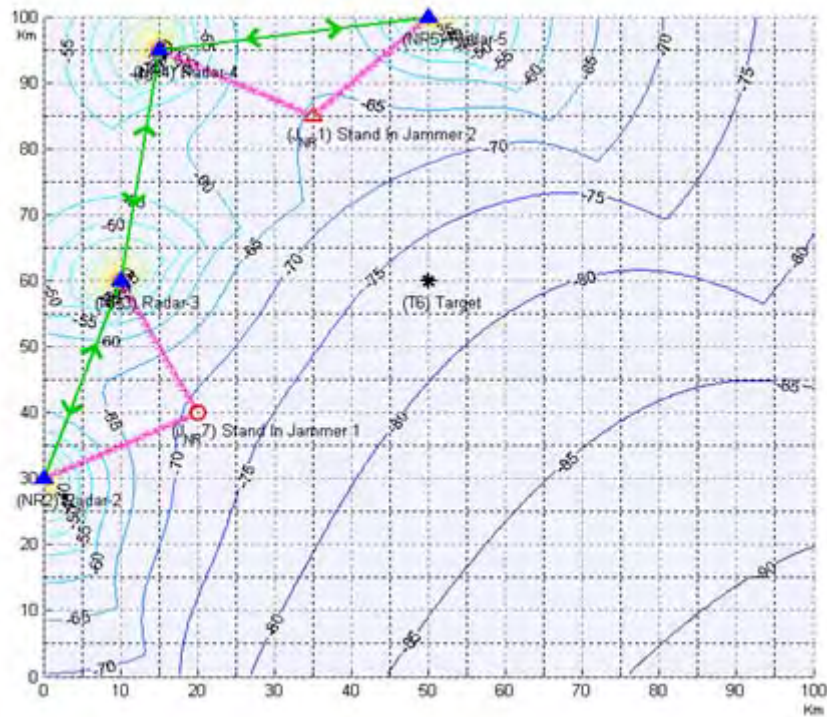

Figure 106. Non-netted SNJR Contour Chart at Time
Index=3

For target at (50, 60):

Node	Radar Echo	Noise Power	Jamming Power	SNJR
2	$4.4646 \cdot 10^{-21}$	10^{-12}	$1.2933 \cdot 10^{-11}$	$3.2043 \cdot 10^{-10}$
3	$2.016 \cdot 10^{-20}$	10^{-12}	$5.8009 \cdot 10^{-12}$	$2.9644 \cdot 10^{-9}$
4	$8.5982 \cdot 10^{-21}$	10^{-12}	$1.2305 \cdot 10^{-11}$	$6.4621 \cdot 10^{-10}$
5	$2.016 \cdot 10^{-20}$	10^{-12}	$1.0191 \cdot 10^{-11}$	$1.8015 \cdot 10^{-9}$

Max SNJR = $2.9644 \cdot 10^{-9}$= -85.2807 dB

f.   S/(J+N) –Netted

Figure 107. Netted SNJR Contour Chart at Time Index=3

For target at (50, 60):

Node	Radar Echo	Noise Power	Jamming Power	SNJR
2	$2.9635 \cdot 10^{-20}$	10^{-12}	$1.2933 \cdot 10^{-11}$	$2.127 \cdot 10^{-9}$
3	$6.2974 \cdot 10^{-20}$	10^{-12}	$5.8009 \cdot 10^{-12}$	$9.2597 \cdot 10^{-9}$
4	$4.1126 \cdot 10^{-20}$	10^{-12}	$1.2305 \cdot 10^{-11}$	$3.0909 \cdot 10^{-9}$
5	$6.2974 \cdot 10^{-20}$	10^{-12}	$1.0191 \cdot 10^{-11}$	$5.6271 \cdot 10^{-9}$

Total SNJR = $2.0105 \cdot 10^{-8}$ = -76.967 dB

	Network disabled	Network enabled	Network improvement
SNJR (dB)	-85.2807 dB	-76.967 dB	**8.3137 dB**

Table 15 summarizes the results of the simulation.

Scenarios			Max SNJR (Non-Netted)or Total SNJR (Netted)	SNR_{Ri}	TARGET DETECTION
Scenario 1	step 1	Non-Netted	-92.5288 dB	-92.65 dB	YES
		Netted	-83.9260 dB	-92.65 dB	YES
	Step 2	Non-Netted	-95.5245 dB	-92.65 dB	NO
		Netted	-82.4976 dB	-92.65 dB	YES
	step 3	Non-Netted	-93.4090 dB	-92.65 dB	NO
		Netted	-81.0730 dB	-92.65 dB	YES
Scenario 2	Step 1	Non-Netted	-92.6182 dB	-92.65 dB	YES
		Netted	-80.1218 dB	-92.65 dB	YES
	Step 2	Non-Netted	-88.6722 dB	-92.65 dB	YES
		Netted	-78.4656 dB	-92.65 dB	YES
	Step 3	Non-Netted	-82.6774 dB	-92.65 dB	YES
		Netted	-75.6283 dB	-92.65 dB	YES
Scenario 3	Step 1	Non-Netted	-92.7302 dB	-92.65 dB	NO
		Netted	-83.1963 dB	-92.65 dB	YES
	Step 2	Non-Netted	-89.9903 dB	-92.65 dB	YES
		Netted	-80.7247 dB	-92.65 dB	YES
	Step 3	Non-Netted	-85.2807 dB	-92.65 dB	YES
		Netted	-76.9670 dB	-92.65 dB	YES

Table 15.   Summary of Simulation Results

Having all other parameters constant (radar positions, radar characteristics, target RCS, target movement, etc.) and changing only the type of operation (netted versus non-netted mode of operation), the preceding results are heavily dependent on the jammer characteristics (jammer ERP, jammer capability), the jammer's distance from the radar nodes and the Target's distance from the radar nodes.

A careful study of Table 15 indicates that the netted configuration has no problem detecting the target in any scenario and at any time step. In fact, the netted configuration has a significant advantage over the non-netted one, not only in terms of higher SNR, JSR and SNJR values, but also by achieving 100% detection probability.

For the analysis of the non-netted configuration we examine each scenario separately:

- Non-Netted Scenario 1

Scenario 1 is a pure Self Screening Jamming (SSJ) scenario where the target and jammer coincide. In this specific scenario, the on-board jammer has a moderate ERP (10 Watts) and a good (0.75) jamming capability. In time steps 2 and 3 of the non-netted configuration, the jamming was effective and there was no detection by the radar grid. This can be explained by two factors: (1) the jammer is on-board the target so there is no additional free space loss--as, for instance in the case of Stand-off Jamming (SOJ); and (2) the jammer has good ERP jamming capabilities.

If we examine more closely time step 1 of scenario 1 we'll see that even though there is target

248

detection, the SNJR is slightly higher than the threshold value (0.1212 dB higher than SNR_{Ri}).

- Non-Netted Scenario 2

Scenario 2 is a pure SOJ scenario, where the target and the jammer have an offset (jammer behind target). In this scenario, the Jammer has the same characteristics as in scenario 1; the only difference is its offset with the target. The analysis of scenario 2 LPIsimNet data indicates that all radar nodes could easily detect the target. This can be explained by the offset between the target and the jammer: given the fact that the target is closer to the radar nodes, it provides higher returns than the stand-off jammer can effectively mask. A stand-off jammer with higher ERP and jamming capability could probably prevent the target detection in the non-netted operation.

- Non-Netted Scenario 3

Scenario 3 is a stand-in jamming scenario, where two slow moving stand-in jammers are used. Both jammers were selected to have low jamming capability (0.3) and low ERP (1 Watt), but they are much closer to the radar nodes. At time step 1 the radar nodes fail to detect the target. This can be attributed to two factors: (1) the small initial distance between the jammers and the radar nodes (less jamming power losses) and (2) the large initial distance between the target and the radar nodes (low signal returns due to losses).

The detection at time steps 2 and 3 can be explained by the fact that the target is approaching the radar nodes

249

faster than the stand-in jammers do; this causes the target's returns into the radar nodes to increase faster than the jamming power does. Two stand-in jammers with higher ERP and/or jamming capability or at closer distance to the radar, or moving at higher speed could probably prevent the target detection in the non-netted operation.

In all scenarios the netted version has an additional effect on SNJR that varies from +7.049 dB (minimum improvement) to +13.0269 dB (maximum improvement) which in layman terms--keeping the noise power the same in all cases)--means that jamming power into the radar receiver has to be from 5.069 to 20.077 times higher in order to mask the target.

This advantage of the netted configuration ,set against the non-netted configuration is mathematically explained in the work of Hume and Baker, and Papoutsis, Barker and Griffiths (Hume and Barker, 2001; Papoutsis, et. al, 2003): By netting several radars, and assuming that all radars are transmitting and are capable of receiving apart from their own echo the echoes from the other radars and that there is network synchronization, we get an increase in SNR by the square of the number of the total number of radar systems comprising the network. The formula for the SNR of the netted radar system is:

$$SNR = \sum_{\mu=1}^{n} \frac{ERP_r(\mu)}{\left(4\pi R_\mu\right)^2} \sum_{\nu=1}^{n} \frac{A_e(\nu)}{\left(4\pi R_\nu\right)^2 Noise(\nu)} \quad (8.1)$$

Where:

$ERP_r(\mu)$: Effective radiated power of radar μ.

$A_e(\nu)$: Effective antenna area of radar ν.

Noise(ν): Noise power of radar ν.

R_μ: Range from radar μ to target.

R_ν: Range from target to radar ν.

THIS PAGE INTENTIONALLY LEFT BLANK

IX. CONCLUSIONS

This thesis provides a comprehensive view of two major elements in Electronic Warfare: LPI assets and network configurations. With the existing scholarly efforts dealing individually with either of these two elements being not only extensive but also constantly updated, we attempted to fill the literature gap and provide a more comprehensive work discussing and linking both areas within the same work.[39]

The simulations to achieve our data were performed with MATLAB-based software, using a standardized data set (LPIsimNet). Utilizing this tool, it was possible to numerically prove that the netted LPI IADS is less vulnerable to jamming attack than a non-netted LPI IADS. Although the results are not surprising (we expected a netted LPI IADS to be less susceptible to jamming than a non-netted one), the accuracy of the output data is affected by several factors pertaining to the limitations of the software used.

Running the LPIsimNet, we noted that the absence of a parameter precisely describing the ease of flow between the assets is among the most notable factors affecting the accuracy of the output data. To account for this parameter, LPIsimNet requires a value for the "capability of

---

[39] The 2008 paper of Chen and Pace presents a basic framework for simulation of network enabled radar systems, but, apart from being limited in breadth, its scope is limited in the evaluation of the jamming effect in general radar topology. Y. Q. Chen and Phillip E. Pace, "Simulation of Information Metrics to Assess the Value of Networking in A General Battlespace Topology," in *Proc. of the IEEE International Conf. on System of Systems Engineering* (IEEE, June 2008).

information" of each of the nodes utilized;[40] however, this parameter lacks a mathematical formula for its precise calculation. In the absence of such a formula, and in order to reflect the reduced capabilities of nodes 2 and 3 in our simulation scenario, we arbitrarily assumed that their "capability of information" was 0.7 instead of 1 (maximum).In order to enhance the computation accuracy and provide real operational results, the extraction of a mathematical formula computing precisely the "capability of information" is recommended for future work.

A second parameter that affects the output data of the simulation pertains to the RCS, as LPIsimNet assumes that the RCS of the target/jammer remains the same throughout its approach towards the radar grid. Such an arbitrary assumption generates extra inaccuracies, as the RCS is affected by several parameters.[41]As detailed computation of the netted vs. non-netted configuration performance was outside the scope of this paper, no alteration of the existing program code was attempted. In this context, the introduction of a real time RCS computational tool--within the LPIsimNet code if feasible-is highly recommended as a means to enhance the realism of the scenarios and provide more realistic results for existing assets.

Our work asserts that networks of radar systems present many advantages compared to the traditional concept

---

[40] The min value for the "capability of information" input is 0, and the max value is 1.

[41] Among the major factors are: the material of which the target is made; the absolute size of the target; the relative size of the target (that is, in relation to the wavelength of the illuminating radar); the incident angle, which depends upon the shape of the target and its orientation to the radar source; the reflected angle; the strength of the radar emitter; and the distance between the radar and the emitter.

of autonomous radar assets. Simple independent networks offer a subset of these advantages and are a logical first step. More sophisticated coherent networks offer the ultimate in performance. However, further research is required to truly establish the merits of this mode of operation and to overcome the technical challenges it presents.

THIS PAGE INTENTIONALLY LEFT BLANK

APPENDIX. DETAILED DESCRIPTION OF PHASE MODULATING TECHNIQUES, FREQUENCY SHIFT KEYING TECHNIQUES AND NOISE TECHNIQUES

A. PHASE MODULATING TECHNIQUES

1. BPSK Codes

BPSK is a phase shift technique primarily used in the communication sector rather than as modulation technique for LPI radar. In BPSK modulation two output phases are generated for a single carrier frequency. One output phase represents the logic 1 and the other the logic 0. When the input digital changes state (1 to 0 or 0 to 1) the phase of the output carrier shifts between two angles that are 180° apart.

This can easily been seen in Figure 108 (red arrows).
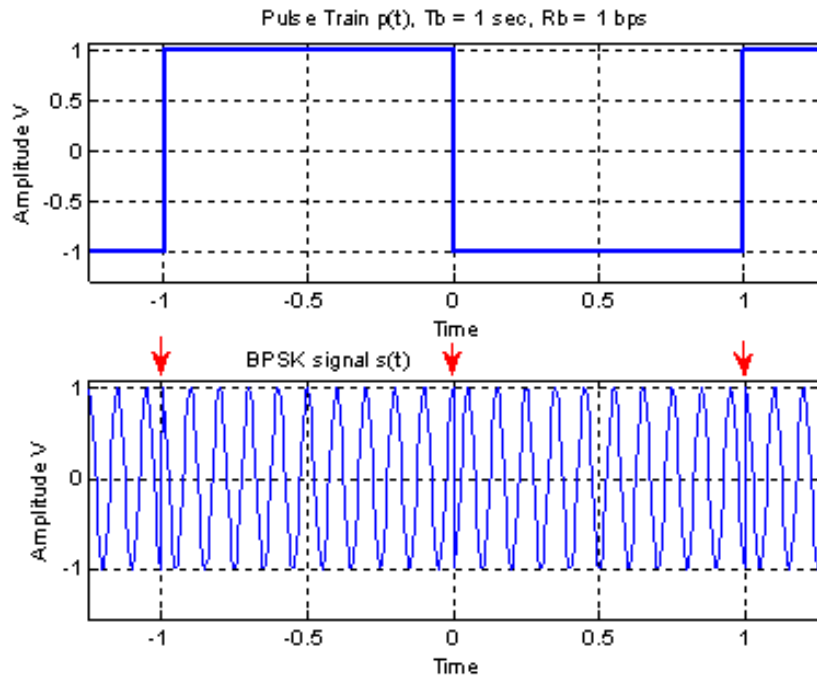
Figure 108. Figure BPSK Modulation

The typical BPSK codes used for BPSK modulation are the Barker Codes. The binary Barker sequences are finite-length discrete time sequences with constant magnitude and a phase of either $\varphi_k = 0$ or $\varphi_k = \pi$. The only known lengths of Barker sequences are $N_c = 2,3,4,5,7,11,13$. The nine different Barker codes along with their respective peak sidelobe level (PSL) with respect to main lobe level can be seen in Table 16 below(Pace 2009, 128):

Code Length	Code Elements	PSL (dB)
2	- + , + -	-6.0
3	+ + -	-9.5
4	+ + - +, + + + -	-12.0
5	+ + + - +	-14.0
7	+ + + - - + -	-16.9
11	+ + + - - - + - - + -	-20.8
13	+ + + + + - - + + - + - +	-22.3

Table 16.   Barker Codes

Another BPSK technique is to use Compound Barker Codes, which creates a sequence by implementing a Barker code within a Barker code. In this way we can create a larger sequence code that has a sequence of:

$$N_c^{compound} = N_c N_c = N_c^2 \text{ (A.1)}$$

A compound 4 Barker code is presented in Table 17.

Primary code	+				+				-				+			
Embedded Code	+	+	-	+	+	+	-	+	+	+	-	+	+	+	-	+
Final Code	+	+	-	+	+	+	-	+	-	-	+	-	+	+	-	+

Table 17.   Compound Barker Code for $N_c = 4$

258

In Figure 109, by using the MATLAB LPIT TOOLBOX, we see an example of a Barker code BPSK wave modulated by a 7 code length Barker code and added white Gaussian noise, with parameters: $f_c = 1kHz$, $f_s = 7kHz$, $SNR = 0dB$, $N_c = 7$.
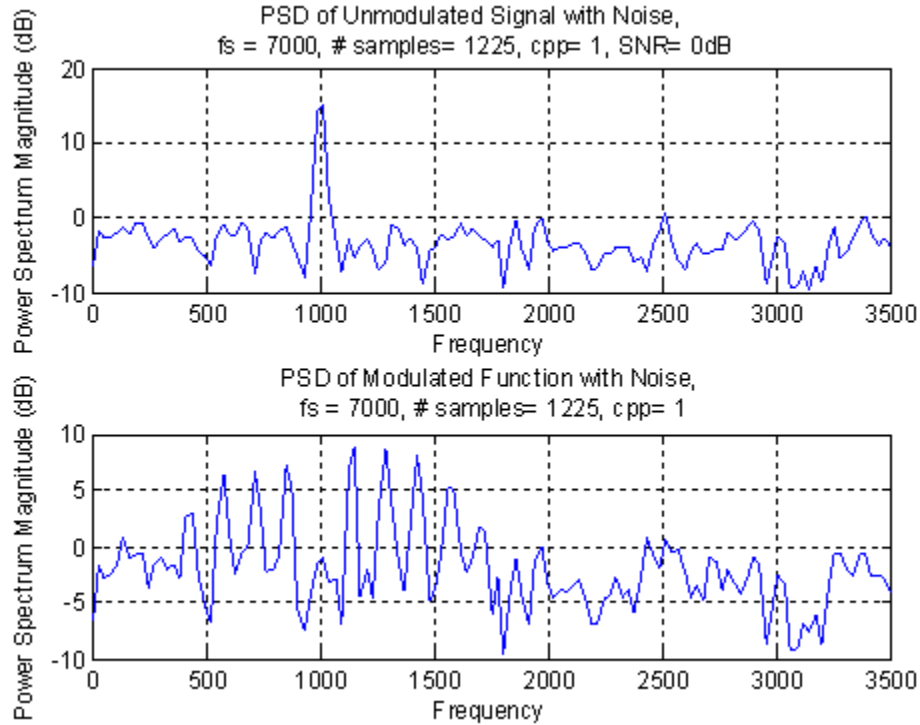
Figure 109. BPSK Signal Modulated by Barker Code (length 7)

Compound Barker codes give a very large length of code sequences that can improve range resolution and also give a higher compression gain, but their peak sidelobes are not proportionally decreased (due to this higher compression gain)(Pace 2009, 128).

There are three major disadvantages with the use of Barker codes.

- There are only few (9) known Barker code sequences that have a very limited length and thus limit the range resolution.

- Even in the case of compound Barker codes that can have very large sequences of codes their peak sidelobes are not proportionally decreased due this high compression gain.

- They are very sensitive to Doppler shifts. The Doppler shift of the return waveform can compress the waveform within the filter such that the matched filter gives incorrect results.

2. Polyphase Codes

Polyphase sequences are finite length, discrete time complex sequences with constant magnitude and variable phase φ_k. Polyphase coding is the phase modulation of the CW carrier by a polyphase sequence that has a number of discrete phases (Pace 2009, 133).

Various codes satisfy the above criteria; Polyphase Barker codes, Frank, P1, P2, P3 and P4 codes. Polyphase codes derive from approximating a stepped (in the case of Frank, P1 and P2) or linear (in the case of P3 and P4) frequency modulation waveform, where the phase steps vary as needed to approximate the underlying waveform, but the time spent at any given phase state is constant. A short description of the polyphase codes follows.

a. Polyphase Barker Codes

Polyphase sequences that satisfy the Barker criteria are under investigation in order to try finding

longer sequences. Various algorithms have been used and/or developed in order to develop longer polyphase Barker codes. Currently $N_c \leq 63$ codes have been discovered (Pace, 2009, 134).

b. Frank Code

Frank code, developed by R.L. Frank in 1963, has been used successfully in LPI radar. The Frank code is derived from a step approximation to a linear frequency modulation waveform using M frequency steps and M samples per frequency. Its length (or processing gain) is $N_c = M^2$. The phase of the Frank code is given by the following formula (Pace 2009, 143):

$$\varphi_{i,j} = \frac{2\pi}{M}(i-1)(j-1) \text{ (A.2)}$$

Where:

$\varphi_{i,j}$: Phase of the ith sample of the jth frequency

$i = 1,2,...,M$

$j = 1,2,...,M$

In Figures 110 and 111, by using the MATLAB LPIT TOOLBOX, we see a Frank code modulated CW wave, signal phase and code phase diagrams, with parameters: $f_c = 1kHz$, $f_s = 7kHz$, $SNR = 0dB$ and $M = 16$.
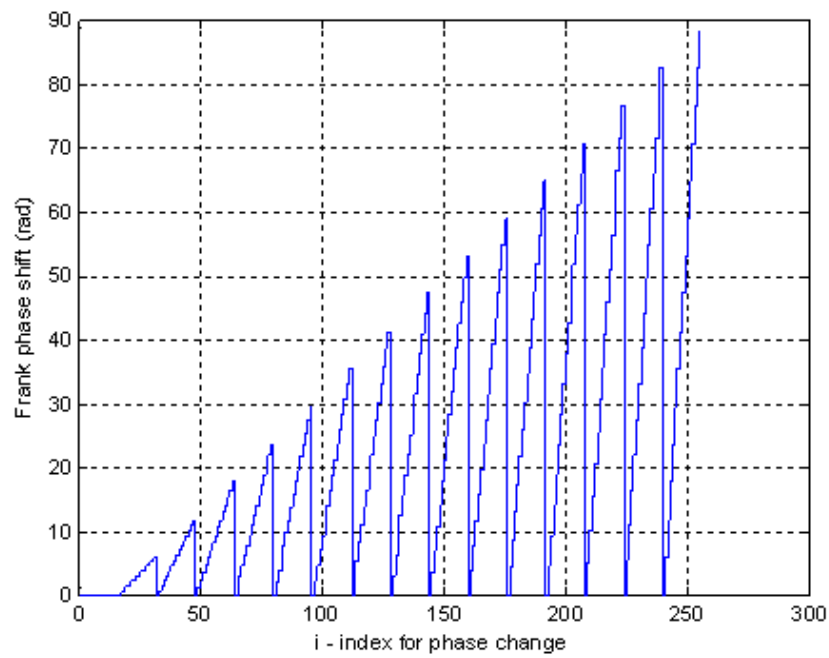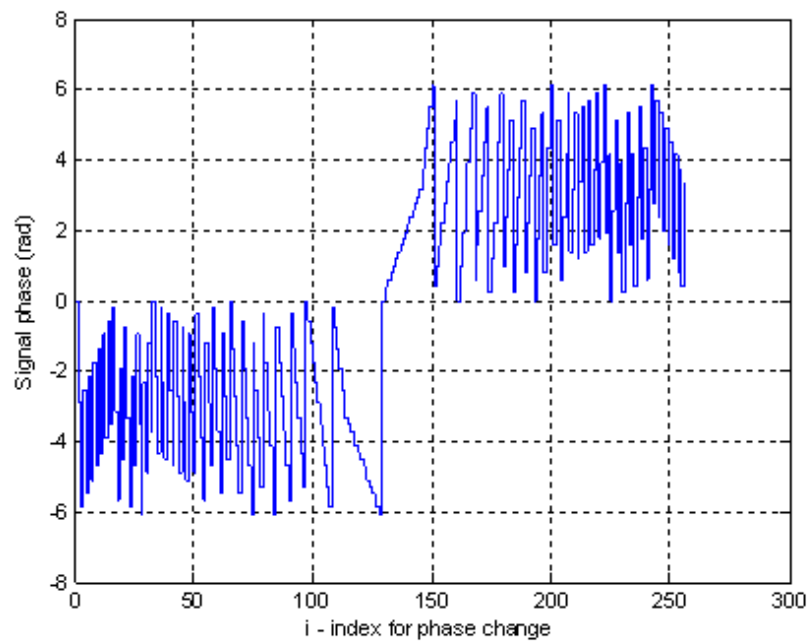
Figure 110. Frank Code Phase
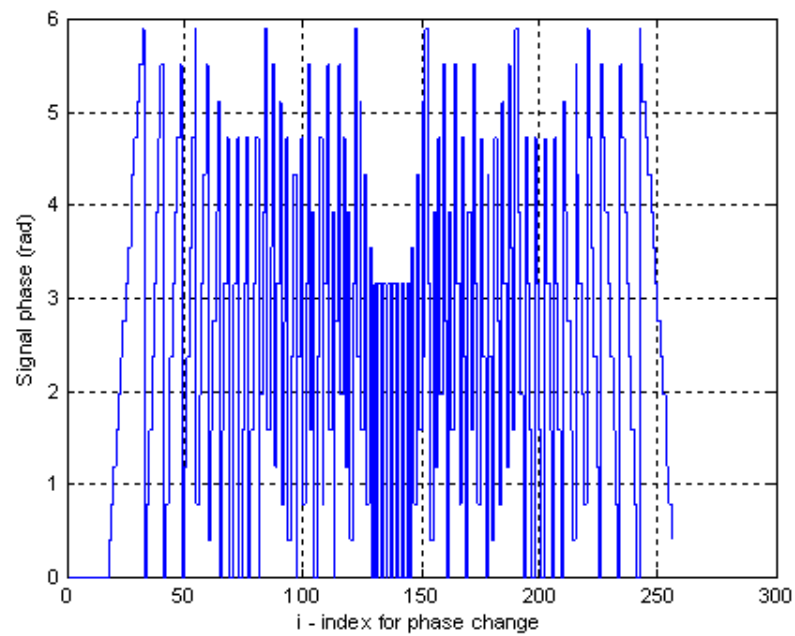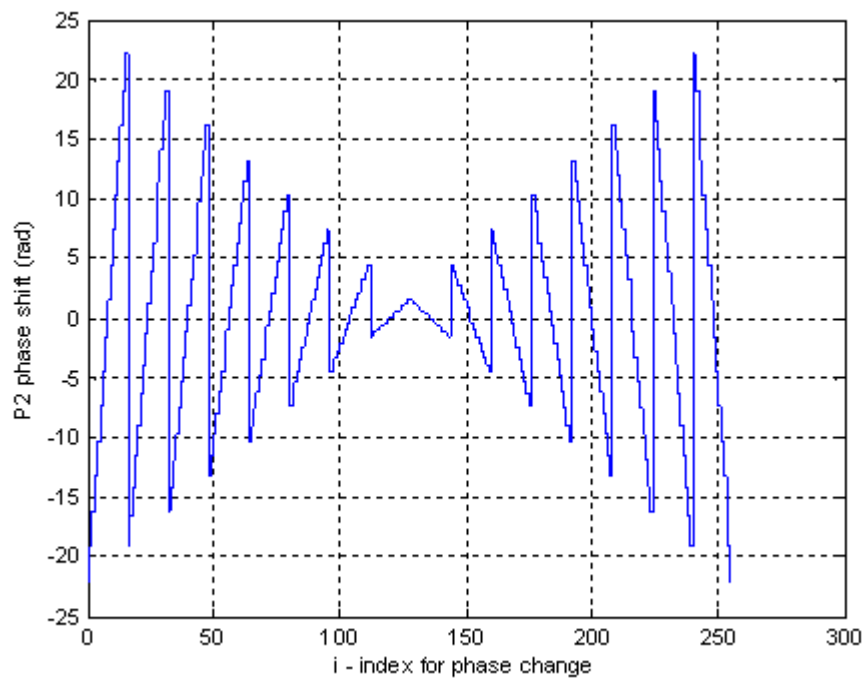

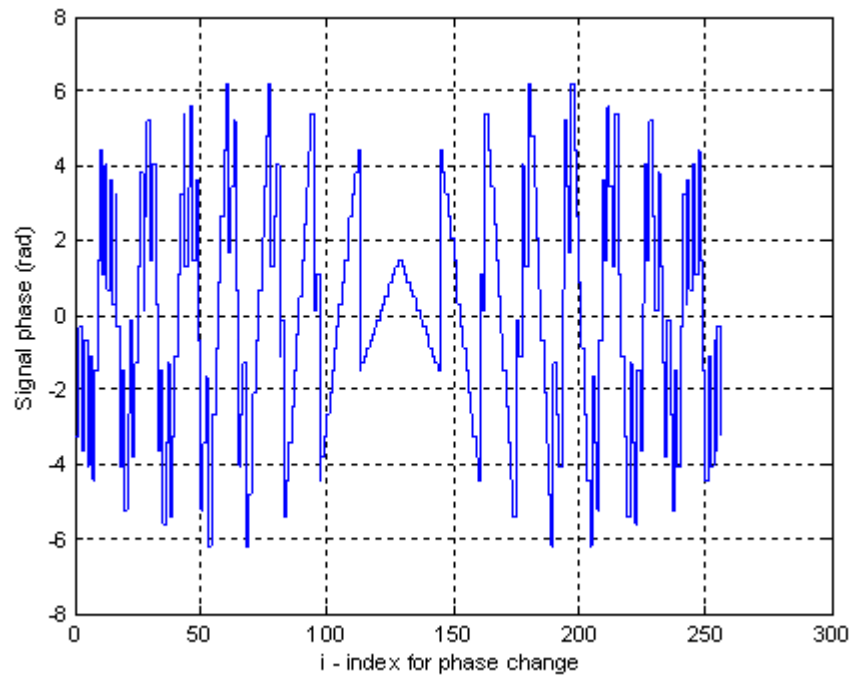Figure 111. Signal Phase (Modulated by Frank Code)

c. P1 Code

P1 code is similar to the Frank code. It is also derived from a step approximation to a linear frequency modulation waveform using M frequency steps and M samples per frequency. Its length (or processing gain) is $N_c = M^2$. The phase of the P1 code is given by the following formula (Pace 2009, 148):

$$\varphi_{i,j} = \frac{-\pi}{M} \big[M - (2j-1) \big] \big[(j-1)M + (i-1) \big] \ (\text{A.3})$$

Where:

$\varphi_{i,j}$: Phase of the ith sample of the jth frequency

$M = 1,2,3,....$

$i = 1,2,...,M$

$j = 1,2,...,M$

In Figures 112 and 113, by using the MATLAB LPIT TOOLBOX, we see a P1 code modulated CW wave, signal phase and code phase diagrams, with parameters: $f_c = 1kHz$, $f_s = 7kHz$, $SNR = 0dB$ and $M = 16$.

263
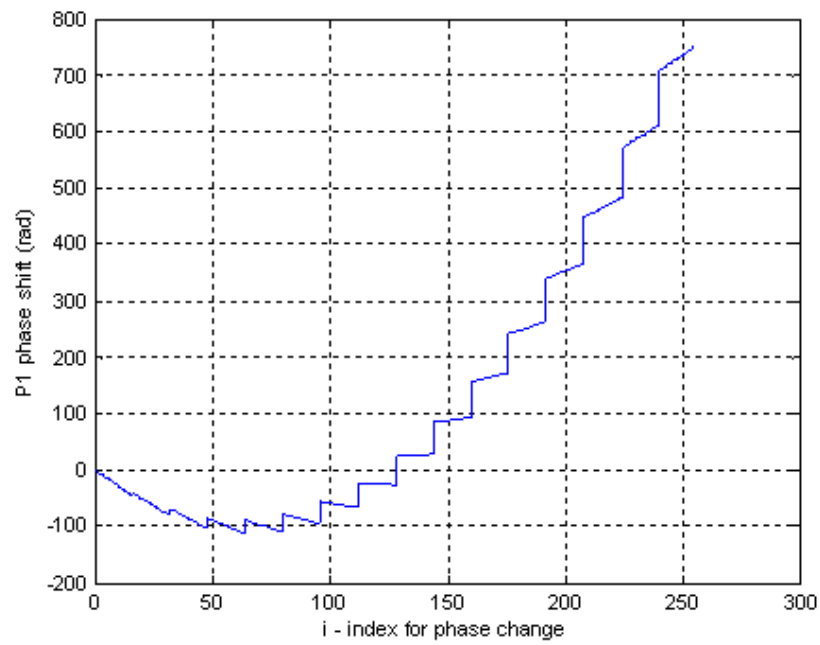
Figure 112. P1 Code Phase

Figure 113. Signal Phase (Modulated by P1 Code)

264

d.   P2 Code

P2 code is similar to P1 code, but   should be even and the starting phases are different than with P1 code. It is also derived from a step approximation to a linear frequency modulation waveform using M frequency steps and M samples per frequency. Its length (or processing gain) is $N_c = M^2$. The phase of the P2 code is given by the following formula (Pace 2009, 152).

$$\varphi_{i,j} = \frac{-\pi}{2M}(2i-1-M)(2j-1-M) \quad (A.4)$$

Where:

$\varphi_{i,j}$: Phase of the ith sample of the jth frequency

$M = 2,4,6,....$

$i = 1,2,...,M$

$j = 1,2,...,M$

In Figures 114 and 115, by using the MATLAB LPIT TOOLBOX, we see a P2 code modulated CW wave, signal phase and code phase diagrams, with parameters: $f_c = 1kHz$, $f_s = 7kHz$, $SNR = 0dB$ and $M = 16$.
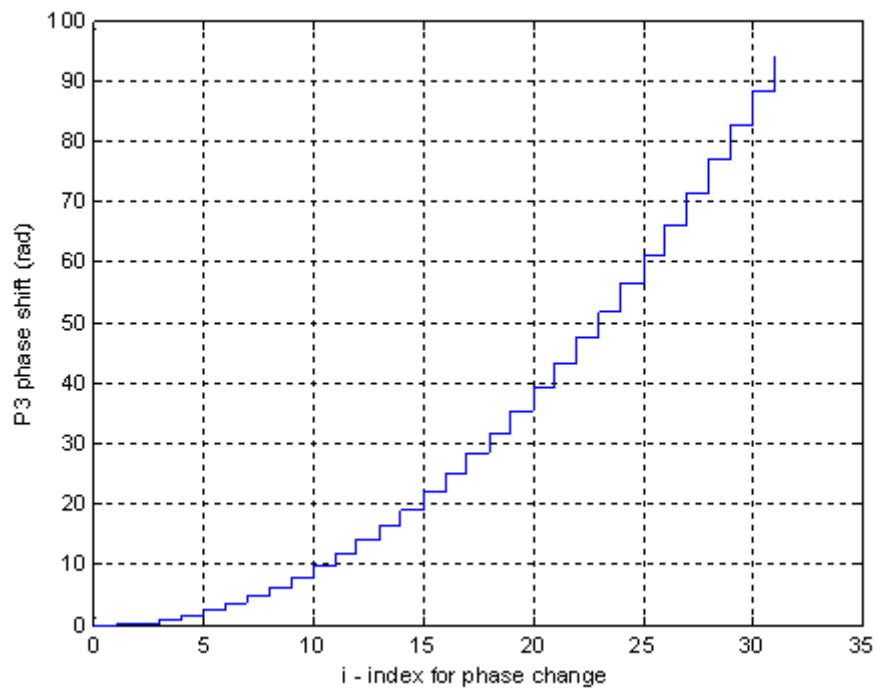
Figure 114. P2 Code Phase

Figure 115. Signal Phase (Modulated by P2 Code)

266

e.   P3 Code

P3 code is derived by converting a linear
frequency modulation waveform to baseband. That is done by
using a synchronous oscillator on one end of the frequency
sweep and sampling the in-phase (I) and quadrature (Q)
channels at the Nyquist rate (the sampling frequency $f_s \leq 2W$
where W is the highest frequency of the signal) resulting
in a single sideband detection. The phase of the P3 code is
given by the following formula (Pace 2009, 152):

$$\varphi_i = \frac{\pi}{N_c}(i-1)^2 \quad (A.5)$$

Where:

φ_i : Phase of the ith sample

N_c : Compression ratio

$i = 1, 2, ..., N_c$

In Figures 116 and 117, by using the MATLAB LPIT
TOOLBOX, we show a P3 code modulated CW wave, signal phase
and code phase diagrams, with parameters: $f_c = 1kHz$, $f_s = 7kHz$,
$SNR = 0dB$ and $M = 32$.

Figure 116. P3 Code Phase
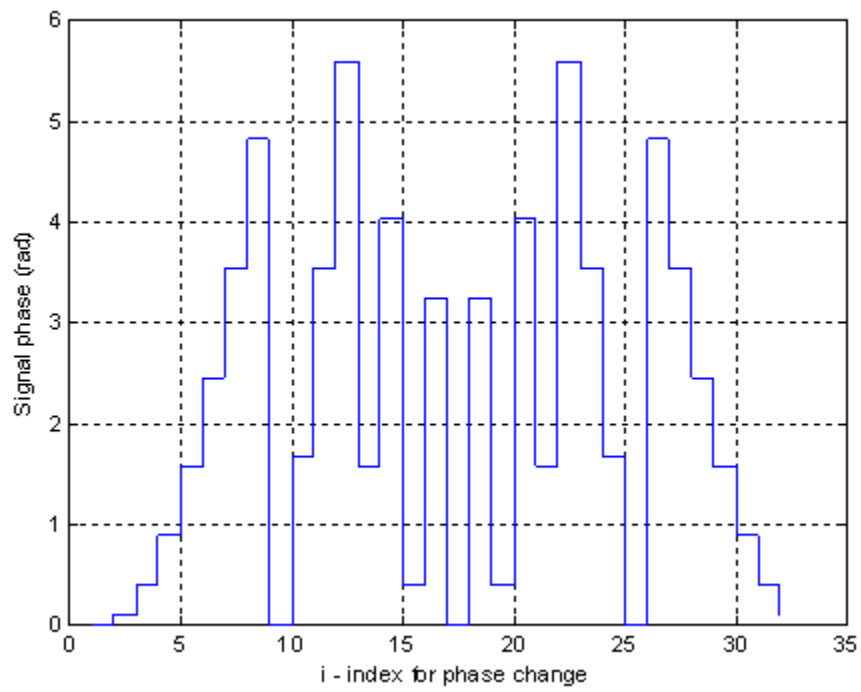
Figure 117. Signal Phase (Modulated by P3 Code)

f.   P4 Code

P4 code is similar to P3 code, but the oscillator that does the sampling of the in-phase (I) and quadrature (Q) channels has an offset between I and Q channels, resulting in coherent double sideband detection. Again, the sampling is done at the Nyquist rate (the sampling frequency $f_s \leq 2W$ where W is the highest of the signal). The phase of the P4 code is given by the following formula (Pace 2009, 157).

$$\varphi_i = \frac{\pi(i-1)^2}{N_c} - \pi(i-1) \quad \text{(A.6)}$$

Where:

φ_i: Phase of the ith sample

N_c: Compression ratio

$i = 1,2,...,N_c$

In Figures 118 and 119, by using the MATLAB LPIT TOOLBOX, we show a P4 code modulated CW wave, signal phase and code phase diagrams, with parameters: $f_c = 1kHz$, $f_s = 7kHz$, $SNR = 0dB$ and $M = 32$.
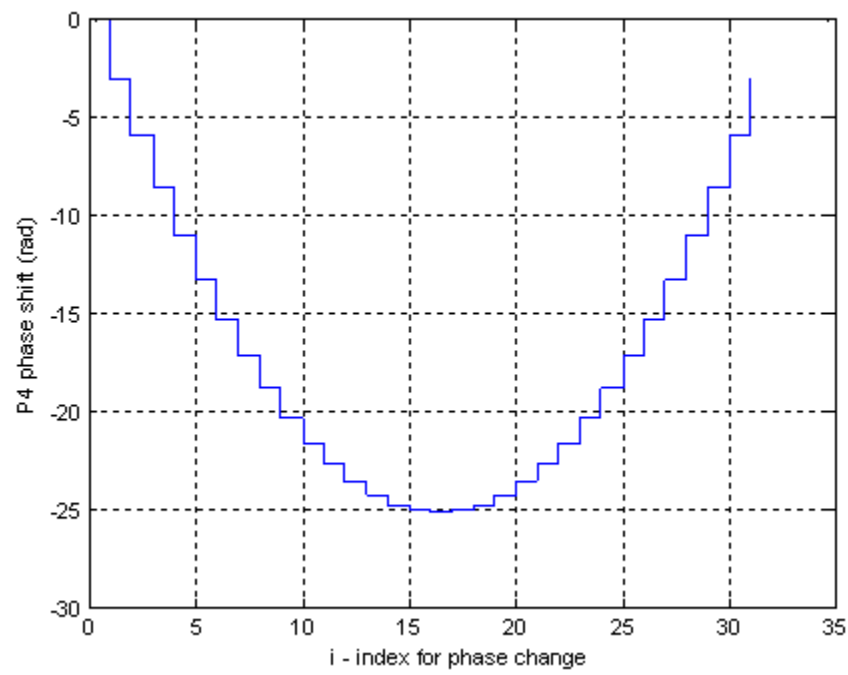
Figure 118. P4 Code Phase
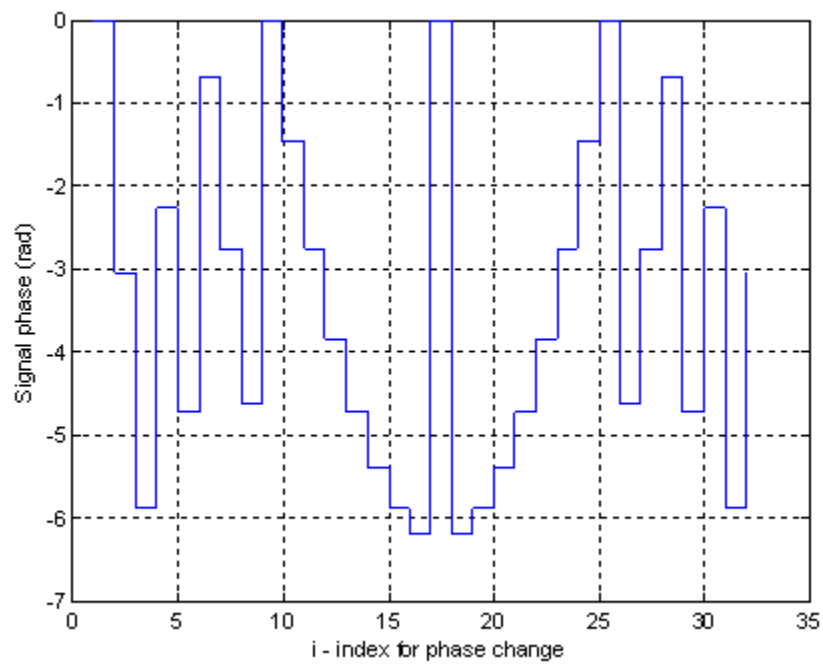
Figure 119. Signal Phase (Modulated by P4 Code)

270

3.   Polytime Codes

Polyphase codes derive from approximating a stepped (in the case of Frank, P1 and P2) or linear (in the case of P3 and P4) frequency modulation waveform, where the phase steps vary as needed to approximate the underlying waveform, but the time spent at any given phase state is constant. For polytime codes there is different process; the underlying waveform is quantized into a user-selected number of phase states. So for polytime codes the phase states are fixed, but there are varying time periods at each phase state (Pace 2009, 163). There are four polytime sequences as follows.

a.   T1(n)

T1(n) is generated from a stepped frequency waveform where n is the number of phase states used to approximate the underlying waveform. The formula of the phase of the polytime sequence T1(n) is as follows(Pace 2009, 163).

$$\varphi_{T1}(t) = \text{mod}\left\{ \frac{2\pi}{n} INT\left[(kt - jT)\frac{jn}{T} \right], 2\pi \right\} \quad (A.7)$$

Where:

n : Number of phase states in the code sequence

k : Number of segments in the T1 code sequence

T : Overall code duration

$j = 0,1,2,...,k-1$: Segment number in the stepped frequency waveform

In Figures 120 and 121, by using the MATLAB LPIT TOOLBOX, a T1(2) code modulated CW wave, stepped frequency phase shift and time domain waveform, with parameters: $f_c = 1kHz$, $f_s = 7kHz$, $SNR = 0dB$, $n = 2$, $T = 0.016\sec$, $\Delta F = 250Hz$ and $k = 4$ are depicted.
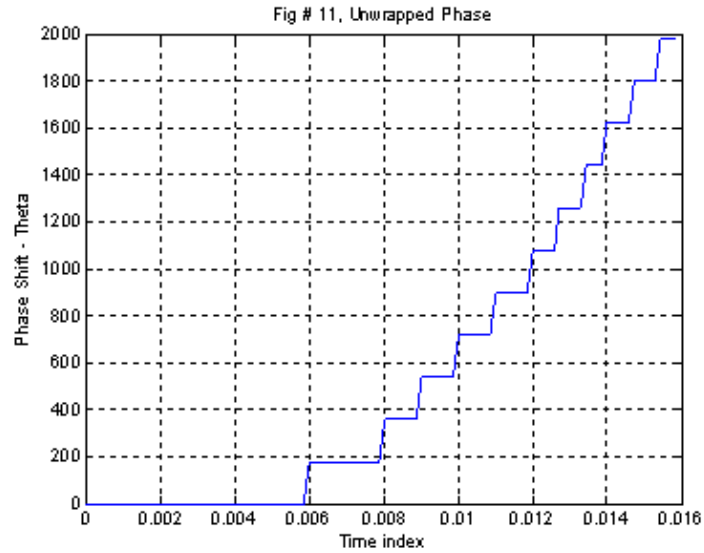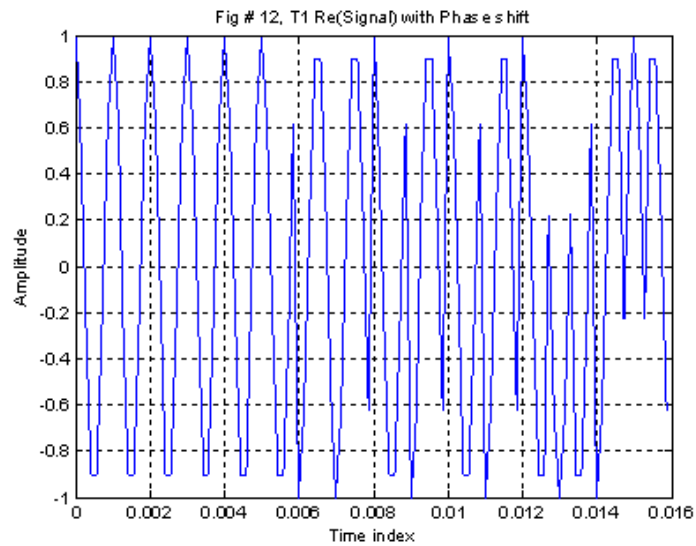

Figure 120. T1(2) Stepped Frequency Phase

Figure 121. T1(2) Modulated Signal Time Domain Waveform

b. T2(n)

T2(n) is generated from a stepped frequency waveform where n is the number of phase states used to approximate the underlying waveform. The formula of the phase of the polytime sequence T2(n) is as follows(Pace 2009, 165).

$$\varphi_{T2}(t) = \mod\left\{\frac{2\pi}{n} INT\left[(kt - jT)\left(\frac{2j - k + 1}{T}\right)\frac{n}{2}\right], 2\pi\right\} \quad (A.8)$$

Where:

n: Number of phase states in the code sequence

k: Number of segments in the T1 code sequence

T: Overall code duration

$j = 0,1,2,...,k-1$: Segment number in the stepped frequency waveform

In Figures 122 and 123, by using the MATLAB LPIT TOOLBOX, a T2(2) code modulated CW wave, stepped frequency phase shift and time domain waveform, with parameters: $f_c = 1kHz$, $f_s = 7kHz$, $SNR = 0dB$, $n = 2$, $T = 0.016\sec$, $\Delta F = 250Hz$ and $k = 4$ are depicted.
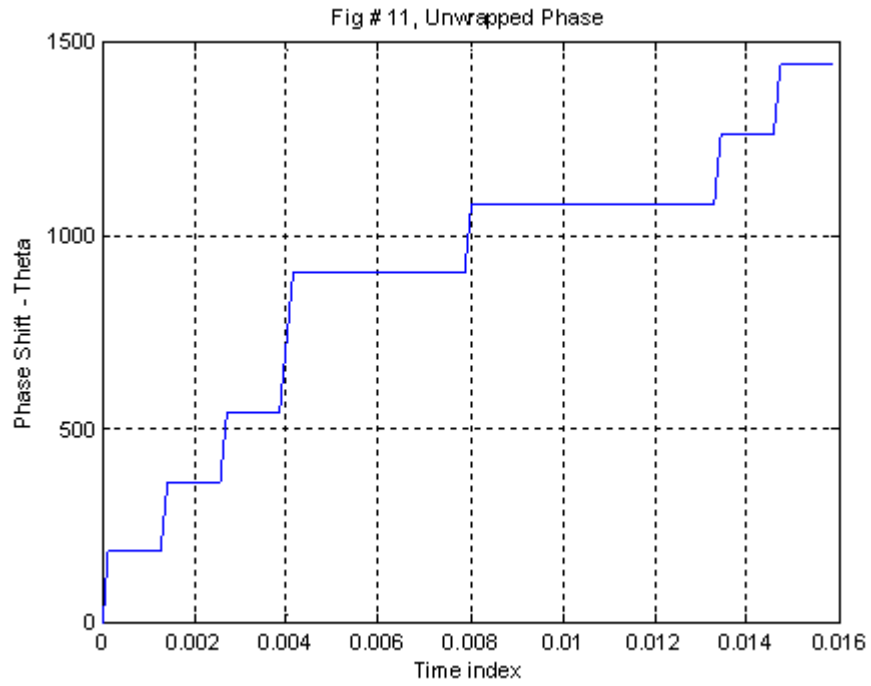
273

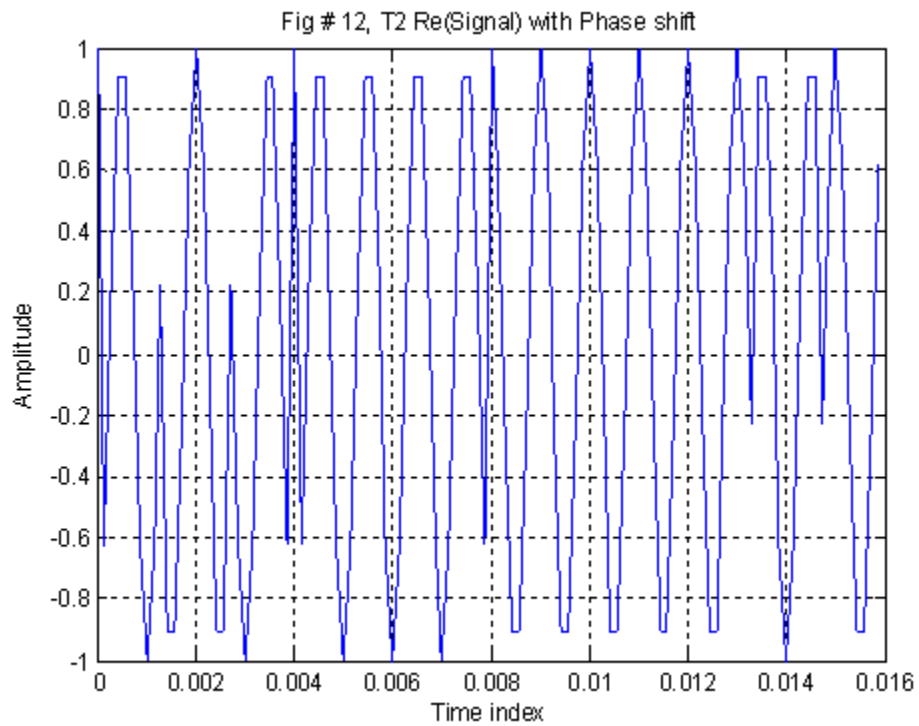Figure 122. T2(2) Stepped Frequency Phase

Figure 123. T2(2) Modulated Signal Time Domain Waveform

274

c.   T3(n)

T3(n) is generated from approximations of a linear frequency model, where n is the number of phase states used to approximate the underlying waveform. The formula of the phase of the polytime sequence T3(n) is the following (Pace, 2009, 169):

$$\varphi_{T3}(t) = \mod\left\{\frac{2\pi}{n} INT\left[\frac{n\Delta Ft^2}{2t_m}\right], 2\pi\right\} \quad \text{(A.9)}$$

Where:

n : Number of phase states in the code sequence

ΔF : Modulation bandwidth

t_m : Modulation period

In Figures 124 and 125, by using the MATLAB LPIT TOOLBOX, we see a T3(2) code modulated CW wave, stepped frequency phase shift and time domain waveform, with parameters $f_c = 1kHz$, $f_s = 7kHz$, $SNR = 0dB$, $n = 2$ and $\Delta F = 250Hz$.
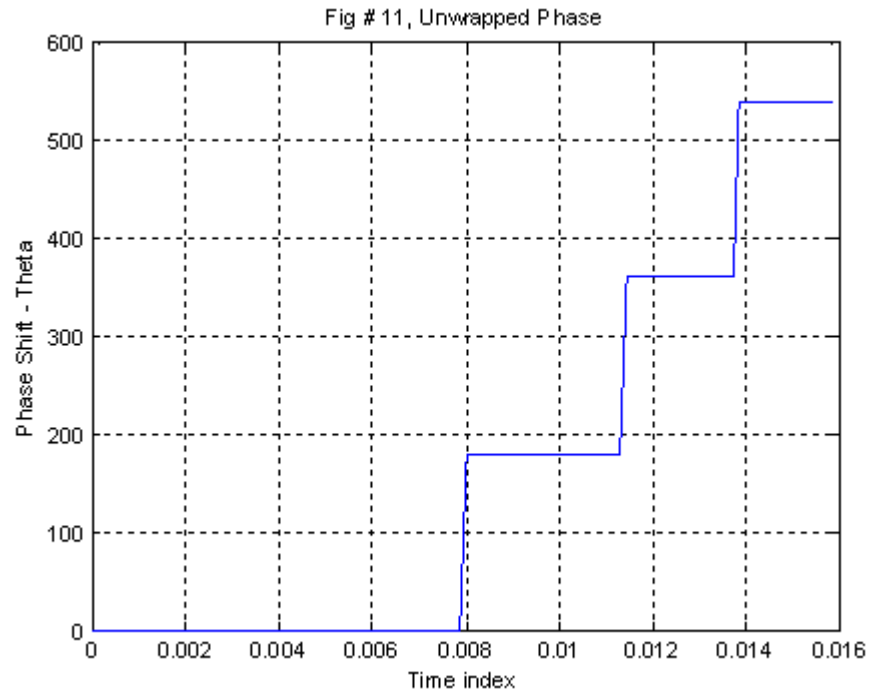
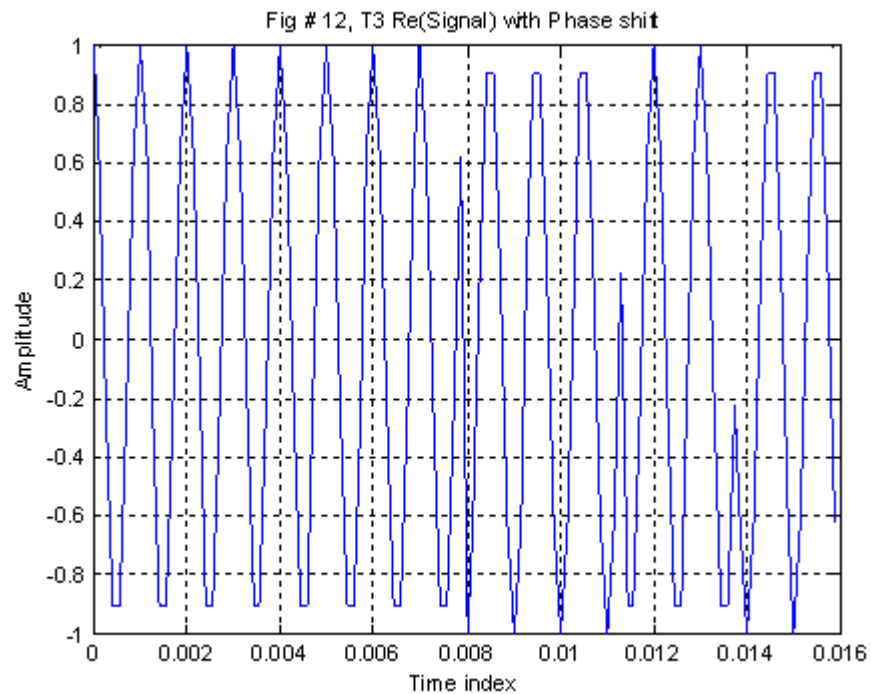Figure 124. T3(2) Stepped Frequency Phase

Figure 125. T3(2) Modulated Signal Time Domain Waveform

276

d.   T4(n)

T4(n) is generated from approximations of a linear frequency model, where n is the number of phase states used to approximate the underlying waveform. The formula of the phase of the polytime sequence T4(n) is the following (Pace 2009, 169):

$$\varphi_{T4}(t) = \mathrm{mod}\left\{ \frac{2\pi}{n} INT\left[\frac{n\Delta F t^2}{2t_m} - \frac{n\Delta F t}{2} \right], 2\pi \right\} \quad (A.10)$$

Where:

n : Number of phase states in the code sequence

ΔF : Modulation bandwidth

t_m : Modulation period

In Figures 126 and 127, by using the MATLAB LPIT TOOLBOX, a T4(2) code modulated CW wave, stepped frequency phase shift and time domain waveform, with parameters $f_c = 1kHz$, $f_s = 7kHz$, $SNR = 0dB$, $n = 2$ and $\Delta F = 250Hz$.
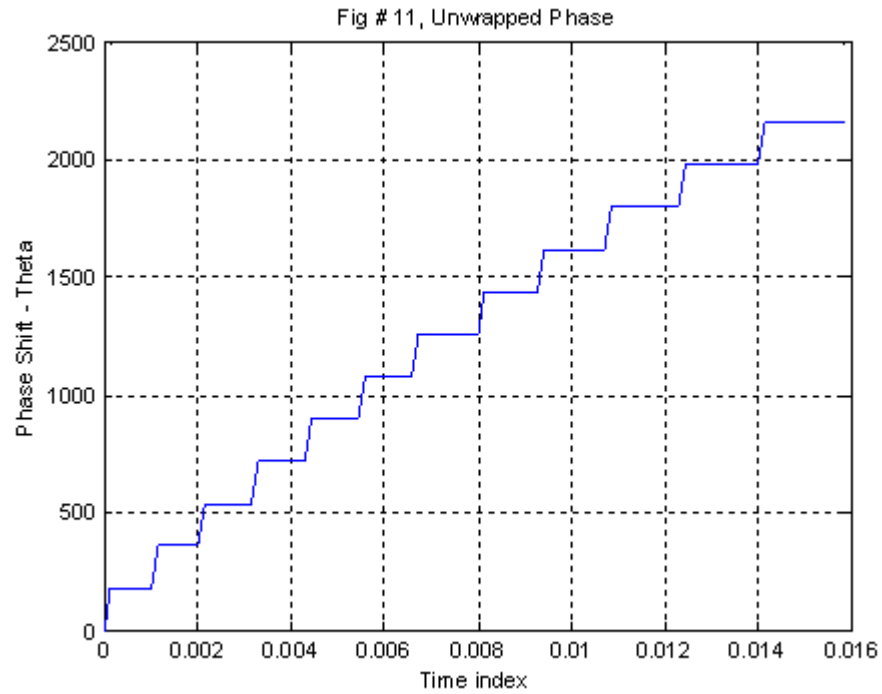
277

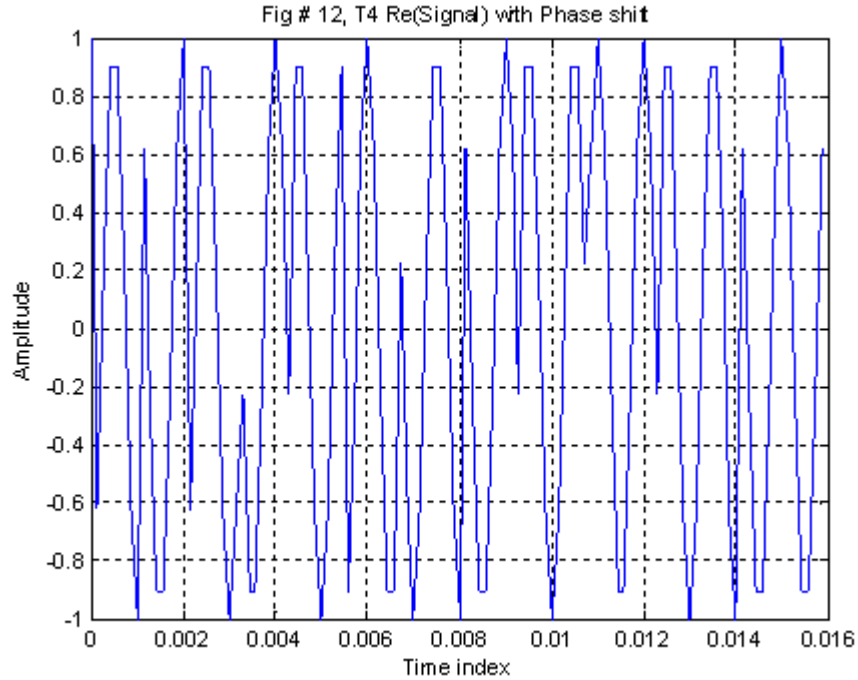Figure 126. T4(2) Stepped Frequency Phase

Figure 127. T4(2) Modulated Signal Time Domain Waveform

278

B.   FREQUENCY SHIFT KEYING (FSK) TECHNIQUES

1.   Costas Codes

Costas codes were developed by J.P. Costas. They are a sequence of frequencies that provide unambiguous range and Doppler measurements while minimizing the cross talk between frequencies. They have peak sidelobes that are down from the mainlobe by a factor of $1/N_F$ (N_F is the number of contiguous frequencies within a band B and each frequency lasts t_p seconds)(Pace 2009, 191).

There are various methods to construct a Costas sequence, such as the Welch construction, the Lempel construction, the Golomb construction, Taylor's T_4 construction, and the G_4 and G_5 constructions. An exhaustive search to find all $n \times n$ Costas arrays (which has currently been completed for $n \leq 26$), as well as others being developed (Golomb 2006), is not within the scope of the present thesis to enumerate.

Instead, by using the MATLAB LPIT TOOLBOX, for the known Costas sequence $\{2, 4, 8, 5, 10, 9, 7, 3, 6, 1\}(kHz)$, for $SNR = 0dB$, $t_p = 0.1\sec$, $f_s = 15kHz$ we present in Figures 128 and 129 the PSD plots of the I channel with and without noise (AWGN).
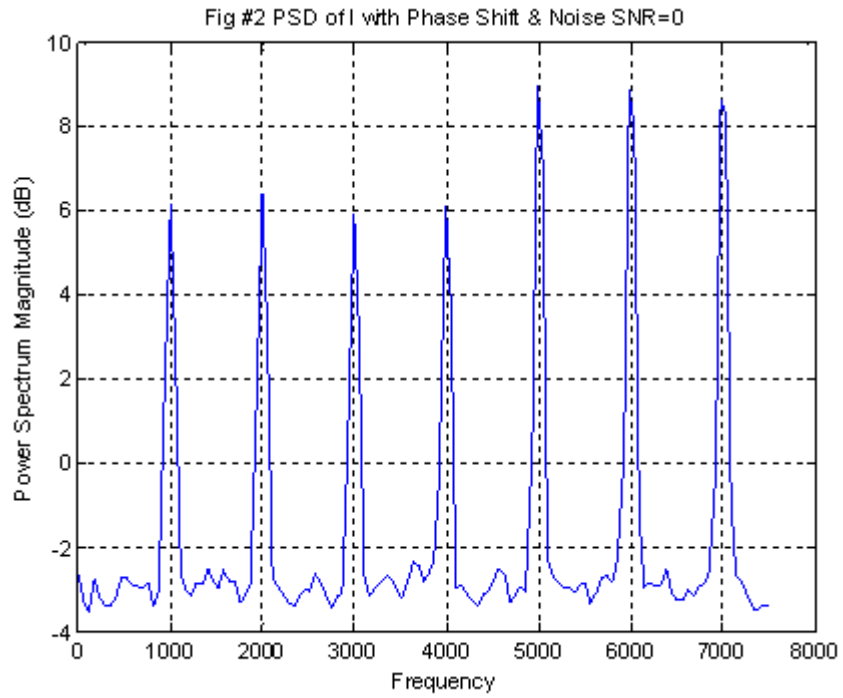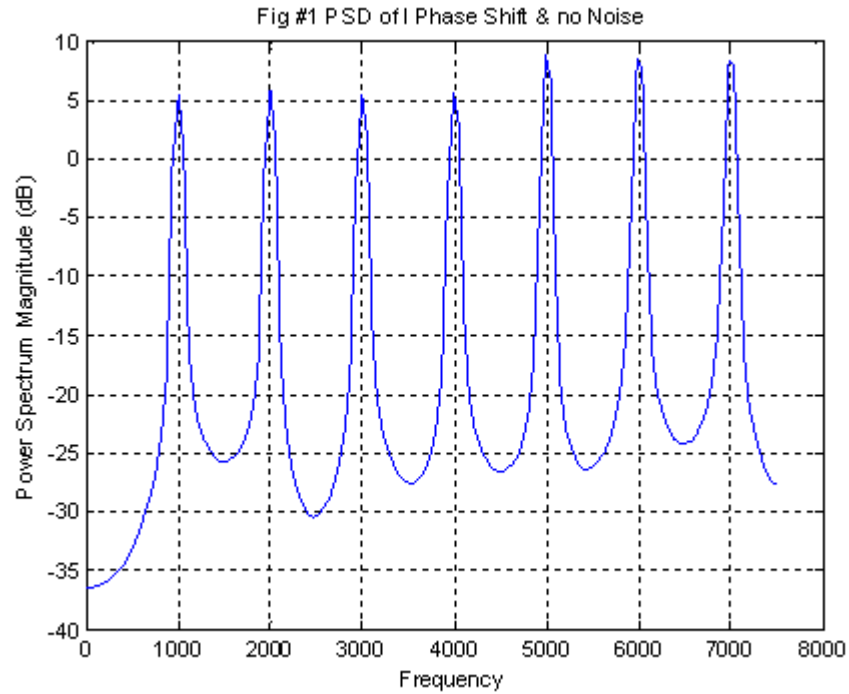
Figure 128. I Channel PSD with Noise SNR=0dB

Figure 129. I Channel PSD with No Noise

2.   Hybrid FSK/PSK Technique

The proposed technique(Pace 2009, 195) combines an FSK technique (Frequency Hoping using Costas sequences) with a PSK technique. The FH LPI radar waveform has N_F frequencies within a bandwidth B. Every frequency lasts t_p seconds in duration. The proposed hybrid technique subdivided each subperiod t_p (that one of the N_F frequencies is transmitted) into N_B phase slots, each with duration t_b. The mathematical relationships of the proposed scheme are:

$$T_B = t_p = t_b N_B \quad \text{(A.11)}$$

$$N_T = N_F N_B \quad \text{(A.12)}$$

$$T = t_p N_F = t_b N_B N_F \quad \text{(A.13)}$$

Where:

t_p : Duration of each frequency

t_b : Duration of each phase slot

N_F : Number of frequencies

N_B : Number of phase slots

T : Total code (FSK/PSK) period

T_B : PSK code period

The formula of the complex envelope of the transmitted CW FSK/PSK wave is the following (Pace 2009, 196):

$$s(t) = A e^{j2\pi f_j t + \varphi_k} \quad \text{(A.23)}$$

Where:

φ_k : One of the PSK codes

f_j : One of the   FSK frequencies

In Figures 130 and 131, by using the MATLAB LPIT TOOLBOX, we present the plot of PSD of a FSK (Costas) CW LPI waveform and an FSK(same Costas)/PSK(Barker) CW LPI waveform with the parameters: Barker code length 5, Costas sequence $\{3, 2, 6, 4, 5, 1\}(kHz)$, $f_s = 15kHz$, $SNR = 0dB$ and $t_p = 0.006 \sec$.
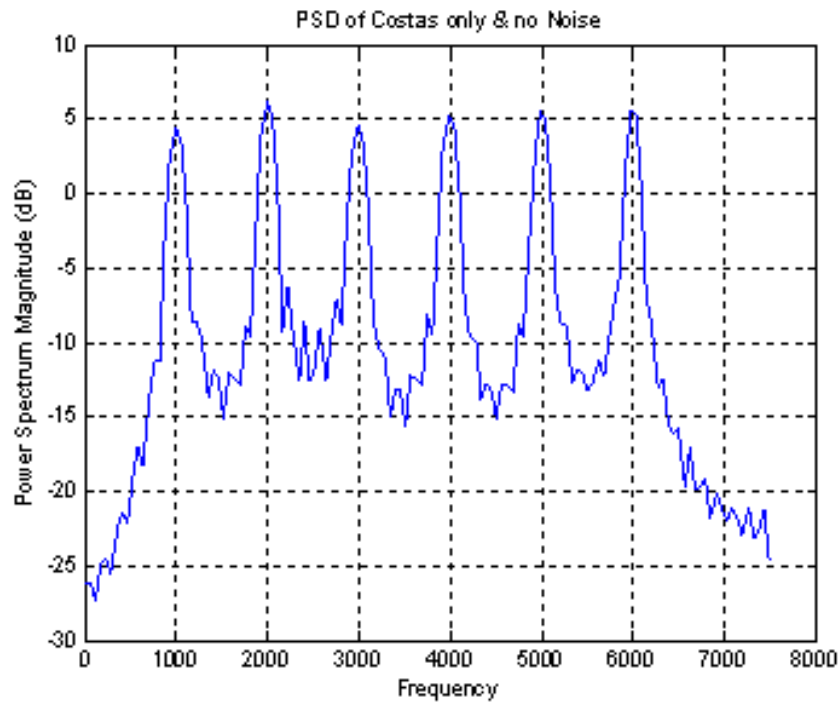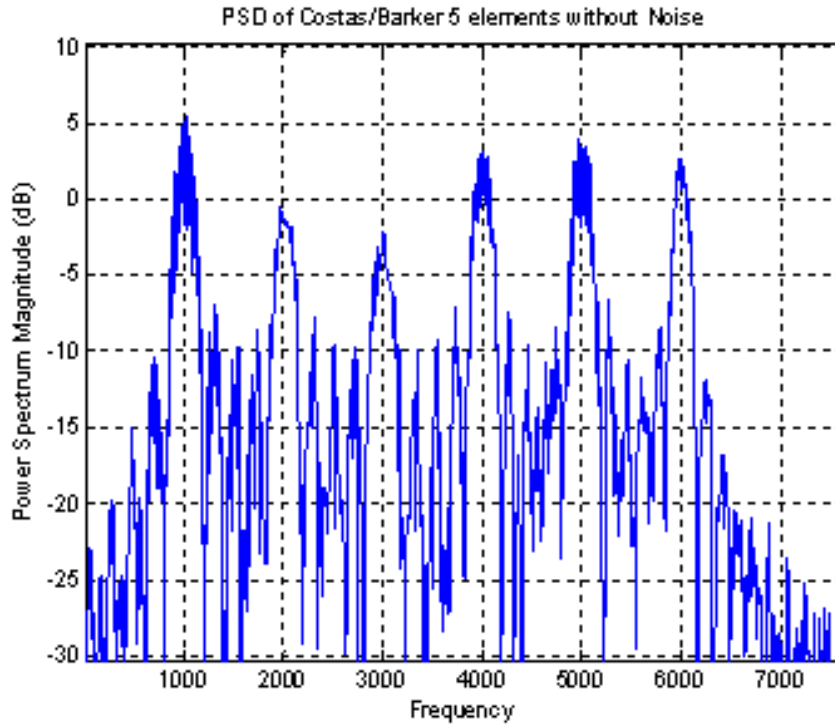

Figure 130. FSK (Costas Only) PSD

Figure 131. Hybrid FSK (Costas)/PSK (Barker) PSD

3. Matched FSK/PSK Technique

This type of technique generates FSK/PSK signals optimally matched to an arbitrary target's spectral response. Radar uses FSK/PSK signal but instead of selecting the frequency from a Costas sequence (as in the Hybrid case above), the frequencies are selected by a random process with a probability density function which is based on the target's spectral content. In this way the frequencies transmitted more frequently by the radar are the ones that correspond to the spectral peaks of the target's spectral response (Skinner 1994).

These kinds of signals can be considered as spread spectrum signals, but instead of trying to equally spread the power over the given spectrum bandwidth, more energy is

283

focused at frequencies of special interest with respect to the target's spectral response.

The resulting FH sequence appears random to an intercept receiver, so it is considered an LPI waveform. However, there is one characteristic that can enhance LPI behavior--the reuse of frequencies (due to the spectral response of the target that it is trying to match), which increases the possible number of sequences even more (Skinner 1994).

C. NOISE TECHNIQUES

1. RNR

RNR was first introduced by Narayanan. A Gaussian noise waveform is transmitted; target detection is accomplished by cross-correlating the received signal with a time-delayed and frequency shifted replica of the transmitted signal in the heterodyne correlation receiver (Narayanan 1998). RNR waveforms are not suitable for unambiguous range rate estimation due to their extended Doppler spread parameter (Dawood 2003).

The signal characteristics employed in RNR are the following (Pace 2009, 213,217):

XMIT complex form: $S(t) = [X(t) + jY(t)]e^{j2\pi f_c t}$ (A.15)

XMIT real part: $S_t(t) = X(t)\cos(2\pi f_c t) - Y(t)\sin(2\pi f_c t)$ (A.16)

RCV real part:

$$S_r(t) = X'(t)\cos\left\{\omega_c\left[(1+\alpha)t - t_d\right]\right\} - Y'(t)\sin\left\{\omega_c\left[(1+\alpha)t - t_d\right]\right\} \quad (A.17)$$

Where:

f_c: Carrier frequency

$X(t), Y(t)$: Gaussian processes (zero mean and bandwidth B)

$\alpha = (c-v)/(c+v) \approx 1 - 2v/c$

v: Relative velocity of the target

$X'(t) = AX[(1+\alpha)t - t_d)$

$Y'(t) = AY[(1+\alpha)t - t_d)$

A^2: Power reflection coefficient

t_d: Return signal delay

2. RNFR

RNFR was first introduced by Liu. A Gaussian noise wave is modulated linearly by a FMCW waveform. A portion of the transmit signal is used as a local oscillator input to the receiver, where the correlation between target return and transmitted signal takes place (L. X. Guosui 1991). RNFR has good distance measurement capability, but the CW leakage makes it difficult to measure speed and detect long range targets (L. H. Guosui 1999).

The signal characteristics employed in the RNFR are the following (Pace 2009, 223-224):

XMIT signal: $e(t) = E \cos[\omega_c t + \theta(t)]$ (A.18)

RCV signal: $e_R(t) = E_R \cos[(\omega_c + \omega_d)(t - t_d) + \theta(t - t_d)]$ (A.19)

Where:

$\omega_c = 2\pi f_c$: Carrier angular frequency

E : Amplitude of transmitted signal

$$\theta(t)=\int_0^t D_f \xi(t_1)dt_1$$: Angular deviation of FMCW modulation

D_f : Angular frequency per volt of the FMCW chirp

$\xi(t_1)$: Noise voltage of a stationary process with zero mean

E_R : Amplitude of echo signal

t_d : Return signal delay

ω_d : Doppler angular frequency

3.   RNFSR

RNFSR is very like RNFR but it also uses an additional sine signal, at frequency f_m that modulates the noise source. The composite signal is then modulated by the FMCW waveform. The additional sine helps minimize the leakage from the transmitter to the receiver that happens to the RNFR as described previously (L. X. Guosui 1991). Even with the addition of sinusoidal modulation, the RNFSR cannot measure the speed of a moving target or detect a long range target (as does RNFR), but it is suitable for short-range applications (harbor control, missile fuse systems, UAV landings, etc.) (Pace 2009, 229).

The signal characteristics employed in the RNFR are as follows (Pace 2009, 229):

XMIT signal:　　　　　　　$e(t)=E\cos[\omega_c t+\theta_1(t)+\theta_2(t)]$ (A.20)

Where:

$\omega_c=2\pi f_c$: Carrier angular frequency

E: Amplitude of transmitted signal

$$\theta_1(t) = \int_0^t \Delta F \cos(\omega_m t_1)dt_1 = \frac{\Delta F}{\omega_m}\sin(\omega_m t_1):$$ Angular frequency deviation

of sine modulation

$$\theta_2(t) = \int_0^t D_f V(t_2)dt_2:$$ Angular frequency deviation of FMCW

modulation

D_f: Angular frequency per volt of the FMCW chirp

$V(t_2)$: Noise voltage of a stationary process with zero mean

4. RBPC

Random binary phase code emitters use a random phase modulation, of binary phase code 0 or π radians, of a carrier to achieve LPI noise characteristics. To improve the performance of the RBPC emitter, we can use several pulse compressors in series. The maximum measurable Doppler frequency is defined by the length of the single pulse compressor. RBPC can detect long range targets and high speed targets, has good Doppler sensitivity and overcomes the limitations of RNFR and RNFSR radar with respect to long range detection and speed measurements; however the CW leakage problem still remains(Pace 2009, 235).

Some characteristics of the RBPC are as follows.

Range Resolution: $$\Delta R = \frac{ct_b}{2} \quad \text{(A.21)}$$

Maximum Range: $$R_{max} = \frac{N_c ct_b}{2} \quad \text{(A.22)}$$

(M pulse compression in series) $R_{max} = \dfrac{MN_c ct_b}{2}$ (A.23)

Doppler tolerance: $f_d^{max} = \dfrac{1}{2N_c t_b}$ (A.24)

Where:

t_b: Subcode width

N_c: Number of pulse codes

LIST OF REFERENCES

Adamy, David L. EW 101: A First Course in Electronic Warfare. Norwood, MA: Artech House, 2001.

Adamy, David L. EW 102: A Second Course in Electronic Warfare. Norwood, MA: Artech House Publishers, 2004.

Adamy, David L. "Jamming LPI Signals." Journal of Electronic Defense (Association of Old Crows) 32, no. 5 (May 2009): 53-54.

Adamy, David. "RADAR Part 10 - LPI RADAR." Journal of Electronic Defense, 2001.

Baker, C. J., and A. L. Hume. "Netted Radar Sensing." IEE Aerospace and Electronic Systems Magazine, Febuary 2001: 3-6.

Barton, D. K. Radar System Analysis. Norwood, MA: Artech House, 1982.

Boyd, John R. A Discourse on Winning and Losing. 1987.

Burgos-Garcia, M., J. Sanmartin -Jara, F. Perez-Martinez, and J. A. Retamosa. "Radar Sensor Using Low Probability of Interception SS-FH Signals." IEEE Aerospace and Electronic Systems Magazine 15, no. 4 (April 2000): 23-28.

Chen, Y. Q., "Simulation of Network-Enabled Electronic Warfare Metrics to Assess the Value of Networking in A General Information and Radar Topology", Naval Postgraduate School Thesis, September 2007.

Chen, Y. Q., and Phillip E. Pace. "Simulation of Information Metrics to Assess the Value of Networking in A General Battlespace Topology." Proc. of the IEEE International Conf. on System of Systems Engineering. IEEE, June 2008.

Chernyak, Victor S. Fundamentals of Multisite Radar Systems - Multistatic Radars and Multiradar Systems. Amsterdam: Overseas Publishers Association, 1998.

Cohen, Leon. "Time-Frequency Distributions-A review." Proceedings of IEEE 77, no. 7 (1989): 241-265.

Dawood, M., and Narayanan, R. M. "Generalized wideband ambiguity function of a coherent ultrawideband random noise radar." IEEE Proceedings-F Radar, Sonar, Navigation Vol.150 No. 5. 2003. 379-386.

Denk, Aytug. Detection and Jamming Low Probability of Intercept (LPI) Radars. Master's Thesis, Electronic Warfare, Naval Postgraduate School (NPS), Monterey: NPS, 2006.

Derham, T. E., S. Doughty, K. Woodbridge, and C. J. Baker. "Design and Evaluation of a Low-Cost Multistatic Netted Radar System." IET Radar, Sonar and Navigation (IET) 1, no. 5 (October 2007): 362-368.

Fuller, K. L. "To See and not be Seen [Radar]." Radar and Signal Processing, IEE Proceedings F (IEEE Proceedings) 137, no. 1 (February 1990): 1-10.

Gau, Jen Yu. Analysis of Low Probability of Intercept (LPI) Radar Signals Using the Wigner Distribution. Master's Thesis, Information Science Department, Naval Postgraduate School, Monterey: Naval Postgraduate School, 2002.

Golomb, Solomon W. "The Status of Costas Array Construction." 40th Annual Conference on Information Sciences and Systems. 2006. 522.

Guosui, L., Hong, G., and Weimin, S. "Development of Random Signal Radars." IEEE Transactions on Aerospace and Electronic Systems, Vol.35, No. 3. 1999. 770-777.

Guosui, L., Xiangquan, S., Jinhui, L. Guoyu, Y., and Yaaoliang, S. "Design of Noise FMCW Radar and its Implementation." IEEE Proceedings-F Radar, Sonar, Navigation, Vol 138, No. 5. 1991. 420-426.

Haimovich, A. M., R. S. Blum, and L. J. Cimini Jr. "MIMO Radar with Widely Separated Antennas." IEEE Signal Processing Magazine, January 2008: 116-129.

Hume, A. L., and C. J. Baker. "Netted Radar Sensing." Proc. of the CIE International Conference on Radar. CIE, October 2001. 110-114.

Huyng, Ill Choi, and William J. Williams. "Improved Time-Frequency Representation of Multicomponent Signals Using Exponential Kernels." IEEE. Trans. Acoustics, Speech, Signal Processing 37, no. 6 (June 1989): 862-871.

Kadambe, S., and T. Adali. "Application of Cross-Term Deleted Wigner Representation (CDWR) for Sonar Target Detection- Classification." Record of the 31st Asilomar Conference on Signals, Systems & Computers. 1998. 822-826.

Katkovnik, V., and L. Stankovic. "Instantaneous Frequency Estimation Using the Wigner Distribution with Varying and Data-Driven Window Lenght." IEEE Trans. on Signal Processing 46, no. 9 (September 1998): 2315-2325.

Kruse, J., M. Adkins, and K. A. Holloman. "Network-Centric Warfare in the U.S Navy's Fifth Fleet." Proc. of the IEEE 38th Hawaii International conf. on Systems Sciences. IEEE, 2005.

Lee, Jim P. Interception of LPI Radar Signals. Technical Note, Ontario: Defense Research Establishment Ottawa , 1991.

Lehman, N. H., A. M. Haimovich, R. S. Blum, and L. Cimini. "High Resolution Capability of MIMO Radar." Record of the Fortieth Asilomar Conference on Signals, Systems and Computers. 2006. 25-30.

Lima, Antonio Jr. F. Analysis of Low Probability of Intercept (LPI) Radar Signals Using Cyclostationary Processing. Master's Thesis, Electrical Engineering Department, Naval Postgraduate School, Monterey: Naval Postgraduate School, 2002.

Ling, F. M., T. Moon, and E. Kruzins. "Proposed Network-Centric Warfare Metrics: From Connectivity to the OODA Cycle." Military Operations Research 10, no. 1 (2005): 5-13.

Lynch Jr., David. Introduction to RF Stealth. Vols. 13 of IEEE Radar, Sonar, Navigation and Avionics Series SPIE Monograph . SciTech, 2004.

McRitchie, W. K., and S. E. McDonald. "Detection and Jamming of LPI Radars." MC Countermeasures (INC), 1999: W7714-7-0133/003/SV.

Milne, P. R., and Phillip E. Pace. "Wigner Distribution Detection and Analysis of FMCW and P-4 Polyphase LPI Waveforms." IEEE International Conference on Acoustics, Speech, and Signal Processing. 2002.

Narayanan, R. M., Xu, Y., Hoffmeyer, P. D. and Curtis, J. O. "Design performance and applications of a coherent ultra-wideband random noise RADAR." Optical Engineering, Vol.37 No 6, June 1998: 1855-1869.

Naval Air Systems Command. "Electronic Warfare and RADAR System Engineering Handbook." Washington, DC: Naval Air Warfare Center, 1999 April.

Papoutsis, I. and C.J. Baker and H.D. Griffiths, "Fundamental Performance Limitations of Radar Networks", EMRS DTC First Annual Technical Conference, Edinburg, UK 2003.

Pace, Phillip E. Detecting and Classifying Low Probability of Intercept Radars. 2nd Edition. Norwood, MA: Artech House, 2009.

Ruffe, L. I., and G. F. Stott. "LPI Considerations for Surveillance Radars." Radar 92. International Conference. Conf.Publ.no.365, 1992. 200-202.

Sammartino, P. F., C. J. Baker, and J. D. Griffiths. "Target Model Effects on MIMO Radar Performance." Proc. of the IEEE International Conf. on Acoustics, Speech and Signal Processing. IEEE, May 2006. V1129-V1132.

Schleher, Curtis D. Electronic Warfare in the Information Age. Norwood, MA: Artech House Publishers, 1999.

Schrick, Gerd. "Interception of LPI Radar Signals." Radar Conference 1990. Arlington : Record of the IEEE 1990 International, 1990.

292

Shannon, Claude E. "A Mathematical Theory of Communication." The Bell System Technical Journal 27 (July-October 1948): 379-423.

Skinner, B. J., Donohoe, J. P., Ingels, F. M. "Matched SK/PSK RADAR." IEEE National Radar Conference. Atlanta, 1994. 251-255.

Skolnik, Merril Ivan. Introduction to RADAR Systems, 3rd Edition. New York: McGraw-Hill, 2001.

Stankovic, L., and S. Stankovic. "On the Wigner Distribution of Discrete Time Noisy Signals With Application to the Study of Quantization Effects." IEEE Trans. on Signal Processing 42, no. 7 (July 1994): 1863-1867.

Stein, F., J. Garska, and P. L. McIndoo. "Network-Centric Warfare: Impact on Army Operations." EUROCOMM 2000 Information Systems for Enhanced Public Safety and Security (IEEE/AFCEA), May 2000: 288-295.

Stephens, J. P. "Advances in Signal Processing for Electronic Warfare." IEEE Aerospace and Electronic Systems Magazine, November 1996: 31-38.

Stove, A. G., A. L. Hume, and C. J. Baker. "Low Probability of Intercept Radar Strategies." IEEE Proceedings-Radar Sonar and Navigation (Artech House) 151, no. 5 (October 2004): 249-260.

Teng, Y., H. D. Griffiths, C. J. Baker, and K. Woodbridge. "Netted Radar Sensitivity and Ambiguity." IET Radar and Sonar Navig. (IET) 1, no. 6 (2007): 479-486.

Wiley, Richard G. Electronic Intelligence: The Analysis of Radar Signals. Norwood, MA: Artech House, 1976.

Wiley, Richard G. ELINT: The Interception and Analysis of Radar Signals. Norwood, MA: The Arthech House Radar Library, 2006.

THIS PAGE INTENTIONALLY LEFT BLANK

INITIAL DISTRIBUTION LIST

1. Defense Technical Information Center
   Ft. Belvoir, Virginia

2. Dudley Knox Library
   Naval Postgraduate School
   Monterey, California

3. Dr. Dan C. Boger
   Department of Information Sciences
   Naval Postgraduate School
   Monterey, California

4. Edward Fisher
   Department of Information Sciences
   Naval Postgraduate School
   Monterey, California

5. Dr. Wolfgang Baer
   Department of Information Sciences
   Naval Postgraduate School
   Monterey, California

6. Major Charalampos Fougias HAF
   Hellenic Air Force
   Athens, Greece

7. Lieutenant Charalampos Menychtas HN
   Hellenic Navy
   Athens, Greece